


1-1-2017

Biomechanics Of Concussion: The Importance Of Neck Tension

Ron Jadischke
Wayne State University,

Follow this and additional works at: https://digitalcommons.wayne.edu/oa_dissertations

 Part of the [Biomechanics Commons](#), [Biomedical Engineering and Bioengineering Commons](#), and the [Other Mechanical Engineering Commons](#)

Recommended Citation

Jadischke, Ron, "Biomechanics Of Concussion: The Importance Of Neck Tension" (2017). *Wayne State University Dissertations*. 1812.
https://digitalcommons.wayne.edu/oa_dissertations/1812

This Open Access Dissertation is brought to you for free and open access by DigitalCommons@WayneState. It has been accepted for inclusion in Wayne State University Dissertations by an authorized administrator of DigitalCommons@WayneState.

**BIOMECHANICS OF CONCUSSION:
THE IMPORTANCE OF NECK TENSION**

by

RONALD JADISCHKE

DISSERTATION

Submitted to the Graduate School

of Wayne State University,

Detroit, Michigan

in partial fulfillment of the requirements

for the degree of

DOCTOR OF PHILOSOPHY

2017

MAJOR: BIOMEDICAL ENGINEERING

Approved By:

Dr. Albert I. King Date

Dr. David C. Viano Date

Dr. King Yang Date

Dr. John Cavanaugh Date

Dr. Priya Prasad Date

© COPYRIGHT BY

RONALD JADISCHKE

2017

All Rights Reserved

ACKNOWLEDGEMENTS

Thank you to McCarthy Engineering Inc. and the Institute for Injury Research for providing funding to support this dissertation. Without the support it simply would not have been possible. Thank you to my dissertation advisors Dr. David Viano and Dr. Albert King for urging me to pursue my degree and their continued support throughout the research, whether it was by answering questions, steering me in the right direction, or providing me a couple of short words that just made things ‘click.’ I would also like to thank the staff of McCarthy Engineering Inc. for their assistance in various aspects of testing and preparation of this manuscript, and especially Mr. Joe McCarthy for his interest, insight, and continued support throughout this research.

I would also like to extend a thank you to Mr. Jeff Crandall, of BioCore LLC, and to the National Football League for providing better quality game videos related to the case study in Chapter 6. Thank you to Dr. King Yang, Dr. Xin Jin, and Mr. Rohit Raut, of Wayne State University, for not only providing the GHBMC finite element model for this research but also for its segmentation and guidance on use of the model. Thank you to Livermore Software Technology Corporation (LSTC) for supporting the first year of my research.

Most importantly, thank you to my wife, Kristy, for encouraging and supporting me throughout my schooling and research and to my children, Emmerson, Presley, and Brooks for providing me inspiration for the research. I could not have done it without you.

TABLE OF CONTENTS

Acknowledgements	ii
List of Tables	v
List of Figures	vii
Chapter 1 – Background and Significance	1
Chapter 2 – Anatomy and Physiology	11
Chapter 3 – Specific Aims	26
Chapter 4 – The Effects of Helmet Weight on Hybrid III Head and Neck Responses in Pendulum Impacts.....	28
Introduction.....	28
Materials and Methods.....	29
Results.....	35
Discussion.....	39
Chapter 5 – A New Laboratory Method to Simulate Player-to-Player Collisions in Contact Sports.....	51
Introduction.....	51
Materials and Methods.....	52
Results.....	59
Discussion.....	62
Chapter 6 – Concussion without Primary Head Impact and the Role of the Tensile Forces in the Upper Neck: A Case Study	65
Introduction.....	65
Materials and Methods.....	67

Results.....	74
Discussion.....	80
Chapter 7 – A Laboratory Study of Injurious and Non-Injurious Helmet-to-Helmet Hits in American Football Simulated Using the Hybrid III ATD: A New Look at Head and Neck Responses	85
Introduction.....	85
Materials and Methods.....	87
Results.....	94
Discussion.....	104
Chapter 8 - Strain and Strain Rate in the Brain Stem and Cervical Spine or Power at the Atlanto-Occipital Joint as Biomechanical Predictors of Concussion	109
Introduction.....	109
Materials and Methods.....	111
Results.....	119
Discussion.....	127
Chapter 9 – Conclusions	136
References.....	194
Abstract.....	210
Autobiographical Statement.....	212

LIST OF TABLES

Table 2.1 - Range of motion of the motion segments of the cervical spine based upon select in-vivo imaging studies.....	14
Table 4.1 – Pendulum Impact Test Matrix.	33
Table 4.2 – Results from Test Series One – Pendulum Impact Testing.	36
Table 4.3 – Results from Test Series Two – Linear Impactor Testing.	38
Table 5.1 – Summary of player masses and speeds and impactor capability.	54
Table 5.2 - Test Series 1 - Repeatability of impactor speeds and impactor synchronization.	59
Table 5.3 – Test Series 2 – Repeatability of impactor speed and ATD responses when using the impactors in three different configurations.....	61
Table 6.1 – Biomechanical responses to chest impacts for the Hybrid III ATD in the helmeted and un-helmeted conditions.	75
Table 6.2 – Biomechanical responses to chest impacts for the Hybrid III ATD in the reconstructed game hits resulting in concussion.....	77
Table 6.3 – Estimated strain in the cervical spinal canal based upon the head rotation angle and tensile loads.	80
Table 7.1 – Summary of input data for the laboratory reconstructions.	88
Table 7.2 – Calculated impact force, ATD head kinematics and head kinematics relative to T1.....	94
Table 7.3 - ATD upper neck forces and moments.	95
Table 7.4 - Comparison of the ATD kinematic data to the original dataset.	102
Table 8.1 - Change in length of the cervical spinal canal per unit of head rotation or per unit of neck tension.	120
Table 8.2 - Summary of calculated changes in length of the cervical spinal canal, strains in the spinal cord and brain stem and power at the atlano-occipital joint for the injured and uninjured players.....	123
Table 8.3 – Summary of calculated binary logistic regression parameters for the NFL reconstruction data.....	124

Table 8.4 – Summary of calculated strain and strain rates in the spinal cord and brain stem of eight human volunteer exposures in sled testing conducted by the NBDL.131

LIST OF FIGURES

Figure 1.1 – The potential location of common symptoms related to concussion based upon 1740 concussions in the National Football League.	2
Figure 1.2 – A 20 year history of the incidence of concussion in the NFL.	5
Figure 2.1 – The upper and lower cervical spine.	12
Figure 2.2 – Osteoligamentous anatomy of the cervical spine.	13
Figure 2.3 – The cranium.	15
Figure 2.4 – Inferior view of the skull.	16
Figure 2.5 – Dural infoldings.	17
Figure 2.6 – Dural venous sinuses.	17
Figure 2.7 – The meninges.	19
Figure 2.8 – Ventricles of the brain.	21
Figure 2.9 – Cisterns of the neurocranium.	21
Figure 2.10 – Surface anatomy of the brain stem.	22
Figure 4.1 – Changes in helmet mass from early 1970s until 2010.	29
Figure 4.2 – Locations for linear impact to shell and facemask.	30
Figure 4.3 – Computer model of pendulum test setup.	33
Figure 4.4 – Sample impact from impact location C comparing un-helmeted and helmeted responses.	40
Figure 4.5 – The percent increase in upper neck force versus the percent increase in head mass in all impact locations.	41
Figure 4.6 – Headform resultant acceleration and headform delta-V in the un-helmeted and helmeted impacts.	43
Figure 4.7 – Headform linear momentum and resultant upper neck forces in the un-helmeted and helmeted impacts.	45

Figure 4.8 - Summary of increase in headform effective mass and percentage change in headform kinematics.	46
Figure 5.1 – Sample reconstruction setup used by Pellman et al.	51
Figure 5.2 – Schematic of the impactor layout.	55
Figure 5.3 - Sample test setup to assess the repeatability of the impactor system when used in a ram configuration striking a stationary helmeted ATD.....	57
Figure 5.4 - Sled acceleration and deceleration profile from five tests overlaid on one another at a target speed of 8 m/s (n = 5).....	60
Figure 5.5 – Pneumatic impactor repeatability (speed from Viano et al. (n = 380)).....	62
Figure 5.6 – Impact location on helmet of ATD on impactor 2 from a set of five tests with two moving ATDs.....	64
Figure 6.1 – Impact configuration for test series 1.	67
Figure 6.2 – Pre- and Post-Impact impact kinematics for Case A.....	71
Figure 6.3 – Pre- and Post-Impact impact kinematics for Case B.....	72
Figure 6.4 - Comparison of helmeted versus un-helmeted chest impact.	76
Figure 6.5 – Post-impact kinematics in laboratory reconstruction of Case A compared to game video.....	77
Figure 6.6 - Upper neck tension and head acceleration responses to chest impacts for the Hybrid III ATD in the helmeted and un-helmeted conditions.	78
Figure 7.1 - Summary of instrumentation and filtering of the ATDs.	91
Figure 7.2 – Average impact force and impulse force representing the striking (uninjured) player and the ATD representing the injured player.	96
Figure 7.3 - Headform ΔV relative to T1 and headform $\Delta\omega$ relative to T1 for the uninjured and injured players.....	98
Figure 7.4 - Upper neck force and head rotation relative to T1 for a representative case of a struck an injured player (Case 38).	99
Figure 7.5 - Head kinematics and neck kinetics for the striking and struck player compared temporally with the peak impact force.....	100

Figure 7.6 - Comparison of head resultant translational acceleration from the struck players in the original dataset [1] to this study.	103
Figure 7.7 - Comparison of the neck tensile forces in this dataset to neck tensions reported in human volunteers, cadaveric studies and other biomechanical studies.	105
Figure 8.1 - Coordinate system setup for in-vivo studies and sample of measurement points in the spinal canal.....	113
Figure 8.2 – Location of loading applied to FE model.....	114
Figure 8.3 – Relationship of the change in length of the cervical spine to strain in the CNS	116
Figure 8.4 - Graphical comparison of the change in length of the spinal canal per unit if head rotation [%/deg] or per unit of neck tension [%/N].....	121
Figure 8.5 – Binary logistic regression plots of probability of concussion for various injury predictors.....	124
Figure 8.6 - Tolerance for concussion based upon predicted strain and strain rate in the spinal cord and brain stem.	129

CHAPTER 1 – BACKGROUND AND SIGNIFICANCE

Concussion Definition and Symptoms

Concussion in sport is defined as “*a complex pathophysiological process affecting the brain induced by biomechanical forces*” [1]. The concussion working group indicates that “*Concussion may be caused either by a direct blow to the head, face, neck or elsewhere on the body with an “impulsive” force transmitted to the head.*” The signs of concussion include any loss of consciousness, slow to get up after contact, balance problems, vacant gaze, disorientation, and/or clutching of the head after contact. There are several other symptoms that rely upon player reporting, including headache, dizziness, balance/coordination problems, nausea, amnesia, cognitive problems, sensitivity to light and sound, disorientation, visual disturbance, and tinnitus [2].

The National Football League (NFL) [3, 4] and the National Hockey League (NHL) [5] have reported on concussion symptoms in 1740 and 559 concussions, respectively. The most common symptoms of concussion in these datasets are general symptoms, such as, headaches and neck pain and cranial nerve symptoms, such as, dizziness and blurred vision. In the NFL data, 64% of the injured players had general symptoms and 54% had cranial nerve symptoms. In total, 82% had general and/or cranial nerve symptoms. Players who sustained more severe injuries, resulting in the player being out greater than 7 days, had more initial symptoms (4.62 in 1996-2001, 4.43 in 2002-2007) than players being out less than 7 days (2.75 in 1996-2001 and in 2002-2007). Players with repeat concussions were more likely to be out for greater than 7 days. The most common symptoms in these more-severely injured players were headaches (70%), dizziness (46%), and information processing (43%). Most (93%) of the symptoms reported in the NFL study correlate to injury of the spinal cord, brain stem, and/or midbrain (Figure 1.1). A table illustrating the symptoms associated with these regions is shown in Appendix A.1. Most of

these injuries were the result of direct impact to the helmet; however, some (53 of 854 from 2002-2007) did occur as a result of an indirect force being transferred to the head.

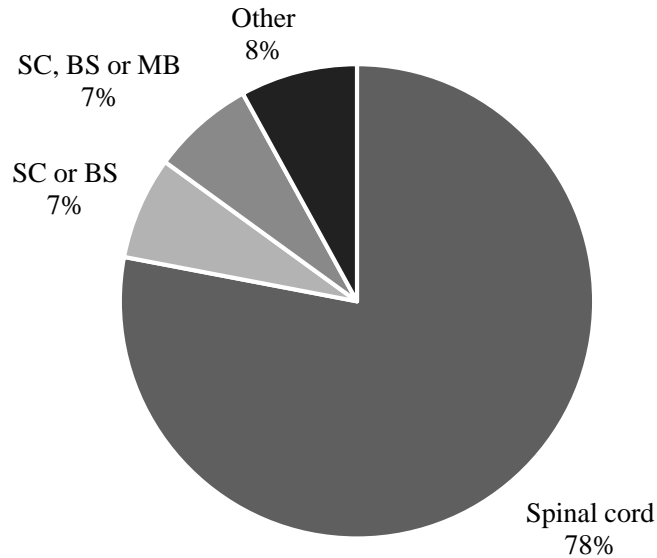


Figure 1.1: The potential location of common symptoms related to concussion based upon 1740 concussions in the National Football League [3,4]. The potential location of the symptoms is courtesy of Dr. Ira Casson. A more detailed table is included in Appendix A.1. **SC** – Spinal cord, **BS** – Brain stem, **MB** – Midbrain. Other – these players did not report symptoms in the table in Appendix A.1.

In the NFL, loss of consciousness (a sign of concussion) was much less frequent than the reported symptoms of concussion with 6.6% of these injured players (115 out of 1740) having a loss of consciousness. These players missed, on average, 5.2 days in 1996-2001 and 16.4 days in 2002-2007. The difference in time lost may reflect the changes in concussion management protocols over this period. McCrory and Berkovic [6] conducted a video analysis of players who sustained a loss of consciousness in Australian football. They concluded that the tonic posturing often seen in these players could be due to temporary brain stem dysfunction. Others [7, 8] have found cellular damage in the brain stem of people who have had short or long periods of unconsciousness prior to succumbing to a fatal injury.

In animal studies [9, 10, 11], loss of consciousness, drowsiness, sluggishness, and poor coordination are common signs used to assess experimental concussion. Transient physiological changes include bradycardia, tachycardia, respiratory failure, and loss of corneal reflex. These physiological changes are primary functions of the brain stem [12]. Sances et al. [13] measured evoked potentials in the spinal cord and brain in response to static and dynamic tensile loading applied to the head. They found a reduction in evoked potentials in the spinal cord and that changes in heart rate and respiration occurred shortly after these changes in evoked potentials. They concluded that the changes in evoked potentials and heart rate and respiration were due to distraction of the brain stem. In primate studies, both Lenox et al. [14] and Sances et al. [13] have reported reduced spinal cord function occurs at approximately half of the failure level in tensile loading conditions.

A Brief Historical Look at Concussion in the National Football League (NFL)

Since 1982, it has been prohibited for a defensive player to use the crown of his helmet as the primary point of contact against a *defenseless* player; defined as a passer, a receiver while catching a pass, or a rusher who is already being tackled by other players. The mild traumatic brain injury (MTBI) committee was formed in 1994 to conduct research regarding the biomechanics of concussion in the National Football League (NFL). In 1995, the defenseless player rule was expanded to include kickoff/punt returners and a player who is already on the ground. The rule was also modified to cover the defensive player not only striking with the crown of the helmet but also the forehead part of the helmet to the defenseless player's head, neck, or face. In 2009, the rule was further expanded to include the initial force of contact from the defensive player as being the defender's helmet, forearm, or shoulder to the receiver's head. In 2010, all defenseless players were protected from blows to the head from the defenders, and

kickers and punters were also protected from blows to the head by the opponent's helmet, forearm, and shoulder. Further extensions to this rule occurred in 2012, 2013, and 2015 to add additional defenseless players to the list: defensive players on blocks, long snappers on field goals and point-after attempts, and an intended receiver as defenseless player.

From the years 2009 to 2011 several other rule changes were implemented. These rule changes focused on the reduction of direct blows to the head from the tackler's or blocker's helmet, forearm, or shoulder. In 2011, additional rule changes regarding kickoffs were made in an attempt to increase the number of touchbacks and reduce the speed of the players on the kickoff team by reducing the amount of a running head start that they may have. Direct hits to the head delivered by the opponent's helmet, shoulder, or forearm were found to be the most frequent hits causing concussion in the NFL [15]. There is no doubt that these rule changes have had a positive effect on the battle against concussion injuries.

In parallel to the rule changes, helmet manufacturers have improved helmet designs in an attempt to help protect against concussion in football. Viano et al. [16, 17] conducted two studies assessing the impact performance of 17 models of football helmets spanning from the 1970s to 2010. Of the helmets tested, four modern helmets resulted in a reduction (10 to 20%) in head response when compared to a baseline 1990s helmet (Riddell VSR-4). There has also been an increasing trend in the size and weight of helmets over the same period. Despite the rule changes and helmet improvements, the NFL data indicates that the average number of reported concussions in the regular season from 1996 to 2000, 2001 to 2005, 2006 to 2010, and 2011 to 2015 was 105, 90, 123, and 157, respectively (Figure 1.2).

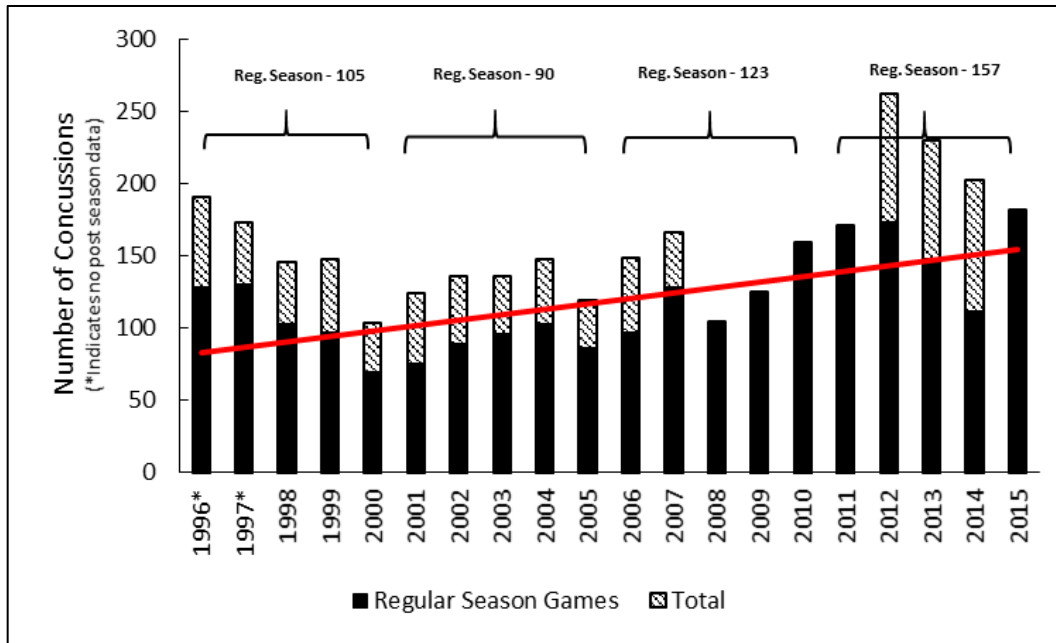


Figure 1.2: A 20 year history of the incidence of concussion in the NFL

There are several other factors that confound these injury data. Some of the teams in 1996 through 2001 may not have been reporting their injury data. However, even if the injury data was being under-reported by 10%, as has been suggested [18], the regular season injury data still indicates there is an increase in the number of diagnosed concussions per year. New concussion protocols have now been implemented, and there have also been unaffiliated neurological consultants added to the sidelines in NFL games and injury spotters overseeing the game to help spot suspicious impacts [19]. The decline in NFL injury numbers from 1996 to 1999 may be, in part, due to the rule changes regarding direct hits to the head. There was an increasing trend in the number of concussions reported per year in the NFL despite improvements to helmets and relatively few rule changes from 2000 to 2010. In the year 2000 there were only 69 regular season concussions reported, which is a 20 year low, and in 2010 there were 159 regular season concussions reported. A factor that may help to explain the increasing trend during this time is the increasing size and mass of the players during this time period. Based upon the NFL

combine data from 2000 to 2010, the average 40 yard dash speed increased from 7.60 m/s in 2000 to 7.70 m/s in 2010, equating to an increase of 1.3%, and the average mass of the players increased from 110.3 kg to 111 kg. The average momentum was increased by 2.0% from the year 2000 to 2010. The increasing player momentum (players' mass and speed) during this time may be contributing to the increasing trend of concussions in the NFL; however, it seems there are also other factors.

Other Historical Research

Most attention is paid to the roles of translational and rotational accelerations or velocities of the head causing concussion. Little recent attention has been paid to forces and deformation at the atlanto-occipital joint and brain stem [20]. There is compelling new and older data on the importance of forces and deformation of the brain stem causing concussion [15, 16, 18, 19, 21, 22, 23, 24, 25, 26, 27, 28, 29, 31, 32, 33].

Gurdjian et al. [22] discussed the mechanism of concussion and concluded that it involves a specific area of the brain - the brain stem - based on animal research. Gurdjian et al. [23] studied the upper cervical spine and found that tissue damage from a head impact is caused by shear forces at the craniocervical joint. Hodgson [24, 25] and Gurdjian et al. [26] found high strains in the area of the foramen magnum in occipital impacts to primates and dogs. Gurdjian et al. [27] and Hodgson [24] reported that impacts to the occiput of dogs caused the brain stem and cerebellum to be extruded through the foramen magnum and that dogs were more susceptible to concussion than primates in these impacts. Hodgson and Thomas [21] also found relative motion and strain in the craniocervical joint and brain stem in primates when a brain hemisphere was subjected to rotational and translational movement. They deduced that the strain in the brain

stem was due to forces from the spinal cord and indicated that their results suggest the mechanism of brain stem injury is due to stretching of the cervical cord.

Friede [10, 11] studied the mechanics of concussion by evaluating the symptoms and neuropathology in the upper spinal cord and brain stem of cats as a result of impacts and drop tests with the head supported. The latter were non-impact tests and resulted in forces being transferred through the foramen magnum and the cervical spine stretching. Each of these loading conditions resulted in the same symptoms: loss of consciousness, drowsiness, sluggishness, and poor coordination. Temporary physiological changes included bradycardia, tachycardia, respiratory failure, and loss of corneal reflex. The loss of corneal reflex lasted less than four minutes in all cats, with most being less than one minute. Both conditions also resulted in, first, a lesion at the level of C1-C2 in the spinal cord in which the thick fibers underwent Wallerian degeneration. Second, there was a subsequent axonal reaction, resulting in chromatolytic cells concentrated in the reticular formation and lateral vestibular nucleus of the brain stem. The more severe injuries also resulted in chromatolytic cells in the red nucleus. The lesion at the level of C1 occurred, but chromatolytic cells in the brain stem did not, in the subjects that expired as a direct result of the testing, supporting that a degenerative process occurs. Friede [10, 11] concluded that craniocervical stretch and flexion are the most important factors for the mechanics of concussion. In these tests, when the cervical spine muscles were tetanized it reduced the potential for injury [30].

Denny-Brown and Russell [31] conducted pendulum impacts to the occiput of cats with the head either fixed or free to move upon impact. They found when the head was fixed relative to the body, no concussion occurred; however, when the head was free to move, a concussion did occur. They also found concussion signs in the decerebrate animal; indicating the involvement

of the brain stem. Ommaya et al. [29] impacted the occiput of collared and un-collared primates. They found when the primates were wearing a cervical collar they were very difficult to be concussed. The collared primates sustained head accelerations nearly twice as high as the un-collared primates without concussive symptoms. Ommaya et al. [29] identified that this could be due to the reduction in tensile strains along the brain stem. The animal research indicates the brain stem may play an important role in a mechanism of concussion.

Breig [28] analyzed the biomechanics of the central nervous system, including the spinal canal, the spinal cord, and the brain stem, in 183 cadavers. He found that the spinal cord motion is coupled with the spinal canal motion by the denticulate ligaments and nerve roots. He studied flexion, extension, and lateral bending of the cervical spine and reported flexion results in an overall elongation of the spinal canal and spinal cord, coupled with narrowing of the spinal cord. Extension resulted in an overall shortening of the spinal canal and a thickening of the spinal cord. Others have imaged the living human [34, 35] and primate [36] head and neck with X-ray or MRI and found elongation of the cervical spinal cord in flexion and shortening in extension. Breig [28] indicated the tension generated in the spinal cord can be transmitted from the spinal cord to the brain stem (medulla oblongata, pons, and midbrain), cerebellum, and cranial nerves (V – XII), resulting in elongation of these brain tissues. The largest elongation occurred in the medulla oblongata, and no elongation was apparent superior to the midbrain. This cadaveric study points to the upper cervical spinal cord and brain stem being susceptible to injury due to their coupled motion.

Ishii et al. [37, 38, 39] conducted in-vivo, three-dimensional imaging studies of the head undergoing axial rotation and lateral bending in the living human. The in-vivo studies indicated that, during axial rotation of the head, the largest rotational movement occurs at C1-C2. Lateral

bending resulted in elongation on the contralateral side and shortening on the ipsilateral of the spinal canal, similar to Breig [28]. In lateral bending, there is coupled axial rotation that occurs at C1-C2 which is consistent with the findings of White and Panjabi [40]. Research has also shown that when tensile loads are applied to the head, resulting in tensile loads at the atlanto-occipital joint, the greatest amount of elongation occurs at the upper cervical spine (Occiput–C2) [13, 18, 41, 42]. These studies indicate that the stretching in the upper cervical spine and spinal cord has the greatest magnitude during tension, flexion, and axial rotation. People do not sustain concussion under normal range of motions in axial rotation and flexion. This suggests that tensile (distraction) forces in the upper cervical spine, which is not a common range of motion in the human due to our upright posture, and the rate of these movements may be important.

Pellman et al. [43] reported on the analyses of 182 severe game impacts in the NFL and the reconstruction of 31 impacts using the Hybrid III 50th percentile anthropomorphic test device (ATD). The Head Injury Criteria (HIC) was one of the best predictors of concussion from these reconstructions; however, Viano et al. [44] has recommended further study of the head kinematics, such as, neck axial rotation, and neck tension after the impact has occurred, and their relation to concussion since neck stiffness can affect headform delta-V. Collins et al. [45] indicated that lowered neck strength is a significant predictor of concussion; however, they recommended that further research is necessary to understand why.

Finite element modeling is another approach to assess tissue level strains in the brain stem and spinal cord. Giordano and Kleiven [46] studied axonal strain in the brain by conducting finite element modelling using a head and cervical spine model based upon the NFL reconstructions [40]. They found strain in the axonal direction is a better predictor of injury than maximum principal strains and that axonal strain in the brain stem was the best predictor of

injury. However, they indicate the neck model used was not a biofidelic model. Antona-Makoshi et al. [47] studied a head and cervical spine finite element model of the monkey by reproducing experimental test data of Ono et al. [48] and found strains in the brain stem to be the best predictor of concussion. Other finite element modeling studies [20, 49, 50, 51] do not incorporate a biofidelic finite element model of the neck. Therefore, their ability to calculate the strains in the brain stem and spinal cord is questionable.

Significance

Concussion signs and symptoms found in NFL, NHL players, and boxers and physiological changes found in animals can be correlated to injury to the upper cervical spinal cord or brain stem. Historical and current research using cadavers, animal models, and finite element modelling indicate that strains occur in the brain stem and upper spinal cord during head movement and impacts to the head. They also indicate that strain in the brain stem is one of the best biomechanical predictors of concussion. It is my hypothesis that an important mechanism of concussion is related to the strain and strain rate in the brain stem and upper spinal cord, or in an anthropomorphic test device, the forces at the upper neck and velocity of these forces. If this proves to be a predictor of concussion these findings can have significant influence on understanding a mechanism of concussion. These data can then be applied to assess helmet performance and identify alternative methods to protect against concussion. The findings will highlight the importance of the need for more biomechanical research in this field to assess the interaction between the brain stem and upper spinal cord by way of cadaveric testing and finite element modeling.

CHAPTER 2 – ANATOMY AND PHYSIOLOGY

A general overview of the anatomy of the brain and osteoligamentous upper cervical spine is provided in this section. The overview is limited to the cranium and its meninges, the surface anatomy of the cervical spinal cord and brain stem, and the internal architecture of the brain stem, highlighting some of the key functional pathways and the ventricles of the brain and cerebral spinal fluid (CSF) flow. Details of the anatomical structures can be readily found in various published sources [12, 40, 52]. The complex musculature related to the head and cervical spine is not discussed.

Osteoligamentous Cervical Spine

The cervical spine consists of seven motion segments (OC-C2, C2-C3, C3-C4, C4-C5, C5-C6, C6-C7, C7-T1), extending from the skull to the first thoracic vertebrae. The cervical spine can further be subdivided into two regions: the upper cervical spine (UCS) (OC-C2) and the lower cervical spine (LCS) (C2-T1) (Figure 2.1). There are differences in both the anatomical structures and the functions of the UCS and LCS. There are various ligaments attaching the vertebrae to one another. Intervertebral discs absent between the skull and C1 and between C1 and C2.

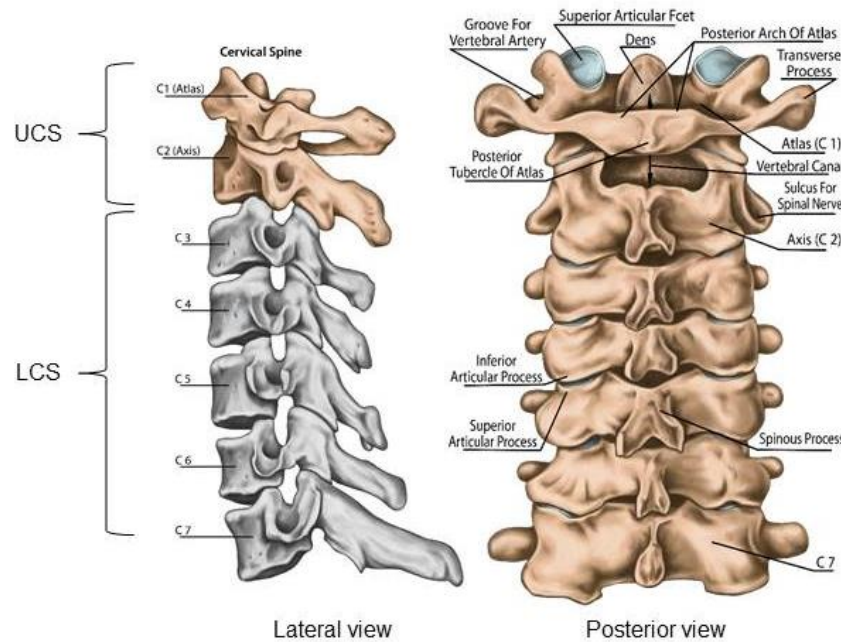


Figure 2.1: The upper and lower cervical spine

The skeletal structures in the UCS (Figure 2.2) are the base of the skull, atlas (C1), and axis (C2). The atlas and axis are specialized vertebrae. The atlas is a ring-shaped structure and differs from the other vertebrae since it has no vertebral body, but it does have enlarged facets on the lateral aspect of the ring. The base of the skull rests on the surface of these facets of the atlas. This motion segment, known as the atlanto-occipital joint (AO), is responsible for a large portion of the nodding (flexion/extension) motion of the head. The axis consists of a vertebral body and a posterior arch, similar to the vertebrae in the LCS; however, it has an additional feature, the odontoid process. The odontoid process is positioned superiorly, protrudes near the anterior arch of the atlas, and articulates with this arch. The atlantoaxial (AA) motion segment (C1-C2) provides approximately half of the axial rotation (“No”) range of motion of the head. This segment (AA) is also responsible for approximately 20 deg in flexion/extension [53].

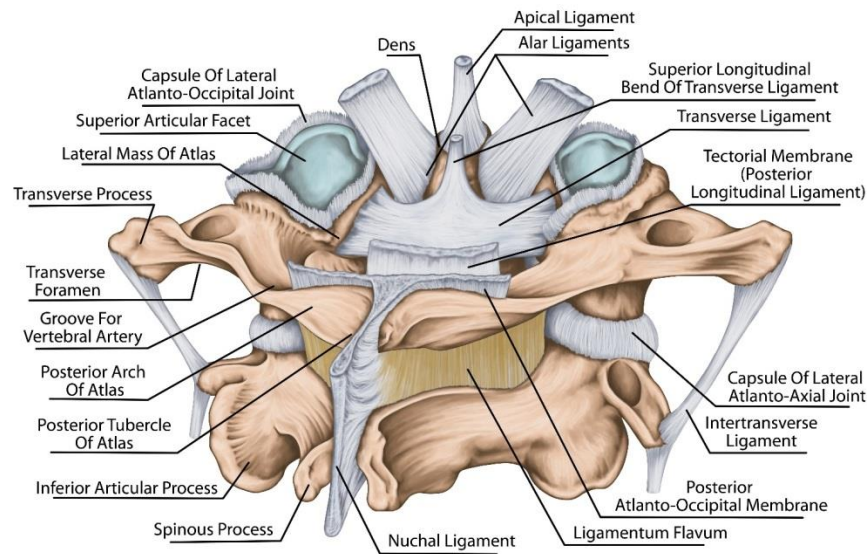


Figure 2.2: Osteoligamentous anatomy of the cervical spine

The ligamentous portion of the UCS includes a continuation of the posterior longitudinal and anterior longitudinal ligaments (PLL and ALL) in the LCS; however, there are ligaments that are unique to the UCS. These ligaments are the cruciform (superior, transverse, and inferior), apical, and alar ligaments. The PLL and ALL insert into the base of the skull and are continuous with the tectorial membrane at this location. The transverse cruciform ligament connects the medial aspect of the lateral mass of C1 to the odontoid process, constraining posterior movement of the odontoid process. The inferior and superior cruciate ligaments attach to the anterior portion of the foramen magnum and posterior aspect of the vertebral body of C2. The apical ligament attaches the superior point (apex) of the odontoid process to the base of the skull, while the alar ligaments connect the odontoid process laterally to the base of the skull.

Table 2.1 summarizes the ranges of motion based upon in-vivo imaging studies of the living human cervical spine. This table reports only the primary direction of motion. Coupled motion also occurs in the cervical spine. The magnitude of these coupled motions is discussed in the cited literature.

Level	Lateral Bending One side [39] [deg]	Flexion [53, 54] [deg]	Extension [53, 54] [deg]	Axial Rotation One Side [37, 38] [deg]
C0-C1	1.9	12.6	17.8	1.7
C1-C2	1.6	15.4	7.3	36.2
C2-C3	3.7	5	3	2.2
C3-C4	3.5	6	5	4.5
C4-C5	3.3	7	8	4.6
C5-C6	4.3	6	5	4.0
C6-C7	5.7	7	4	1.6
C7-T1	4.1	-	-	1.5
Total	28.1	59.0	50.1	56.3

Table 2.1: Range of motion of the motion segments of the cervical spine based upon select in-vivo imaging studies

The Cranium

The cranium (or skull) is the skeletal section of the head (Figure 2.3). It is segmented into the neurocranium, which is the bony covering of the brain (cranial vault), and the viscerocranium, which is the facial skeleton. There are eight bones that make up the neurocranium: the frontal, parietal (left and right), temporal (left and right), occipital, sphenoid, and ethmoid. The inferior and external aspect of the occipital bone contains the occipital condyles which articulate with the condylar surfaces on the atlas. The union of the bones of the neurocranium are known as sutures. The coronal suture forms the connection between the frontal and parietal bone; the lambdoid suture between the parietal, temporal, and occipital bones; and the sagittal suture between the left and right parietal bones. The pterion suture is an H-shaped formation that unites the frontal, parietal, sphenoid, and temporal bones. In the infant, the sutures are not rigidly formed. They begin to form at approximately the age of one and a half to two and a half, and it is not until the second or third decade of life that the sutures are completely formed.

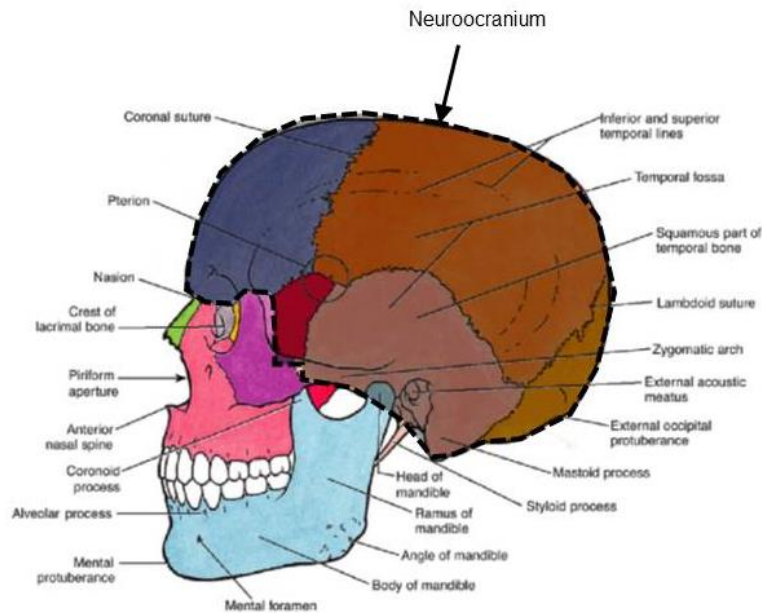


Figure 2.3: The cranium

The cranial base is the inferior aspect of the neurocranium (Figure 2.4). In the cranial base, the occipital bone interfaces with the temporal, parietal, and sphenoid bones. The sphenoid bone consists of a body and three pairs of processes known as the greater and lesser wings and the pterygoid processes. The ethmoid bone lies anterior-superior to the sphenoid bone. It interfaces anteriorly and superiorly with the frontal bone and posteriorly and inferiorly with the sphenoid bone. The cranial base is divided into three separate regions: the anterior, middle, and posterior fossae. The anterior fossa is formed by the frontal bone anteriorly and the sphenoid bone posteriorly. The middle cranial fossa is composed of deep depressions on each side of the sella turcica of the sphenoid bone and the petrous portion of the temporal bone. The pituitary gland is contained within the sella turcica. The posterior fossa is the posterior aspect of the cranial base.

There are broad grooves in the posterior fossa that are formed by the transverse and sigmoid sinuses. There is also an internal occipital crest which sub-divides the posterior fossa into two cerebellar fossae.

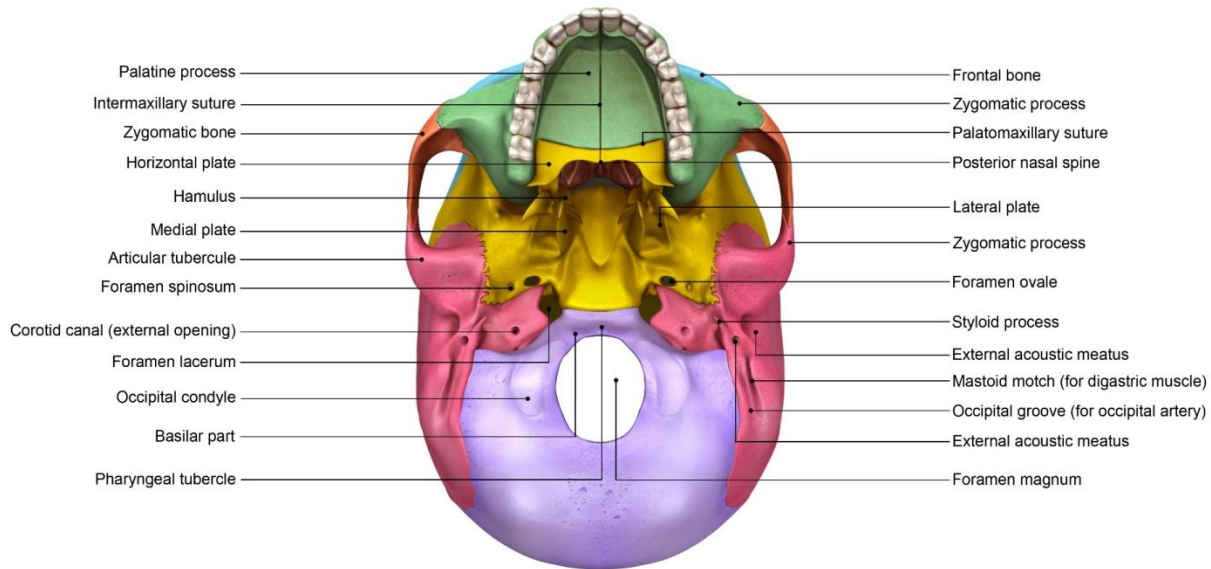


Figure 2.4: Inferior view of the skull

In the cranial base there are several openings (foramina) to allow for cranial nerves and other structures to enter and exit the neurocranium. The largest opening in the cranial base is the foramen magnum which is the entrance of the spinal cord. This is located at the center of the posterior fossa. There are two jugular foramen which are anterior and lateral to the foramen magnum and allow for the exit of the left and right jugular veins.

The Meninges (Dura, Arachnoid, and Pia Mater)

The neurocranium houses the brain and the spinal column houses the spinal cord. The brain and spinal cord make up the central nervous system (CNS) and are covered externally by the meninges, which are the dura, arachnoid, and pia mater. The meninges act to protect the brain

and spinal cord and also form the supporting framework for various arteries, veins, and venous sinuses.

The outermost layer is the dura mater which is a tough, thick, fibrous layer. There are two layers that make up the dura mater: the outer periosteal layer which is attached to the skull and the inner meningeal layer. The dura compartmentalizes the neurocranium and supports parts of the brain. There are several dural infoldings that branch off of the dura mater: the cerebellar tentorium, the cerebral falx, the cerebellar falx, and the sellar diaphragm (Figures 2.5 and 2.6). The cerebral falx is the largest dura infold and it separates the right and left cerebral hemispheres. It stretches from the crystal galli on the frontal bone to the internal occipital protuberance posteriorly and attaches to the cerebellar tentorium in its midline. The cerebellar tentorium divides the cerebrum (superior) from the cerebellum and brain stem (inferior). The dura is attached to the foramen magnum and the periosteum covering the upper cervical spine and ligaments. The dura continues inferiorly and the epidural space separates the dura mater and the spinal canal inferior to the UCS. The dura lines the external surface of the spinal nerve roots.

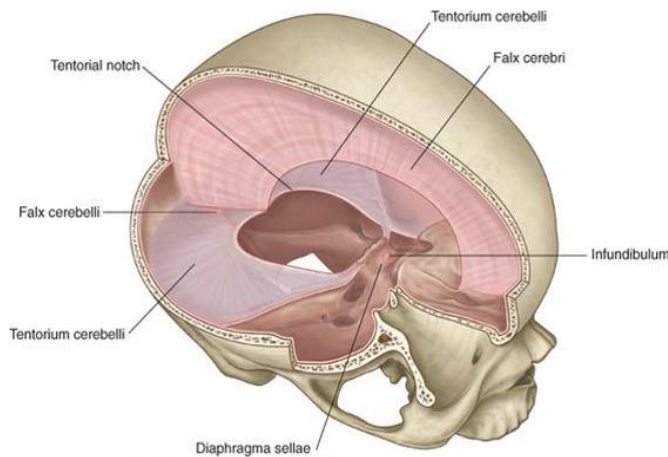


Figure 2.5: Dural infoldings

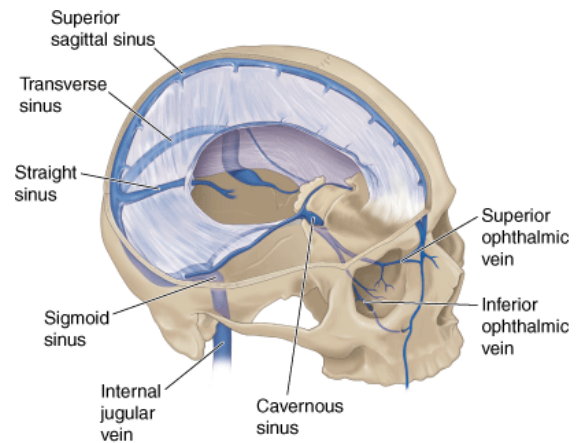


Figure 2.6: Dural venous sinuses

In the neurocranium, the periosteal and meningeal layers of the dura separate to make room for the dural venous sinuses (Figure 2.6). The dural venous sinuses collect blood from the larger veins on the surface of the brain and drain inferiorly toward the cranial base. The superior sagittal sinus and inferior sagittal sinus run along the exterior and interior borders of the cerebral falx, respectively. The straight sinus is formed by the union of the inferior sagittal sinus and the cerebral vein. The straight sinus and superior sagittal sinus meet at the confluence of sinuses which then transitions to the transverse sinuses, the sigmoidal sinuses, and then feed to the internal jugular veins. Inferior to the confluence of sinuses is the occipital sinus. The occipital sinus drains inferiorly towards the marginal sinus which surrounds the foramen magnum and then to the vertebral venous plexus (VVP), the suboccipital veins, or through the internal jugular vein.

The periosteal layer of the dura is attached to the bone, and the arachnoid mater is held against the inner meningeal layer of the dura by the pressure of the CSF and conforms to the shape of the dura mater. The space between the meningeal layer of the dura mater and the arachnoid mater is known as the subdural space. This is a potential space and does not normally exist. The arachnoid mater is a thin, avascular, intermediate layer (Figure 2.7). The space between the arachnoid and pia mater is a real, natural, physical space versus the spaces between the cranium and dura or dura and arachnoid which are not physical spaces. The subarachnoid space contains trabecular cells, veins, arteries, and the cerebral spinal fluid (CSF). The pia mater is a delicate internal vascular layer that adheres to the surface of the brain and follows its contour. Since the arachnoid mater follows the dura and the pia mater follows the surface of the brain, there are areas where the pia and arachnoid mater separate. These are known as cisterns. The cisterns in the brain are spaces that contain a greater volume of CSF.

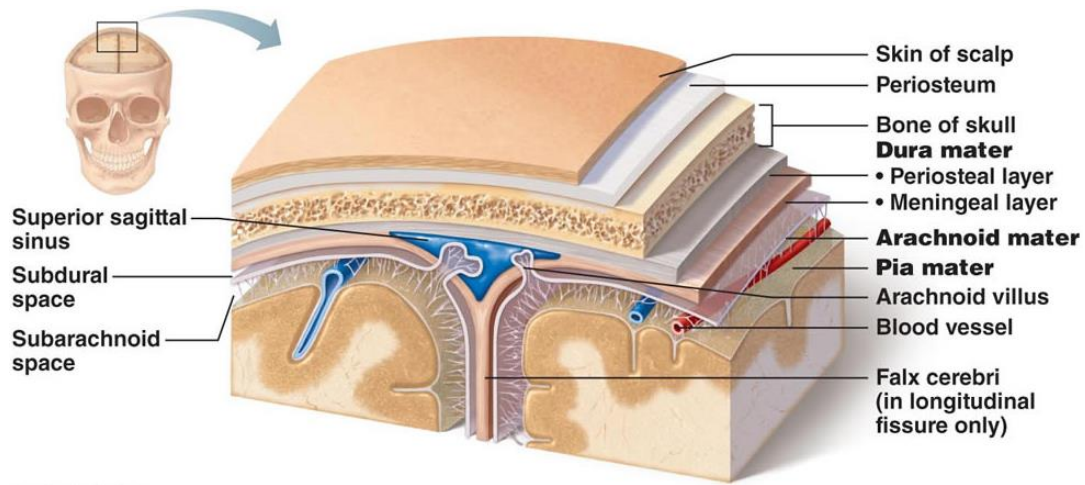


Figure 2.7: The meninges

The subarachnoid space continues inferiorly and surrounds the spinal cord. On the spinal cord, the internal surface of the dura/arachnoid mater is tethered to the pia mater and spinal cord by 21 pairs of ligaments, known as the denticulate ligaments (DL). The DLs are located laterally on the spinal cord between the ventral and dorsal nerve roots. Each ligament has various triangular extensions running from the lateral aspect (dura mater) that converge to a single narrow strip and are attached medially to the pia mater covering the spinal cord [55]. The DLs are made of collagen fibres and begin at the craniovertebral junction, with pairs present on the spinal cord inferiorly to the level of T12. The DLs are larger in diameter in the cervical spine and there is a greater number than in the thoracic spine. The first DL is attached to the spinal cord in close proximity to the spinal accessory nerve rootlets (cranial nerve XI). In the cervical spine, the DLs penetrate the pia and the collagen fibres attach to the spinal cord directly [55].

Cerebrospinal Fluid

CSF is produced primarily by the choroid plexuses which are located in the ventricles of the brain at a rate of 400-500 mL/day. CSF is a clear fluid, and its flow is pulsatile and varies with

heart rate and respiration. It surrounds both the brain and spinal cord and acts to perform cleanup by removing metabolic waste and its flow helps to regulate intracranial pressure. There is approximately 150 mL of CSF within the CNS. Approximately 40-50 mL is located in the cranium, with 20-25 mL in the ventricles and 20-25 mL in the subarachnoid space, and 100 mL is within and surrounds the spinal cord. The normal CSF pressure with the patient lying on his/her side by lumbar puncture is 8 – 15 mmHg, which is similar to the normal intracranial pressure in this orientation, and this pressure varies by approximately 1 mmHg in the normal adult.

There are four ventricles of the brain (Figure 2.8): the lateral ventricles (2), the third ventricle, and the fourth ventricle. The lateral ventricles are the most superior within the brain and are paired structures located above the cerebellar tentorium. CSF is primarily produced in these ventricles then converges at the septum pellucidum and flows inferiorly towards the third ventricle, which is located superior to the mesencephalon. The flow then continues inferiorly and posterior to the brain stem through the cerebral aqueduct toward the fourth ventricle which is located posterior to the pons and anterior to the cerebellum. From this location, some CSF flows through the lateral apertures towards the arachnoid mater lining the surface of the neurocranium, some flows inferiorly and into the central canal of the spinal cord, and some flows inferiorly and into the arachnoid mater lining the spinal cord. The remainder flows inferiorly through the median aperture towards the basal cistern, which is located posterior to the brain stem and inferior to the cerebellum.

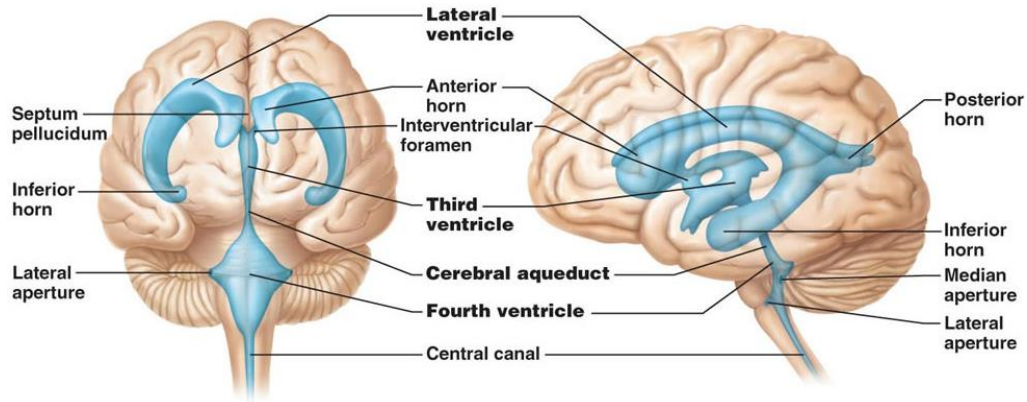


Figure 2.8: Ventricles of the brain

There are various cisterns located in the neurocranium (Figure 2.9), which are areas located mainly at the base of the brain. These are spaces where the arachnoid and pia mater are separated by large pools of CSF. The main cisterns are the cerebellomedullary cistern, the pontocerebellar cistern, the interpeduncular (basal) cistern, the chiasmatic cistern, and the quadrigeminal cistern. CSF from these various cisterns flows through the sulci and fissures on the cerebral hemispheres and around the cranial nerves. The CSF is then reabsorbed into the blood stream. The main site of reabsorption is through the arachnoid granulations which are protrusions of the arachnoid villa into the dural venous sinuses. By way of the dural sinuses the CSF flows out of the neurocranium.

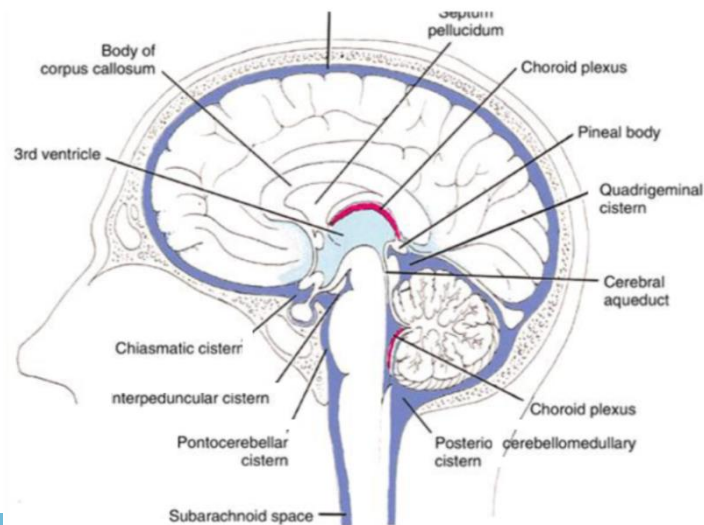


Figure 2.9: Cisterns of the neurocranium

Surface Anatomy of the Brain Stem and Upper Spinal Cord

The brain stem and cerebellum are located in the posterior cranial fossa. They are surrounded posteriorly by the occiput, anteriorly by the occiput and sphenoid, and superiorly by the cerebellar tentorium. The brain stem is encapsulated by CSF. The basal and pontomedullary cisterns separate the ventral aspect of the brain stem and the occiput and sphenoid bones. The third ventricle is superior to the brain stem and the cerebral aqueduct, and fourth ventricle and cerebellomedullary cistern are dorsal to the brain stem. The brain stem is subdivided into 3 parts: the medulla, the pons, and the mesencephalon (midbrain) (Figure 2.10). The mesencephalon travels through the opening in the cerebellar tentorium (tentorial hiatus) to communicate with the upper compartment of the brain (diencephalon and telencephalon).

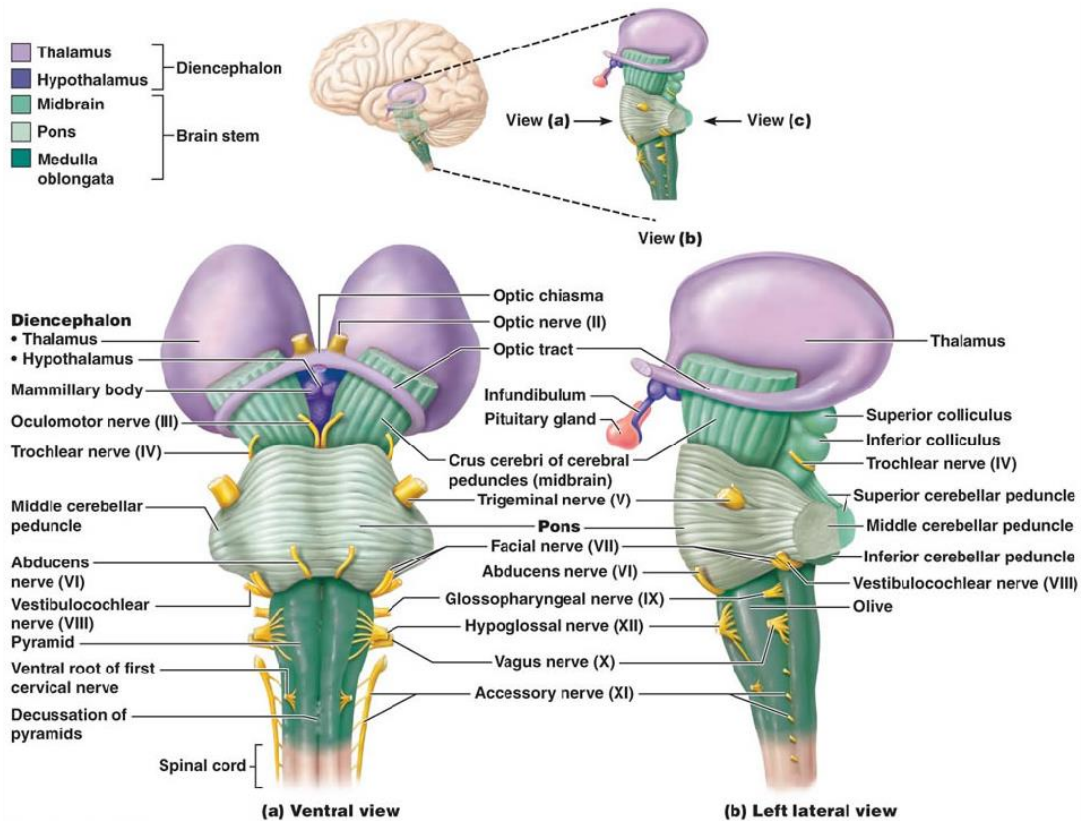


Figure 2.10: Surface anatomy of the brain stem

Inferiorly, the brain stem travels through the foramen magnum and is continuous with the cervical spinal cord. The inferior aspect of the brain stem is defined as being just above the first pair spinal nerve roots, which can be approximated by a transverse plane through the apex of the dens and the middle of the posterior arch of the atlas.

The nerve roots for cranial nerves (CN) III through XII originate in the brain stem and exit the neurocranium through various foramen. The CNs contain sensory and/or motor fibres to innervate muscles or glands within the body or carry impulses from sensory receptors.

Major Functions of the Brain Stem

The brain stem plays an important role in sensory, motor and autonomic functions of the body. The brain stem also provides pathways to integrate information between the cerebrum, cerebellum, and spinal cord. Naidich et al. [52] provides a detailed overview of the major functions of the brain stem and the interested reader is referred to this reference for specific details on the sensory and motor functions of the brain stem. Some of these primary functions are briefly discussed herein.

Some of the primary functions of the brain stem are the regulation of consciousness and the control of heart rate and respiration, and therefore, it is essential for life. The control centers for these processes lie within the reticular formation of the brain stem. The precise location of the regulation of consciousness is difficult to pin point; however, it is generally thought that the pontine tegmentum, located in the pons, is an integral part of consciousness. Autonomic control of heart rate is completed through the glossopharyngeal (CN IX) and vagus (CN X) nerves with their control centers located at the nucleus of solitary tract and the dorsal motor nucleus of the vagus nerve. The medulla is the primary control center for respiration with secondary control occurring in the pons.

The vestibular area of the brain stem is responsible for balance, posture and the sensing of head position and movement. The vestibular nuclei are located in the floor of the fourth ventricle and it is subdivided into four sub-regions: 1) the inferior vestibular nucleus (Roller), 2) the medial vestibular nucleus (Schwalbe), 3) the lateral vestibular nucleus (Deiter), and 4) the superior vestibular nucleus (Bechterew). The vestibular/ocular motor reflex is integrated in the medial vestibular nucleus of the brain stem. This reflex regulates eye movements to stabilize images while the head is moving. Diagnostic testing related to this reflex has recently been shown to be a sensitive diagnostic tool for concussion [56]. The lateral vestibular nucleus is linked to the spinal cord through the vestibulospinal tract and is responsible for control of balance.

The trigeminal nucleus is a large network of nuclei that lie on the brain stem and extend through the midbrain, pons and medulla. The superior part of the trigeminal nucleus is known as the mesencephalic nucleus, the medial part is the pontine nucleus and the inferior part is the trigeminocervical nucleus. The trigeminal nerve is the largest of the cranial nerves and is responsible for the sensory functions in the face and upper cervical spine and motor functions in the face such as mastication. The spinal trigeminal nucleus (inferior part) integrates pain and temperature sensation from the face as well as from the first three cervical nerves. The pain sensation in the cervical nerves is a possible mechanism of cervicogenic headache [57, 58].

A brief overview of the major functions of the brain stem has been provided. In animal studies, concussion has previously been diagnosed based upon loss of consciousness and has been associated with changes in heart rate and respiration. In the human, the most common symptoms (Chapter 1) of concussion in 1740 NFL players were general symptoms (64%) or cranial nerve (54%) symptoms. Eighty two percent of players had general and/or cranial nerve

symptoms. The most common general symptoms were headache (57%) and neck stiffness (13%) while the most common cranial nerve symptoms were dizziness (41%) and blurred vision (17%). This brief overview of major brain stem functions indicates that most signs and symptoms of concussion could be related to a mechanism of injury involving the upper cervical spinal cord and/or brain stem.

CHAPTER 3 – SPECIFIC AIMS

The motivation for this study is that, despite advancements in helmet technology to reduce head accelerations, the incidence of concussion has not reduced. This suggests a different mechanism of injury that that which helmets protect against. In the NFL, the lack of reduction in the incidence of concussion is complicated by ongoing rule changes, changes to concussion protocol, and evolving definition of concussion. However, there is compelling older and new research to point to tension or strain in the brain stem and the upper cervical spine as a potential source for signs and symptoms related to concussion. Helmets are not designed to reduce strain in the brain stem.

The central hypothesis of this dissertation is that the strain and strain rate in the upper cervical spine and brain stem correlate to concussion. In the Hybrid III ATD this could be quantified as the power at the upper neck. The hypothesis is based upon the cited research involving animal, cadaveric and finite element mathematical models and that elongation of the cervical spine can result in tension in the spinal cord, brain stem, and cranial nerves. This is supported by the fact that the signs of and most common symptoms of concussion are related to injury in the upper cervical spinal cord and brain stem.

The overall aim of this research is to understand whether the strain and strain rate in the upper spinal cord and brain stem and/or the power at the upper neck, when measured in an ATD, is a biomechanical predictor of concussion. The data in this dissertation were collected and analyzed as several smaller scale studies and each Chapter is organized as a separate scientific paper. Therefore, there will be some repetition in the Introduction and Discussion sections of the chapters.

The specific aims for each chapter are outlined below.

Chapter 4 – To assess the effects of helmet weight on Hybrid III head and neck responses by comparing un-helmeted and helmeted impacts.

Chapter 5 – To develop and assess repeatability of a new laboratory method to simulate player-to-player collisions in contact sports.

Chapter 6 – To assess the head kinematics and neck kinetics in concussion with no head contact and to assess the effects of helmet weight in un-helmeted and helmeted impacts to the chest.

Chapter 7 – To reconstruct several injury causing collisions in football and assess the head and neck responses as predictors of concussion in football.

Chapter 8 – To estimate the strains in the spinal cord and brain stem as a result of head movement relative to the body and combine this with the reconstruction data to estimate the strains and strain rates in the upper cervical spinal cord and brain stem of injured and uninjured players.

CHAPTER 4 – THE EFFECTS OF HELMET WEIGHT ON HYBRID III HEAD AND NECK RESPONSES BY COMPARING UN-HELMETED AND HELMETED IMPACTS

This chapter has been previously published in the Journal of Biomechanical Engineering. The citation for the publication is:

Jadischke R, Viano DC, McCarthy J, King AI. The Effects of Helmet Weight on Hybrid III Head and Neck Responses by Comparing Unhelmeted and Helmeted Impacts. J Biomech Eng. 138(10). 2016.

INTRODUCTION

Football helmets in the early 1900s were made of leather and included a marginal amount of padding. In the early 1970s, the National Operating Committee on Standards for Athletic Equipment (NOCSAE) was formed and collaborated with Wayne State University to develop standards and biofidelic headforms for use in impact testing. Currently, the NOCSAE football helmet standard for newly-manufactured football helmets requires the NOCSAE headform to experience a Gadd Severity Index (GSI) of less than 300 to 1200 in drop tests to various locations on the helmet [59]. The drop velocities range from 3.46 to 5.46 m/s.

Viano et al. [16, 17] conducted two studies assessing the impact performance of 17 models of football helmets spanning from the 1970s to 2010. When compared to linear impactor tests of the un-helmeted headform, there was, on average, a decrease of head accelerations of 20%, 22%, 21%, and 33% for the 1970, 1980, 1990, and 2010 helmets, respectively. Of the helmets tested, four modern helmets resulted in a significant reduction (10 to 20%) in head response when compared to a baseline 1990s helmet. Viano et al. [16] further reported helmet increases in length of 4.3 cm, in height of 7.6 cm, in width of 4.9 cm, and in mass of 1.18 kg (from 0.73 to 1.91 kg), on average, from the 1970s to 2010 (Figure 4.1).

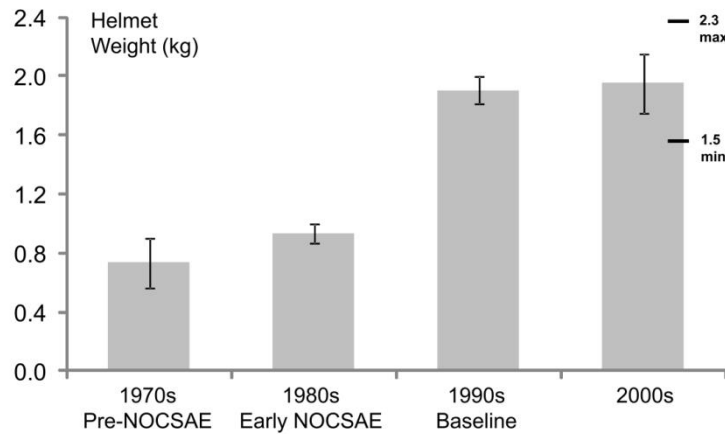


Figure 4.1: Changes in helmet mass from early 1970s until 2010

The current study hypothesizes that the addition of the mass of a helmet on a headform will result in an increase in upper neck loads due to the helmet's mass and inertia. The aims of this study are to conduct impact testing, to assess the response of the head and upper neck, and to investigate the effects of adding the mass of a helmet to an un-helmeted Hybrid III headform and Hybrid III neck.

MATERIALS AND METHODS

The impact locations in this study were developed based upon the analysis of game films. Pellman et al. [60] studied 182 game films of concussion and severe helmet impacts in the NFL. They found that 29.3% of severe helmet impacts occurred to the facemask represented by impact locations A, A', and A'' (Figure 4.2). Viano et al. [61] found that 30.5% of these severe impacts occurred to areas connecting the facemask to the shell (locations F, B, and UT), and 40.2% occurred to the shell (locations C, D, and R). Most of these impact locations are representative of the struck/injured player.

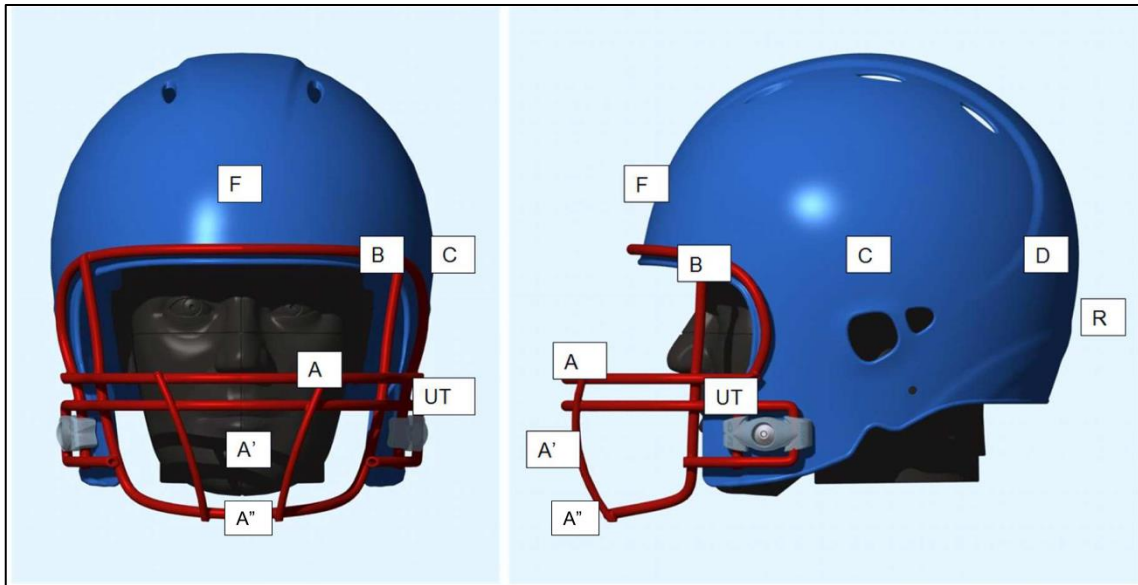


Figure 4.2: Locations for linear impact to shell and facemask

Two independent test series were performed. The first test series was performed at McCarthy Engineering Inc. (McCarthy) (Windsor, Ontario, Canada). This test series was conducted using the same helmet, and the mass of the helmet was varied (1.3 to 2.3 kg) to cover the range of masses found in modern football helmets (Figure 4.1) (1.5 kg to 2.3 kg). The same helmet was used to keep the helmet-to-head boundary conditions constant. The second test series was conducted at Biokinetics (Ottawa, Ontario, Canada). This test series evaluated the performance of seventeen different makes and models of football helmets. The headform response data was presented previously by Viano et al. [17]. Upper neck forces were measured in some of these tests, and the un-helmeted Hybrid III headform was impacted at some of the impact speeds and locations. These results were not previously published.

In the first test series (McCarthy), all tests were conducted using the same Riddell Revolution (size large) helmet with a standard face mask. The helmet, which had been previously used, had no damage other than superficial markings to the shell at the commencement of this test series.

A large-sized helmet was used in accordance with the manufacturer's fitting instructions which indicated that this size is recommended for the circumference of the Hybrid III head and based on the findings of Jadischke et al. [62] which indicated that the large-sized helmet on the 50th percentile Hybrid III head is similar to the average volunteer fit. The bladders in the jaw pads were inflated to just contact the jaw of the headform. It was difficult to install the football helmet on the Hybrid III headform due to the high friction between the padding and the surface of the headform. A nylon stocking was placed over the Hybrid III headform to reduce the friction at this interface and to provide a more realistic response of the helmet on the headform. This is consistent with NFL helmet testing [17, 43].

Four mass conditions were studied: 1) The un-helmeted Hybrid III headform (4.54 kg), 2) The helmet shell and padding with no facemask on the Hybrid III headform (5.80 kg), 3) The helmet shell, padding, and facemask on the Hybrid III headform (6.46 kg), and 4) The helmet shell, padding, facemask, with 350 grams of lead tape added to the inside surface of the shell on the Hybrid III headform (6.81 kg). For the last case, the helmet padding was removed, and 350 g of 1.0 mm thick lead tape was distributed evenly within the gap between the padding and the helmet shell. The lead tape was fixed to the helmet shell and the padding was replaced over top of the lead tape.

The struck Hybrid III headform and Hybrid III neck were mounted to a linear slide table that was free to move upon impact with only bearing-slide friction, similar to that described by Pellman et al. [60]. The mass of the slide table and bearings was 20.5 kg without the Hybrid III head, neck, and instrumentation. The helmet, when used, was fitted onto the Hybrid III headform with the brow pad positioned 2.54 cm (1 inch) above the top of the nose. This location was marked at the beginning of the testing and used as a reference for all tests. The chin strap

was attached so that it fit snugly over the Hybrid III chin. This chin strap tightness was set at the beginning of testing, and the straps were marked. After each test, the chin straps were inspected for any evidence of their becoming unbuckled or loose. The chin strap was subsequently unbuckled and the helmet repositioned in preparation for the next test. There were no provisions for the replacement of the facemask in this testing. In the higher energy facemask impacts (A and B), slight facemask deformation was noted. The helmet itself was inspected after individual tests, and no damage occurred.

These tests were conducted using a pendulum impactor with an arm radius of 1.58 m and ballasted to 31 kg (Figure 4.3). The impactor mass was similar to the pendulum discussed by Pellman et al. [64]. The target impact speeds were 4.1 m/s and 5.2 m/s. These impact speeds result in headform delta-Vs that are representative of typical NFL game impacts [60]. A Hybrid III headform was mounted on the pendulum arm via a rigid neck and fitted with a Riddell VSR-4 helmet (size large) to simulate a helmet-to-helmet impact. Each of the described impact configurations was repeated three times ($n=90$). The test matrix for this test series is illustrated in Table 4.1. The testing was conducted using a blocked approach. At a given helmet condition and impact location, the impacts were first conducted at 4.1 m/s then at 5.2 m/s. The impact location was then changed. After each impact location and speed was tested, the helmet condition was then changed, and this was repeated until the test matrix was complete.

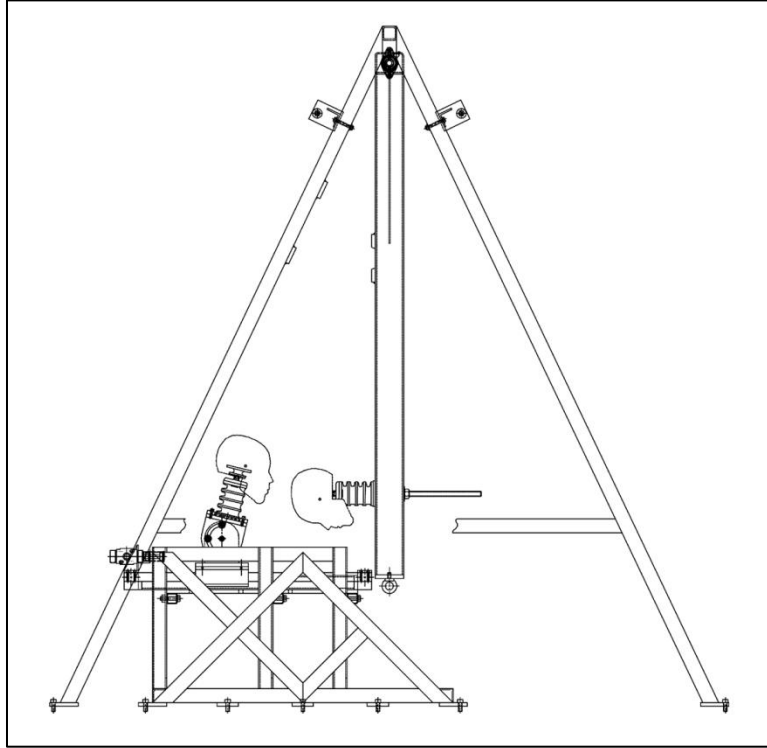


Figure 4.3: Computer model of pendulum test setup

Condition	Un-helmeted		No facemask		Helmet		Helmet + 350 g	
Helmet and Headform mass (kg)	4.54		5.8		6.46		6.81	
Velocity (m/s)	4.1	5.2	4.1	5.2	4.1	5.2	4.1	5.2
A	3	3	-	-	3	3	3	3
B	3	3	3	3	3	3	3	3
C	3	3	3	3	3	3	3	3
D	3	3	3	3	3	3	3	3

Table 4.1: Pendulum Impact Test Matrix

The struck Hybrid III headform was instrumented with a DTS 6DX-PRO 2000-18K system (www.dtsweb.com) mounted to a machined mounting block to measure linear acceleration at the center of gravity of the headform. The system was capable of measuring rotational velocity; however, the data acquisition system inadvertently clipped the rotational velocity data and it could not be used. A six-axis upper neck load cell (www.mg-sensor.de) for a 50th percentile male Hybrid III dummy was also used. The data were acquired at 10 kHz using a National

Instruments cDAQ-9178 data acquisition system and were filtered using an antialiasing hardware filter. Head accelerations were digitally filtered at CFC 180, upper neck forces were filtered at CFC 1000, and upper neck moments were filtered at CFC 600 using the algorithm defined in SAE J211. An optical encoder (Celesco Model CH25-2048) mounted on the pendulum arm was used to trigger the data acquisition system and to calculate the linear impact velocity of the headform. High speed video was recorded at 1000 frames per second for, at minimum, two tests per impact location and condition.

The methods of the second test series are described in detail by Viano et al. [17]. In short, this test series was conducted using the Biokinetics linear impactor impacting a Hybrid III headform and neck that was mounted to a linear slide table. The Hybrid III headform was equipped with nine single axis accelerometers in a 3-2-2-2 configuration and a six-axis upper neck load cell. The data were collected at a 10 kHz sampling rate and filtered with an anti-aliasing hardware filter. The head linear acceleration data were then digitally filtered with CFC 180 filtering and the rotational accelerations and velocities were calculated [65]. The entire test matrix included seventeen football helmet make and models, impacted at eight locations (F, A, A', B, UT, C, D and R) and speeds of 5.5, 7.4, 9.3, and 11.2 m/s. In fourteen of these helmets the upper neck loads were measured. The un-helmeted Hybrid III headform was tested at impacts speeds of 7.4 and 9.3 m/s for impact location C and D. The subset of data, including the fourteen helmets wherein upper neck forces and moments were measured and the un-helmeted Hybrid III headform was tested, is presented in this paper. In this test series, each of the fourteen helmets was impacted two times at impact location D at 7.4 m/s ($n=28$) and 9.3 m/s ($n=28$). At impact location C the helmets were impacted two times at a speed of 5.5 m/s ($n=28$) and 7.4 m/s

($n=28$) and four times at a speed of 9.3 m/s ($n=56$). The un-helmeted headform was impacted two times at each impact location and speed ($n = 10$). A total of 178 tests were conducted.

The average and standard deviation of the peak headform linear acceleration, peak headform delta-V, peak headform rotational velocity (for Biokinetics test series only), and peak upper neck forces and moments, as well as headform linear momentum, were calculated across each impact location, condition, and speed. The mean difference and the 95th percentile confidence intervals of the difference for each of the helmeted conditions when compared to the un-helmeted headform were computed across all impact locations. In the first test series, the differences between the un-helmeted Hybrid III headform and each of the helmeted headform conditions were assessed using a paired sample, two-tailed, student-t test, assuming no variance of the mean values. A $p < 0.05$ was considered significant.

RESULTS

Table 4.2 summarizes the test data from the first test series. Appendix B.1 includes the data from each individual test. Across all impact locations and speeds, the resultant head acceleration for helmets with no facemask, with facemask, and with 350 grams added mass was reduced by an average of 26.2 g (36%), 32.3 g (43%), and 33.0 g (44%), respectively, when compared to the un-helmeted headform ($p < 0.001$). The resultant headform delta-V was reduced by 0.06 m/s ($p = 0.704$), 0.23 m/s ($p = 0.017$), and 0.23 m/s ($p = 0.034$), respectively, which equates to an average reduction of headform delta-V of 1.5%, 4.6%, and 4.5%.

Impact Location	Helmet Condition	Impact Speed (m/s)	Acceleration (g)	Headform		Lin. Momentum			Upper Neck Forces			Upper Neck Moments	
				ΔV (m/s)	ΔV (m/s)	(kgm/s)	(kgm/s)	(kgm/s)	Fx (N)	Fy (N)	Fz (N)	Resultant (N)	Resultant (Nm)
Location A	Un-helmeted	4.1	61.4	4.43	623	20.10	375	339	719	41.0			
		5.2	99.9	6.30	882	28.62	460	670	975	59.2			
	No facemask	4.1	-	-	-	-	-	-	-	-			
		5.2	-	-	-	-	-	-	-	-			
	Helmet	4.1	36.0	4.33	783	27.95	461	625	1023	59.5			
5.2		53.6	6.01	987	38.82	632	1194	1569	77.7				
Helmet + 350 g	4.1	35.3	4.46	741	30.34	504	649	1050	62.1				
	5.2	56.5	5.99	908	40.82	761	1294	1637	77.6				
Location B	Un-helmeted	4.1	59.4	4.42	370	20.07	652	468	751	42.9			
		5.2	82.5	5.96	472	27.07	853	895	1065	56.5			
	No facemask	4.1	32.2	4.55	438	26.39	766	641	991	56.8			
		5.2	62.8	6.29	459	36.49	898	1122	1407	79.4			
	Helmet	4.1	31.9	4.31	354	27.86	959	664	1088	75.8			
5.2		40.6	5.57	404	36.01	1118	1200	1491	88.6				
Helmet + 350 g	4.1	29.4	4.29	342	29.19	1021	595	1127	84.0				
	5.2	44.5	6.00	464	40.86	1331	1119	1598	109.8				
Location C	Un-helmeted	4.1	65.7	4.35	91	19.75	543	538	673	34.7			
		5.2	87.8	5.84	186	26.51	739	948	1083	44.5			
	No facemask	4.1	39.5	4.35	99	25.21	583	733	912	35.5			
		5.2	55.9	5.83	169	33.80	791	1257	1416	51.0			
	Helmet	4.1	37.5	4.35	177	28.09	608	809	1012	24.7			
5.2		53.4	5.77	304	37.29	809	1420	1601	47.4				
Helmet + 350 g	4.1	39.1	4.33	133	29.48	676	801	1019	33.7				
	5.2	51.8	5.65	286	38.45	844	1518	1709	47.9				
Location D	Un-helmeted	4.1	61.7	4.49	690	20.40	396	501	880	55.8			
		5.2	84.7	6.03	1000	27.38	497	936	1413	75.4			
	No facemask	4.1	41.8	4.14	696	24.04	435	733	1085	52.4			
		5.2	52.2	5.58	924	32.37	526	1079	1507	72.0			
	Helmet	4.1	38.2	4.09	633	26.44	457	828	1129	46.1			
5.2		53.4	5.53	941	35.72	566	1364	1737	70.1				
Helmet + 350 g	4.1	35.5	4.01	758	27.33	478	915	1263	50.9				
	5.2	47.2	5.25	1055	35.77	539	1408	1832	74.5				
Comparison to Un-helmeted	No facemask	Mean Difference	-26.2	-0.06	-4	6.19	53	213	242	6.2			
		95% Upper CI	-23.2	0.28	21	9.35	73	243	286	11.0			
	95% Lower CI	-29.2	-0.40	-29	3.02	34	184	198	1.4				
	p	<0.0001	0.704	0.763	<0.0001	0.354	<0.0001	<0.0001	<0.0001	0.017			
	Helmet	Mean Difference	-32.3	-0.23	58	8.54	120	351	386	10.0			
95% Upper CI		-28.8	-0.09	119	9.59	157	399	436	17.1				
95% Lower CI	-35.8	-0.37	-3	7.49	83	304	337	2.9					
p	<0.0001	0.017	0.068	<0.0001	<0.0001	<0.0001	<0.0001	<0.0001	0.009				
Helmet + 350 g	Mean Difference	-33.0	-0.23	47	10.29	205	375	460	16.3				
	95% Upper CI	-30.2	-0.05	69	11.66	268	448	514	24.8				
95% Lower CI	-35.8	-0.41	25	8.93	142	303	405	7.8					
p	<0.0001	0.034	<0.0001	<0.0001	<0.0001	<0.0001	<0.0001	<0.0001	0.001				

Table 4.2: Results from Test Series One - Pendulum Impact Testing

Conversely, the helmeted headform conditions sustained higher resultant upper neck forces and moments in all impact conditions. Across all impact locations and speeds, the addition of the helmet resulted in an increase of resultant upper neck forces of 26%, 41%, and 49%, respectively ($p < 0.001$). Neck tension (F_z) increased significantly ($p < 0.001$) as mass was added to the headform. The resultant upper neck moment also increased with helmet mass by 12%, 20% and 32%, respectively ($p < 0.02$). The difference in shear neck loading (F_x and F_y) in the un-helmeted headform compared to the helmeted conditions was not as great; however, it was significant in most conditions.

Table 4.3 summarizes the results from the second test series and illustrates the averaged results across all impact speeds. Appendix B.2 is a supplementary file for the individual impact speeds. The fourteen helmets tested resulted in differences for the un-helmeted condition when compared to the various helmet makes and models. These helmets followed the same trend as seen in the first test series. The mass of the helmets resulted in an average increase in head mass of 42% (± 4 %). The head acceleration was reduced by 30.5 g (± 14.6 g) which equates to a reduction of 23% (± 6 %). Delta-V was reduced by 0.9 m/s (± 0.6 m/s) and rotational velocity was reduced by 3.8 rad/s (± 3.8 rad/s). This equates to a 13% (± 6 %) and 7% (± 7 %) reduction in delta-V and rotational velocity, respectively. This resulted in an increase of linear momentum of the headform of 24% (± 8 %) and increases in the resultant upper neck forces (32% (± 13 %)), upper neck tension (44% (± 20 %)), and resultant upper neck moment (29% (± 18 %)).

Impact Location	Helmet	Helmet Mass (kg)	Total Mass (kg)	Acceleration (g)	ΔV (m/s)	Rotational Velocity (rad/s)	Linear Momentum (kgm/s)	Resultant Neck Force (N)	Neck Tension (Fz) (N)	Resultant Neck Moment (Nm)
Location C	Hybrid III - Head	0.00	4.54	124.5	7.14	50.4	32.4	1759	1398	49.6
	Helmet A	1.50	6.04	109.9	6.79	47.1	41.0	2937	2747	70.3
	Helmet B	1.59	6.13	98.6	6.94	48.8	42.5	2971	2761	72.2
	Helmet C	1.84	6.38	93.5	6.68	49.1	42.6	2277	2050	72.7
	Helmet D	1.84	6.38	101.4	6.78	49.7	43.3	2340	2076	68.1
	Helmet E	1.85	6.39	101.2	6.55	44.5	41.8	2382	2225	74.6
	Helmet F	1.85	6.39	106.1	6.74	47.6	43.1	2273	2207	69.3
	Helmet G	1.91	6.45	102.4	6.50	43.8	41.9	2357	2232	70.7
	Helmet H	1.93	6.47	86.4	6.40	42.3	41.4	2397	1988	69.1
	Helmet I	1.98	6.52	100.0	6.87	45.8	44.8	2739	2206	77.4
	Helmet J	1.99	6.53	85.8	6.25	39.6	40.8	2361	1881	68.9
	Helmet K	2.00	6.54	89.0	6.34	41.1	41.5	2382	1754	70.6
	Helmet L	2.06	6.60	86.5	6.55	47.0	43.2	2123	2176	73.1
	Helmet M	2.08	6.62	87.3	6.57	49.2	43.5	2184	2559	83.9
	Helmet N	2.19	6.73	87.8	6.35	45.0	42.7	2030	1696	66.3
	Location D	Hybrid III - Head	0.00	4.54	138.2	8.56	56.9	38.9	2251	1820
Helmet A		1.50	6.04	112.4	7.37	60.8	44.5	2812	2305	97.4
Helmet B		1.59	6.13	119.0	7.33	55.4	44.9	2925	2358	101.6
Helmet C		1.84	6.38	105.8	7.13	58.1	45.5	2882	2419	97.2
Helmet D		1.84	6.38	121.0	6.99	57.8	44.6	2813	2389	91.0
Helmet E		1.85	6.39	107.4	7.33	53.0	46.8	2978	2363	111.6
Helmet F		1.85	6.39	117.3	7.10	58.9	45.3	2836	2603	95.4
Helmet G		1.91	6.45	122.8	7.09	51.7	45.8	2738	2504	102.1
Helmet H		1.93	6.47	96.7	6.71	49.1	43.4	2899	2442	97.8
Helmet I		1.98	6.52	109.4	6.74	52.9	43.9	2833	2479	106.0
Helmet J		1.99	6.53	106.6	6.46	52.0	42.2	3003	2448	91.5
Helmet K		2.00	6.54	92.2	6.54	51.5	42.8	2795	2397	97.9
Helmet L		2.06	6.60	107.5	7.40	53.9	48.8	3028	2393	104.8
Helmet M		2.08	6.62	107.9	7.33	59.8	48.5	2999	2510	102.5
Helmet N		2.19	6.73	101.7	6.74	50.7	45.3	2344	2053	78.2
Comparison to Unhelmeted		Mean Difference			-30.5	-0.90	-3.84	8.7	641	742
	95% Upper CI			-25.9	-0.72	-2.65	9.6	733	842	22.3
	95% Lower CI			-35.0	-1.08	-5.03	7.8	548	641	16.9
	p			<0.0001	<0.0001	<0.0001	<0.0001	<0.0001	<0.0001	<0.0001

Table 4.3: Results from Test Series Two - Linear Impactor Testing

DISCUSSION

Figure 4.4 illustrates an example un-helmeted and helmeted impact for location C. During an impact to the un-helmeted headform, the peak resultant accelerations occur in the initial 10 milliseconds of the collision. In the example case shown, these accelerations are primarily acting laterally (y-axis) on the headform. The bimodal lateral acceleration is due to the striking helmet padding compression and the helmet moving on the headform. The accelerations result in the un-helmeted headform reaching a peak ΔV , in this case, approximately 12 to 13 milliseconds after the impact occurred. As the headform begins to rotate, the resultant acceleration reduces and the upward (z-axis) acceleration of the headform dominates the acceleration pulse during the time 10 to 20 milliseconds after impact, with its peak occurring at 13 milliseconds. The upward acceleration of the headform, relative to the neck, and its subsequent motion results in the upper neck forces increasing and the headform pulling the neck and sled (or torso in the case of a player) along with it. Due to the rotation of the headform, the peak neck forces are primarily due to neck tension and occur at approximately 13 milliseconds.

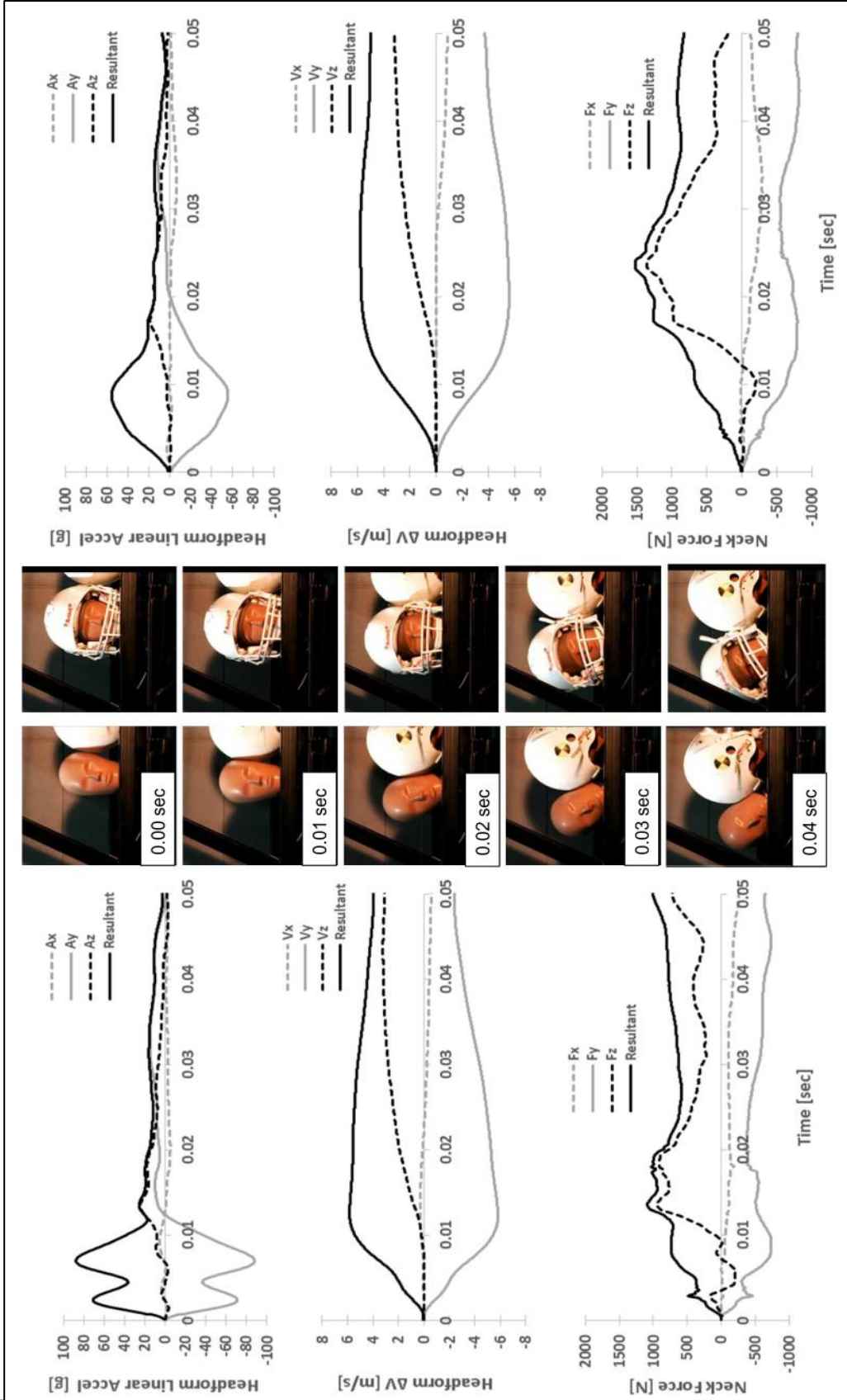


Figure 4.4: Sample impact from impact location C comparing un-helmeted and helmeted responses

The helmeted impact results in lower resultant head accelerations, with the resultant un-helmeted head accelerations in this case being 88 g versus the helmeted impact reaching a peak of 56 g. This occurs due to compression of the helmet padding and the headform accelerations occurring over a longer period of time. The longer acceleration pulse results in the peak upward accelerations of the head occurring later (17 milliseconds versus 13 milliseconds) and the peak headform delta-V also occurring later (28 milliseconds versus 13 milliseconds). The peak headform delta-V was only reduced by 0.07 m/s (5.85 m/s, un-helmeted versus 5.78 m/s, helmeted). In the helmeted case, the neck forces increased when compared to the un-helmeted case and occurred at approximately 24 milliseconds.

The three helmet conditions resulted in an increase of head mass of 28% (5.80 kg), 42% (6.46 kg), and 50% (6.81 kg) when compared to the un-helmeted headform (4.54 kg). The headform delta-V was only reduced by 1.5%, 4.6%, and 4.5% across all impact locations and speeds. This resulted in an increase in the headform momentum. The increased headform momentum caused higher resultant upper neck forces, which increased by 26%, 41%, and 49% across all impact locations and speeds. The increase in upper neck forces corresponded to the increase in mass of the headform due to the helmet (Figure 4.5) and was primarily the result of an increase in neck tension.

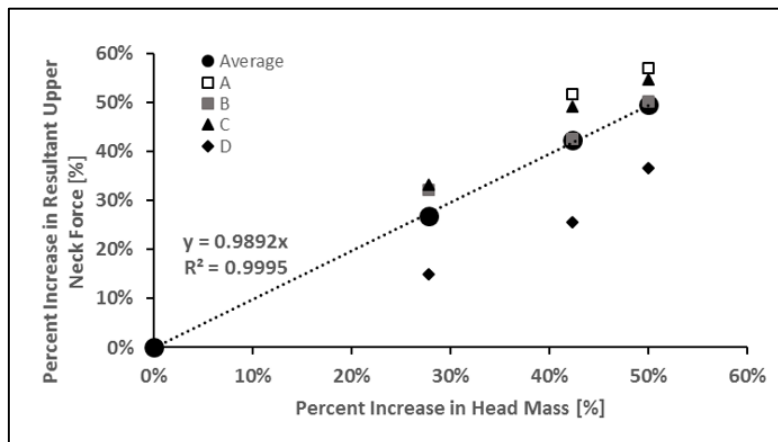


Figure 4.5: The percent increase in upper neck force versus the percent increase in head mass in all impact locations. The un-helmeted head mass = 4.54 kg.

In location D, an impact to the rear of the helmet, the resultant upper neck forces did not increase as substantially as at other locations. In this location, helmet rotation relative to the headform was noted, and since the chin strap is located on the front of the helmet, it would experience a reduction in loading relative to side and oblique impacts. Since the helmet becomes decoupled from the head to a greater degree in this impact orientation, this results in a lower delta-V and momentum of the headform and a smaller increase in upper neck forces. Locations A, B, and C result not only in the helmet remaining more tightly coupled to the headform but also in higher delta-Vs than at impact location D.

Figure 4.6 illustrates the acceleration and delta-V from the un-helmeted headform compared to the helmet and facemask condition in the 5.2 m/s impacts. These data illustrate that the helmeted conditions reduce peak head accelerations by increasing the duration of the acceleration pulse. Due to the increase in duration of the acceleration pulse, a corresponding increase in time occurred until the maximum delta-V was achieved in all impact conditions.

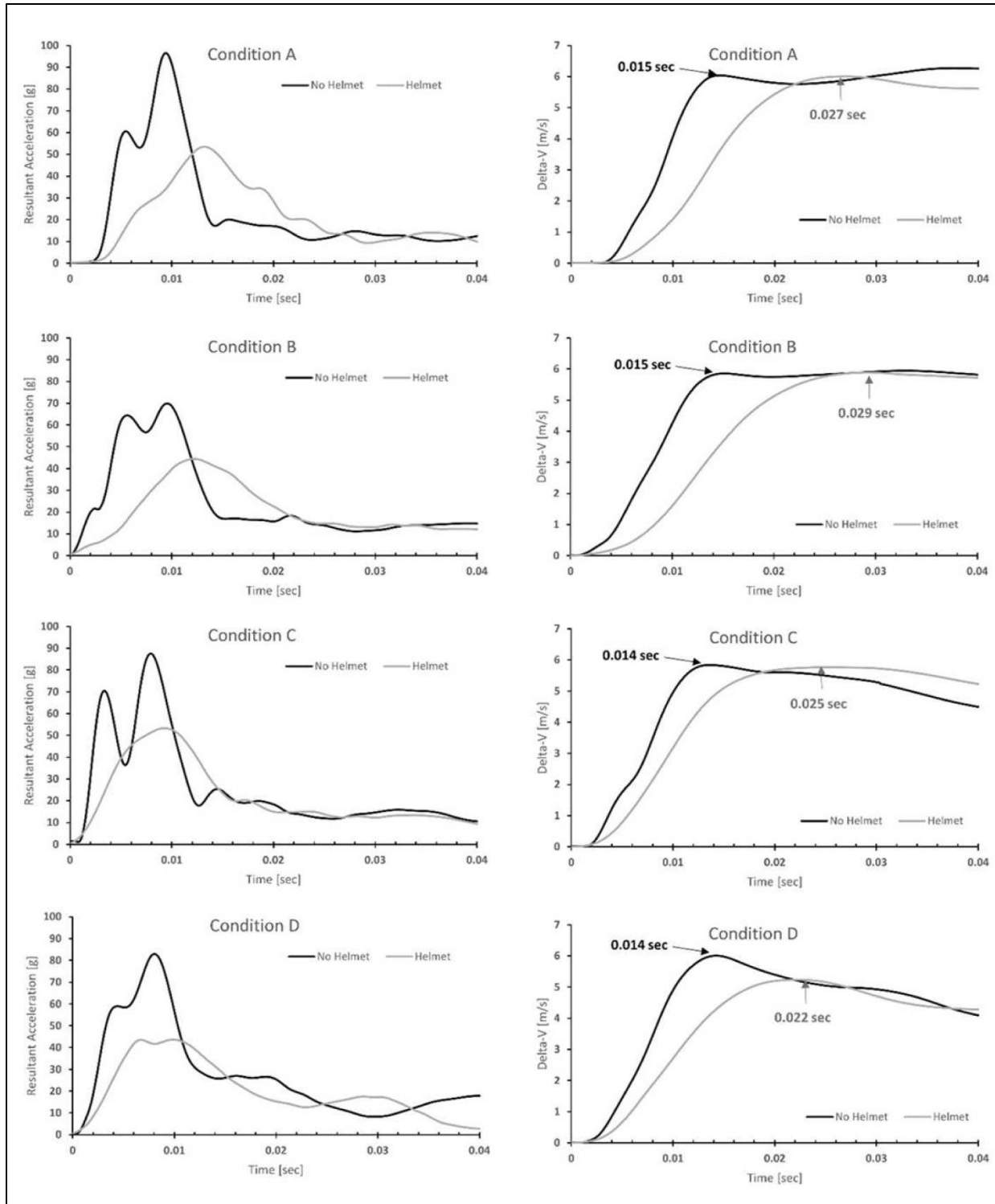


Figure 4.6: Headform resultant acceleration and headform delta-V in the un-helmeted and helmeted impacts

An increase in the upper neck forces and moments occurred with the addition of the helmet onto the headform. The increase in mass of the headform exceeded the reduction in delta-V of the headform. This resulted in an overall increase in the momentum of the headform. As the momentum of the headform increased, the upper neck forces also increased to restrain the head and helmet onto the neck. The maximum upper neck forces occurred after the peak acceleration of the headform and corresponded more closely to the time at which delta-V and headform momentum reached their maximum (Figure 4.7).

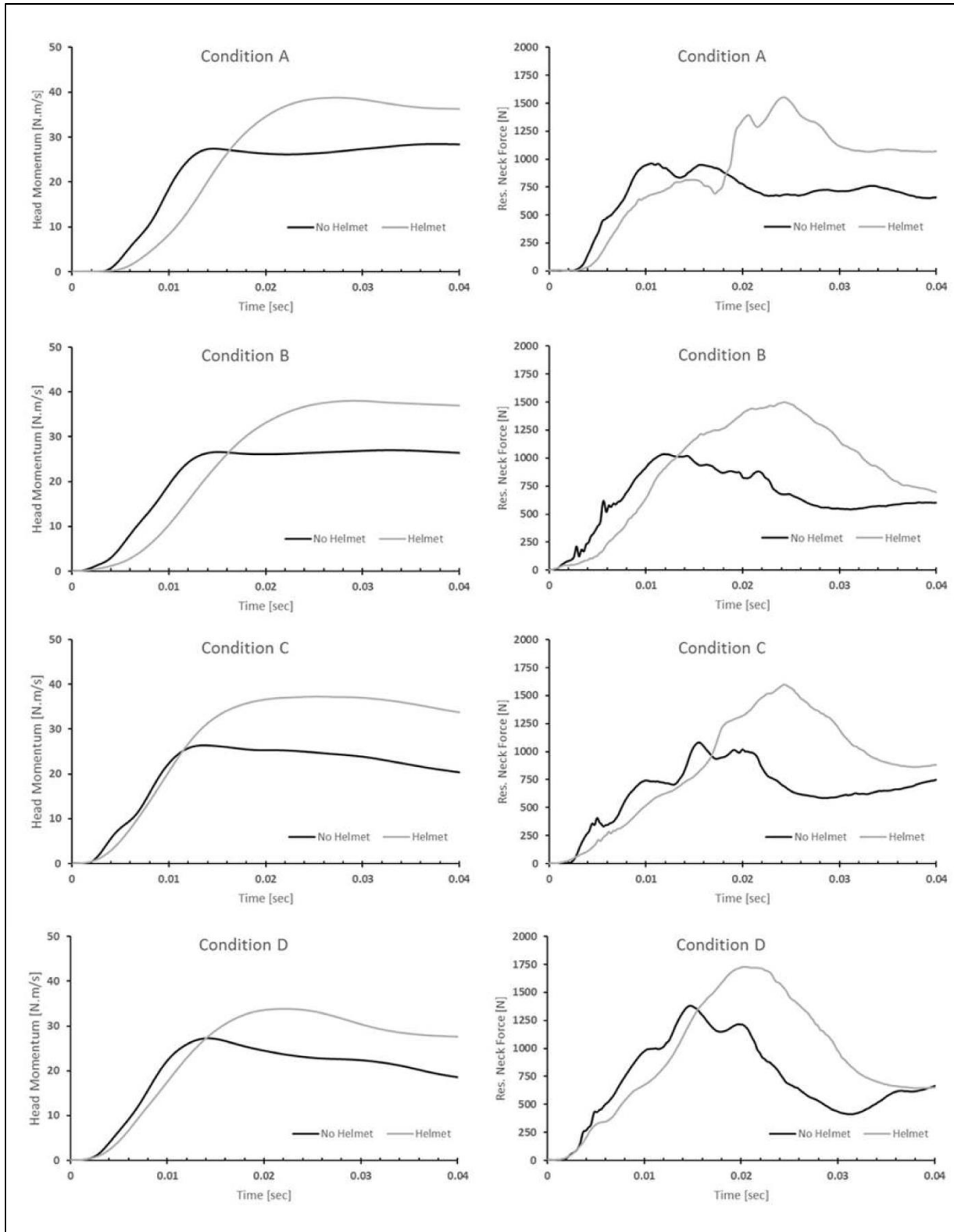


Figure 4.7: Headform linear momentum and resultant upper neck forces in the un-helmeted and helmeted impacts

For test series two, the data for the fourteen helmets in which upper neck loads were measured indicates the helmet increased the overall head mass by 42% ($\pm 4\%$) (Figure 4.8). In impact location C, this resulted in an average reduction in head linear acceleration of 23% ($\pm 6\%$) and an average increase in resultant upper neck force of 37% ($\pm 15\%$). The greatest increase in neck forces was observed in neck tension (Fz) which resulted in an average increase of 56% ($\pm 23\%$). The lower speed impact (5.5 m/s) increased the upper neck tension by a greater magnitude ($198\% \pm 68\%$) than the higher speed impacts (9.3 m/s) which resulted in an increase of neck tension of $30\% \pm 12\%$. This suggests the increase may be due to the helmet remaining more tightly coupled to the head in the lower speed impacts; however, this effect was not fully investigated in this study. Since the higher impact speeds are representative of professional football impacts resulting in concussion in open field helmet-to-helmet collisions, this indicates that during more frequent, sub-concussive impacts in professional football, the percentage increase in tensile neck loads is substantial.

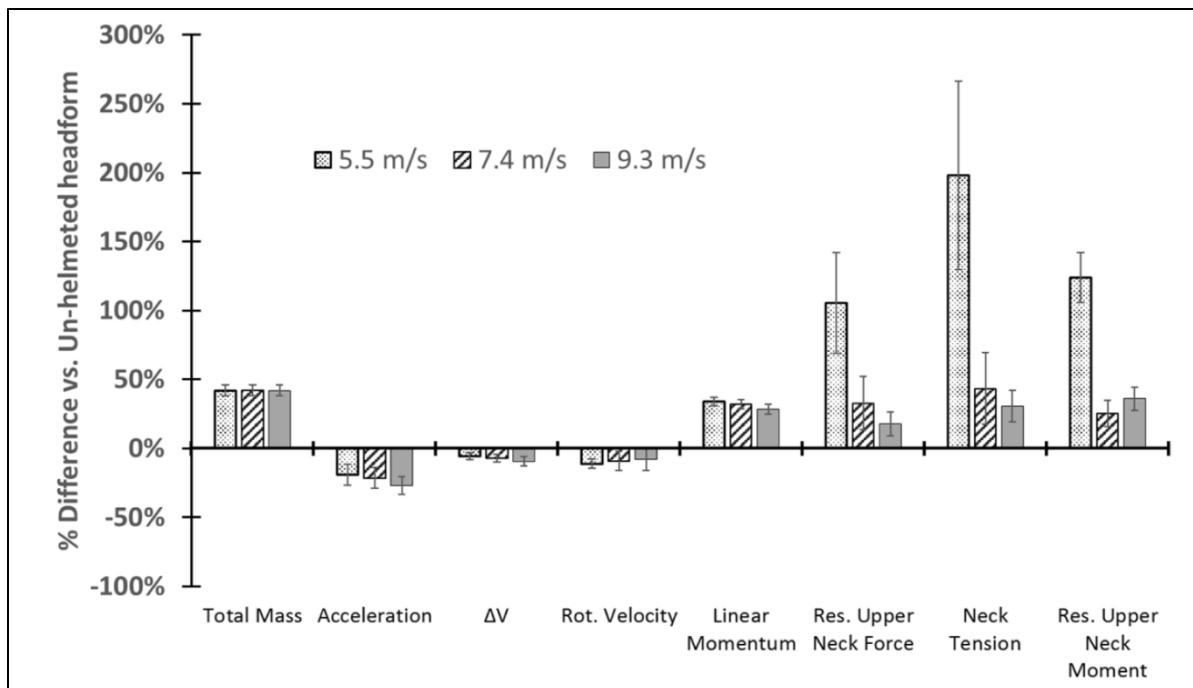


Figure 4.8: Summary of increase in headform effective mass and percentage change in headform acceleration, delta-V, momentum, resultant upper neck forces, and neck tension for the fourteen helmets (average \pm std dev) at impact speeds of 5.5 m/s, 7.4 m/s, and 9.3 m/s. The data is summarized from Viano [2, 3] for impact location C.

High school and youth football helmets also have a similar mass to the helmets presented herein. However, in comparison to collegiate or professional football players, youth-aged players have, on average, less head mass and weaker necks, based on anthropometric and tolerance data [66]. Collins et al. [45] found that neck strength was a significant predictor of concussion in high school athletes. The findings of the current study suggest that, for a given impact speed, if upper neck loading contributes to concussion, youth football players, who are less conditioned than professionals, would have a higher potential for concussion while wearing professional level helmets due to their reduced neck strength. The weaker neck strength of younger athletes would provide less restraint of the head on the neck. As a result, for a given upper neck force an athlete with a weaker neck would have greater movement of the head relative to the body. As Breig [28] has indicated, this has the potential of generating tension in the brain stem, cerebellum, and cranial nerves. Cranial nerve symptoms are some of the most common symptoms in concussion as reported in NFL studies [3]. Therefore, this could increase the potential for concussion symptoms in young athletes.

The improvements to helmets to reduce head accelerations have resulted in increases in helmet mass, size, and, therefore, inertia from the 1970s to the present. These helmets would be expected to increase the loading on the upper neck, as was observed in this study. Hardy et al. [67, 68] reported that a Riddell VSR4 helmet on a cadaver reduced head accelerations, did not affect head angular speed but increased brain strain in the cerebrum. The present study has confirmed that using a helmet reduces head accelerations and the second test series illustrated there is only a small reduction in rotational velocity ($7\% \pm 7\%$); however, adding the mass of the helmet to the head results in an increase in resultant upper neck forces and, specifically, neck tension. Increases in neck tension could result in an increase in brain strain by exerting forces on

the brain stem. Hodgson et al. [21] also deduced that shear strain in the brain stem was due to stretching of the spinal cord. Various other studies have reported strain in the brain stem [24, 25, 26] as well as downward movement of the brain stem through the foramen magnum [21, 27]. It has also been shown that neck tensile forces result in the highest spinal cord strains in the upper cervical spinal cord [41] that is continuous with the brain stem. Therefore, it is expected that, as upper neck forces (and cervical spinal cord strains) increase, a corresponding increase in brain stem strain would also occur [28].

Since improvements in helmet design to reduce head acceleration have not resulted in a corresponding decrease in the reported incidence of concussion, a possible explanation is that the incidence of concussion may not entirely relate to the magnitude of head acceleration. Forces in the upper neck may be a factor. There may be other factors related to concussion, such as angular velocity of the head [67]; however, angular velocity of the head can also result in forces and moments in the upper neck. This study postulated that upper neck forces may be related to concussion. If that proves to be true through further research, then upper neck loads should be considered in the evaluation of concussion risks and in the development of protective equipment.

The limitations of this study must be recognized. This study was performed using the Hybrid III headform and Hybrid III neck. The Hybrid III headform provides a biofidelic response; however, it is not human so, tissue level strains cannot be assessed. Additionally, the Hybrid III has a neck simulating some muscle tensing but there is no active musculature in any of the current test dummies. The effects of active and passive neck musculature were not investigated in this study since this would require a comprehensive and biofidelic finite element model of the human, which was beyond the scope of this parametric study. As such, this study was conducted

to alert the biomechanics community of the potential relationship of helmet and head mass and concussion, and it is not meant to imply that helmet and head mass is responsible for concussion.

The Hybrid III dummy was designed for frontal impact testing; however, the Hybrid III head and neck are regulated for frontal (FMVSS 208) and rear (FMVSS 202) impact testing where head and neck criteria are specified for comparison to tolerance levels. In addition, the Hybrid III head and neck are used on various dummies for side impact testing; and, Piziali et al. [69] found the head and neck were reasonable for rollover testing where a range of oblique head impacts and neck responses can occur. NOCSAE helmet certification standards do not currently specify a neck to be used. For research purposes, the current standard for head impact testing related to helmet performance appears to be the Hybrid III head and neck and it has been used extensively in impact testing related to helmet performance and boxing punches [16, 17, 61, 62, 70, 71, and others]. The Hybrid III head and neck is a reasonable tool for the type of parametric testing done in this study.

For the first test series, we chose a single helmet with added mass to limit the amount of variables, such as helmet inertia, fit, chin strap design, and padding style. In test series two, an increase in forces at the upper neck was also found across the fourteen different makes and models of helmets when compared to the un-helmeted headform. The effects of other helmet boundary conditions, such as, padding to headform friction, helmet fit, and chin strap effects, were not investigated in this study; however, the test data from the fourteen different makes and models of helmets suggests these may play a role. In addition, the base of the neck was fixed to the linear slide; in a human, the torso is free to rotate. The effects of this boundary condition were not investigated in this study.

A motivation for this study was to understand whether the forces and moments at the atlanto-occipital joint could be contributing to concussion in football since a reduction in concussions in the NFL has not been observed from 1996 until the present. The definition of a concussion is evolving, as are the means to diagnose the various signs and symptoms. There is also an increased emphasis on concussion education and awareness leading to increased identification and reporting. In addition, players may be getting bigger and faster at a pace that is masking the benefits of improved helmets. At the same time, rule changes and the reduction of direct hits to the head may be responsible for a reduced number of injuries. All of these factors, and others, confound the trends in concussion rates in professional, collegiate, and high school data.

CHAPTER 5 – A NEW LABORATORY METHOD TO SIMULATE PLAYER-TO-PLAYER COLLISIONS IN CONTACT SPORTS

INTRODUCTION

In the laboratory reconstruction of concussive impacts in the NFL [43, 44, 72], the *struck* player (in the actual game) was dropped from a height to achieve the proper closing speed at impact. The struck player was represented by a helmeted 50th percentile male Hybrid III ATD headform and neck, with the base of the neck attached to a 7.1 kg carriage system [44]. The carriage was equipped with rollers that allowed for primarily vertical motion on its track (Figure 5.1). The *striking* player was represented by a stationary, helmeted Hybrid III head, neck, and upper and lower torso that was supported by cables.

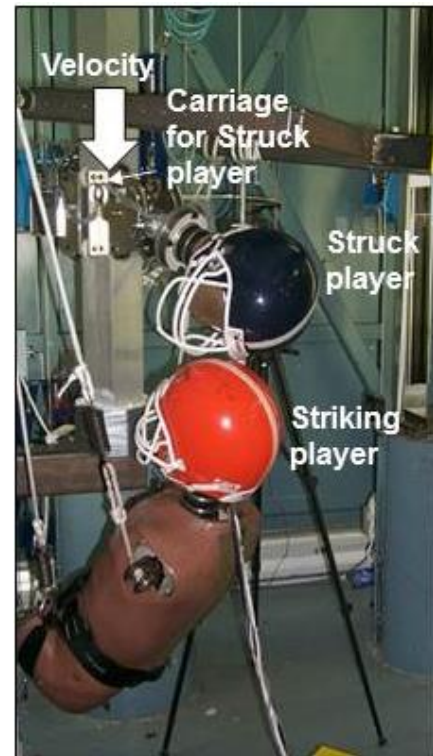


Figure 5.1: Sample reconstruction setup used by Pellman et al. [3]

There were some limitations to the drop tower method used by Pellman et al. [43, 64]. The drop tower could achieve a similar closing speed at impact; however, there was only one headform and neck moving on a carriage rather than two bodies at higher masses moving at each other. Additionally, the effect of the carriage restraint on head kinematics and neck kinetics is also unknown. Lastly, the NFL videos were taken from network video and were post-processed to extract the video at sixty frames per second. In one to two frames (0.033 seconds) much of the impact is already over. The stop at the end of the carriage limits the duration of data that can be used.

Pellman et al. [64] reported on the development of a helmet test method involving a 14.2 kg pneumatically driven impactor striking a stationary Hybrid III 50th percentile male anthropomorphic test device (ATD) head and neck that is attached to a base, constrained to motion along linear rails. The linear impactor tests correlated to the data based upon reconstruction of game impacts [64] that were conducted with the injured player being represented by the Hybrid III 50th head and neck in a drop tower-style impact [44]. The pneumatic linear impactor method is currently in use by some laboratories to assess helmet performance, providing a method to assess helmet performance in hits producing both linear and angular headform response. This test method is proposed for helmet testing but has not been accepted by the National Operating Committee on Standards for Athletic Equipment (NOCSAE).

The NOCSAE football and ice hockey helmet standards for newly-manufactured helmets require the NOCSAE headform to experience a Gadd Severity Index (GSI) of less than 1200 in drop tests to various locations on the helmet [59, 73]. These drop velocities range from 3.46 to 5.46 m/s. This test only assesses the performance of helmets to attenuate impacts by reducing linear acceleration.

The aims of this study were to (1) develop a new laboratory impactor to simulate player-to-player collisions in high speed contact sports, (2) develop an alternative helmet test method to the pneumatic linear impactor, and (3) assess the repeatability of the system.

MATERIALS AND METHODS

Test Apparatus

The NFL combine data [74] was analyzed to assess the speeds and masses of NFL prospects. The fastest players in these tests were defensive backs (DB) and wide receivers (WR) at speeds of 8.09 ± 0.11 m/s and 8.07 ± 0.16 m/s, respectively. These players also had the lowest average

weights at 86.6 ± 3.8 kg and 91.7 ± 7.1 kg. The slowest players were the offensive linemen (OL) at a speed of 6.89 ± 0.20 m/s and weighing 141.9 ± 6.7 kg. The average height of these players was $1.87 \text{ m} \pm 0.07 \text{ m}$ with tight ends (TE) being the tallest ($1.94 \pm 0.03 \text{ m}$) and running backs (RB) being the shortest ($1.80 \pm 0.06 \text{ m}$). The speed and mass data indicate, with exception of quarterbacks (QB), as the mass of a player increases his speed decreases.

Mertz et al. [75, 76] have summarized the size and weight of the Hybrid III ATDs. The average player in the NFL combine data is similar to the Hybrid III 95th percentile adult male ATD and the lightest player was the Hybrid III 50th percentile adult male. In designing a new method to simulate player-to-player collisions, it was thought that, at minimum it should be capable of accelerating a mass equivalent to the upper body of NFL players. The Hybrid III ATD data was used to scale the player masses. This data indicate that the upper body (head, neck, arms, upper and lower torso) is approximately 70% of the total ATD mass [75, 76, 77]. The NFL combine data, scaled to account for upper body mass only, indicate that the system should be capable of propelling a mass of approximately 75 kg to a speed of 7.7 m/s, resulting in a total momentum of 572 ± 67 kgm/s and/or kinetic energy of 2185 ± 161 J (Table 5.1). The impactor developed for these player-to-player impacts has the capacity to accelerate a mass of 100 kg to a speed of 9 m/s. This mass is inclusive of hardware not associated with the ATD.

Position	Speed [m/s]	Mass [kg]	Upper body mass [kg]	KE [J]	Momentum [kgm/s]
DB	8.09	86.6	60.6	1982	490
WR	8.07	91.7	64.2	2091	518
S	7.97	92.7	64.9	2061	517
RB	7.93	99.0	69.3	2177	549
LB	7.72	108.6	76.0	2262	586
TE	7.63	114.5	80.2	2336	612
QB	7.54	98.6	69.0	1964	521
DL	7.21	133.6	93.5	2431	674
OL	6.89	141.9	99.3	2357	684
Average	7.67	107.5	75.2	2185	572
Stdev	0.38	18	13	161	67
Impactor Capability	9	100		4050	900

Table 5.1: Summary of player masses and speeds and impactor capability

Figure 5.2 illustrates the impactor test system. The test system was designed to be used to carry and propel the upper body of a Hybrid III 50th percentile male ATD to simulate on field collisions but could also be used as an impactor ram for helmet and/or other biomechanical impact testing. The impactor system could be duplicated and the two impactors could be synchronized to simulate on-field collisions in contact sports to achieve closing velocities up to 18 m/s with a total pre-impact momentum and energy exceeding 1800 kgm/s and 8100 J, respectively. In this configuration, the ATDs could collide while in free flight with no other constraints acting on the ATDs. The system was designed to be portable so that it could be moved to different testing locations and also so that the individual player heading angles could be varied. If the system is used as an impactor ram, higher impactor speeds could be achieved when accelerating a mass lower than 100 kg.

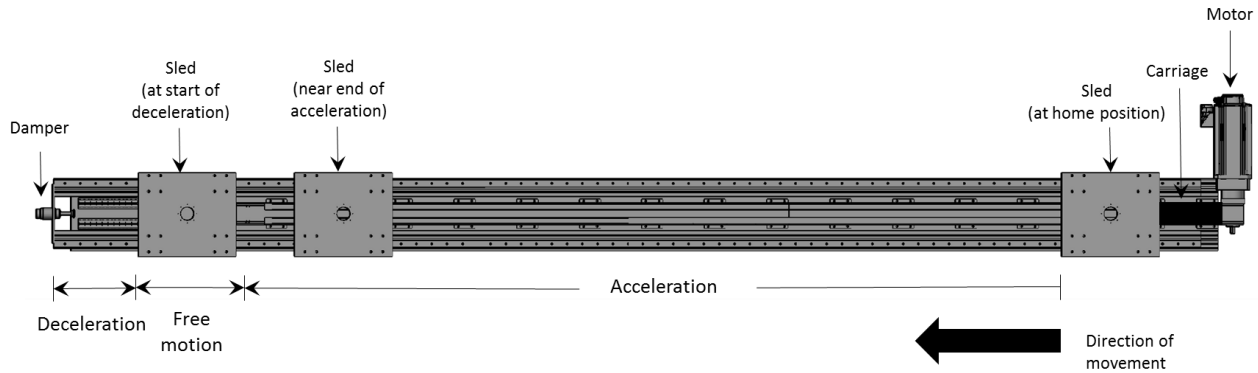


Figure 5.2: Schematic of the impactor layout

The test system used a servo motor which powered a linear drive module with a carriage mounted to it. The motor drives the carriage, accelerating a sled which was mounted on high speed bearings along a set of parallel linear rails. At a prescribed location the carriage decoupled from the sled allowing it to move freely for a short distance just prior to impact. The sled was then decelerated using a passive braking system. A shock absorber was located at the end to provide a positive stop for the sled in the event it travels through the braking section. The braking phase also acts to decouple the ATD from its mount allowing it to move forward relative to the sled and become air borne.

Impactor Repeatability Study

Test Series 1 – Impactor Repeatability

A series of tests was conducted to assess the system repeatability. These tests were designed not only to assess the repeatability of the speed of the individual impactors, but also to assess the synchronization between the motion profiles of the two impactors. Each impactor was accelerated to a speed of 2 m/s to 8 m/s in 1 m/s increments and each test was repeated five times for a total of 35 tests per impactor. The carriage propelled a sled weighing 14 kg. An ATD was not used in this series of tests. The speed and position of the carriage on each impactor and the

synchronization of the carriages between impactors was monitored using a rotary encoder mounted on the linear drive module. The synchronization was calculated by calculating the absolute difference between the time of impactor 1 and impactor 2 when the carriage started to decelerate. The impactor position and speed data were acquired through the impactor control panel at 1000 Hz. One of the impactors had a triaxial accelerometer (+/- 100g) (www.dtsweb.com) mounted to the sled. The sled acceleration was acquired using a Diversified Technical Systems (DTS) slice micro (www.dtsweb.com) at 1000 Hz and filtered using a CFC60 filter [82].

A coefficient of variation (CV) and root mean square error (RMSE) were calculated to assess the repeatability of the impactors' speed relative to its target speed and the synchronization between the two impactors. A correlation analysis was conducted on the sled acceleration profile by comparing each individual test acceleration curve to the average curve for a given impact speed. CV was calculated for the peak deceleration of the sled.

Test Series 2 – Repeatability of ATD kinematic response

A second series of tests was conducted to assess the repeatability of the ATD measurements. These tests do not necessarily reflect the repeatability of the impactor itself but are a measure of the repeatability of the initial positioning of the ATD and the repeatability of the ATD instrumentation. There were four different configurations tested; (**Configuration A**) An impactor ram with a 38 mm thick vinyl nitrile endcap covered by a hard plastic impactor striking a stationary un-helmeted ATD (Figure 5.3), (**Configuration B**) An impactor ram with endcap striking a stationary helmeted ATD, (**Configuration C**) The impactor carrying the helmeted head, neck, upper torso, lower torso and arms of the Hybrid III ATD and propelling it to strike a stationary, helmeted head, neck, upper torso and lower torso Hybrid III ATD and

(**Configuration D**) two moving ATDs striking one another in a helmet-to-helmet impact at a 90 degree impact orientation.



Figure 5.3 – Sample test setup to assess the repeatability of the impactor system when used in a ram configuration striking a stationary helmeted ATD.

The tests involving a single, stationary ATD (**A and B**) were all conducted with an impactor ram speed of 5 m/s and the total mass of the sled and ram was 45 kg. In these tests the impactor was used as a ram and the ATD was positioned independent of the impactor on a height adjustable table. In the case of one moving ATD striking a stationary ATD (**C**), the stationary ATD was positioned on a height adjustable table and the moving ATD was initially positioned on the impactor sled. The sled was accelerated to speed and decelerated which resulted in the ATD becoming decoupled from the sled and the collision occurred with the moving ATD in flight. In the case of two moving players (**D**) at a 90 degree impact orientation, the ATDs were each traveling at a target speed of 6 m/s resulting in a closing velocity of 8.48 m/s. The impactors were arranged in a 90 degree impact orientation to provide a worst case scenario and

to maximize the potential variability in the test data. The ATD on impactor 1 was aligned such that the crown of the helmet was to strike the left side of the ATD's helmet on impactor 2. The ATDs were angled such that the pelvis angle on the ATD on impactor 1 was 30 degrees above horizontal and the pelvis angle on impactor 2 was 60 degrees above horizontal. This angle was measured on the pelvis insert. Lasers were utilized to document the position of each ATD at the start of each test and these lasers remained in the same position for each set of tests to confirm that the ATDs were setup consistently. This was necessary due to the compliance in the lumbar spine and neck of the ATDs. The ATDs were simultaneously accelerated up to speed and subsequently decelerated. The impact occurred with both ATDs in free flight and they were free to move post-impact with no boundary conditions.

The stationary ATD was instrumented with a DTS 6DX-PRO 2000-8K (www.dtsweb.com) to measure linear acceleration and rotational velocity of the head and a six-axis upper neck load cell (www.mg-sensor.de) for a 50th percentile male Hybrid III ATD to measure the forces at the upper neck. The data was acquired using a SLICE Micro (www.dtsweb.com) mounted inside the ATD at a rate of 10,000 Hz. Head accelerations and angular rates were filtered at CFC 180, upper neck forces at CFC 1000, and upper neck moments at CFC 600 using the algorithm defined in Society of Automotive Engineers (SAE) J211. High speed video was recorded at 1000 frames per second. In the case with two ATDs striking one another while moving, the instrumentation was duplicated on the second ATD.

A CV and curve correlation analysis were completed on the resultant head translational acceleration, resultant head rotational velocity, resultant upper neck force and resultant upper neck moment.

RESULTS

Test Series 1

Carriage speed and synchronization

Table 5.2 is a summary of the data for test series 1. The carriage speed on impactor 1 and impactor 2 had an RMSE of 0.07% and 0.05%, and CVs of 0.02% and 0.03%, respectively. The average standard deviation for a given target speed was 0.001 m/s. The actual speed achieved by the carriage matched the target test speed to two decimal accuracy at each target speed. The time that the carriage began to decelerate was also repeatable on each impactor with CVs of 0.02% and 0.05%, respectively. The synchronization between impactor 1 and impactor 2 was within 0.77 ± 0.41 milliseconds (ms).

Target Speed	Impactor 1				Impactor 2				Synchronization	
	Average Speed	Std. Dev. Speed	RMSE Speed	CV Speed	Average Speed	Std. Dev. Speed	RMSE Speed	CV Speed	Avg. Diff. Time	Std. Dev. Time
[m/s]	[m/s]	[m/s]	[%]	[%]	[m/s]	[m/s]	[%]	[%]	[ms]	[ms]
2	2.00	0.001	0.05%	0.05%	2.00	0.001	0.09%	0.07%	0.00	0.00
3	3.00	0.001	0.15%	0.02%	3.00	0.001	0.03%	0.02%	1.00	0.00
4	4.00	0.001	0.04%	0.02%	4.00	0.000	0.03%	0.01%	0.00	0.00
5	5.00	0.001	0.07%	0.02%	5.00	0.001	0.03%	0.02%	1.40	0.89
6	6.00	0.001	0.07%	0.01%	6.00	0.001	0.08%	0.02%	1.00	0.71
7	7.00	0.000	0.07%	0.01%	7.00	0.001	0.01%	0.01%	1.80	0.84
8	8.00	0.003	0.04%	0.04%	8.00	0.004	0.07%	0.05%	0.20	0.45
Average		0.001	0.07%	0.02%		0.001	0.05%	0.03%	0.77	0.41

Table 5.2 – Test Series 1 - Repeatability of impactor speeds and impactor synchronization. Five tests were conducted on each impactor for each test speed (n = 70), sled mass = 14 kg.

Sled acceleration profile

The sled is decoupled from the carriage prior to the free motion phase. The acceleration profiles were compared using a correlation analysis. The average curve correlation coefficient

was 0.9992 (std. dev $\pm 7.76 \text{ e-}05$). The curves were essentially the same. The lowest correlation coefficient occurred at the 2 m/s target speed (0.9975) and at each of the other target speeds the correlation coefficient exceeded 0.9990. The correlation was high at all target speeds; however, there was a trend of better correlation as the speed increased. The CV of peak deceleration of the sled was 0.5%. The CV followed the same trend as the correlation coefficient indicating that with higher speeds the CV decreased. This CV value is a measurement of the braking system repeatability in this test setup and would not affect the impactor speed repeatability since the impact had already occurred prior to braking. Figure 5.4 illustrates the sled acceleration and deceleration profile at a target speed of 8 m/s.

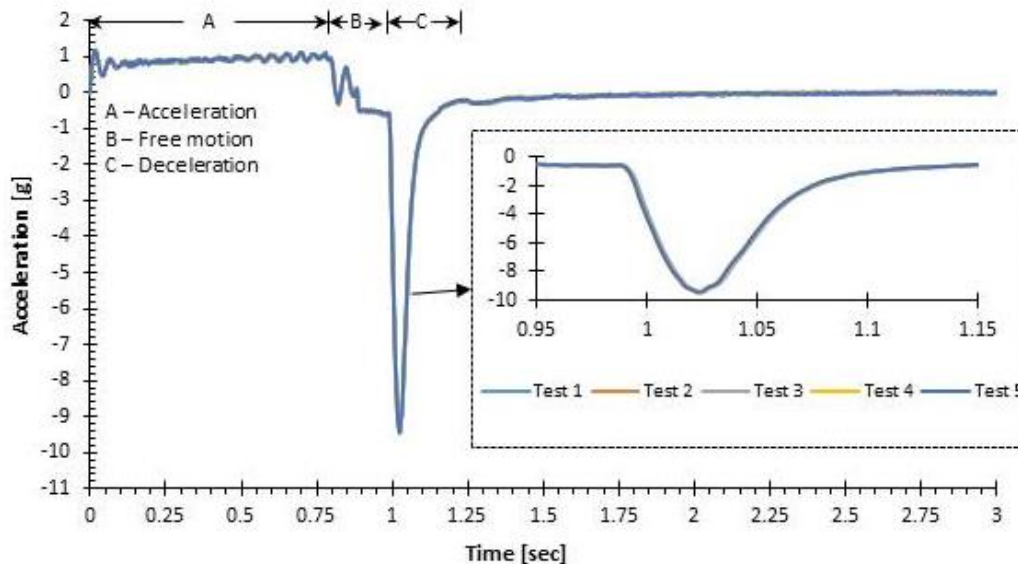


Figure 5.4 – Sled acceleration and deceleration profile from five tests overlaid on one another at a target speed of 8 m/s (n = 5).

Test Series 2

Impactor ram striking a stationary un-helmeted and helmeted ATD

The carriage speed maintained its level of repeatability as in test series 1. The CV of carriage speed was 0.02 % for this test series which is equivalent to an average standard deviation of

speed of 0.001 m/s. In the case of the ram striking the un-helmeted ATD (n=10) the average CV for the upper neck forces (CV=3.4%), upper neck moments (CV=2.5%), head acceleration (CV=1.5%) and head angular speed (CV=0.6%) was 2.0%. The average correlation coefficient for these curves was 0.9991. The helmeted impacts (n=10) resulted in an average CV of the ATD responses of 2.7% with a correlation coefficient of 0.9964 (Table 5.3).

Configuration	Target Speed [m/s]	Number of Tests	Impactor 1 Speed			ATD 1 Avg. of head and neck		ATD 2 Avg. of head and neck	
			Average	Std. Dev.	CV	CV	Correl.	CV	Correl.
			[m/s]	[m/s]	[%]	[%]	[-]	[%]	[-]
Ram into unhelmeted ATD	5	10	5.00	0.001	0.02%	-	-	1.98%	0.999
Ram into helmeted ATD	5	10	5.00	0.001	0.02%	-	-	2.66%	0.996
Moving ATD into Stationary ATD	5	5	5.01	0.001	0.03%	-	-	4.28%	0.995
Moving ATD into Moving ATD [¶]	6	5	6.02	0.001	0.02%	6.47%	0.975	8.07%	0.986

[¶]The speed data includes impactor 1 and impactor 2.

Table 5.3 – Test Series 2 - Repeatability of impactor speed and ATD responses when using the impactors in three different configurations (n = 30).

Moving ATD striking a stationary ATD

In these tests (n=5) the impactor was used to accelerate a helmeted ATD and propel it to strike a stationary ATD. The stationary ATD had an average CV of 5.2% for the upper neck forces, 1.8% for the upper neck moments, 5.1% head translational acceleration and 5.0% for head angular velocity. The average CV was 4.3% with a correlation coefficient of 0.9953. These tests were much more complex than the previous tests since they included the positioning of two ATDs, fitting a helmet to each ATD, and releasing the moving ATD from the impactor.

Two moving ATDs striking in a 90 degree helmet-to-helmet impact

In these tests (n=5) the two impactors were used to accelerate two helmeted ATDs and propel each of them to strike one another in free flight. The average CV of the kinematic responses on the striking ATD (impactor 1) was 6.5% with a correlation coefficient of 0.975. The average CV

on the struck ATD (impactor 2) was 8.1% with a correlation coefficient of 0.986. The ATD head responses had a lower average CV (4.9%) than the upper neck forces and moments (10.2%).

DISCUSSION

The speed of the impactor and timing of the two impactors relative to one another are the primary inputs to simulate player-to-player collisions in contact sports. The impactor speed from these electric servo-driven impactors was repeatable within ± 0.001 m/s. The precision, when used in the ram configuration, and pushing a 14 kg (n=70) or 45 kg (n=20) mass reached the target speed with an average absolute error from the target speed of 0.002 m/s and a CV of 0.025%. A similar study could not be located for the pneumatic linear impactor in the published literature. The actual impact speed and target impact speed data from one of the labs utilized in the testing reported from Viano et al. [17, 63] was analyzed to assess the precision (target speed – actual speed) and variability (standard deviation and CV) in the pneumatic impactor test data (n = 380 tests) (Figure 5.5). The pneumatic impactor test data had an average absolute error of 0.05 m/s (Std. dev = ± 0.07 m/s) with a CV of 0.35%. These data indicate that the servo-driven impactor has the capability of delivering an impactor ram with at least at the same level of accuracy as, and with less variation than the pneumatic linear impactor.

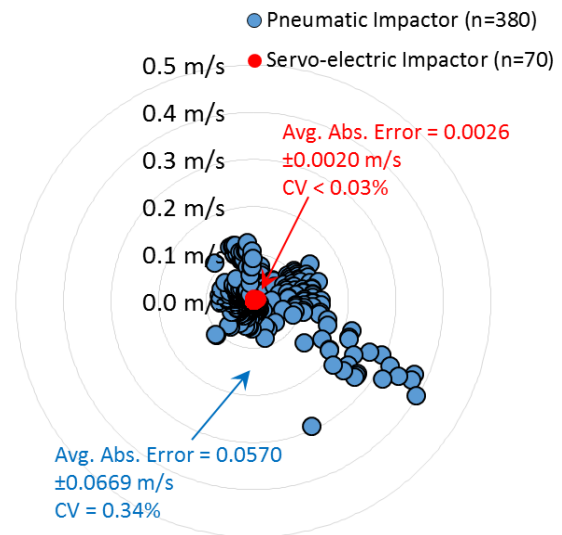


Figure 5.5 – Pneumatic impactor repeatability (speed data from Viano et al. (n = 380)).

The data presented for the servo-driven impactors included two separate pieces of equipment; however, the testing was conducted in the same laboratory. In test series 1, impactor 1 and impactor 2 had average absolute errors from the target speed of 0.003 m/s and 0.002 m/s, and CV's of 0.025% and 0.031%, respectively. Therefore, this study illustrated that the servo-driven impactors were reproducible to a high level of precision and accuracy. The pneumatic impactor data only considered a single laboratory and do not account for any laboratory to laboratory variation or equipment variation. The laboratory-to-laboratory and equipment variation in the pneumatic impactor is unknown; however, a small-scale study was conducted at Wayne State University (WSU) [79] (n=47). In this study, the pneumatic impactor had an average absolute error from the target speed (9.3 m/s) of 0.112 m/s and a CV of 1.75%. This indicated that the pneumatic impactor was less reproducible due to laboratory, equipment or operator variation. The servo-driven impactor should have similar laboratory to laboratory performance or operator to operator performance since it is a control system and the operator is only required to input a target speed.

The impactors, when used with ATDs, were capable of simulating on-field player-to-player collisions with one or two moving ATDs. Test series 2 illustrates that as the complexity of the impact event increased the CV of the ATD response increased. The CV was lowest (2.0%) when striking an un-helmeted ATD with a ram and increased to a CV of 2.7% when the helmet was added to the struck ATD headform. In collisions with one moving and one stationary ATD the CV increased to 4.3% and CVs further increased to 6.5% to 8.1% with two ATDs moving. The CVs with two ATDs moving were less than 10% despite the complexity of propelling two independent ATDs to impact in free-air. These CVs are in the range of CVs found in automotive

testing to simulate collisions [80, 81] so this appears to be a reasonable level of variation for this type of impact simulation.

This study presented data on repeatability of ATD to ATD impacts using a first generation of ATD support and release system. Steps have been taken since the time of the testing to improve repeatability of these impacts. It is known that the impactors can deliver the ATDs to impact at a consistent speed and synchronized within 1 millisecond of one another. Therefore, the variation exists in the ATD setup and support of the ATD during the acceleration phase of the impactor. In the repeatability testing, it was often seen that the ATD would move from its initial position during the acceleration phase. Paint transfer markings from the ATD's helmet on impactor 1 to the helmet of the ATD on impactor 2 indicated the impact occurred within +/- 1.5 cm (Figure 5.6). This small movement could explain most of the differences in CV seen from the one ATD moving (4.3%) to the two ATD moving (6.5% to 8.1%) conditions. The first generation support and release of the ATD was accomplished using a specially made harness. Modifications have been made to the ATD support system on the sled to provide a more positive support of the ATD and prevent this movement during the acceleration phase. Once these modifications have been fully implemented and tested the target is to minimize the CV to a level of 5%, or less.



Figure 5.6 – Impact location on helmet of ATD on impactor 2 from a set of five tests with two moving ATDs.

CHAPTER 6 – CONCUSSION WITHOUT PRIMARY HEAD IMPACT AND THE ROLE OF THE TENSILE FORCES IN THE UPPER NECK: A CASE STUDY

INTRODUCTION

The 2012 consensus statement on concussion in sport included the statement that “*concussion may be caused by a direct blow to the head, face, neck or elsewhere on the body with an impulsive force transmitted to the head.*” [1]

Quite a lot is known about direct impacts to the head causing injury, but there are few studies on concussion without head impact. Friede [10, 11] studied the mechanics of concussion by evaluating the signs and neuropathology in the upper spinal cord and brain stem of cats in a non-impact condition. He concluded that craniocervical stretch and flexion are the most important factors in concussion. Ommaya et al. [29] produced signs of cerebral concussion, hemorrhages on, and contusions over the surface of the brain and upper cervical cord by rotational displacement of the head on the neck, without direct head impact. They concluded that multiple mechanisms are involved in cerebral concussion, among them are rotational acceleration of the head, flexion-extension-tension of the neck, and intracranial pressure gradients. Hodgson [82] concluded that relative movement at the craniocervical junction may be an important factor in whether consciousness is lost in impacts resulting in inertial loading of the head.

In the human, sled testing conducted by Col. John P. Stapp [83] resulted in the loss of consciousness of one volunteer at a peak sled deceleration of 38 g with an onset rate of 1370 g/sec. The volunteer reportedly did not follow the experimental protocol to minimize potential for injury [82]. Hutchinson [84] conducted a video analysis of 174 concussion-causing hits in the National Hockey League (NHL). Twenty percent of these injuries had a primary shoulder-to-chest contact, but less than 5% had no secondary head contact. Elkin et al. [85] noted that the clinical symptoms of whiplash and concussion have considerable overlap. They determined the

strain in the brain during rear-end car crashes and found that strains correlated best with the change in head angular velocity.

While direct head impact is the most common cause for concussion and head injury, the study of a blow to the body causing concussion may shed light on a mechanism of brain injury. Jadischke et al. [86] studied the effect of the increase in helmet weight on head kinematics and neck kinematics and concluded that the increased mass of a football helmet added to the head caused an increase in neck forces. This provided a possible explanation why there has not been a reduction in concussion rates despite improvements in a helmet's ability to reduce head accelerations. Ommaya [87] and Hodgson [82] indicated that the mass of the helmet aggravates the potential for injury by adding bending, axial, and shear loads at the craniocervical junction. King et al. [88] used a discrete parameter model of the head and neck to study the response of the neck of pilots who ditch in the ocean and fail to eject before the jet aircraft sank. The model assumed no direct head impact but considered active muscle tension in the neck. Results showed that, with the added weight of a helmet, one of the reasons for the pilots failing to eject was cord concussion due in part to upper cervical cord stretch during the combined vertical acceleration and forward deceleration of the aircraft. The computed head linear and angular accelerations were below concussive levels.

The aim of this study was to assess the biomechanical response and estimate the strain in the upper cervical spine and brain stem as a result of direct impact to the chest in the sport of American football. This study was completed first by conducting impact testing to the chest of a stationary anthropomorphic test device (ATD), both helmeted and un-helmeted. Second, a case study of two National Football League (NFL) game collisions was conducted to assess biomechanical forces in real-life collisions resulting in concussion. In each collision, the

primary impact to the struck player was to the chest, and the players experienced a concussion with a delayed return to play. Third, a finite element study of the head and neck from the Global Human Body Model Consortium (GHBMC) Average Male model was conducted to estimate the elongation of the cervical spine under tensile and flexion loading conditions. The results of the finite element study were then compared to the neck loads obtained in the laboratory reconstructions to estimate the strain in the central nervous system (CNS).

MATERIALS AND METHODS

Test Series 1 - Impact Testing

Impact tests were conducted with head, neck, and upper torso of a Hybrid III 50th percentile anthropomorphic test device (ATD) struck at the centre of gravity of the chest (Figure 6.1). The pelvis of the ATD was replaced with a mount of equal mass. The first set of tests was conducted by striking the stationary ATD with an impactor with a 38.1 mm (1.5 inch) thick deformable vinyl nitrile end cap. This end cap is used commonly in helmet-to-helmet testing to simulate a helmeted player [64]. A servo-controlled electric impactor was used to accelerate a mass of 45 kg to a desired impact velocity. The impact velocities were increased from 5 m/s to 10 m/s and each impact velocity was repeated back-to-back in the helmeted and the un-helmeted condition. The addition of the helmet to the headform resulted in a 47% increase in effective head mass (6.69 kg) versus the un-helmeted impacts (4.54 kg). In the



Figure 6.1 – Impact configuration for test series 1

9 m/s and 10 m/s impact speed, the facemask was removed to prevent it from striking the ram, resulting in effective head mass (6.02 kg) and only a 32% increase when compared to the un-helmeted headform. The struck ATD torso angle was set at 90 degrees above horizontal, it was placed on a height-adjustable table, and the impactor was aligned to the centre of gravity of the chest.

The Hybrid III 50th percentile male ATD was instrumented with a DTS 6DX-PRO 2000-8K system (www.dtsweb.com) mounted to a machined mounting block to measure translational acceleration at the center of gravity of the headform and rotational velocity of the headform. A six-axis upper neck load cell (www.mg-sensor.de) for a 50th percentile male Hybrid III ATD was used to measure the forces and moments at the upper neck. A triaxial accelerometer SLICE (+/- 100 g) and triaxial angular rate sensor SLICE (+/- 140 rad/s) were integrated into the Diversified Technical Systems (DTS) Slice Micro data acquisition system (www.dtsweb.com) mounted on the Hybrid III ATD spine to measure linear acceleration and angular velocity of the chest. These data were used to calculate the accelerations at the centre of gravity of the chest. The data were filtered using an antialiasing hardware filter. Head translational accelerations were digitally filtered at Channel Frequency Class (CFC) 1000, neck forces were filtered at CFC 1000, and neck moments were filtered at CFC 600 using the algorithm defined in SAE J211 [78]. Angular velocities and chest translational acceleration were filtered at CFC 180. The polarities of the sensors follow those set out in SAE J211.

Test Series 2 - Laboratory Reconstructions

Game video was analyzed from multiple camera views to assess the heading angles, torso angles, and closing speeds of two cases in the NFL involving concussion with no primary head contact. The orientation of the camera was first calculated in 3D Studio Max software using the

perspective match utility. A 0.25 m diameter sphere, which is representative of the size of modern American football helmets, was then placed on the helmet in the camera view in a scaled 3-dimensional model of the playing field. This was done just prior to the collision and repeated at the time of the collision for three camera views. The analysis resulted in the sphere positions in 3D-space overlaying each other from the three separate camera views. The scaled model of the playing field, distance travelled by the player's helmet, and the time between frames were used to estimate the pre-impact speed and heading angle of each of the players. The torso angle of each of the players was also estimated for use in the reconstruction. The players' speeds were checked using a 2-dimensional analysis of the markings on the playing field.

In the laboratory, the upper body of two Hybrid III 50th percentile ATDs were used to represent the football players involved in these collisions. The ATDs consisted of the Hybrid III head, neck, upper torso, shoulders, arms (on striking player only), standing lumbar spine, and pelvis. The ATDs were fitted with a weight vest such that the ATD mass could be ballasted to represent the player's upper body mass. The upper body mass was assessed by scaling the ATD mass up to the player mass. A large-sized American football helmet weighing 2.15 kg was fitted onto the struck Hybrid III headform, and a large-sized American football helmet weighing 1.85 kg was fitted onto the striking Hybrid III headform. The brow pads were positioned 2.54 cm (1 inch) above the top of the nose. The chin strap was attached so that it fit snugly over the Hybrid III chin. A nylon stocking was placed over the Hybrid III headforms to reduce the friction at this interface and to provide a more realistic response of the helmet on the headform. This is consistent with NFL helmet testing [17, 43].

The data acquisition and instrumentation for each of the ATDs was similar to that described in test series 1. An electric servo-controlled acceleration sled was used to accelerate

independently the two ATDs towards one another at the calculated closing speed. Just prior to impact, the ATDs were released from their sled, and at impact, they were in free flight. Encoders mounted on the acceleration sleds were used to control the acceleration sleds and to measure the speed and position of the two Hybrid III ATDs just prior to impact. High speed video was recorded at 1000 frames per second.

Case A

The injured player was 1.78 metres tall and weighed approximately 81 kilograms. He played the wide receiver position and was struck by a defender who was 1.78 metres tall and weighed approximately 83 kilograms. The wide receiver caught a football while running sideline-to-sideline on the field, took one step and, just prior to impact, he was looking in the direction of another defender. The striking player's helmet struck his chest and right shoulder area (Figure 6.2), and during the response of the struck player, the struck player's head flexed forward. The struck player's forward torso motion was stopped immediately upon impact and displaced rearward, indicating the torso's change in speed was greater than the player's running speed. After the impact, the struck player lay motionless for approximately 70 seconds, and he was subsequently helped off the field by the athletic training staff. The team injury report indicates he suffered a concussion and missed the remainder of the game as well as the two subsequent games. This is approximately three weeks of game play.



Figure 6.2a - Pre-Impact



Figure 6.2b - Impact



Figure 6.2c - Post-Impact

Figure 6.2 – Pre- and Post-Impact images for Case A.

Case B

The injured player was 1.91 metres tall and weighed approximately 112 kilograms. He played the tight end position and caught a football while airborne and moving downfield toward the end zone. The defender's helmet struck the chest and right shoulder area of the injured player while he was airborne (Figure 6.3). The defender was 1.91 metres tall and weighed approximately 105 kilograms. When he was struck, the struck player was not looking at the defender but was still looking in the direction from which the ball had come. After the impact, he fell to the turf on his back and subsequently got up under his own power. No head-to-ground

impact occurred. He left the field and did not return to play that game. The team injury report indicates he suffered a mild concussion, and he returned to game play 7 days later.

Figure 6.3a – Pre-Impact

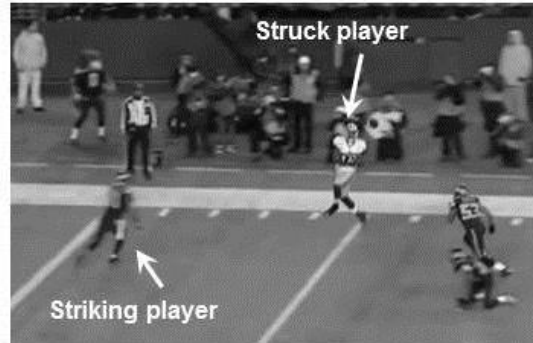


Figure 6.3b – Impact

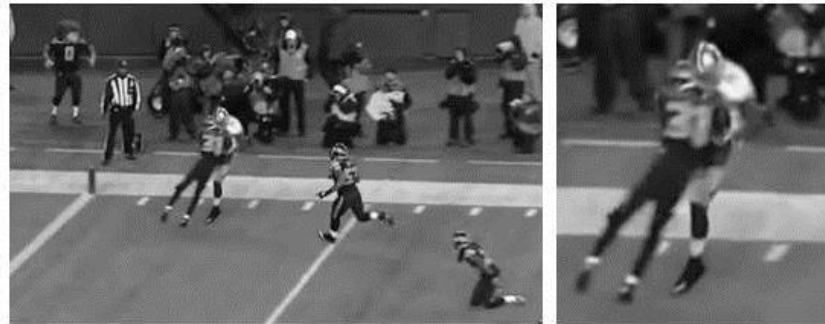


Figure 6.3c – Post-Impact



Finite Element Modeling

The head and neck were segmented from the whole GHBM 50th percentile male model at the first thoracic vertebrae along with all relevant musculature and ligaments. Validation of the head and neck model was previously completed by others [89, 90] using cadaveric and volunteer experimental data. In the present study, the model was not used to assess tissue level strains in the brain stem and spinal cord directly because there was no specific validation related to the

brain stem and upper cervical spinal cord discussed in the literature. Rather, the kinematics of the vertebrae and skull were studied to assess the craniocervical stretch in the vertebral column. The overall elongation of the cervical column because of tensile or flexion loading was computed using discrete points defined on the anterior, left, right, and posterior sides of each cervical vertebrae, and the location and orientation of the skull was monitored by tracking its centre of gravity

LS-Dyna (Livermore Software Technology Corporation, Livermore, CA) was used to run the simulations. The scalp, skull, and each vertebrae were converted to rigid bodies. The nodes at the base of the model (base of C7 vertebral body) were fully constrained. The tensile and flexion loading conditions were applied independently of one another to the same node, located on the top of the scalp and above the occipital condyles. The tensile load curve was developed based upon the upper neck tension in Viano et al. [44] (Case 38) and the curve was scaled to have peak neck tensions of 500, 1500, and 2500 N occurring at 20 milliseconds. The simulations were run for 30 milliseconds. A second set of simulations was completed for the flexion loading condition. The head was rotated forward to simulate flexion of the head and neck and to assess the change in length of the spinal canal per degree of head rotation. The simulations were conducted for a duration of 30 milliseconds, and the head reached a maximum forward flexion of 51 degrees during this time. The average strain in the upper cervical spine was assessed at the level of C1-C5 since the literature [35, 36] has shown there to be not only caudal (downward) displacement of the spinal cord relative to the spinal column in this level but also cephalad (upward) displacement of the spinal cord below this level. The strain in the spinal canal was multiplied by a 0.65 coupling ratio to estimate the strain in the upper cervical spinal cord and brain stem. The basis for this coupling ratio is discussed in Chapter 8.

The simulations were conducted using a dual quad core 64-bit Dell Precision M6600 computer with an Intel i7-2760 CPU at 2.4 GHz. The kinematics predicted by the finite element simulations were compared to existing human volunteer [35, 91] and cadaveric studies [92, 93].

RESULTS

Test Series 1 – Impact Testing

The primary ATD response to the chest impacts was in the sagittal plane. Table 6.1 illustrates the biomechanical responses for various closing velocities. The helmeted responses resulted in a $40\% \pm 10\%$ ($t=9.84$, $p<0.001$) increase in upper neck tensile forces when compared to their equally severe un-helmeted impacts. There was also an increase of $8\% \pm 3\%$ ($t=7.267$, $p<0.001$) in head flexion angle. There was a reduction in head displacement of $18\% \pm 4\%$ and a reduction of rotational velocity of $18\% \pm 6\%$ because of the increased mass and inertia of the helmeted headform. For the helmeted impacts, the head flexed more forward prior to it being displaced rearward with the torso causing the head motion to lag behind the torso motion. This resulted in significantly greater neck forces and moments when compared to the un-helmeted impacts. High speed video of a 10 m/s chest impact is illustrated in Figure 6.4.

Test ID	Helmet	Impactor Speed [m/s]	Impactor Force [N]	Head Kinematics						Chest Kinematics						Upper Neck Kinetics													
				Translation			Rotation			Translation			Rotation			Forces			Moment										
				Accel. res [g]	Vel. x [m/s]	Vel. y [m/s]	Vel. z [m/s]	Displ. x [m]	Displ. y [m]	Displ. z [m]	Rot. Y [deg]	Rot. X [deg]	Rot. Z [deg]	Accel. res [g]	Vel. x [m/s]	Vel. y [m/s]	Vel. z [m/s]	Displ. x [m]	Displ. y [m]	Displ. z [m]	Vel. X [rad/s]	Vel. Y [rad/s]	Vel. Z [rad/s]	Rot. X [deg]	Rot. Y [deg]	Rot. Z [deg]	Shear [N]	Tension [N]	Moment Flexion [Nm]
M8B	no	5	4187	12.3	-6.19	3.11	0.20	-0.34	0.20	0.20	-13.9	-24.8	10.7	10.7	-2.5	0.5	0.5	-0.20	0.03	0.03	6.2	16.2	-326	387	15.0				
M8A	yes	5	4026	11.1	-4.73	2.62	0.20	-0.27	0.20	0.20	-12.3	-25.7	10.0	10.0	-2.4	0.7	0.7	-0.19	0.04	0.04	5.1	12.3	-421	522	16.0				
M8C	no	6	4931	15.1	-7.36	3.81	0.24	-0.40	0.24	0.24	-17.8	-30.5	12.9	12.9	-3.1	0.6	0.6	-0.23	0.05	0.05	7.4	18.3	-384	484	17.7				
M8D	yes	6	4931	13.7	-6.16	3.21	0.24	-0.32	0.24	0.24	-15.6	-33.1	12.5	12.5	-2.9	0.6	0.6	-0.23	0.04	0.04	6.9	15.8	-481	676	19.0				
M8F	no	7	5736	17.9	-8.20	4.92	0.31	-0.44	0.31	0.31	-20.9	-34.8	15.3	15.3	-3.6	0.8	0.8	-0.27	0.06	0.06	8.6	20.4	-448	602	19.4				
M8E	yes	7	5655	16.1	-6.96	4.14	0.30	-0.36	0.30	0.30	-16.4	-38.0	14.8	14.8	-3.4	0.9	0.9	-0.26	0.06	0.06	7.5	17.3	-587	868	19.8				
M8G	no	8	6681	21.2	-9.46	6.01	0.37	-0.50	0.37	0.37	-25.2	-40.1	18.0	18.0	-4.1	1.0	1.0	-0.31	0.07	0.07	9.6	22.5	-533	696	22.0				
M8H	yes	8	6621	19.2	-7.60	4.74	0.37	-0.39	0.37	0.37	-18.5	-42.5	17.8	17.8	-3.8	1.1	1.1	-0.30	0.07	0.07	6.7	15.3	-682	1094	22.3				
M8K	no	9	8029	25.7	-10.33	7.60	0.47	-0.56	0.47	0.47	-29.3	-44.5	21.4	21.4	-4.5	1.2	1.2	-0.35	0.09	0.09	10.3	24.6	-650	868	23.8				
M8J	yes*	9	8130	25.2	-8.94	6.35	0.44	-0.48	0.44	0.44	-23.4	-48.6	21.0	21.0	-4.4	1.2	1.2	-0.35	0.09	0.09	6.9	17.2	-747	1195	26.9				
M8L	no	10	11449	35.6	-11.44	9.04	0.55	-0.63	0.55	0.55	-36.0	-48.2	31.2	31.2	-5.1	1.3	1.3	-0.40	0.10	0.10	11.0	27.8	-816	1322	34.7				
M8M	yes*	10	11771	37.2	-10.16	7.29	0.50	-0.55	0.50	0.50	-29.3	-53.7	32.1	32.1	-5.0	1.3	1.3	-0.39	0.10	0.10	7.7	19.1	-955	1687	39.7				
Avg. (Helmet / Un-helmeted)				0.94	0.83	0.83	0.97	0.82	0.82	0.82	1.08	1.08	0.98	0.98	0.95	1.07	1.07	0.97	1.00	1.00	0.78	0.78	1.24	1.24	1.40	1.40	1.07		
Std Dev (Helmet / Un-helmeted)				0.06	0.04	0.02	0.03	0.04	0.03	0.03	0.03	0.03	0.03	0.03	0.02	0.12	0.12	0.01	0.01	0.09	0.09	0.11	0.11	0.07	0.10	0.06			
t				2.495	9.040	18.733	2.031	12.110	2.031	7.817	-7.177	1.657	6.422	-1.516	5.421	4.828	7.267	-8.900	-9.839	-3.322									
p (one-tail, 0.05)				0.027	<0.001	<0.001	0.049	<0.001	<0.001	<0.001	<0.001	<0.001	0.079	0.001	0.095	0.001	0.002	<0.001	<0.001	<0.001	<0.001	<0.001	<0.001	<0.001	<0.001	<0.001	<0.001		

*Facemask removed to prevent contact with impactor ram.

Table 6.1: Biomechanical responses to chest impacts for the Hybrid III ATD in the helmeted and un-helmeted conditions. The Hybrid III ATD was struck by a 45 kg impactor with a deformable end cap.

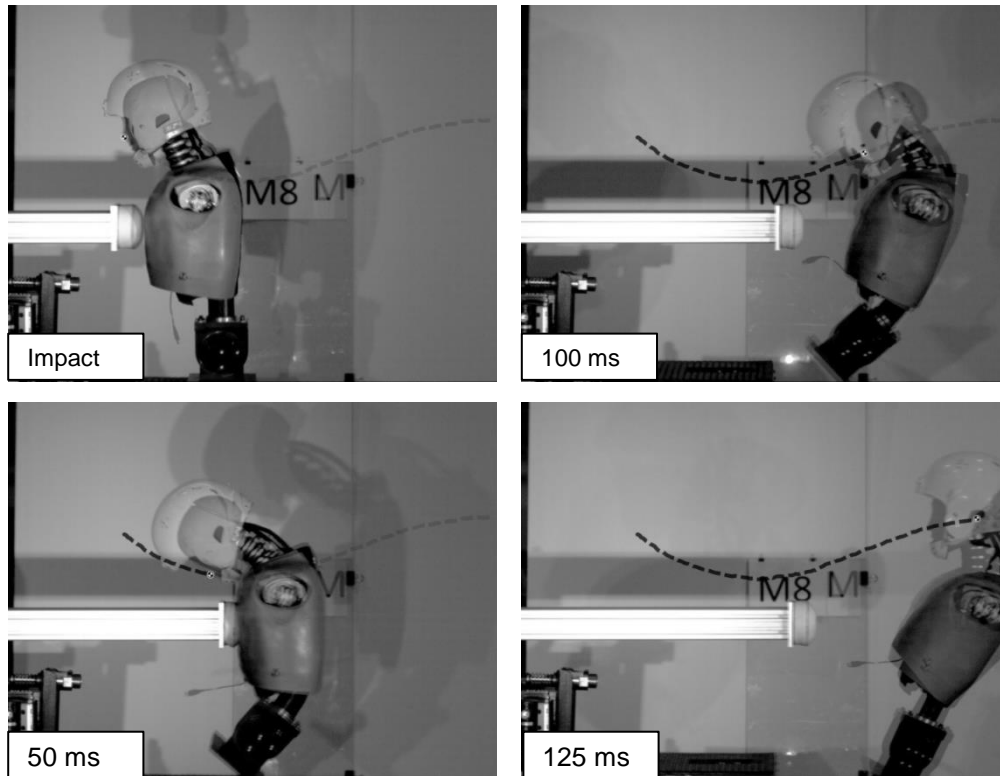


Figure 6.4: Comparison of helmeted versus un-helmeted chest impact. In the helmeted impact the head movement lags behind the torso rotation, resulting in greater forward rotation of the head relative to the torso and higher neck force and moments

Test Series 2 - Laboratory Reconstructions

The closing velocities for Case A and Case B were 12.6 and 9.8 m/s, respectively. The closing velocity in Case A was higher than any of the closing velocities reported by Pellman et al. [43] in their reconstruction of helmet-to-helmet hits resulting in concussion, and the closing velocity in Case B was higher than the average reported by Pellman et al. [43]. The reconstructed laboratory impacts for Case A and Case B both resulted in the struck player's kinematics being similar to the actual impact as well as the impact testing in test series 1. These kinematics are also similar to a seat-belted occupant in an automotive frontal collision. The reconstruction data from the struck ATD are summarized in Table 6.2. A comparison of the post-impact kinematics of Case A is illustrated in Figure 6.5. A comparison of these laboratory

reconstructions to the Test Series 1 results for the helmeted and un-helmeted ATDs is illustrated in Figure 6.6.

Case	Closing		Kinematics									Upper Neck Kinetics			
	Speed	Location	Trans. Accel.			Trans. ΔVel.		Trans. Disp.		Rot. Acc.	Rot. Vel.	Rot.	Forces		Moment
	[m/s]		x	z	res	x	z	x	z	y	y	y	Shear	Tension	Flexion
			[g]	[g]	[g]	[m/s]	[m/s]	[m]	[m]	[rad/s ²]	[rad/s]	[deg]	[N]	[N]	[Nm]
A	12.6	Head	-38.2	49.7	49.3	-12.20	7.89	-0.73	0.55	-3110	-41.1	-51.0	-1074	2646	49.3
		Chest	-36.6	18.0	41.8	5.1	1.6	-0.42	0.08	-	8.2	10.1	-	-	-
B	9.8	Head	-15.6	-15.0	18.7	-6.10	-3.40	-0.16	-0.14	-1264	-26.5	-46.0	-799	1342	36.0
		Chest	-19.2	9.7	19.0	3.8	0.9	-0.17	0.03	-	4.6	3.0	-	-	-

Table 6.2: Biomechanical responses to chest impacts for the Hybrid III ATD in the reconstructed game hits resulting in concussion

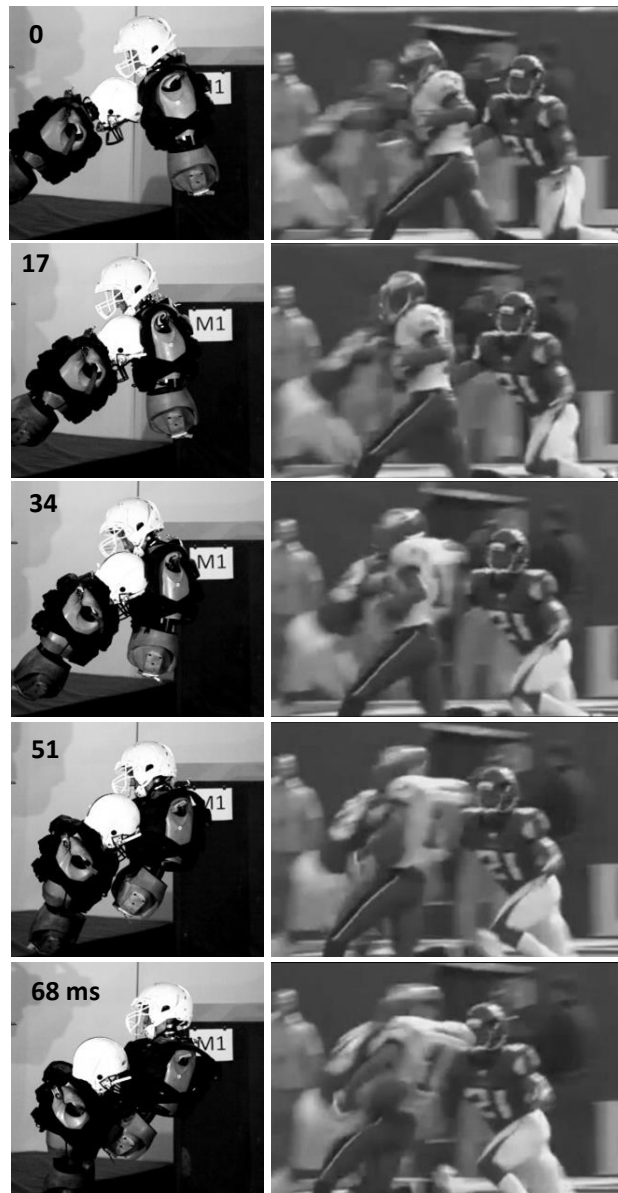


Figure 6.5 – Post-impact kinematics in laboratory reconstruction of Case A compared to the game video.

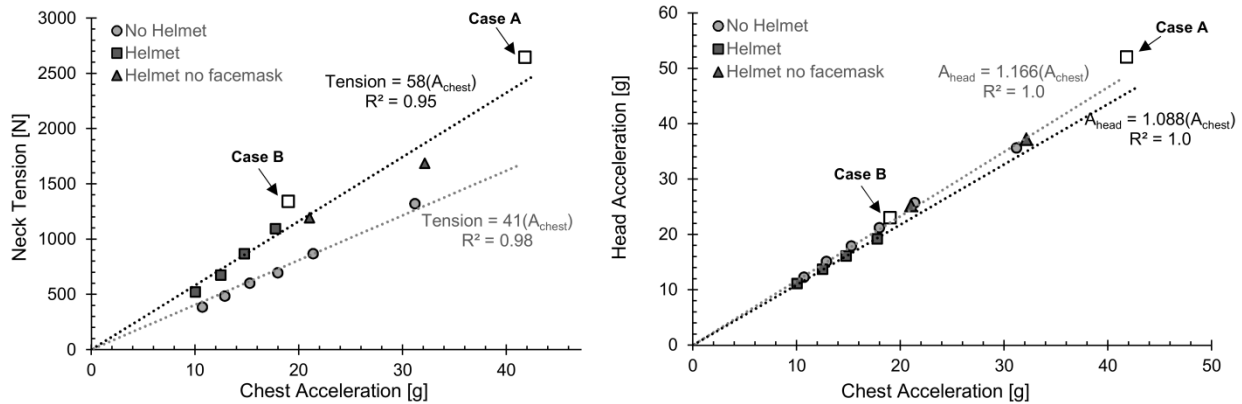


Figure 6.6 – Upper neck tension and head acceleration responses to chest impacts for the Hybrid III ATD in the helmeted and un-helmeted conditions. The laboratory reconstructions (Case A and Case B) are overlaid onto this data and show good agreement with the impact testing to the chest of the Hybrid III ATD.

The translational head accelerations in these cases (Case A = 52 g, Case B = 23 g) are in the range of the uninjured striking (56 ± 22 g) and uninjured struck (60 ± 24 g) player data from Pellman et al. [43], in their reconstruction of helmet-to-helmet collisions. These are well below the average of concussed player's (98 ± 28 g). The lowest translational accelerations reported by Pellman et al. [43] resulting in concussion were 48 g and 52 g, and neither of these resulted in loss of consciousness. The translational head accelerations in Cases A and B are below other proposed translational acceleration injury thresholds for a concussion [48, 49, 94, 95, 96].

In the laboratory reconstructions of Cases A and B, the ATD head flexed forward 51 and 46 degrees, respectively, relative to the torso and reached angular speeds of 41.1 rad/s and 26.5 rad/s, respectively. The forward flexion angle of the ATD head was within the normal range of motion of the human [35]. The head angular velocity in Case A was similar to the average injured player by Pellman et al. [43] (34.8 ± 15 rad/s). The head angular velocity in Case B was similar to the average uninjured players by Pellman et al. [43] (26.1 ± 10 rad/s).

The upper neck had a peak neck tension of 2646 N in Case A and 1342 N in Case B. These neck tension forces exceed those previously reported in volunteer research [97, 98, 99]. They are

generally in the range of those reported by Viano et al. [44] (1704 ± 432 N) in the reconstruction of five players who sustained concussion with no loss of consciousness in the NFL. However, in this case study, Case A had a greater neck tension and did result in a loss of consciousness. The chest acceleration in Case A was of similar magnitude to the case reported in the literature [82] in which a volunteer lost consciousness after undergoing a severe frontal deceleration event.

Finite Element (FE) Modeling

Finite element modeling indicated that the strain in the cervical spine increased linearly with head flexion or tensile loading; however, it varied along the length of the cervical spine. The average strain in the vertebral column in flexion was 0.21 % strain/degree of head rotation and 4.6 % strain/1000 N of tensile load. The maximum strain in the vertebral column was predicted to occur in the upper cervical spine (C1-C2) and was 0.28 % strain/degree of head rotation and 6.5% strain/1000 N of tensile load for flexion and tension, respectively. This is consistent with previous biomechanical testing and finite element modeling that has predicted the highest strains to occur in the upper cervical spine [100].

A spinal cord coupling ratio of 0.65 [41, 101] was used to estimate the central nervous system (CNS) strain relative to vertebral body strain. Using this coupling ratio, a maximum strain in the CNS for a flexion angle of 55 degrees is predicted to be 7.5% to 10.0%. These estimates using finite element modeling were comparable to in-vivo volunteer data which measured a maximum strain in the spinal cord of approximately 10.2% at a 55 degree flexion angle [35]. This comparison suggests that the coupling ratio in the human may be higher than 0.65. A coupling ratio was also applied to the tensile loading condition to estimate the strain in the CNS due to neck tension. The average strain in the CNS was predicted to be 1.6%, 4.6% and

6.8% for neck tension loads of 500 N, 1500 N, and 2500 N, respectively. The peak strains, in the upper cervical spine (C1-C2), were predicted to be 1.3%, 6.0% and 11.0%, respectively.

The laboratory reconstruction data for Case A and Case B, as well as the FE data, were used to estimate the strain in the CNS in these concussed NFL players. The strain in the CNS was estimated to be 14.4 to 20.5% in Case A and 10.1 to 14.1% in Case B due to combined tension and forward flexion. This assumes that the peak strains due to the tensile load and flexion occur at the same time. This laboratory reconstruction and FE data indicates that the maximum strain in the CNS (Table 6.3) exceeds the levels that have been documented to cause changes in functional and structural response in spinal nerve roots at high strain rates [102]. The strains are similar to those documented in in-vivo tests with primates which resulted in functional changes in the spinal cord as well as changes in heart rate and respiration [13].

Case	Force	Tension				Rotation	Flexion			
		Avg. Strain C1-C5		Max. Strain C1-C2			Avg. Strain C1-C5		Max. Strain C1-C2	
		Spinal Canal	CNS	Spinal Canal	CNS		Spinal Canal	CNS	Spinal Canal	CNS
[N]	[%]	[%]	[%]	[%]	[%]	[deg]	[%]	[%]	[%]	[%]
FE Study	500	2.4%	1.6%	2.1%	1.3%	35	7.4%	4.8%	9.8%	6.4%
FE Study	1500	7.1%	4.6%	9.2%	6.0%	45	9.5%	6.1%	12.6%	8.2%
FE Study	2500	10.5%	6.8%	16.9%	11.0%	55	11.6%	7.5%	15.4%	10.0%
Case A	2646	11.5%	7.5%	17.3%	11.2%	51	10.7%	7.0%	14.3%	9.3%
Case B	1342	5.9%	3.8%	8.7%	5.7%	46	9.7%	6.3%	12.9%	8.4%

Table 6.3 – Estimated strain in the cervical spinal canal based upon the head rotation angle and tensile loads. The strain in the CNS (spinal cord and brain stem) was estimated by multiplying the spinal canal strain by a 0.65 coupling ratio.

DISCUSSION

While translational acceleration, rotational velocity, and rotational acceleration of the head have been discussed as biomechanical correlates with concussion, craniocervical stretch resulting from tension and flexion in the upper cervical spine has been reported to be an important factor in concussion [10, 11, 82]. In the human, neck tension and head flexion have each been shown

to result in strain of the upper cervical spinal cord and the brain stem. Breig [28] studied the biomechanics of the CNS in 183 human cadavers. He found that tension generated in the spinal cord can be transmitted from the spinal cord to the brain stem, resulting in elongation of these brain tissues. The largest elongation occurred in the medulla oblongata, and no elongation was apparent superior to the midbrain. The reticular formation of the brain stem controls heart rate, respiration, and consciousness. Changes in heart rate, respiration, and alteration of consciousness are common signs of concussion in animal studies [10, 11, 13, 87]. These changes have also been observed in the decerebrate animal [31] indicating there is brain stem involvement. In histological animal studies related to concussion [10, 11, 31] cellular damage in the reticular formation of the brain stem has been identified. The loss of consciousness evident in one of the players in this case study is consistent with injury to the brain stem.

In Case A and Case B, the struck Hybrid III ATD underwent 51 and 46 degrees of head flexion, respectively. The forward flexion of the head was combined with neck tension as a result of the inertial loading of the head. The flexion of the head is within normal range of motion of the human for quasi-static movement; however, in the human [34, 35, 91, 103, 104] and primate [36], imaging studies have reported elongation of the cervical spinal canal and cord in flexion. The FE modelling results combined with a coupling ratio would estimate strains in the CNS of 9.3 % and 8.4 % as a result of forward flexion, in Cases A and B, respectively. These strains, by themselves, are within the range that has been documented for the human [35] as part of the normal range of flexion motions.

The neck tensions in the concussed NFL players in this case study (Case A = 2646 N, Case B = 1342 N) are greater than neck tensions found in volunteer studies [97, 98, 99] and greater than uninjured NFL players [15] (670 ± 405 N). The neck tensions are similar to those reported by

Viano et al. [44] in their reconstruction of struck and injured players in the NFL (1704 ± 432 N) and are less than the neck tensions resulting in failure of the cervical spine in musculoskeletal cadaveric studies [92, 93, 105, 106]. Neck tension is not a typical range of motion or loading condition in the human due to our upright posture. The tensile loads in Case A and Case B correspond, respectively, to approximately 3.27 and 1.10 times the player's body weight which must be supported by the soft tissues of the neck. In these cases, the struck players did not appear to have the opportunity to ready themselves for the impact. From our FE study, and by applying a coupling ratio, the maximum strain in the CNS due to neck tension was estimated to be 11.2% and 5.1% for Cases A and B, respectively.

The strain in the CNS due to combined tension and flexion for Case A and Case B was on the order of 14.4 to 20.5% and 10.1 to 14.1%, respectively, assuming that peak strains occurred simultaneously. The data presented in this case study supports the mechanism of injury discussed by Friede [10, 11] and Hodgson and Thomas [21] and Hodgson [82] who have indicated that strain in the upper spinal cord and brain stem are important factors in concussion. The brain stem's relation to concussion is further supported by the early work of Denny-Brown and Russell [31] who produced concussion signs in the decerebrate animal. This level of strain exceeds the strains [110] that resulted in changes in heartrate and respiration as well as reduced evoked potentials in the spinal cord in in-vivo primate testing. These are common signs of concussion in animal studies. The estimated strains in this study also exceed the strain that resulted in temporary dysfunction of spinal nerve roots with a tensile loading applied [13]. Therefore, the magnitude of these strains support that elongation of the cervical spinal cord and brain stem could be a mechanism of concussion.

The addition of the helmet to the ATD headform in test series 1 resulted in an increase in neck tension and forward flexion of the head. The neck tension increased by 40% and forward flexion increased by 8% as a result of the added helmet mass. A similar trend in the neck forces was also found previously in simulated head impacts [86]. Others [29, 82] have indicated that the mass of the helmet added to the head can increase the strain at the craniocervical junction. If, through further research, neck tension is found to be a biomechanical predictor of concussion, helmet and equipment manufacturers could use this information to apply greater emphasis on helmet mass and inertia when optimizing helmet performance and also to develop alternative methods of protecting against concussion.

There are several limitations of this case study that should be noted. This case study was performed using the Hybrid III ATD in a laboratory test environment. The case study is limited since only two cases were reconstructed. However, the reconstruction of these two cases may help shed some light on a potential mechanism of concussion since they investigated impacts to the chest. The Hybrid III headform and neck provide a biofidelic response in the loading condition analyzed; however, it is not human. Therefore, tissue level strains could not be directly assessed. The data acquired was used in conjunction with FE modelling to estimate the stretch in the upper cervical spine and a coupling ratio was applied to assess the strain in the CNS under these loading conditions. Additionally, the design of the Hybrid III has a neck simulating some muscle tensing, but there is no active musculature in any of the current test dummies. The effects of active and passive neck musculature were not investigated since this was beyond the scope of this case study; however, our review of the videos indicated that neither of the injured players appeared to be looking in the direction of the defender and, therefore, it is unlikely they were able to actively prepare for the impact.

The Hybrid III ATD was designed for frontal impact testing; in this case study the post-impact kinematics of the ATD are representative of a frontal impact in an automotive collision. Therefore, it appears to be a suitable mechanical surrogate for this testing. In addition, for research purposes, the current standard for head impact testing related to helmet performance appears to be the Hybrid III head and neck, and they have been used extensively in impact testing related to helmet performance and boxing punches [16, 17, 61, 62, 70, 71].

In Case B, it was clear that no primary or secondary head contact occurred between the striking player and the struck player's head; however, the motion blur in the video for Case A was a limiting factor. In Case A, upon impact, the torso's forward motion stopped and the head continued to move and flex forward. This indicates that the primary contact was to the chest of the struck player. Due to the severity of this collision, the bottom of the struck player's facemask may have made contact with the top of the defending player's helmet as his head flexed forward. This was simulated in our reconstruction of the collision and appears to have reduced the forward flexion of the head and increased the neck tension in comparison to test series 1.

In this study, only peak strain in the neck has been considered from an impact to the chest. The rate of loading indicates the strain-rate effect may be a factor in the concussion and deserve further attention in the future.

CHAPTER 7 – A LABORATORY STUDY OF INJURIOUS AND NON-INJURIOUS HELMET-TO-HELMET HITS IN AMERICAN FOOTBALL SIMULATED USING THE HYBRID III ATD: A NEW LOOK AT HEAD AND NECK RESPONSES

INTRODUCTION

Pellman et al. [43] reported on the analyses of 182 game impacts in the National Football League (NFL) and the laboratory reconstruction of 31 impacts using the Hybrid III 50th percentile anthropomorphic test device (ATD). Twenty-five of these reconstructed impacts resulted in concussion to one of the players involved. Viano et al. [44] have recommended further study of the head kinematics, such as, neck twist (z-axis rotation) and neck tension after the impact has occurred, and their relation to concussion since neck stiffness can affect headform delta-V. Collins et al. [45] more recently indicated that a lowered neck strength is a significant predictor of the potential for concussion; however, they recommend that further research is necessary to understand why.

It is generally thought that translational and rotational acceleration and velocity of the head are biomechanical predictors of concussion. Each of these can result in head movement relative to the torso and lead to forces and deformation in the cervical spine. There are important data to support the theory that concussions can occur from forces and deformation at the atlanto-occipital joint and brain stem [10, 11, 13, 21, 22, 29, 32, 32, 33]. In animal studies, concussion is typically diagnosed if a loss of consciousness, change in heart rate or respiration, or loss of corneal reflex occurs. These are primary functions of the brain stem [12]. In the human, Casson et al. [3] have reported on concussion symptoms in 1740 National Football League (NFL) players. Most of these symptoms correlate to injury of the spinal cord, brain stem, and/or midbrain (Chapter 1). McCrory et al. [6] have discussed posturing of injured players through a video analysis and concluded this also could be a sign of brain stem injury.

Neck tension (distraction), lateral rotation (x-axis rotation), flexion (y-axis rotation), and twist (z-axis rotation) can each result in elongation of the cervical spine and, therefore, tension in the central nervous system (CNS) [107]. Breig [28] observed that tension generated in the spinal cord can be transmitted from the spinal cord to the brain stem, cerebellum, and cranial nerves (V – XII), resulting in tension in these brain tissues. The role of neck tension and motion of the head relative to the torso as a mechanism for concussion needs further evaluation since these kinematics could result in strain in the brain stem.

In the study by Pellman et al. [43], the laboratory reconstructions incorporated a drop tower where the struck player was represented by the falling, helmeted, ATD headform with neck attached to a carriage. This moving head and neck impacted a stationary ATD which consisted of the head, neck, and torso supported by stretchable cables. The upper neck forces and the carriage acceleration were not measured in the moving head and neck. There was no instrumentation to measure the upper torso kinematics in the stationary ATD. The aim of this study is to generate new data of a subset of the reconstruction cases presented by Pellman et al. [43] to better understand head motion relative to torso and the upper neck forces in the injured and uninjured players. In this study, eighteen of the thirty-one cases have been re-created using different laboratory methods. The impacts were re-created by matching the helmet-to-helmet impact location and closing velocities reported in previously-published work [60] and through new video analysis of the heading angles, torso orientation, and relative speeds of the players. The aim of this study was not to re-create the head kinematics from the initial work but rather to generate a new independent data set using new laboratory methods.

MATERIALS AND METHODS

Video Analysis

The methods used in the original reconstructions are described in detail elsewhere [43, 72, 108]. In the present study, the closing speeds and impact location on the helmets were used from the published research [60], and the game videos were re-analyzed to assess the players' pre-impact vectors. The players' heights and weights were also established.

The same game videos were analyzed from a minimum of two views to assess the heading angles, torso angles relative to the field, and the relative distance traveled from a time just prior to impact until the impact occurred. The orientation of the camera was first calculated in 3D Studio Max software using the perspective match utility. A 0.25 m diameter sphere, which is representative of the size of the Riddell VSR4 size large helmet, was then placed on the helmet in the camera view in a scaled 3-dimensional model of the playing field. The sphere was connected to two different-sized ellipsoids to represent the neck and upper torso of the players. The 3-dimensional position of the sphere and ellipsoids was established just prior to the collision (typically 10 frames prior) and repeated at the time of the collision for each camera view. The analysis resulted in the sphere positions overlaying each other in 3D-space. The sphere was then rotated about its center point to establish the approximate torso orientation relative to the horizontal plane of the playing field. The scaled model of the playing field, calculated distance travelled by the player's helmet, time between frames, and the previously-published closing speeds were used to estimate the pre-impact vector of each of the players. Table 7.1 summarizes the data used for this new data set of laboratory reconstructions.

Case	Player	Injured	Helmet Contact Location			Player Weight [kg]	ATD Weight		Closing Velocity		Closing Momentum		Torso Angle [deg]
			Facemask	Top View	Side View		Target [kg]	Actual [kg]	Target [m/s]	Actual [m/s]	Target [kgm/s]	Actual [kgm/s]	
7	striking	0	N	L 0-45	+Q4	112	41	41	6.9	6.9	266	283	
7	struck	1	N	R 90-135	+Q1	96	36	36					
9	striking	0	N	R 45-90	+Q4	99	58	58	10.3	8.0	610	464	
9	struck	1	N	L 45-90	+Q3	104	60	60					
38	striking	0	N	R135-180	+Q4	104	61	61	9.5	8.8	523	536	56
38	struck	1	Y	L 45-90	-Q1	84	49	49					73
39	striking	0	N	L 0-45	+Q4	88	52	52	10.9	8.9	649	460	36
39	struck	1	Y	R 45-90	-Q2	115	67	67					52
57	striking	0	N	R 0-45	+Q3	86	50	50	8.8	8.9	519	444	51
57	struck	1	Y	L 45-90	-Q1	116	68	68					61
59	striking	0	N	L 0-45	+Q4	96	41	41	5.3	5.3	205	217	
59	struck	0	N	R 90-135	+Q2	102	36	36					
69	striking	0	N	R 45-90	+Q4	94	55	55	10.3	10.3	556	556	60
69	struck	1	Y	R 0-45	-Q1	91	53	53					71
71	striking	1	N	R 0-45	+Q2	84	49	49	10.3	8.0	507	391	
71	struck	0	Y	R 45-90	+Q1	84	49	49					
77	striking	0	N	R 0-45	+Q3	82	48	48	9.9	9.9	590	589	65
77	struck	1	Y	R 0-45	-Q2	122	71	71					75
84	striking	0	N	R 45-90	+Q4	102	60	60	9.4	9.4	627	630	69
84	struck	1	Y	L 0-45	+Q2	126	74	74					49
92	striking	0	N	R 90-135	+Q4	92	54	54	11.1	11.1	744	716	40
92	struck	1	N	L 90-135	+Q4	137	80	75					54
98	striking	0	N	L 0-45	+Q4	85	50	50	9.6	9.6	509	509	53
98	struck	1	N	L 45-90	+Q2	96	56	56					42
113	striking	0	N	R 90-135	+Q3	98	57	57	7.0	7.0	367	399	41
113	struck	1	N	L 0-45	+Q2	82	48	48					77
118	striking	0	N	R 0-45	+Q4	90	53	65	10.7	8.9	579	579	40
118	struck	1	Y	R 0-45	-Q1	95	56	56					71
125	striking	0	N	R 0-45	+Q4	124	72	72	11.4	11.4	712	713	46
125	struck	1	Y	L 45-90	-Q1	90	53	53					54
148	striking	0	N	R 0-46	+Q4	147	71	71	6.6	6.6	410	469	45
148	struck	1	Y	L 0-45	+Q1	98	54	54					74
157	striking	0	N	R 0-45	+Q4	88	41	50	10.8	8.3	417	415	54
157	struck	1	Y	R 0-45	+Q1	79	36	36					89
164	striking	0	N	R 45-90	+Q4	98	57	57	10.8	10.8	609	610	26
164	struck	1	N	L 90-135	+Q2	95	56	56					36

Table 7.1 – Summary of input data for the laboratory reconstructions. The helmet impact location is defined in the original dataset [1]. The player weights were established by reviewing game video. The ATD weight is the scaled weight of the player to represent the upper torso mass. The ATD weight and closing velocity were varied to more closely represent the closing momentum.

Laboratory Reconstructions

The upper body of two Hybrid III 50th percentile ATDs were used to represent the football players involved in these collisions. These ATDs were positioned and accelerated toward one another to simulate the torso angles and closing momentum determined from the video analysis. An electric servo-controlled acceleration sled (Chapter 5) was used to move each ATD independently to achieve the target closing momentum. For some of the reconstructions, both ATDs were accelerated toward each other and impact occurred with both ATDs in free flight. Other tests were performed with one moving ATD in free flight at impact and the stationary

ATD resting on a height-adjustable table and supported overhead by a tear-away hook and loop strap.

The ATDs consisted of the Hybrid III head, neck, upper torso, shoulders, standing lumbar spine, and pelvis. The ATDs were fitted with a weight vest such that the ATD mass could be ballasted with up to 30 kg of additional weight in 1 kg increments to represent the player's upper body mass. The upper body mass was assessed by scaling the ATD mass up to the estimated mass of the player's upper torso. This was based upon the weight distribution of the ATD [75, 76]. The unballasted ATDs weighed 45 kg; therefore, the maximum upper body mass that could be achieved was 75 kg.

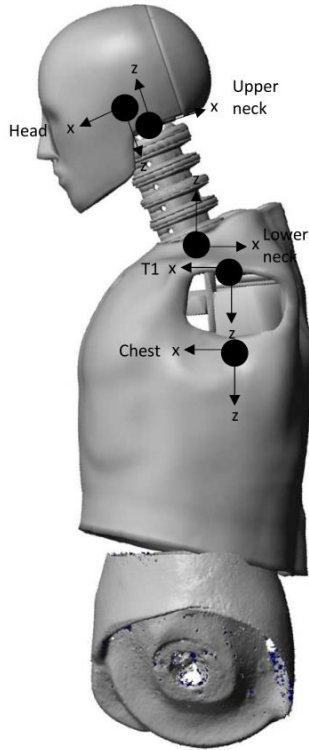
A nylon stocking was placed over the Hybrid III headforms to reduce the friction at this interface and to provide a more realistic response of the helmet on the headform. This is consistent with NFL helmet testing [16, 43]. A large-sized Riddell VSR-4 helmet [62] weighing 1.85 kg was fitted onto the each of the Hybrid III headforms. The brow pads were positioned 2.54 cm (1 inch) above the top of the nose. The chin strap was attached so that it fit snugly over the Hybrid III chin. The Riddell VSR-4 helmets were no longer for sale for game use at the time of this study. The helmets used for this study were replica helmets that were acquired from Riddell. The padding arrangement and overall appearance were identical to a game-worn Riddell VSR-4 helmet. On one of these helmets, a grid was created on the shell to match the impact locations that Pellman et al. [60] had previously defined. This grid on the helmet shell assisted with positioning the ATDs for impact.

ATD Instrumentation and Filtering

Each Hybrid III 50th percentile male ATD was instrumented with a DTS 6DX-PRO 2000-8K system (www.dtsweb.com) mounted to a machined block to measure translational acceleration

at the center of gravity of the headform and rotational velocity of the headform. A six-axis upper neck load cell (www.mg-sensor.de) for a 50th percentile male Hybrid III ATD was used to measure the forces and moments at the upper neck of each ATD. One of the ATDs was equipped with a DTS 6DX-PRO 2000-8K at the center of gravity of the ATD chest. The other ATD had a triaxial accelerometer SLICE (+/- 100 g) and triaxial rotational rate sensor SLICE (+/- 140 rad/s) that were integrated into the Diversified Technical Systems (DTS) Slice Micro data acquisition system (www.dtsweb.com) mounted on the Hybrid III ATD spine to measure linear acceleration and rotational velocity of the chest. These data were used to calculate the accelerations at the center of gravity of the chest. This ATD was also equipped with a six-axis lower neck load cell (www.mg-sensor.de) and three additional accelerometers in the ATD headform to measure linear and rotational acceleration of the head and rotational velocity directly.

The data were first filtered using an antialiasing hardware filter. Head translational accelerations and rotational velocities were digitally filtered at Channel Frequency Class (CFC) 180, neck forces were filtered at CFC 1000, and neck moments were filtered at CFC 600, using the algorithm defined in SAE J211 [78]. Chest rotational velocities and chest translational acceleration were filtered at CFC 180. The polarities of the sensors follow those set out in SAE J211 and are summarized in Figure 7.1. The head rotational accelerations were measured in ATD 1, and in ATD 2, they were calculated by taking the derivative of the CFC 180 rotational velocity data. In the chest, the rotational velocities were first filtered at CFC 60 then differentiated to calculate rotational acceleration. Post-processing was completed using National Instruments LabVIEW and Microsoft Excel. The first 100 milliseconds of data after the collision were analyzed.



Location	Parameter	Channel Name	ATD 1	ATD 2	CFC
Head	Trans. Accel.	Acc	M	M	180
Head	Trans. Vel.	Δv	C	C	180
Head	Rot. Accel.	α	M and C	C	180
Head	Rot. Vel.	$\Delta\omega$	M	M	180
Upper Neck	Forces	F	M	M	1000
Upper Neck	Moments	M	M	M	600
Lower Neck	Forces	-	M	-	1000
Lower Neck	Moments	-	M	-	600
T1	Trans. Accel.	-	C	C	180
T1	Rot. Vel.	-	C	C	180
Chest	Trans. Accel.	-	C	M	180
Chest	Rot. Vel.	-	C	M	180

M - Measured
C - Calculated

Figure 7.1 – Summary of instrumentation and filtering of the ATDs. The channel name is provided as it relates to the results and discussion section. The subscripts x, y and z correspond to the axis of measurement. The subscript R corresponds to a resultant. Rotational acceleration (if not measured) was calculated by first filtering rotational velocity at CFC60 and then differentiating the velocity to calculate acceleration.

Calculated Biomechanical Parameters

The head translational and rotational displacements, velocities, and accelerations of the head relative to T1 were each calculated. The Head Injury Criteria (HIC) is an injury criterion that is based upon linear acceleration and the Wayne State Tolerance Curve. It is traditionally used for the assessment of head protection in the automotive industry when an impact occurs with an interior vehicle component. It is utilized as a measure of head injury assessment in various Federal Motor Vehicle Safety Standards (FMVSS). When applying HIC in the automotive testing environment, it has been recommended that the duration over which HIC is calculated is less than 15 ms (HIC_{15}) [109]. The expression to calculate HIC_{15} is:

$$HIC_{15} = (t_2 - t_1) \left[\frac{1}{t_2 - t_1} \int_{t_1}^{t_2} a_r(t) dt \right]^{2.5}$$

The impact force vector was calculated for each of the collisions [110]. The magnitude of the impact force is equal to the sum of the inertial forces acting on the head and the neck reaction forces. It is determined as:

$$\Sigma P = ma - F$$

Where,

P = Resultant impact force vector

m = The sum of the mass of the helmet (1.85 kg) and headform (4.54 kg)

a = Translational acceleration at the center of gravity of the headform

F = Neck reaction force vector

The location of the impact force radius vector is determined by solving the following equation:

$$\Sigma M = \dot{H} = M_N + \rho_N \times N + \rho_P \times P$$

Where,

M_N = Neck reaction moment vector

ρ_N = Neck reaction force radius vector

ρ_P = Radius vector of the impact force

M = Applied moment vector

\dot{H} = Euler's Equations, where,

$$I_{xx} = 0.03190 \text{ kgm}^2 \text{ (headform} = 0.0160 \text{ kgm}^2, \text{ helmet} = 0.0159 \text{ kgm}^2)$$

$$I_{yy} = 0.04165 \text{ kgm}^2 \text{ (headform} = 0.0240 \text{ kgm}^2, \text{ helmet} = 0.01765 \text{ kgm}^2)$$

$$I_{zz} = 0.03912 \text{ kgm}^2 \text{ (headform} = 0.0220 \text{ kgm}^2, \text{ helmet} = 0.01712 \text{ kgm}^2)$$

To solve this equation, the Hybrid III headform was digitized and 3000 points were established on the headform which were evenly distributed and referenced using x, y, and z locations relative to the headform's center of gravity. The location of the impact force on the

headform was solved numerically using a least-squares approximation. An azimuth and zenith were calculated for the impact force using the directional components of the impact force vector. The impact force vector and location of application were plotted in MS Excel at the time of the maximum impact force +/- 10 milliseconds to verify the stability of the calculation.

The impulse acting on the headform was calculated using the impact force. The end of the impulse was defined as the time at which the impact force drops below 500 N. The impulse was then used to calculate the effective mass of the headform and helmet during the collision. The calculation is as follows:

$$Impulse = \int P dt = m_{eff} \Delta V_{head}$$

Where,

P = Impact force

m_{eff} = Effective mass of the head

ΔV_{Head} = Change in velocity of head

Statistical Analysis

In the new data set, the differences between the ATDs representing the injured and uninjured players were assessed using a two-tailed, student-t test, assuming unequal variances. A paired sample t-test was conducted to assess the differences between the impact force and impulse acting on the striking and uninjured players to the struck and injured players. The t-tests were conducted using IBM SPSS version 24. A $p < 0.05$ was considered significant.

This new data set was compared to the original data set [43] to assess ATD response differences due to the laboratory methods used. A *z-test* was conducted to compare translational and rotational resultant head accelerations, changes in velocity, HIC₁₅, upper neck tensile and compressive force for each of the injured and uninjured players. The peak impact forces for the

uninjured players were also compared. This *z-test* was conducted using Microsoft Excel, and p-values were looked up in standard z tables.

RESULTS

The data from these laboratory reconstructions are summarized in Tables 7.2 and 7.3.

Case ID	Injury 0 - No 1 - Yes	Impact Force				Head					Head relative to T1					Head M _{eff} [kg]
		Force [N]	Azimuth [deg]	Zenith [deg]	Impulse [N-s]	Acc _R [g]	ΔV _R [m/s]	HIC	α _R [rad/s ²]	Δω _R [rad/s]	ΔV _{H-T1} [m/s]	Δω _{H-T1} [rad/s]	x [deg]	y [deg]	z [deg]	
7	0	4598	-28.0	-74.3	96.5	33.1	4.4	25.9	2275	11.1	2.25	12.0	7.8	-10.3	16.1	25.7
7	1	4309	-88.1	13.8	55.4	51.0	6.3	113.4	3432	20.7	5.54	13.7	7.2	-6.4	8.8	9.3
9	0	6872	-40.4	-81.7	80.6	49.2	3.3	52.7	3149	18.3	2.54	19.0	21.0	20.1	9.3	23.6
9	1	6505	83.8	-37.4	77.7	71.9	8.2	316.9	4170	44.9	8.19	40.2	47.0	10.1	21.6	9.5
38	0	9695	29.1	-72.1	97.5	81.2	2.8	121.0	8179	18.4	2.90	20.6	4.6	-28.3	7.8	42.9
38	1	8198	-86.7	5.5	96.4	107.1	10.0	480.4	5464	50.4	11.05	42.5	40.7	-20.5	39.0	9.7
39	0	5599	55.3	-75.9	72.8	32.4	3.2	28.7	3091	22.3	2.98	23.0	20.8	-13.0	10.4	22.8
39	1	6997	46.4	1.2	75.1	90.9	9.0	365.9	5011	60.3	8.09	53.2	60.6	23.4	53.9	8.9
57	0	11883	20.7	-62.5	158.3	111.9	7.3	359.9	4225	26.8	5.16	26.4	23.7	11.7	27.3	26.5
57	1	6376	-78.8	-3.4	79.1	79.5	8.7	382.9	6329	51.4	9.67	43.5	40.0	-17.1	25.1	9.2
59	0	3187	27.4	-49.3	27.7	29.3	2.1	22.5	1296	12.7	1.65	8.8	5.1	8.3	1.8	13.4
59	0	4131	78.4	-16.1	27.9	56.3	3.2	71.4	4474	26.4	3.20	24.7	21.1	12.5	28.8	8.5
69	0	6722	-18.6	-81.3	138.4	43.3	6.5	38.3	4960	23.9	2.81	22.2	10.3	-20.7	31.0	17.0
69	1	5302	37.5	-1.0	92.5	63.7	11.1	227.8	4977	26.4	9.63	24.6	11.9	15.8	16.3	11.4
71	1	5163	87.6	-21.3	50.2	73.5	6.5	196.9	6547	40.2	6.83	36.4	36.6	-4.1	30.4	7.8
71	0	6142	1.7	-53.5	51.9	62.4	3.1	76.3	3687	20.4	2.42	18.0	3.1	32.9	9.2	17.2
77	0	8188	71.9	-65.1	93.0	71.5	9.6	128.3	5233	34.7	4.59	33.9	37.2	24.5	12.7	15.8
77	1	6145	40.6	-14.0	82.9	82.0	8.9	382.0	4947	33.9	7.79	29.1	21.7	47.0	7.3	9.1
84	0	6941	75.1	-59.2	69.6	63.3	5.8	106.4	5746	34.7	3.83	35.2	34.2	35.0	11.2	14.3
84	1	5361	-51.9	-40.6	62.2	54.1	6.6	142.4	4260	35.0	6.71	30.2	46.0	29.1	32.1	10.0
92	0	10363	75.0	-69.2	82.3	88.3	6.7	222.5	10609	35.8	4.79	37.8	41.1	17.6	25.4	15.8
92	1	9072	-75.4	-21.2	89.4	119.1	11.0	617.6	7620	44.0	11.38	37.3	53.0	28.6	23.0	8.4
98	0	7167	-80.4	-72.7	103.2	56.3	5.6	62.0	6671	33.7	3.60	35.4	15.6	37.8	54.6	18.8
98	1	5080	-73.5	-28.0	73.3	61.2	7.7	203.7	3469	31.4	8.07	26.0	32.6	28.8	20.3	10.1
113	0	4612	-80.3	-75.4	46.5	33.7	2.4	29.8	3131	14.6	2.22	12.9	12.8	-3.1	4.7	19.7
113	1	3835	84.4	6.6	49.2	54.8	6.0	132.1	5616	34.1	6.54	31.2	37.4	9.3	25.3	7.9
118	0	9715	-34.7	-78.8	162.2	74.4	6.4	162.4	3557	18.5	4.69	21.2	5.0	-24.6	4.9	27.8
118	1	4100	41.8	-3.6	67.3	48.8	7.8	106.8	5795	57.6	5.87	54.0	21.2	-29.7	75.6	11.3
125	0	9459	-72.4	-69.0	67.2	76.9	3.9	162.4	10987	24.6	3.62	20.9	21.3	17.6	19.7	18.3
125	1	7988	-86.1	-9.6	79.9	113.8	10.5	558.5	10100	64.7	12.82	55.9	36.4	-24.7	66.5	8.2
148	0	4755	-74.1	-72.9	46.3	31.4	1.9	25.3	1433	14.5	1.88	13.6	11.8	12.5	11.1	23.8
148	1	3607	-51.4	-10.0	46.0	51.3	5.8	113.8	4696	36.8	5.66	32.5	36.0	22.1	37.1	7.7
157	0	7321	53.0	-79.6	84.1	59.7	4.8	48.0	3302	14.4	3.42	15.7	21.1	-5.4	7.2	22.9
157	1	5381	33.2	-8.4	76.3	68.1	8.5	229.0	4564	31.3	5.58	24.1	25.1	14.1	37.4	9.1
164	0	8208	-87.7	-64.7	75.8	72.7	6.4	123.5	6954	34.8	4.93	36.1	41.1	29.4	14.8	14.9
164	1	6693	82.2	-15.7	67.0	88.7	7.9	308.7	7247	47.4	8.53	43.1	38.6	14.2	32.3	8.6
Average Injured	1	5889	-3.2	-11.0	71.8	75.3	8.3	287.0	5544	41.8	8.1	36.3	34.8	8.2	32.5	9.2
Std Dev Injured	1	1573	71.5	15.2	15.2	22.4	1.7	159.2	1670	12.3	2.2	11.6	13.9	21.9	18.5	1.1
Average Uninjured	0	7135	-1.5	-67.0	83.2	59.3	4.7	98.3	4893	23.2	3.34	23.0	18.9	8.1	16.2	20.5
Std Dev Uninjured	0	2364	60.4	15.3	38.2	22.5	2.1	85.2	2753	8.3	1.1	9.0	12.3	20.6	12.7	7.6
p		0.0696	0.9404	<0.0001	0.2383	0.0409	<0.0001	0.0002	0.3923	<0.0001	<0.0001	0.0006	0.0010	0.9885	0.0051	<0.0001
t		1.879	0.075	-11.031	1.209	-2.126	-5.617	-4.359	-0.868	-5.245	-8.140	-3.808	-3.620	-0.015	-3.040	6.577

Table 7.2 – Calculated impact force, ATD head kinematics and head kinematics relative to T1. A p < 0.05 is considered significant.

Case ID	Injury 0 - No 1 - Yes	Upper Neck Forces						Upper Neck Moments					Tensile Force per N body mass [-]
		x - Rwd [N]	x - Fwd [N]	y* [N]	z - Tens [N]	z - Comp [N]	Resultant [N]	x* [Nm]	y - Ext [Nm]	y - Flex [Nm]	z* [Nm]	Resultant [Nm]	
7	0	228	-140	224	173	-3920	3921	10.7	31.6	-20.8	17.4	34.3	0.16
7	1	69	-151	1062	1606	-100	1845	71.9	11.0	-7.5	11.0	72.0	1.71
9	0	261	-175	164	390	-6242	6243	54.5	10.7	-10.2	3.6	55.5	0.40
9	1	41	-171	1031	1103	-3010	3162	51.8	11.6	-12.2	11.8	53.9	1.08
38	0	70	-568	277	144	-8029	8045	15.1	45.2	-36.7	4.1	46.4	0.14
38	1	45	-583	1757	1645	-147	2205	120.0	10.5	-36.0	25.4	121.3	2.00
39	0	63	-324	362	597	-4666	4682	33.9	20.4	-6.6	7.5	40.1	0.69
39	1	1044	-457	1214	2040	-1035	2580	97.1	76.6	-42.4	38.1	124.5	1.80
57	0	896	-228	716	340	-7608	7647	47.6	143.3	-10.9	8.2	147.3	0.40
57	1	134	-291	1787	2002	-477	2109	129.9	8.4	-18.7	26.0	130.6	1.76
59	0	407	22	219	626	-2099	2147	16.4	27.7	-13.4	2.5	31.9	0.66
59	0	85	-18	483	303	-1243	1319	28.7	2.7	-10.0	14.2	30.4	0.30
69	0	894	-39	284	657	-5464	5465	13.3	77.8	-26.0	15.6	79.6	0.71
69	1	2432	-254	1236	2704	-1411	3422	125.3	188.2	-35.8	15.0	226.5	3.04
71	1	223	-185	452	890	-1537	1587	26.8	20.0	-3.7	27.8	36.5	1.08
71	0	472	-46	132	450	-5069	5070	24.4	27.9	-16.9	5.4	35.3	0.54
77	0	670	-478	540	1363	-6965	6997	28.7	46.9	-18.8	14.9	47.3	1.69
77	1	958	-165	857	3373	-1450	3573	52.6	63.2	-36.3	6.0	74.0	2.83
84	0	566	-76	428	677	-5281	5291	48.9	19.8	-22.8	8.4	52.7	0.68
84	1	657	-64	564	1323	-2931	3040	30.8	71.5	-24.0	20.9	73.2	1.07
92	0	393	-68	521	709	-8248	8258	63.2	24.3	-19.8	7.3	63.3	0.78
92	1	335	-51	1104	2831	-2586	3005	46.8	19.3	-25.2	8.6	50.4	2.11
98	0	1047	-136	437	489	-6234	6247	30.2	54.4	-55.2	23.1	62.2	0.58
98	1	474	-44	1207	1444	-2668	2849	66.1	33.0	-20.9	6.8	72.0	1.53
113	0	100	-124	318	481	-4049	4055	24.6	8.7	-12.5	5.1	24.7	0.50
113	1	167	-267	494	1190	-509	1286	43.1	18.4	-16.1	20.3	49.2	1.49
118	0	427	-422	254	306	-7426	7436	60.5	114.6	-26.4	8.1	127.2	0.35
118	1	1446	-366	1251	1700	-891	2371	135.5	132.4	-28.0	48.3	190.4	1.82
125	0	158	-412	547	1053	-7174	7201	53.2	7.6	-25.8	10.1	59.2	0.87
125	1	229	-544	1253	1408	-1050	1817	45.1	27.0	-34.6	42.2	58.4	1.60
148	0	284	-76	255	301	-4207	4211	19.0	10.9	-19.3	8.6	21.1	0.21
148	1	312	-162	439	589	-669	780	22.8	16.4	-19.9	20.2	35.7	0.61
157	0	409	-334	282	330	-6209	6215	29.3	44.2	-32.1	4.6	46.4	0.38
157	1	1041	-89	691	1799	-1239	2093	40.0	75.9	-19.0	23.1	80.7	2.31
164	0	317	-88	925	523	-6010	6017	60.8	127.6	-19.6	16.7	137.9	0.55
164	1	206	-158	1091	1104	-1307	1700	56.0	13.2	-20.1	22.5	60.6	1.18
Average Injured	1	577	-235	1029	1691	-1354	2319	68.3	46.9	-23.5	22.0	88.8	1.7
Std Dev Injured	1	637	165	407	728	933	782	38.2	50.1	10.8	12.2	53.6	0.6
Average Uninjured	0	408	-196	388	522	-5586	5603	34.9	44.5	-21.3	9.8	60.1	0.6
Std Dev Uninjured	0	294	174	200	297	1910	1902	17.6	42.0	11.4	5.6	37.5	0.3
p		0.3257	0.4950	<0.0001	<0.0001	<0.0001	<0.0001	0.0032	0.8822	0.5385	0.0010	0.0765	<0.0001
t		-1.005	0.690	-5.887	-6.184	-8.583	6.903	-3.305	-0.149	0.621	-3.798	-1.839	-6.645

Table 7.3 – ATD upper neck forces and moments. A $p < 0.05$ is considered significant.

Impact Force Vector

The striking and uninjured players had a more horizontal torso angle relative to the playing field (45 ± 12 deg) when compared to the struck and injured players (63 ± 15 deg). This typically resulted in the top part of the striking player's helmet striking the side or front of the struck and injured player's helmet. The zenith (or elevation) of the impact force vector in the struck players acted on the side or front of the headform in the horizontal plane (-11.0 ± 15.2 deg, $t=-11.031$, $p<0.0001$), while in the striking players, the impact force vector was aligned with

the torso and acted vertically on the headform (-67.0 ± 15.2 deg) (Figure 7.2). The impact force and impulse curves for each of the struck and striking players are included in Appendix C.1.

The magnitude of the impact force vector for the ATD representing the striking and

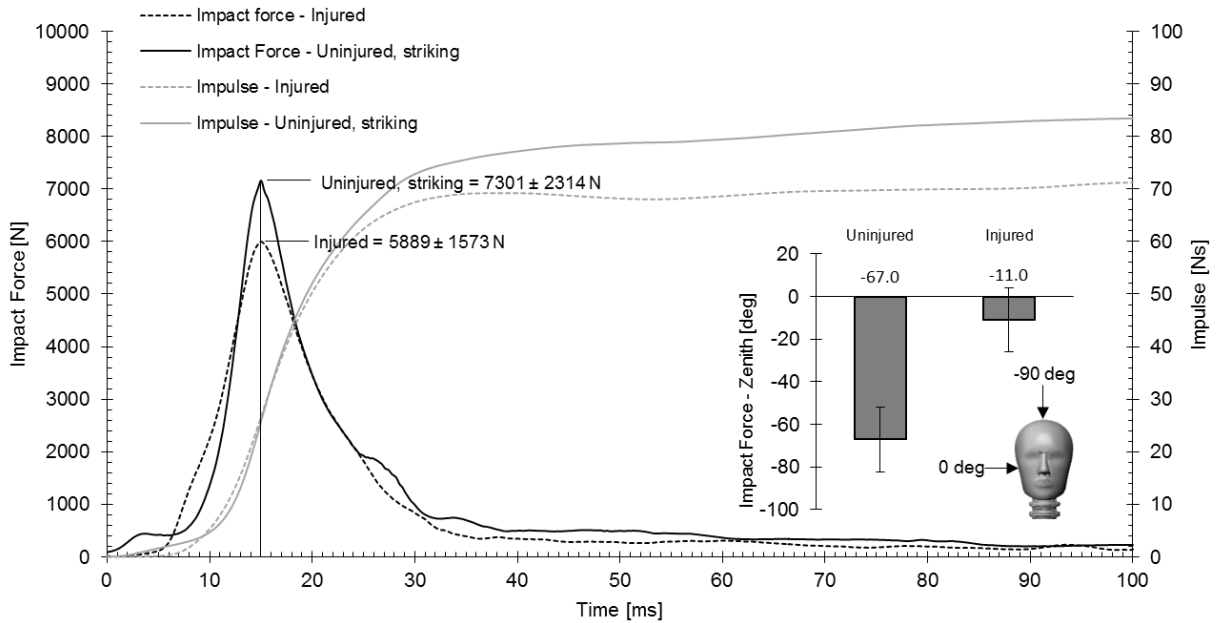


Figure 7.2 – Average impact force and impulse force representing the striking (uninjured) player and the ATD representing the injured player. The data is aligned at the peak calculated impact force.

uninjured players was greater (7135 ± 2364 N, $t=1.879$, $p = 0.0696$) than the ATD representing the struck and injured players (5889 ± 1573 N). In a paired samples analysis, removing case 59 in which neither player was injured, the injured player had a significantly higher impact force than the uninjured player with a mean difference of 1655 N ($t=4.043$, $p=0.0009$). The impulse acting on the headform was also 18 Ns greater in the striking players ($t=2.428$, $p=0.0274$) in a paired samples analysis. This equates to approximately a 20% higher impact force and impulse in the striking players when compared to the struck players.

The calculation of the magnitude of impact force involves the assumption that the helmet mass (1.85 kg) and the headform mass (4.54 kg) remain coupled during the impact to give the

total headform mass (6.39 kg). The helmet mass makes up 29% of the total headform and helmet mass. This is a source of uncertainty in the calculation of impact force. The high speed video illustrates that the impact to the side of the headform results in movement of the helmet on the headform and a decoupling of the helmet and headform mass in the struck players. The striking players' helmets, which involved an impact with the crown of the helmets, engaged the padding, and the relative movement of the helmet on the headform was not as great. This is a possible explanation for the difference in impact force magnitude in the striking and struck players.

Headform Kinematic Responses

The head kinematics and head relative to T1 kinematics are illustrated in Table 7.2. HIC_{15} was higher in the struck and injured players (287 ± 159) when compared to the striking and uninjured players (98 ± 85) ($t = -4.359$, $p = 0.0002$). The higher headform accelerations resulted in greater changes in translational velocity ($t = -8.140$, $p < 0.0001$) and rotational velocity for the struck and injured players relative to the striking and uninjured players ($t = -3.808$, $p = 0.0006$). Although both of the translational and rotational changes in velocity were significantly different between the uninjured and injured players, the translational ΔV for this data set had a specificity and a sensitivity = 1.0 (Figure 7.3). Most of these impacts were from the crown of the striking players' helmets impacting the side of the struck players' helmets. This resulted in the struck players' heads undergoing significantly more rotation about the x-axis ($t = -3.620$, $p = 0.001$) (i.e., lateral bending in the coronal plane) and z-axis ($t = -3.040$, $p = 0.0051$) (i.e., twist in the transverse plane).

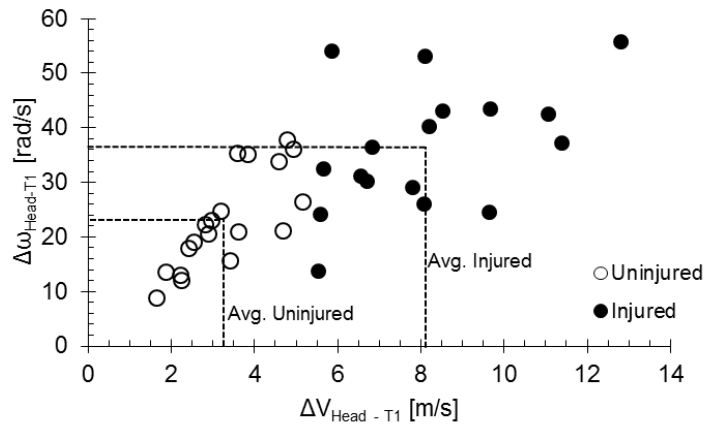


Figure 7.3 – Headform ΔV relative to T1 and headform $\Delta \omega$ relative to T1 for the uninjured and injured players.

Upper Neck Forces and Moments

The upper neck forces and moments were significantly different between the striking and uninjured players and the struck and injured players. As a result of the torso alignment with the crown of the helmet, the striking players' necks underwent high compressive neck loading ($t = -8.583$, $p < 0.0001$), transmitting most of the impact force ($78 \pm 12\%$) through the neck and into the torso. The average compressive force in the neck of the striking players was 5586 ± 1910 N. The struck and injured players underwent neck tension forces of 1691 ± 728 N that were significantly higher than the striking players' neck tension ($t = -6.184$, $p < 0.0001$). The neck tension in the struck and injured players were 1.7 ± 0.6 times the players' estimated body weight and was significantly higher than in the uninjured striking players (0.6 ± 0.3 , $t = 6.645$, $p < 0.0001$). The neck tension in the struck players was coupled with higher upper neck moments in the x-axis ($t = -3.305$, $p = 0.0032$) and z-axis ($t = -3.798$, $p = 0.001$). The significantly higher neck moments mirror the results found in the head rotation relative to T1, as discussed previously. A representative case (Case 38) is presented in Figure 7.4 which illustrates the temporal relationship between the upper neck forces and the rotation of the head relative to T1.

The upper neck force and moment curves as well as head kinematics relative to T1 are for all cases are included in Appendix C.2.

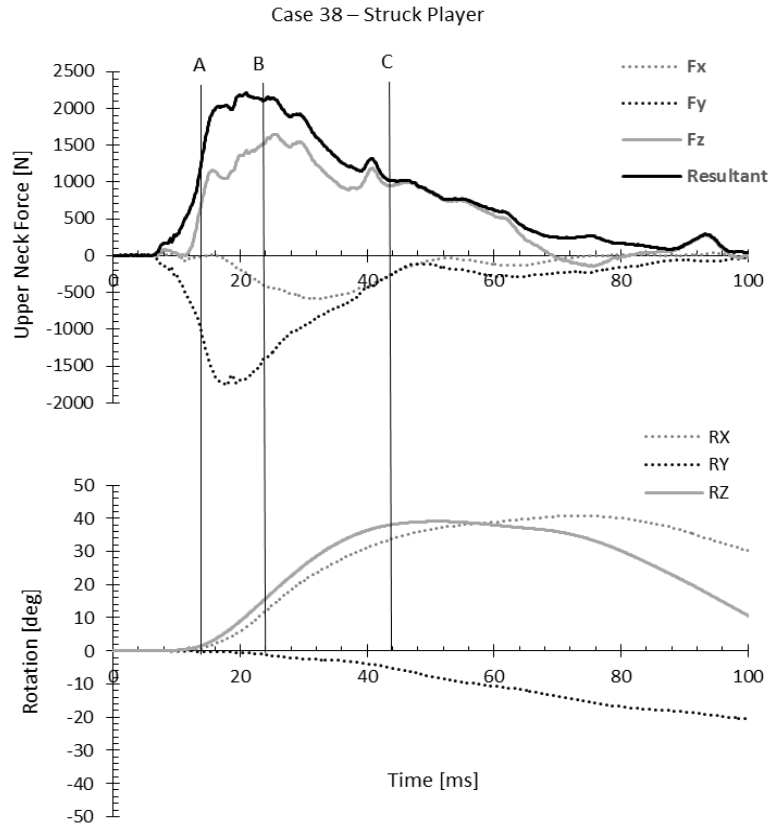


Figure 7.4 – Upper neck force and head rotation relative to T1 for a representative case of a struck an injured player (Case 38). **A** – Maximum impact force, **B** –Maximum neck tension, **C** – Maximum delta-V.

Striking and uninjured kinematics compared to struck and injured kinematics

The average striking and injured player's head kinematics and neck kinetics compared to the average struck and injured players are illustrated in Figure 7.5. Temporally, these data are compared relative to the peak impact force which was defined at 15 ms. The striking player's peak head acceleration and the chest acceleration occurred at 14 ± 0.6 ms and 16 ± 0.5 ms, respectively. The peak neck compression force occurred at 17 ± 0.6 ms. The chest accelerations were greater in the striking players (29.1 ± 10.2 g) than in the struck players (17.6 ± 6.9 g) ($t =$

3.844, $p = 0.0006$). These peak accelerations and compressive neck forces are very close in timing to the peak impact force and confirm that the striking player's torso mass is aligned with the impact force vector, resulting in the impact force being transmitted through the neck to the torso. The $\Delta V_{\text{Head-T1}}$ in the striking players occurred at 32 ± 10.4 ms (or 17 ms after the peak impact force).

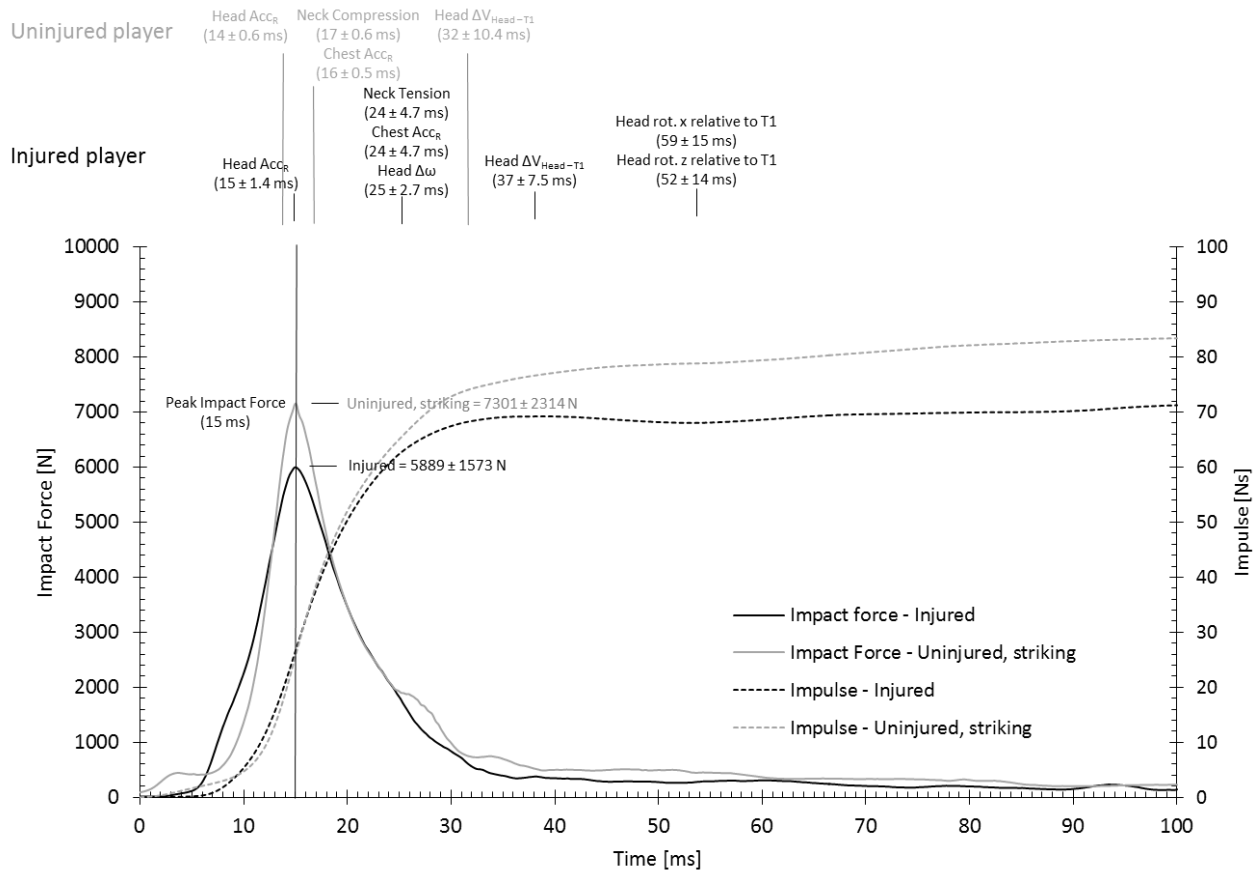


Figure 7.5 – Head kinematics and neck kinetics for the striking and struck player compared temporally with the peak impact force.

The struck and injured players had peak translational head accelerations at 15 ± 1.2 ms (or in line with the peak impact force) and their peak translational chest accelerations occurred at 24 ± 4.7 ms. The peak neck tension forces in these injured players also occurred at 24 ± 4.7 ms, and

peak changes in rotational velocity occurred at 25 ± 2.7 ms. The headform $\Delta V_{\text{Head-T1}}$ occurred later at 37 ± 7.5 ms, and the head continued to rotate relative to T1 until after 50 ms. These data indicate the head is first accelerated in the struck and injured player, and its movement pulls the torso with it. This generates tension in the neck, and the head continues to rotate relative to T1 for approximately 35 ms or greater after the peak impact force and peak head acceleration has occurred.

Effective Head Mass

The effective head mass for each of the striking and struck players was computed using the impulse-momentum relationship. The average effective mass of the struck players was 9.2 ± 1.1 kg compared to the average effective mass of the striking and uninjured players of 21.6 ± 7.0 kg ($t=7.293$, $p<0.0001$). In this calculation Case 59 was removed since neither player was injured. Therefore, these average values are slightly different than Table 7.2. This higher effective mass is the result of the striking player's torso mass being aligned with the impact force vector. This results in a significantly lower headform ΔV_{Head} in the striking and uninjured players than the struck and injured players. The total headform mass of the struck player was measured to be 6.39 kg and the average zenith of the struck player was -11 deg (or 11 degrees downward). This indicates that only a small amount of the struck and injured player's torso mass was involved in the impact.

Comparison to Original Data Set

There were several differences in the laboratory setup between this current study and the original data set. Specifically, the original data set had only a head and neck along with a 7.4 kg carriage that were moving. The impact occurred with the head and neck constrained to the carriage that was riding on a set of rails and with the stationary ATD suspended on a set of

cables. Therefore, it was not the intent to reproduce the original data set; however, it is interesting to see what differences there are between this new data set and the original one. The comparison of several parameters is illustrated in Table 7.4.

Variable	Units	Injured								Uninjured							
		Original			New			z-test		Original			New			z-test	
		mean	std. dev	n	mean	std. dev	n	z	p	mean	std. dev	n	mean	std. dev	n	z	p
Head Acc _R	[g]	94	28	25	75	22	17	2.401	0.016	56	22	27	59	22	19	-0.500	0.618
Head ΔV _R	[m/s]	7.2	1.8	25	8.3	1.7	17	-1.971	0.048	4.1	1.2	27	4.7	2.1	19	-1.146	0.254
Head α _R	[rad/s ²]	6432	1813	25	5544	1670	17	1.633	0.104	3983	1402	27	4893	2753	19	-1.325	0.186
Head Δω _R	[rad/s]	34.8	15.2	25	41.8	12.3	17	-1.642	0.102	26.1	10	27	23.2	8.3	19	1.073	0.284
HIC ₁₅	[-]	381	197	25	287	159	17	1.704	0.090	117	101	27	98	85	19	0.679	0.502
Upper Neck Fz	[N]	1704	432	5	1691	728	17	0.049	0.968	-4221	1885	27	-5586	1910	19	2.401	0.016
Peak Impact Force	[N]	-	-	-	-	-	-	-	-	7191	2352	27	7135	2364	19	0.079	0.944

Table 7.4 – Comparison of the ATD kinematic data to the original dataset [1]. A $p < 0.05$ is considered significant.

The peak impact force as calculated of the striking, uninjured player in the new data set (7135 ± 2364 N) and the original data set (7191 ± 2352 N) were essentially the same ($z = 0.079$, $p = 0.944$). There were significant differences in the struck and injured player ATDs' responses when compared to the original data set. The resultant head acceleration was 75 ± 22 g (new) compared to 94 ± 28 g (original) ($z = 2.401$, $p = 0.016$), and the HIC₁₅ was also lower ($z = 1.704$, $p = 0.090$). The new data set also had significantly higher head ΔV ($z = -1.971$, $p = 0.048$) and higher head rotational velocity ($z = -1.640$, $p = 0.102$). The HIC₁₅, head rotational velocity, and rotational acceleration were not significantly different. The upper neck tension in this data set ($n = 17$, 1691 ± 728 N) was similar to the limited data available from the original data set ($n = 5$, 1704 ± 432 N) ($z = 0.049$, $p = 0.968$).

The differences in head kinematics in the struck and injured players appear to be related to the differences in the duration of the head acceleration in this new data set compared to the original data set (Figure 7.6). The duration of the head acceleration was approximately 19 ms in this new data set compared to 15 ms in the original data set. This equates to an increase in time of

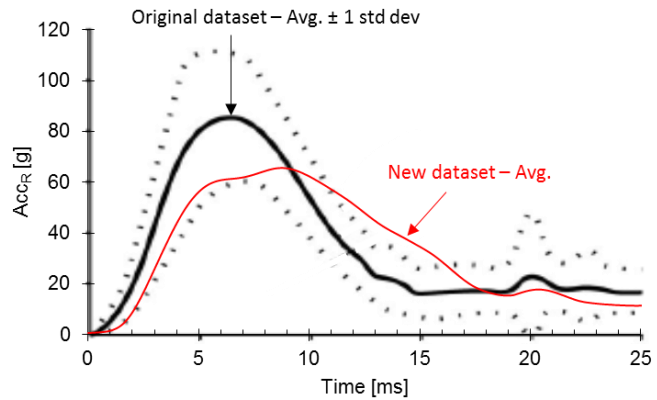


Figure 7.6 – Comparison of head resultant translational acceleration from the struck players in the original dataset [1] to this study. The data in this graph was re-zeroed to correspond to the original dataset so the timing in the graph appears different than previous graphs in this study.

approximately 27%. The head translational and rotational accelerations in this new data set were 20% and 14% lower than the original data set. The peak impact force differed by less than 1% between the two data sets (original = 7191 +/- 2352, new = 7135 +/- 2364). The use of the peak impact force and the peak head acceleration is an alternate method to estimate the effective mass of the headform. The effective mass of the headform in the new data set was 9.7 kg (7135 N / 75 g) and 7.8 kg (7191 / 94 g) in the original data set, using this method of calculation. The effective head mass is greater in this new data set than in the original data set by approximately 25%. This could be due to the higher mass of the head and torso on the struck player used in the new data set (57 ± 12 kg) compared to only the mass of carriage (7.1 kg) [2] and head and neck used in the original data set. This higher effective head mass could explain the lower headform translational accelerations in the struck player for this new data set. This is also consistent with the neck compression forces in this new data set (5586 ± 1910 N) being higher than the neck compression forces in the original data set (4221 ± 1885 N).

DISCUSSION

Eighteen of the original 31 laboratory reconstructions [43] from the helmet-to-helmet hits resulting in concussion in the NFL have been re-created in this study to generate a new data set related to these impacts using new laboratory methods. The laboratory methods presented herein are an improvement on the original data set since they more closely represent the pre-impact closing momentum of these players. This new data set also includes additional information related to the upper neck forces and moments on each of the ATDs representing the striking and struck players. These data indicate that the striking and uninjured players in this data set delivered a tackle by orientating their torsos more horizontally than the struck players. This orientation resulted in the crown of the striking player's helmet impacting the side of the struck player's helmet with the mass of the striking player's torso aligned with the impact. The striking player's torso alignment with the head resulted in a higher effective mass of the striking player's head when compared to the struck player. The impact to the side of the struck player's helmet caused the struck player's head to accelerate prior to the torso, first resulting in higher tension in the struck player's upper neck, and later, in higher neck moments and rotation of the head relative to the torso in the coronal (x-axis) and transverse planes (z-axis). These measurements, as well as the change in velocity of the head relative to the torso, were all significantly higher in the injured players than in the uninjured players. The higher change in velocity of the injured player (8.12 ± 2.19 m/s) and the larger relative movement of the head to the torso are consistent with the animal experiments of Denny-Brown and Russell [31]. Denny-Brown and Russell [31] found that a change in velocity of approximately 8.7 m/s was required, over a very short period of time, to repeatedly produce concussion in the cats and primates that they studied. They also found that head movement relative to the torso was required for concussion to occur.

Head movement relative to the torso results in tension occurring in the cervical spine. This tension can be generated either by the head rotating (flexion, twist, or lateral bending) relative to the torso or the head being accelerated and pulling the torso mass along with it. The injured players in this study had both of these mechanisms occur. Chancey et al. [106] used a musculoskeletal finite element model and predicted the tolerance limits of 3100 N and 3700 N for the relaxed and tensed neck, respectively, indicating that failure is expected in the upper cervical spine (Atlanto-occipital – C2) due to the larger muscular volume in the lower cervical spine. It has been shown that the upper cervical spine is the least stiff, the highest strains occur in this region when a tensile load is applied to the head [13, 41, 42], and that stiffness reduces with repeated application of tensile load [13]. In the human cadaver, average failure loads from quasi-static tensile testing are approximately 3100 N [92, 113], with most cadaveric subjects having injuries in the upper cervical spine. The neck tensions in these concussed NFL players are less than the neck tensions resulting in failure of the cervical spine in musculoskeletal cadaveric studies when only a tensile load is applied to the head (Figure 7.7).

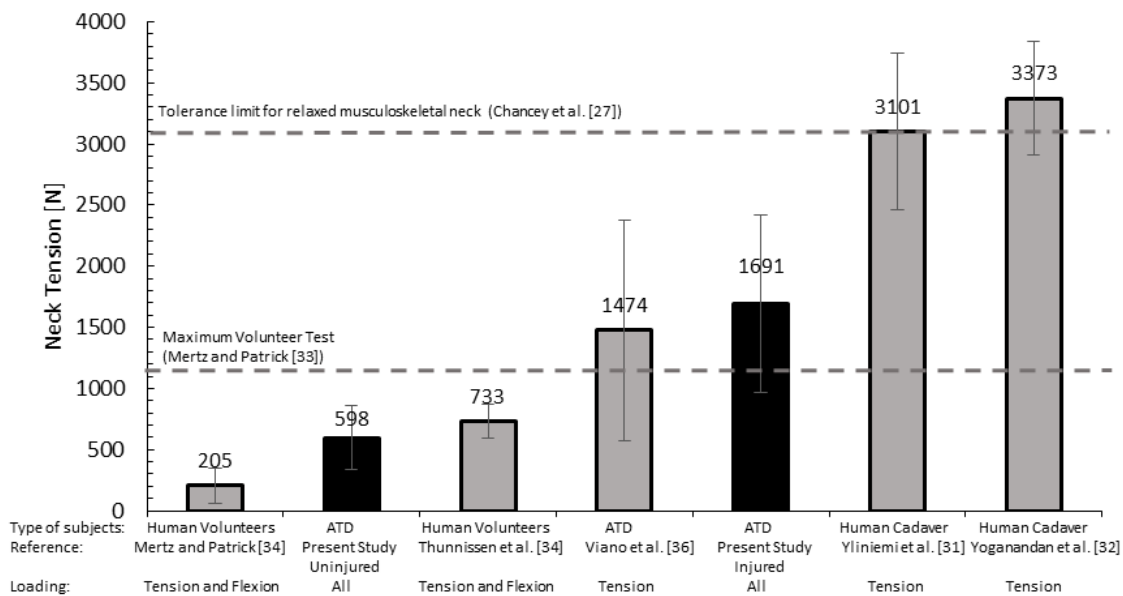


Figure 7.7 – Comparison of the neck tensile forces in this dataset to neck tensions reported in human volunteers, cadaveric studies and other biomechanical studies.

In human volunteer studies, Mertz and Patrick [97] have reported on the highest static tensile loads when applied in pure tension of 1112 N and also tensile loads combined with forward flexion [98]. Thunnissen et al. [99] published corridors of dynamic neck tensile loading to human volunteers exposed to severe frontal sled testing. These volunteers sustained neck tensile loads of 733 N combined with forward flexion of the head. Viano et al. [111] studied ATD responses to Olympic boxers' punches. The uppercut resulted in resultant upper neck loads of 1486 ± 910 N which would be primarily neck tension. The uppercut punch is an effective knockout punch in boxing despite these punches resulting in low HIC_{15} (17 ± 19), low translational accelerations (24.1 ± 12.5 g), and low rotational velocities (17.5 ± 5.0 rad/s). Therefore, these kinematic parameters do not provide an explanation for injury in this condition. The neck tensions in these concussed NFL players are greater than the neck tensions found in human volunteer testing and in the range of the uppercut punch delivered by Olympic boxers. In addition to the high neck tensile loads, the struck players' heads underwent rotation relative to their torsos. The combination of these loads could result in high strains in the upper cervical spine and brain stem [28]. This is consistent with the tensile mechanism of injury discussed by Friede [10, 11] and others [12, 21, 22, 29, 31, 32, 33] who have discussed strains in the upper cervical spine and brain stem related to injury. The location of injury provides a possible explanation for many of the signs and symptoms of concussion in professional athletes (Chapter 1) and an explanation of posturing found in athletes immediately after the injury [6].

In contrast to the struck and injured players, the striking and uninjured players underwent peak neck compression forces which are due to the striking players aligning their heads with their bodies prior to delivering the tackle. Viano and Parenteau [112] have analyzed various drop and pendulum impacts to the crown of cadaver heads. Impacts to the crown of the head

typically result in bony injury to the spine due to compressive forces being transferred through the skull and spine and do not primarily result in brain stem injury. When tensile forces, which could include rotation of the head relative to the torso, are applied to the human head, the load is distributed through the soft tissues, such as, ligaments, muscles, brain stem, and spinal cord, making these tissues susceptible to injury; whereas, in a compressive loading, the load is distributed through the body's bony structure.

The tensile loading at the upper cervical spine and rotation of the head relative to the body each would result in tensile strain along the axis of the upper cervical spine that can be transferred to the brain stem [28]. Neck tensile forces and rotation of the head relative to the torso were significantly higher in the ATD representing the struck and injured players in this study. The headform translational and rotational changes in velocity relative to T1 were also significantly higher in these players. The combination of these suggest that some combination of strain and strain rate [102, 113, 114] or, alternatively, power [115, 116] in the upper cervical spine, may be an important predictor of concussion. King et al. [117] have shown that the product of strain and strain rate was the best predictor of concussion using a finite element model to simulate head response to American football impacts. The injury relationship of neck tensile loading and rotation of the head relative to the torso is significant since it has been previously found that the added mass of the helmet can result in an increase in tensile forces and rotation of the head relative to the torso [82, 86, Chapter 6]. This indicates that the increasing mass of football helmets could have a negative effect on injury, particularly in athletes with lower neck strength [45].

There are several limitations of this study. This study was performed using the Hybrid III ATD in a laboratory test environment. There may be some question regarding the biofidelity of

the Hybrid III ATD in these combined loading conditions; however, it is currently the best available method for reconstructing these on-field collisions in the laboratory. It provides critical information in assessing the injury trends in injurious and non-injurious collisions. The Hybrid III is not human; therefore, tissue level strains could not be directly assessed. The data acquired could now be used in conjunction with FE modelling to estimate tissue level responses more accurately than previous data since this new data set also includes torso motion. Additionally, the design of the Hybrid III has a neck simulating some muscle tensing, but there is no active musculature in any of the current ATDs. These effects could also be studied using a biofidelic human finite element model.

The study is also limited since only eighteen cases were reconstructed and each of these cases simulated a direct helmet-to-helmet impact. The head and neck responses presented in this study would be representative of these types of impacts. Impacts to the ground or body of opponents should also be studied to assess biomechanical impact responses in these conditions. The laboratory reconstruction of these collisions is also limited in that the verification of the reconstruction was based upon a visual comparison of game video to the laboratory reconstruction using a similar camera view. The optimal method of comparison would involve a more detailed analysis of the game film to track the three dimensional helmet kinematics pre and post impact. This data could then be compared more accurately with the ATD response in the laboratory impacts. The present study used the impact orientation and location had also been previously analyzed and published by Pellman et al. [43]. The present study was conducted to provide an improvement on the laboratory methods used to reconstruct these collisions by more closely matching the pre-impact momentum of the players and allowing for uninterrupted post-impact motion.

Chapter 8 – STRAIN AND STRAIN RATE IN THE BRAIN STEM AND CERVICAL SPINE OR POWER AT THE ATLANTO-OCCIPITAL JOINT AS BIOMECHANICAL PREDICTORS OF CONCUSSION

INTRODUCTION

There are important data supporting the forces and deformation at the atlanto-occipital joint and brain stem causing concussion [10, 11, 13, 21, 22, 29, 31, 32, 33]. Common signs of concussion and most symptoms of concussion could correlate to injury of the spinal cord, brain stem, and/or midbrain [3, 12, Chapter 1]. McCrory et al. [6] have also discussed posturing of unconscious athletes and indicated potential brain stem involvement. The role of neck tension and strain in the brain stem could be an important predictor of concussion.

Breig [28] analyzed the biomechanics of the central nervous system on 183 human cadavers. He reported, flexion and lateral rotation resulted in elongation of the spinal canal and spinal cord and that tension generated in the spinal cord could be transmitted from the spinal cord to the brain stem, cerebellum, and cranial nerves (V – XII), resulting in tension of these brain tissues. Neck extension resulted in an overall shortening of the spinal canal and cord and a thickening of the spinal cord. Ji et al. [118] and Ji and Margulies [119] reported on caudal displacement of the brain stem and pons when volunteers underwent flexion in an MRI study. This indicates strains occur in this area. Others have imaged the human [34, 35, 91, 103, 104] and primate [36] head and neck and found elongation of the cervical spinal canal and cord in flexion and shortening in extension. Human volunteers' cervical spine kinematics while undergoing axial rotation [37, 38, 120] and lateral rotation [39] have also been documented using imaging; however the research lacks discussion on the lengthening of the cervical spinal canal under these head motions, and change in length of the spinal cord is only discussed in sagittal plane motion [35, 103, 104].

Friede [10, 11] studied the mechanics of concussion by evaluating the symptoms and neuropathology in the upper spinal cord and brain stem of cats as a result of impacts and drop

tests with the head supported. The latter were non-impact tests and resulted in cervical spine stretching. Each of these loading conditions resulted in the same symptoms: loss of consciousness, drowsiness, sluggishness, and poor coordination. Temporary physiological changes included bradycardia, tachycardia, respiratory failure, and loss of corneal reflex. The loss of corneal reflex lasted less than four minutes in all cats, with most being less than one minute. Both conditions also resulted in, first, a lesion at the level of C1-C2 in the spinal cord in which the thick fibers underwent Wallerian degeneration. Second, there was a subsequent axonal reaction, resulting in chromatolytic cells concentrated in the reticular formation and lateral vestibular nucleus of the brain stem. The more severe injuries also resulted in chromatolytic cells in the red nucleus. The lesion at the level of C1 occurred, but chromatolytic cells in the brain stem did not, in the subjects that expired as a direct result of the testing. Friede [11] concluded that craniocervical stretch is the most important factor for the mechanics of concussion.

Antona-Makoshi et al. [121] studied a head and cervical spine finite element model of the monkey by reproducing experimental test data of Ono et al. [48] and found maximum principal strains in the brain stem to be a significant predictor of concussion. Giordano and Kleiven [46] studied axonal strain in the brain by conducting finite element modelling using a head and cervical spine model based upon the NFL reconstructions [43]. They found strain in the axonal direction is a better predictor of injury than maximum principal strains and that axonal strain in the brain stem was the best predictor of injury. The simulations did not incorporate a biofidelic cervical spine model.

Laboratory testing was conducted to recreate injurious and non-injurious collisions in American football (Chapter 7). Briefly, these data indicated that injured players' heads

underwent higher lateral (coronal plane or x-axis) rotation ($t=-3.620$, $p=0.001$) and axial rotation (z-axis) ($t=-3.040$, $p=0.0051$) relative to the torso and higher neck tensile forces ($t=-6.184$, $p<0.0001$) than uninjured players. The injured players also had significantly higher head changes in velocity relative to the body ($\Delta V_{\text{Head-T1}}$, $t=-8.140$, $p<0.0001$) ($\Delta \omega_{\text{Head-T1}}$, $t=-3.808$, $p=0.0006$) than those of uninjured players. The reconstructed collisions were primarily impacts to the side of the head and, therefore, did not result in flexion of the head in the injured players. This may be an explanation why no significant differences were found with flexion.

The aim of this chapter is to understand 1) The change in length of the cervical spinal canal as a result of movement of the head relative to the body, 2) The potential strain and strain rates along the axis of the spinal cord and brain stem during these movements, and 3) The strain and strain rates in the spinal cord and brain stem as well as power at the atlanto-occipital junction as a biomechanical predictor of concussion in injured and uninjured NFL players.

MATERIALS AND METHODS

Change in length of the cervical spinal canal

Data available in previously published in-vivo imaging studies

A literature review was conducted to locate in-vivo data on segmental vertebral body motion of the cervical spine. Emphasis was placed on finding studies which included both translational and rotational motion of individual vertebrae such that they could be reconstructed in CAD software. There was one study located for each of flexion (+Ry) and extension (-Ry) [91], lateral bending (Rx) [39], and axial rotation (Rz) [37, 38] which included sufficient information to fully reconstruct the cervical spine motion. The study by Dvorak et al. [91] was conducted with combined flexion and extension; therefore, an approximation was made that half of the cervical spine (C1-C7) range of motion is flexion and half is extension [35, 53]. In a tensile loading

condition, cadaveric testing was utilized. The axial tensile testing on cadavers resulted in average neck stiffness of approximately 1700 N/cm [92, 93, 105, 122] with a total displacement at failure of approximately 2 cm. Yliniemi et al. [93] reported the total strain of the cervical spine of 16.7% at failure. This compared closely to the radiographic study conducted on primates by Kroeker and Ching [41] who found an average 16% vertebral column strain at failure. This was an average strain along the length of the cervical spine and these studies both indicated that higher strains occurred in the upper cervical spine. Kroeker and Ching [41] had measured individual vertebral body motion using radiographic markers. This study was used to estimate segmental motion of the vertebral bodies in the human.

The geometrical data from the head and neck model of the GHB model were used in this study [123]. The geometry from each of the cervical vertebrae was exported from the GHB model in neutral posture. The data was imported into Polyworks IMInspect (InnovMetric, Quebec, Canada) and points were defined on the anterior, left, right, and posterior aspects of the spinal canal on each vertebral body (Figure 8.1). Linear measurements were taken in the neutral posture. The translations and rotations from the in-vivo data was then applied to each of the vertebral bodies in the computer model and the measurements were recorded between these same data points. The change in length of the spinal canal (ΔL) between each of the individual vertebral bodies was computed for the full cervical range of motion from the volunteer studies. In the tensile loading condition, the full range of motion was defined as the displacement at failure in the cadaveric studies. Changes in length were computed at each of the anterior, posterior, and lateral locations of the spinal canal. The change in length used in this study is the average change in length in the spinal canal from C1-C5. An increase in length corresponds to a

positive number while a decrease in length is negative. The strain in the spinal canal was estimated using equation 1.

$$\Delta L_{C-spine} = \ln \left(\frac{L_{Cspine-final}}{L_{Cspine-initial}} \right) \times 100 [\%] \dots\dots [1]$$

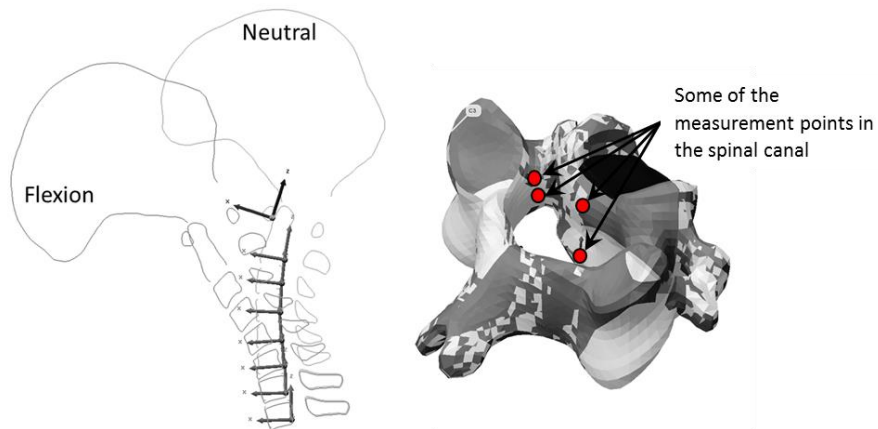


Figure 8.1 - Coordinate system setup for in-vivo studies and sample of measurement points in the spinal canal.

The change in length per unit of head rotation (% per degree of rotation) or translation (% per Newton of force) was calculated so that these data could be used to estimate strain in the spinal canal as a result of head movements.

Finite element model simulations

The head and neck were segmented from the whole GHB model at the first thoracic vertebral body along with all relevant musculature and ligaments. Validation of the head and neck was previously completed using cadaveric and volunteer experimental data. A detailed description of the development and validation of these individual head and neck models has been presented elsewhere [89, 90].

The LS-Dyna Software (Livermore Software Technology Corporation, Livermore, CA) was used to run the simulations. The scalp, skull, and each vertebrae were converted to rigid bodies. The nodes at the base of the model (base of C7 vertebral body) were fully constrained. Loading was applied as a constant force (tension, flexion, extension, and lateral bending) or torque (axial rotation) using the load node command in LS-Dyna (Figure 8.2). The loads were applied independently of one another to the same node, which was located on the top of the scalp and above the occipital condyles, and simulations were conducted for a duration of 30 milliseconds. This was not sufficient time for the dynamic simulation to result in full range of motion of the head and cervical spine; however, the rates of displacement were similar to those reported in helmet-to-helmet hits in the NFL [43]. Three separate tensile loading simulations were performed. The tensile load curve was developed based upon the upper neck tension in Viano et al. [44] (Case 38) and the curve was scaled to have peak neck tensions of 500, 1500, and 2500 N occurring at 20 milliseconds.

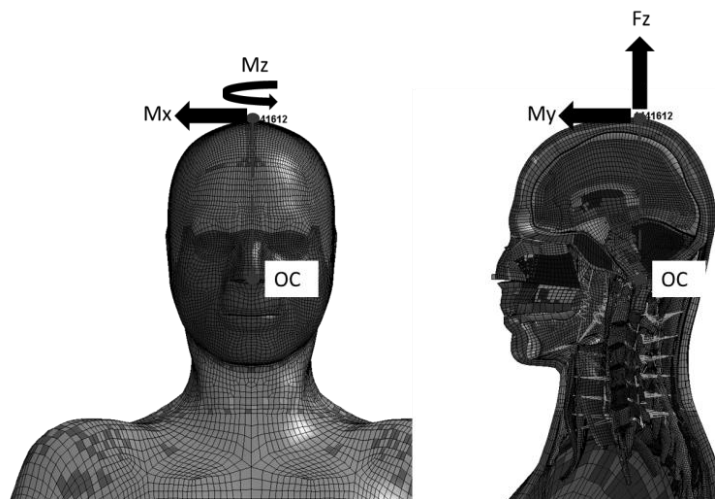


Figure 8.2- Location of loading applied to FE model

The kinematics of the vertebrae and skull were output. The change in length of the cervical spinal canal was measured using points defined on the anterior, left, right, and posterior sides of the spinal canal and a strain per unit of head movement (% / N or % / deg) was estimated. This was done similar to the analysis based upon in-vivo data so that the data could be compared.

Estimate of strain and strain rate in the CNS in injured compared to uninjured American football players

Lau and Viano [113] and Viano and Lau [114] have discussed the importance of considering both the displacement and velocity of displacement when assessing soft-tissue damage and introduced the Viscous Criterion (VC). This criterion considers that at low velocities a tissue can elongate to a greater degree without injury than when subjected to high rates of displacement. This is consistent with the findings of Galbraith et al. [124] who subjected squid giant axons to tensile loading at different rates and found that, for a given elongation, axons that elongated at higher rates sustained more severe, non-reversible damage.

Motion of the head relative to the body can result in strain in the central nervous system (CNS) [28, 107]. The pathways in the brain stem and upper spinal cord travel predominantly superior-inferior along the brain stem and spinal cord axis [52]. Therefore, the change in length of the CNS in this region is expected to be representative of axonal strain in the brain stem and spinal cord. The GHB model was not used to directly assess tissue level strains in the CNS because the version used in this study did not incorporate a biofidelic model of the spinal cord, it did not predict axonal strain and there was no specific validation of the spinal cord and brain stem reported in the literature.

Previous studies [41, 93] discuss a coupling ratio of 0.49 to 0.75 to estimate strain in the CNS compared to spinal canal elongation. The study by Kroeker and Ching [41] based this coupling ratio upon tensile loading applied to primate heads with the primate head in extension. Extension of the cervical spine reduces the length of the cervical spinal canal and can induce slack into the spinal cord.

Therefore, it is expected that head extension would result in a lower than actual coupling ratio in the study by Kroeker and Ching [41]. Yuan et al. [35] and Smith [36] reported caudal (downward) displacement of the spinal cord, relative to the vertebrae, above the C4-C5 vertebrae and rostral (upward) displacement below C4-C5 (Figure 8.3). In the human, the average length from the posterior commissure to the obex is 49 mm [52] and from the obex to C5 vertebrae is approximately 95 mm (from GHBMC model). Based upon these dimensions, a coupling ratio of 0.65 was used to estimate the axonal strain in the cervical spinal cord and brain stem. This coupling ratio was applied to the change in length of the cervical spine from OC-C5 to provide an estimate of strain in the CNS as illustrated in equation 2.

$$\varepsilon_{CNS} = 0.65 \times \Delta L_{C-spine} [\%] \dots \dots [22]$$

Using this method, strain in the CNS was calculated along the individual ranges of motion to characterize the effects of neck tension (ε_{Tz}), lateral rotation (ε_{Rx}), flexion (+) or extension (-) (ε_{Ry}) and axial rotation (ε_{Rz}) of the head relative to T1. These components were calculated by multiplying the change in length of the cervical spinal canal (OC-C5) by a factor of 0.65. Based

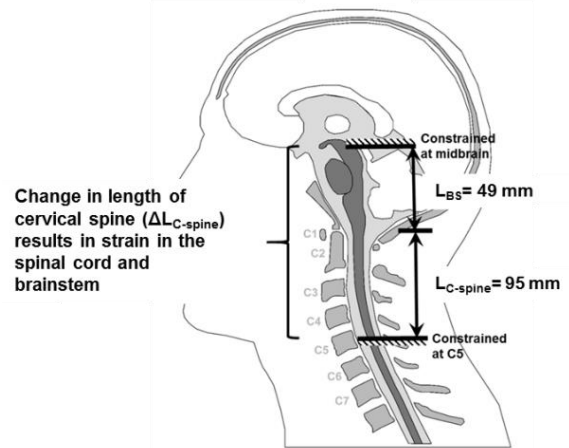


Figure 8.3 - Relationship of the change in length of the cervical spine to strain in the CNS

upon the principle of superposition, the time-varying sum of the individual strains was then calculated to calculate the total strain (ϵ_{Tot}). Strain rate ($\frac{d\epsilon_{Tot}}{dt}$) was calculated by first filtering the total strain with a CFC 60 filter followed by differentiation. The time varying product of $\epsilon_{Tot} \frac{d\epsilon_{Tot}}{dt}$ (strain x strain rate) was calculated for the total strain since this has been shown to be a good predictor of axonal injury [50, 117, 125].

Power at the atlanto-occipital joint as a biomechanical predictor of concussion

DiLorenzo [115] has recommended the use of a power to predict bodily injury. Newman et al. [116], in their development of Head Impact Power (HIP), have illustrated the relationship between power and the Viscous Criteria (VC) [125] when applied to an elemental mass of brain matter. In a rodent head model, Li et al. [126] have utilized an alternative method of calculating power and illustrated that power could be an important predictor of traumatic axonal injury.

The HIP proposed by Newman et al. [116] utilized the mass and inertia of the headform only to calculate the HIP but in the impacts a helmet was actually worn. In helmeted impacts, the mass of the helmet can increase the effective mass of the head by approximately 50% (Chapters 4 and 6). Therefore, it seems important to include the mass and inertia of the helmet in these helmeted impacts. It is difficult to know how the helmet is coupled to the head during the impact due to the helmets' movement relative to the headform. This movement may vary, depending on the impact location or orientation on the headform. Li et al. [126] removed the mass term from the power equation because it was considered to be a constant in their analysis of un-helmeted head impacts using a modified Marmarou model. The method of calculating power utilized by Li et al. [126] is proportional to the Wayne State Tolerance Curve (WSTC) and Gadd Severity Index (GSI) [116] but does not consider headform and helmet mass effects, nor does it consider the rotational component of power.

In the Hybrid III ATD the upper neck power could be calculated directly using the forces measured at the atlanto-occipital joint. In the present study, upper neck power was calculated using two separate methods. The method utilized in equation 3 is a generalized approach that does not consider the time varying effects, similar to the approach by Li et al. [126]. Equation 4 is the time-varying sum of power. The effects of neck elongation have also been incorporated in equation 4 and the components of power that result in elongation of the cervical spine are assigned a positive value while those that result in shortening of the cervical spinal canal result in negative value. The ΔV used in these calculations are $\Delta V_{\text{Head-T1}}$.

$$\text{Power} = \frac{m\Delta V_x^2 + m\Delta V_y^2 + m\Delta V_z^2}{\Delta t_{\Delta V}} + \frac{I_{xx}\Delta\omega_x^2 + I_{yy}\Delta\omega_y^2 + I_{zz}\Delta\omega_z^2}{\Delta t_{\Delta\omega}} \quad [\text{kW}] \dots [3]$$

$$\text{Power} = \sum_{t=0}^n F_x |\Delta V_x| + |F_y| |\Delta V_y| + F_z |\Delta V_z| + |M_x| |\Delta\omega_x| + M_y |\Delta\omega_y| + |M_z| |\Delta\omega_z| \quad [\text{kW}] \dots [4]$$

Statistical Analysis

The differences between the injured and uninjured players were assessed using a two-tailed, student-t test, assuming unequal variances. A $p < 0.05$ was considered significant. The t-tests were conducted using IBM SPSS version 24. Binary logistic regression is a method of analysis used to assess injury probability with one dichotomous variable (not injured (0) and injured (1)). A binary logistic regression analysis was conducted to assess the injury predictors of total strain (ε_{Tot}), strain rate ($\frac{d\varepsilon_{\text{Tot}}}{dt}$), the time varying product of ε_{Tot} $\frac{d\varepsilon_{\text{Tot}}}{dt}$ and upper neck power. Logistic regression analysis was also completed for several global head injury predictor's ($\Delta V_{\text{Head-T1}}$, $\Delta\omega_{\text{Head-T1}}$, Acc_R , HIC_{15} and upper neck tension) to compare the strength of these global injury predictors to injury predictors related to the spinal cord and brain stem strain. The -2Log Likelihood ratio (-2LLR), Chi-squared and fraction of impacts predicted correctly at a 50%

probability of injury were calculated to determine whether there was a statistically significant relationship between injury outcome and the predictor variable.

RESULTS

Change in length of the cervical spinal canal

The in-vivo data indicates the cervical spinal canal elongates in lateral bending, axial rotation, flexion, and tension (Table 8.1). The elongation of the spinal canal in tension (18.2%) is the greatest in comparison to other head motions; however, this represents elongation at failure in comparison to the others which represent elongation at the range of motion of the volunteers. Flexion resulted in an elongation of the posterior of the spinal canal of 14.1%, axial rotation resulted in elongation of 8.9%, and lateral rotation resulted in an elongation of 4.9% on the contralateral side of rotation. The spinal canal elongation values were measured from C1 to C5 based upon previous research [35, 36] reporting caudal movement of the spinal cord relative to the spinal canal above C4-C5. This indicates there is potential for strain in the CNS. In tension, the segmental elongation is greatest at the C1-C2 segment in comparison to C2-C5. The segmental elongation in axial rotation is also the greatest at the C1-C3 segment and the remainder of the cervical spine (C3-C5) had shortened. Extension resulted in a shortening of the anterior of the spinal canal of 2.4% from C1-C5.

	Lateral rotation		Flexion		Extension		Axial rotation		Tension	
	FE Model	In-Vivo	FE Model	In-Vivo	FE Model	In-Vivo	FE Model	In-Vivo	FE Model	In-Vivo
	$\Delta L/\text{head rot}$	$\Delta L/\text{head rot}$	$\Delta L/\text{head rot}$	$\Delta L/\text{head rot}$	$\Delta L/\text{head rot}$	$\Delta L/\text{head rot}$	$\Delta L/\text{head rot}$	$\Delta L/\text{head rot}$	$\Delta L/\text{Newton}$	$\Delta L/\text{Newton}$
	[%/deg]	[%/deg]	[%/deg]	[%/deg]	[%/deg]	[%/deg]	[%/deg]	[%/deg]	[% / N]	[% / N]
Average of C1-C5	0.21	0.18	0.33	0.21	0.03	-0.04	0.03	0.16	0.0048	0.0059
C1-C2	0.19	-0.03	0.50	0.13	0.11	-0.15	-0.04	0.42	0.0061	0.0072
C2-C3	0.23	0.41	0.25	0.18	-0.01	0.02	0.07	0.50	0.0043	0.0054
C3-C4	0.24	0.16	0.30	0.26	-0.04	-0.01	0.03	-0.07	0.0046	0.0053
C4-C5	0.18	0.17	0.29	0.28	0.06	-0.02	0.05	-0.22	0.0040	0.0057
C5-C6	0.14	0.19	0.28	0.46	0.07	-0.11	0.06	0.03	0.0031	0.0057
C6-C7	0.15	0.27	0.40	0.29	0.07	-0.14	0.08	-0.09	0.0026	0.0054
Head rot. or tensile force										
at full range of motion		28.1		66.6		71.8		56.4		3100
(ROM) [deg or N]										
Change in length at full		4.92		14.12		-2.84		8.87		18.24
ROM [%]										
Coupling Ratio		0.65		0.65		0.65		0.65		0.65
CNS strain (C1-C5) [%]		3.20		9.18		-1.84		5.77		11.86
CNS strain (C1-C3) [%]		3.45		6.69		-2.84		16.87		12.65

Table 8.1 – Change in length of the cervical spinal canal per unit of head rotation or per unit of neck tension. The table also calculates the estimated CNS strain based upon a coupling ratio of 0.65.

The in-vivo data for flexion and extension did not report the head angle [91]. This was accounted for by assuming the rotation at the OC-C1 was 12.6 deg in flexion and 17.75 deg in extension [53]. The average head movement from the volunteers in lateral bending and axial rotation were 28.1 deg and 56.4 deg, respectively, and 66.6 deg and 71.8 deg for flexion and extension. Using these head movements, the elongation of the spinal canal per unit of head movement was calculated. These coefficients were calculated for subsequent comparison to the FE simulations and also to provide a convenient means to estimate CNS strain per unit of head movement.

The FE simulations resulted in 17.7 deg, 36.7 deg, 45.5 deg, and 43.5 deg of head movement in lateral bending, axial rotation, flexion and extension. Overall, the FE simulations followed the

same trends as the in-vivo studies (Figure 8.4), resulting in elongation of the cervical spinal canal (C1-C5) in lateral bending, axial rotation, flexion and tension. The FE analysis predicted an elongation in the front of the spinal canal in extension when compared to the in-vivo data which predicted an overall shortening of the spinal canal. There were differences in the distribution of spinal canal elongation between the in-vivo data and the FE data. In axial rotation, the FE model predicted a smaller change in length of the spinal canal per unit of head movement and that most of the change in length occurred in the lower cervical spine. The in-vivo data illustrate the greatest range of motion, and therefore, the greatest change in length of the spinal canal occurs at the C1-C2 and C2-C3 segments. In tension, the FE model predicted a relatively even distribution of the change in length of the spinal canal, with the greatest change in length at C3-C4. The in-vivo data indicate that C1-C2 had the greatest change in length of the spinal canal. Flexion, extension, and lateral bending also illustrated differences between the in-vivo and FE simulations when comparing segmental motion.

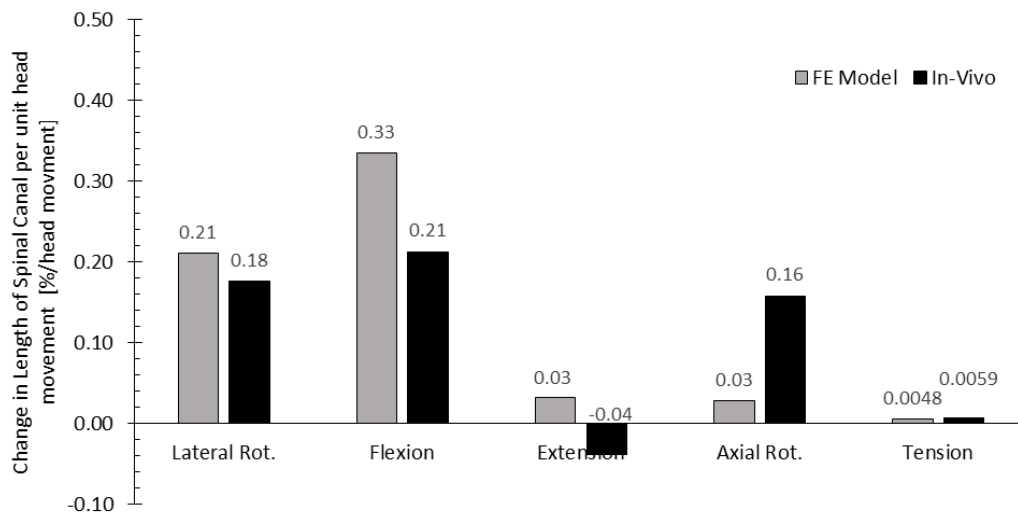


Figure 8.4: Graphical comparison of the change in length of the spinal canal per unit if head rotation [%/deg] or per unit of neck tension [%/N].

The differences between the in-vivo study and the FE simulations suggest that the FE model is stiffer in the upper cervical spine than the in-vivo studies. This is most evident in axial rotation and tension. In axial rotation the FE simulations had more coupled motion between the vertebral bodies, particularly in the upper cervical spine. The in-vivo data will be used to calculate the strain in the CNS using a coupling ratio of 0.65 due to the differences in the in-vivo results and the FE simulations. The estimated strains in the CNS at the ranges of motion in the in-vivo studies are illustrated in Table 8.1. The methods presented in this paper resulted in a 9.2% strain on the posterior surface of the spinal cord in flexion. These data compare closely to the average volunteer in volunteer [35] and cadaveric [127] which reported average strains on the posterior surface of the cord of approximately 10.2% (range = 6.8% to 13.6% and range = 7.5% to 14.2%, respectively).

Estimate of strain and strain rate in the CNS in injured compared to uninjured American football players

The laboratory reconstruction data combined with the in-vivo spinal canal elongation data were used to estimate strains and strain rates in the CNS in the injured and uninjured players (Table 8.2). The calculated strain and strain rate curves are included in Appendix D.1. In these NFL players the strain in the CNS was predicted to be significantly higher in lateral rotation, axial rotation and under tensile loading. This resulted in the total strain in the CNS of the injured players ($10.5 \pm 2.8\%$) being significantly higher than the uninjured players ($5.4 \pm 2.1\%$) ($t=-6.284$, $p<0.0001$). Likewise, the strain rates ($t=-6.4853$, $p<0.0001$) in the injured players and the time-varying product of strain and the strain rate ($t=-4.931$, $p=0.0001$) in the injured players was significantly higher than the uninjured players.

Case ID	Player	Injured	Elongation of the Cervical Spinal Canal (C1-C5)										Estimated Strain in the CNS (C1-C5)					Power (equation 3)			Power (equation 4)		
			0 - No 1 - Yes	ΔL_{Tx} [%]	ΔL_{Rx} [%]	ΔL_{Ry} [%]	ΔL_{Rz} [%]	ΔL_{TOT} [%]	$\Sigma \Delta L$ [%]	ϵ_{Tx} [%]	ϵ_{Rx} [%]	ϵ_{Ry} [%]	ϵ_{Rz} [%]	ϵ_{RTot} [%]	ϵ_{Tot} [%]	$d\epsilon_{Tot}/dt$ [%/s]	$\epsilon_{Tot}(d\epsilon_{Tot}/dt)$ [- / s]	Trans. [kW]	Rot. [kW]	Res. [kW]	Trans. [kW]	Rot. [kW]	Res. [kW]
7	striking	0	1.0	1.4	2.2	2.6	5.5	5.5	0.7	0.9	1.4	1.7	3.6	3.6	144	0.036	1.59	0.27	1.86	0.03	0.15	0.02	
7	struck	1	9.5	1.3	1.3	1.4	3.8	11.5	6.2	0.8	0.9	0.9	2.5	6.8	880	0.410	10.97	0.33	11.30	5.08	0.46	5.48	
9	striking	0	2.3	3.8	0.8	1.5	5.3	6.1	1.5	2.5	0.5	1.0	3.5	3.8	276	0.088	1.66	0.61	2.27	0.39	1.02	0.62	
9	struck	1	6.5	8.5	0.4	3.5	11.6	15.0	4.2	5.5	0.3	2.2	7.5	9.5	1196	0.775	19.44	2.26	21.70	6.71	1.54	7.39	
38	striking	0	0.8	0.8	5.9	1.3	7.4	7.8	0.6	0.5	3.9	0.8	4.8	5.0	181	0.058	3.72	0.95	4.68	1.46	0.41	1.85	
38	struck	1	9.7	7.3	4.3	6.2	16.0	19.8	6.3	4.8	2.8	4.1	10.4	12.8	1100	0.529	26.92	2.74	29.66	17.04	3.44	20.44	
39	striking	0	3.5	3.7	2.7	1.7	8.1	11.6	2.3	2.4	1.8	1.1	5.2	7.2	507	0.328	2.39	0.70	3.09	1.03	0.29	0.98	
39	struck	1	12.0	10.9	0.9	8.6	18.7	23.0	7.8	7.1	0.6	5.6	12.2	14.8	1959	1.385	13.43	3.95	17.38	6.69	2.61	8.36	
57	striking	0	2.0	4.3	1.4	4.4	7.6	8.9	1.3	2.8	0.9	2.8	5.0	5.7	253	0.089	14.55	1.22	15.76	1.76	0.87	1.76	
57	struck	1	11.8	7.2	3.6	4.0	11.8	20.5	7.7	4.7	2.3	2.6	7.7	11.4	1075	0.910	24.88	2.54	27.42	14.94	3.23	18.04	
59	striking	0	3.7	0.9	0.3	0.3	1.4	4.4	2.4	0.6	0.2	0.2	0.9	1.9	433	0.060	0.70	0.13	0.83	0.30	0.12	0.31	
59	struck	0	1.8	3.8	0.5	4.6	8.4	9.0	1.2	2.5	0.3	3.0	5.5	5.8	435	0.130	2.33	0.88	3.20	1.20	0.54	1.51	
69	striking	0	3.9	1.9	4.4	5.0	8.1	11.7	2.5	1.2	2.8	3.2	5.3	7.7	179	0.096	1.68	1.57	3.24	1.56	0.35	1.49	
69	struck	1	16.0	2.1	1.2	2.6	5.3	17.1	10.4	1.4	0.8	1.7	3.4	8.2	2317	1.741	19.04	1.87	20.91	3.86	1.06	4.25	
71	striking	1	5.2	6.6	0.9	4.9	11.6	13.3	3.4	4.3	0.6	3.2	7.6	8.6	1081	0.582	8.49	1.74	10.23	2.56	1.14	3.35	
71	struck	0	2.7	0.5	1.3	1.5	3.0	5.1	1.7	0.4	0.9	1.0	2.0	2.6	370	0.083	1.45	0.52	1.98	0.42	0.24	0.62	
77	striking	0	8.0	6.7	2.9	2.0	9.2	12.3	5.2	4.3	1.9	1.3	6.0	7.9	514	0.260	4.27	2.05	6.32	2.00	0.49	1.98	
77	struck	1	19.9	3.9	1.9	1.2	5.8	21.9	12.9	2.5	1.2	0.8	3.8	12.2	3112	3.255	9.22	1.91	11.14	5.37	0.57	5.49	
84	striking	0	4.0	6.1	1.4	1.8	9.0	12.5	2.6	4.0	0.9	1.2	5.9	8.0	649	0.264	3.39	1.90	5.29	2.01	1.82	2.13	
84	struck	1	7.8	8.3	1.2	5.1	13.9	16.2	5.1	5.4	0.8	3.3	9.1	10.5	1141	0.632	8.93	1.79	10.71	3.50	0.73	4.17	
92	striking	0	4.2	7.4	0.7	4.1	8.8	12.1	2.7	4.8	0.5	2.6	5.7	7.7	792	0.387	5.16	2.05	7.21	1.63	2.03	3.09	
92	struck	1	16.7	9.5	1.1	3.7	11.6	21.3	10.9	6.2	0.7	2.4	7.5	10.6	2349	2.149	30.38	2.11	32.49	14.92	1.06	15.63	
98	striking	0	2.9	2.8	1.5	8.7	11.2	13.0	1.9	1.8	1.0	5.7	7.3	8.5	455	0.158	2.60	2.04	4.64	1.40	2.02	2.29	
98	struck	1	8.5	5.9	1.2	3.2	9.4	12.2	5.5	3.8	0.7	2.1	6.1	7.6	1384	0.747	17.99	1.06	19.05	8.81	1.11	9.43	
113	striking	0	2.8	2.3	0.6	0.8	3.3	5.9	1.8	1.5	0.4	0.5	2.2	3.7	253	0.083	1.32	0.28	1.60	0.63	0.21	0.78	
113	struck	1	7.0	6.7	0.7	4.0	11.5	11.7	4.6	4.4	0.5	2.6	7.5	7.5	777	0.419	10.30	1.31	11.61	4.17	0.84	4.74	
118	striking	0	1.8	0.9	5.2	0.8	5.9	6.3	1.2	0.6	3.4	0.5	3.8	3.9	189	0.052	10.35	0.78	11.13	0.61	0.33	0.59	
118	struck	1	10.0	3.8	6.2	12.1	17.3	22.9	6.5	2.5	4.1	7.9	11.3	14.8	1537	1.007	8.69	5.46	14.15	3.33	3.84	5.96	
125	striking	0	6.2	3.8	0.7	3.2	7.3	10.1	4.0	2.5	0.5	2.0	4.7	6.2	1034	0.474	4.15	0.76	4.92	2.14	0.52	2.39	
125	struck	1	8.3	6.6	5.2	10.6	21.8	24.6	5.4	4.3	3.4	6.9	14.2	15.9	1661	1.199	36.25	4.81	41.06	12.92	2.58	15.14	
148	striking	0	1.8	2.1	0.5	1.8	4.2	5.0	1.2	1.4	0.3	1.2	2.7	3.2	272	0.065	0.79	0.29	1.08	0.39	0.23	0.61	
148	struck	1	3.5	6.5	0.9	5.9	13.3	14.7	2.3	4.2	0.6	3.9	8.6	9.5	664	0.317	6.43	1.61	8.04	2.63	0.88	3.47	
157	striking	0	1.9	3.8	1.1	1.1	4.8	6.3	1.3	2.5	0.7	0.7	3.1	4.0	147	0.051	1.97	0.45	2.42	0.49	0.61	0.61	
157	struck	1	10.6	4.5	0.6	6.0	10.8	13.6	6.9	2.9	0.4	3.9	7.0	8.7	1503	0.793	11.38	1.44	12.82	2.38	0.57	2.44	
164	striking	0	3.1	7.4	1.2	2.4	9.1	10.2	2.0	4.8	0.8	1.5	5.9	6.0	557	0.210	2.92	2.45	5.37	4.09	1.96	4.21	
164	struck	1	6.5	6.9	0.6	5.2	12.5	14.9	4.2	4.5	0.4	3.4	8.1	9.5	1306	0.743	16.92	3.05	19.97	7.72	1.76	8.98	
Average Injured		1	10.0	6.3	1.9	5.2	12.2	17.3	6.5	4.1	1.2	3.4	7.9	10.5	1473	1.035	16.45	2.35	18.80	7.21	1.61	8.40	
Std Dev Injured		1	4.3	2.5	1.8	3.0	4.7	4.4	2.8	1.6	1.2	1.9	3.0	2.8	643	0.752	8.73	1.33	9.25	4.84	1.10	5.56	
Average		0	3.1	3.4	1.9	2.6	6.7	8.6	2.0	2.2	1.2	1.7	4.4	5.4	402	0.157	3.53	1.05	4.57	1.24	0.75	1.47	
Std Dev		0	1.8	2.2	1.6	2.0	2.6	3.0	1.1	1.4	1.1	1.3	1.7	2.1	238	0.128	3.44	0.74	3.69	0.96	0.68	1.07	
p			<0.001	0.001	0.95	0.005	0.001	<0.001	<0.001	0.001	0.947	0.005	<0.001	<0.001	<0.001	<0.001	<0.001	0.002	<0.001	<0.001	0.01	<0.001	
t			-6.174	3.621	0.063	-3.020	4.264	-6.837	-6.194	-3.611	-0.068	-3.049	-4.252	-6.284	-6.485	-4.931	-5.717	-3.581	-5.933	-5.002	-2.796	-5.058	

Table 8.2 – Summary of calculated changes in length of the cervical spinal canal, strains in the spinal cord and brain stem and power at the atlanto-occipital joint for the injured and uninjured players in

The binary logistic regression analysis (Table 8.3, Figure 8.5) indicated $\epsilon_{Tot} \frac{d\epsilon_{Tot}}{dt}$ (strain x strain rate) in the spinal cord/brain stem was the best predictor of concussion in this data set. At a 50% probability of injury, $\epsilon_{Tot} \frac{d\epsilon_{Tot}}{dt}$, predicted 94% of the cases correctly, compared to $\frac{d\epsilon_{Tot}}{dt}$ (92% correct) and ϵ_{Tot} (83% correct). This is similar to others [50, 117, 125] who have indicated $\epsilon_{Tot} \frac{d\epsilon_{Tot}}{dt}$ to be a good biomechanical predictor of injury. In his analysis of primate head impact

data, which also included a primate cervical spine, Antona-Makoshi [121] found strains in the brain stem to correlate to concussion. Strain rates were not reported in that data set.

Predictor	Units	Logistic Regression Parameters					Injury Probability			Range of Injured Players		
		α	β	Fraction correct	-2LLR	χ^2	Nagelkerke R^2	15%	50%	85%	Min.	Max.
Strain x Strain Rate	[s ⁻¹]	-20.199	61.563	0.944	3.932	45.863	0.961	0.30	0.33	0.36	0.32	3.26
Strain Rate	[%/s]	-7.012	0.009	0.917	13.067	36.729	0.854	605	804	1002	664	3112
Strain	[%]	-11.901	1.513	0.833	21.276	28.519	0.730	6.72	7.86	9.01	6.81	15.93
$\Delta V_{\text{Head} - T1}$	[m/s]	-400.7	74.892	1.000	0.000	49.795	1.000	5.33	5.35	5.37	5.85	11.11
Upper Neck Power (eq. 4)	[kW]	-6.314	1.948	0.944	13.082	36.714	0.853	2.35	3.24	4.13	2.44	20.44
Upper Neck Power (eq. 3)	[kW]	-4.961	0.514	0.917	17.946	31.849	0.784	6.27	9.65	13.02	8.04	41.06
Neck Tension	[N]	-5.362	0.006	0.889	18.167	31.629	0.780	604	894	1182	589	3373
HIC ₁₅	[-]	-2.528	0.015	0.806	32.286	17.509	0.514	53	168	284	107	618
$\Delta \omega_{\text{Head} - T1}$	[rad/s]	-3.802	0.126	0.722	37.092	12.703	0.397	16.4	30.2	43.9	20.7	64.7
Acc _R	[g]	-2.315	0.033	0.583	45.349	4.446	0.155	17.5	70.2	122.5	48.8	119.1

Table 8.3 – Summary of calculated binary logistic regression parameters for the NFL reconstruction data (Chapter 7).

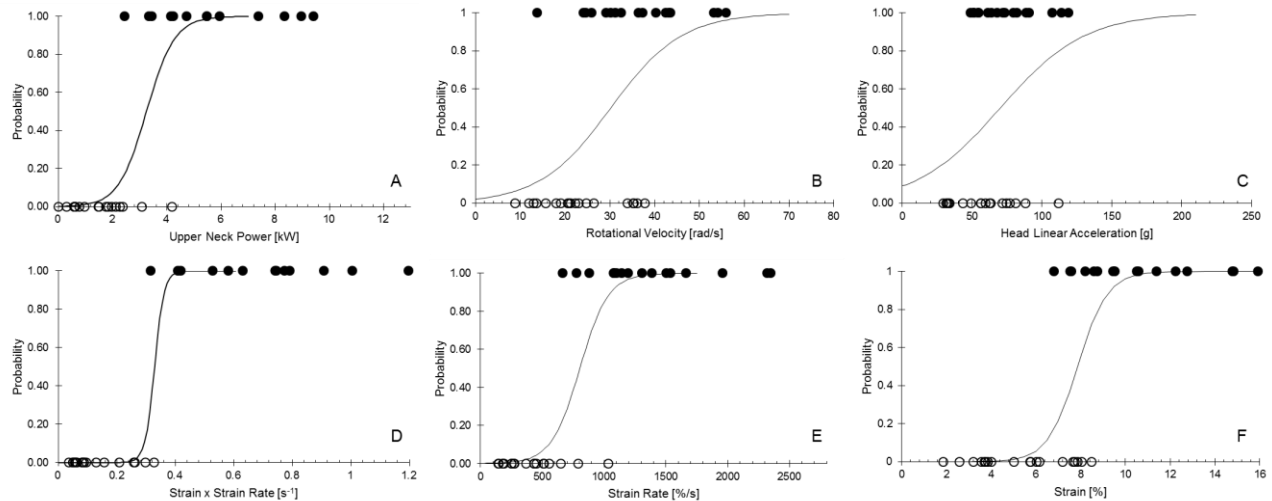


Figure 8.5 – Binary logistic regression plots of probability of concussion for various injury predictors. Upper Neck Power [A], Rotational Velocity relative to T1 [B], Head Resultant Acceleration [C], strain x strain rate [D], strain rate [E] and strain [F].

The product of $\varepsilon_{Tot} \frac{d\varepsilon_{Tot}}{dt}$ in this study is lower than those reported in the literature [50, 117, 125]. The method of calculation in the current study represents a generalized axonal strain in the upper spinal cord and brain stem. The previous FE-based studies utilize an engineering strain as calculated by the FE software and did not include a biofidelic cervical spine and spinal cord. The predicted strain in the brain stem does not include the effects of the upper cervical spine and spinal cord since there was no spinal cord or cervical spine present in previous FE studies. The engineering strain is not equivalent to axonal strain since the axons in the brain travel in different directions. This results in higher predicted strains [46] and when differentiating to calculate strain rate this will also result in higher strain rates. In the spinal cord and brain stem the neural pathways travel along the axis of the spinal cord and brain stem. Therefore, it is expected that the method of analysis used in this study is representative of global axonal strains and strain rates in this area.

There may be local strains and strain rates that are higher or lower than those reported in this study. Three potential causes of higher local strains and strain rates in the upper cervical spine are (1) the attachment of the denticulate ligaments into the spinal cord [28], (2) the relative shear motion of adjacent vertebrae, and (3) excursion of the odontoid process into the spinal canal [10, 11, 88]. Each of these were not accounted for in this analysis; however, it was not the intent to establish the exact threshold value for strain and strain rate, rather it was to assess the potential trend of strains and strain rates in the brain stem as they relate to concussion.

Power at the atlanto-occipital joint as a biomechanical predictor of concussion

The binary logistic regression analysis (Table 8.3, Figure 8.5) illustrates the best predictor of injury was $\Delta V_{Head-T1}$. The average injured player had a $\Delta V_{Head-T1}$ of 8.1 ± 2.2 m/s compared to the average uninjured player who had an average $\Delta V_{Head-T1}$ of 3.3 ± 1.1 m/s. There were no uninjured

players with a $\Delta V_{\text{Head-T1}}$ greater than 5.2 m/s and no injured players with a $\Delta V_{\text{Head-T1}}$ less than 5.5 m/s. These data compare well with the work of Denny-Brown and Russell [31] who found signs of concussion in their animal experiments with primates and cats. They reported signs of concussion began with some animals being injured at head changes of speed of 5.8 m/s and all animals injured at head changes in speed of 8.5 m/s. They also found that head movement relative to the body was an important factor for the injury to occur. When the head of animal was supported it was difficult to produce experimental concussion until higher changes of speed. In addition, they found concussion signs could be reproduced in the decerebrate animal. Both of these findings (head movement relative to torso and signs in the decerebrate animal) indicate there could be brain stem involvement in the concussion injury. Although, $\Delta V_{\text{Head-T1}}$ may be a convenient biomechanical predictor of injury it does not incorporate the effects of rotation or the mass of the helmet.

Upper neck power was calculated using two separate methods. Each of these methods predicted a higher power for the injured player when compared to the uninjured player (equation 3, $t=-5.933$, $p<0.0001$; equation 4, $t=-5.075$, $p<0.0001$) (Table 8.3). Upper neck power incorporates $\Delta V_{\text{Head-T1}}$ and $\Delta \omega_{\text{Head-T1}}$ as well as the upper neck forces which were all significant predictors of injury in this dataset (Chapter 7). The combination of these forces and velocities is advantageous since it may help to shed some light on the directional dependencies associated with injury as well as the potential location of injury. Power also incorporates the effects of the mass and inertia of the helmet since it directly uses the upper neck forces and, it also could incorporate adjustments for the effects of neck strength. This could be important since neck strength has been shown to be a protective factor in concussion [45]. Upper neck power did not predict injury as well as $\epsilon_{\text{Tot}} \frac{d\epsilon_{\text{Tot}}}{dt}$; however, compared to other laboratory based biomechanical

predictors, such as HIC_{15} , resultant head acceleration and resultant rotational velocity, it was a stronger predictor. The current calculation of upper neck power does not incorporate weighting factors to weight the effects of different modes of loading. In the future, a detailed analysis of strains and strain rates provided in this chapter may provide a basis for future weighting these components.

DISCUSSION

Maiman et al. [128] produced spinal cord injury as a result of axial loading to cats. They reported a 10% change in evoked potentials at distraction forces of 1-2 kg/kg of body weight (BW) with a 50% reduction in evoked potentials at 2.5 – 7.0 kg distraction/kg BW and a 95% reduction at 3.5 – 9.0 kg/kg BW in quasi-static testing. The cats with 50% and 95% reduction in evoked potentials suffered from severe quadriplegia that lasted weeks. These injuries are clearly more severe than those involved in concussion. The injured players in this data set sustained tensile forces of 1.7 ± 0.6 kg/kg BW. This is in the range of the 10% change in evoked potentials reported by Maiman et al. [128]; however, the tensile forces in these injured players were combined with rotation of the head relative to the torso and at high strain rates. Axonal injuries have also been found extensively in the brain stem and spinal cord of rats in the Marmarou model [126, 129]; however, the Marmarou model may not be representative of the types of hits that players undergo in football [130].

The calculated strains in the spinal cord and brain stem of these injured players were at the high end of the strains predicted for the normal range of motion of the cervical spine. Viano and Lovsund [125] found that brain and spinal cord tissue demonstrate a rate-sensitive injury response, consistent with VC. At the axonal level this is analogous with product of strain (ϵ) and strain rate ($\frac{d\epsilon}{dt}$). They reported upon in-vivo spinal cord impact testing with impact speeds of 1.5

to 6.0 m/s and compressions of 25 to 65%. Many of these impacts resulted in non-recoverable injury to the spinal cord. The lowest compression (25%) resulted in half of the specimens recovering from injury and the other half having permanent injury. These data were applied to calculate the tensile strain along the length of the spinal cord and it was estimated that the tensile strain was 3% with strain rates ranging from 7500 to 30,000 %/s. No specimens recovered above 20,000 %/s. These strain rates exceed the rates seen in the uninjured and injured players in the present study.

Singh et al. [102] found both strain and strain rate had an effect on functional nerve root injuries in spinal nerves roots of rats. They reported a 50% probability of nerve conduction block at 16%, 9% and 8% for strain rates of 0.1, 10 and 150 %/s. Thibault and Gennarelli [131] conducted tensile testing of the giant axon of the squid at strain rates of above 5000%/s. They reported depolarization of the neurons at 5-10% and illustrated a threshold of injury of 6% in their work. The curve fit in Figure 8.6 illustrates a logarithmic relationship between strain and strain rate from the data in Singh et al. [102], Viano and Lovsund [125] and Thibault and Gennarelli [131].

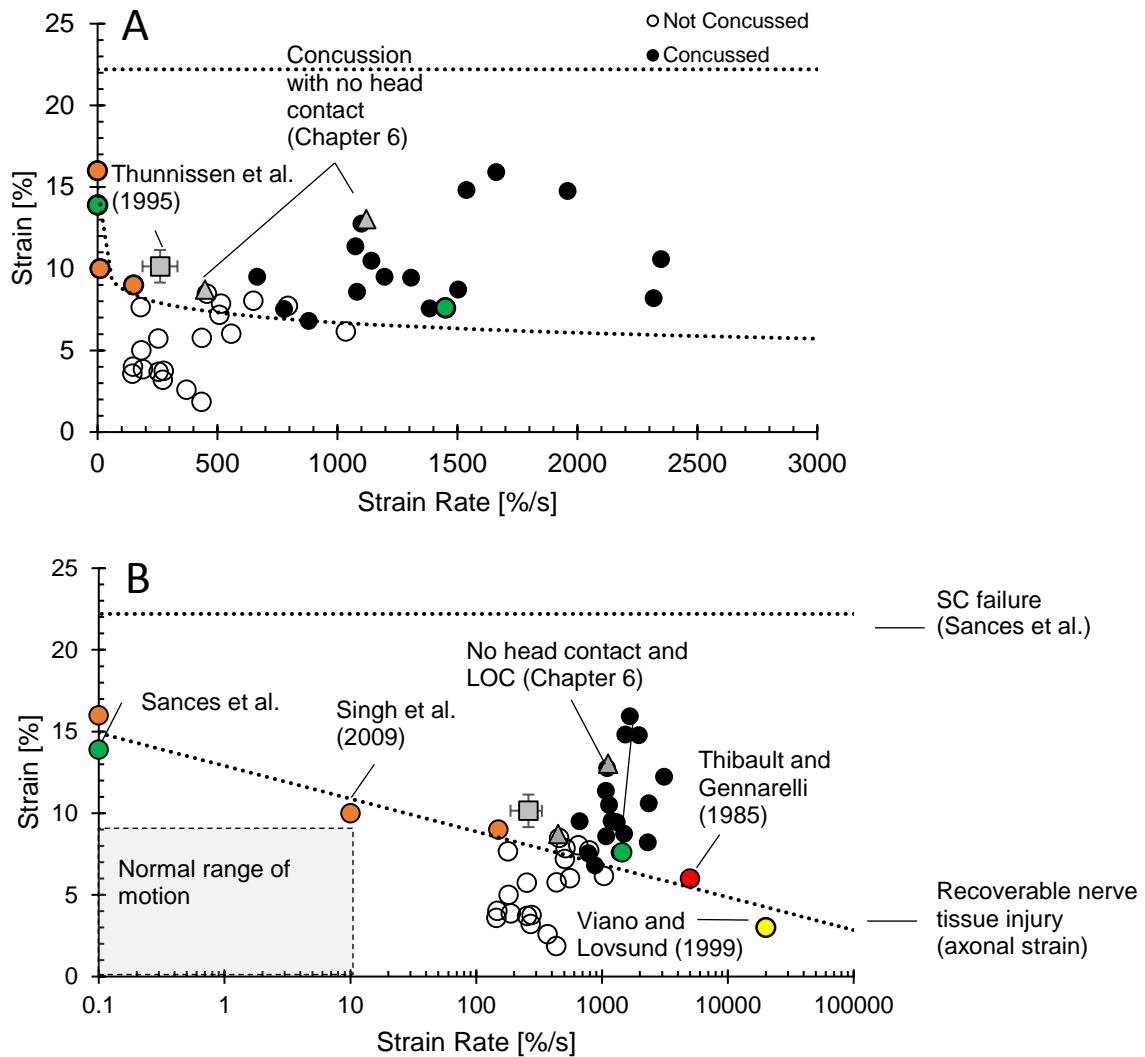


Figure 8.6: Tolerance for concussion based upon predicted strain and strain rate in the spinal cord and brainstem. **(A)** Linear scale. **(B)** Logarithmic Scale. The lower dashed line is a curve fit to Singh et al. (2009), Thibault and Gennarelli (1985) and Viano and Lovsund (1999). The data from Singh et al. was dynamic in-vivo testing conducted on rat spinal nerve roots which represents a 50% probability of recoverable nerve injury. The data point from Thibault and Gennarelli (1985) was taken from the tolerance proposed in their study. It was based upon axial tension test of the giant axon of the squid. The data point from Viano and Lovsund is based upon a calculation to determine the strain due to tension in the spinal cord specimens that recovered from impact. Sances et al. (1981) recorded in-vivo evoked potentials in the CNS while applying static and dynamic tensile loading on primates. These data points represent the strains at which there was a reduction in evoked potentials.

Sances et al. [13] and Cusick et al. [132] conducted tensile tests by pulling vertically on the head of a restrained primate and recorded in-vivo evoked potentials through the brain stem and spinal cord as well as heart rate and respiration. Cusick et al. [132] concluded that brain stem or spinal cord dysfunction are the result of excess tensile stress along the fibre tracts. The tests were conducted quasi-statically and also at rates of 1 m/s (approximately 1450 %/s). The data presented in Sances et al. [13] were used, and it was calculated that in the static and dynamic tests the primates underwent approximately 14.8% and 7.8% strain in the in the spinal cord and brain stem, respectively, prior to a reduction in evoked potentials. Changes in heart rate and respiration occurred shortly after the reduction in evoked potentials.

In the human, a known set of severe volunteer exposures is the sled acceleration testing conducted at the Naval Biodynamics Laboratory (NBDL) [133] involving 17 volunteers with 236 exposures. The volunteers reportedly underwent extensive pre- and post-test medical evaluations. The only injuries reported were minor surface abrasions on the skin under the restraint system. Thunnissen et al. [99] noted movement of the instrumentation located at the T1 vertebrae of these volunteers and provided a method to account for this movement. They confirmed their correction method with video analysis. The method proposed by Thunnissen et al. [99] was applied, and the strains and strain rates of these NBDL volunteers were estimated for eight of the most severe frontal exposures following the same procedure as presented in this chapter. The data was obtained from the National Highway Transportation Safety Administration (NHTSA) website [134]. These severe human volunteer exposures lie close to the curve-fitted line in Figure 8.6. The $\varepsilon_{Tot} \frac{d\varepsilon_{Tot}}{dt}$ was calculated to be $0.16 \pm 0.046 \text{ s}^{-1}$ (Table 8.4). The binary logistic regression analysis indicates that for $\varepsilon_{Tot} \frac{d\varepsilon_{Tot}}{dt}$ the probability of injury is very low.

Test Information				Calculated data		
Subject ID	NBDL Test ID	NHTSA Test ID	Sled Accel. [g]	ϵ_{Tot} [%]	$d \epsilon_{Tot} / dt$ [%/s]	$\epsilon_{Tot}(d \epsilon_{Tot} / dt)$ [s ⁻¹]
H00118	3969	1635	-15.3	11.48	382	0.245
H00120	3954	1625	-14.1	10.85	236	0.160
H00127	3959	1629	-14.7	8.96	159	0.097
H00131	3990	1644	-14.6	9.24	273	0.155
H00132	3957	1627	-14.6	11.16	235	0.147
H00133	3986	1641	-15.5	8.99	317	0.185
H00135	3970	1636	-15.5	10.42	296	0.203
H00136	3962	1631	-14.1	10.07	182	0.124
Average				10.15	260	0.164
Stdev				1.00	73	0.047

Table 8.4 – Summary of calculated strain and strain rates in the spinal cord and brain stem of eight human volunteer exposures in sled testing conducted by the NBDL.

In Chapter 6, two case studies were presented with concussion that occurred as a result of a chest impact to American football players. The resultant strains and strain rates in these two players were calculated for Case A (13.0%, 1119 %/s) and Case B (8.7%, 448 %/sec). These two collisions resulted in different outcomes to the injured player. In Case A the player was unconscious for approximately 70 seconds, he returned to play three weeks later. In Case B, the player returned to game play 7 days later. The product of strain and strain rate were 0.89 s⁻¹ and 0.25 s⁻¹, respectively. These cases were not included in the binary logistic regression analysis. The regression analysis for $\epsilon_{Tot} \frac{d\epsilon_{Tot}}{dt}$ indicates this correlates to a 1% probability of injury for Case B and was below the minimum of any of the players who had sustained concussion in helmet-to-helmet contact. The logistic regression analysis was repeated, including these two cases, and this resulted in a 15% probability of injury for Case B. This suggests that as more data become available this should improve the injury prediction capability of these variables or, alternatively, the injured player in Case B was more susceptible to injury. The data from these

two cases may help to shed some light on the thresholds for AIS1 injury (concussion without loss of consciousness) and AIS2 injury (concussion with loss of consciousness) [135]. Additional data are needed to further understand these thresholds; however, strain in the spinal cord was previously cited as one of the reasons for pilots failing to eject after ditching their planes into the ocean [88] and has been discussed in several animal studies as a biomechanical predictor of concussion.

The sport of boxing provides an additional resource to estimate thresholds for injury. The punch forces of Olympic boxers [111] have been reported. The uppercut punch is an effective knockout punch and resulted in average upper neck forces in the Hybrid III ATD of 1474 ± 903 N, with maximum forces delivered by heavyweight boxers that exceeded 3500 N. This correlates to a strain of 8.7 to 13.4 % (1474 N to 3500 N) and a strain rate of approximately 870 to 1340 %/s, assuming a triangular wave with a peak force at 0.01 sec. These data also coincide with the strain and strain rate calculations for these injured NFL players. The uppercut punches delivered by heavyweight boxers resulted in similar strains and strain rates to the NFL player in Case A; who lost consciousness as a result of an impact to the chest. This may help to provide some insight into the threshold for loss of consciousness; however, more data of these types of severe exposures are required.

In summary, the signs and symptoms as well as posturing [6] of athletes who have sustained a concussion are consistent with injury to the upper cervical spinal cord and/or brain stem. Previous animal studies [10, 11, 13, 22, 29, 31, 32, 33] support the upper spinal cord and brain stem as a potential mechanism of injury. The data presented in this report indicates that the combination of strain and strain rate along the axis of the spinal cord and brain stem is a strong biomechanical predictor of concussion. An analysis of existing volunteer data is also supportive

of this mechanism of injury. The findings from this study could provide important information in understanding the mechanism of concussion in sports and a means to better protect against it. The data indicate that there is an increasing trend in helmet size and mass [16, 86] and also that helmet mass and inertia can result in higher upper neck forces and rotation of the head relative to the torso [16, Chapter 6]. Therefore, if strain in the upper spinal cord and brain stem is considered a mechanism of concussion, helmet manufacturers should pay close attention to the mass, inertia and/or how the mass and inertia of the helmet is coupled to the athlete since these factors may help to optimize helmet performance.

There are several limitations to this study that must be acknowledged. This study was performed using data generated from laboratory reconstructions using the Hybrid III ATD to represent humans in injurious and non-injurious helmet-to-helmet collisions while playing American football. There may be some question regarding the biofidelity of the Hybrid III ATD in these combined loading conditions; however, it is currently the best available method for reconstructing these on-field collisions in the laboratory. It provides critical information in assessing the injury trends in injurious and non-injurious collisions. Additionally, the design of the Hybrid III has a neck simulating some muscle tensing, but there is no active musculature in any of the current ATDs. Therefore, the differences in head kinematics for players who were able to brace for impact, who are generally striking players, compared to those unable to brace for impact could not be assessed. This may be an important factor when comparing the struck (and unprepared) player versus the striking (and prepared) player. In addition to these differences, the effects of neck strength were not studied. However, it is thought that players with stronger necks who were able to prepare for impact would have the ability to reduce head motion relative to the torso. Also, the Hybrid III represents the 50th percentile male. The

dummy is lighter and shorter than the typical football player involved in game impacts and concussion. In this study the weight was increased using a weight vest; however, the height could not be modified.

The laboratory data acquired was used in conjunction with FE modelling and in-vivo volunteer studies to estimate the stretch in the cervical spine. A coupling ratio of 0.65 was applied to assess the tensile strain in the CNS (brain stem and spinal cord). The coupling ratio was supported by previous animal studies that have reported coupling ratios of 0.5 to 0.75. It also appears to be supported by the anthropometry of the human cervical spine, cervical spinal cord, and brain stem. If the coupling ratio is related to the anthropometry of the cervical spine and brain stem then differences in the length of the spinal cord and brain stem will have an effect on its magnitude. A Monte-Carlo simulation was conducted to assess the sensitivity of this coupling ratio to variations in cervical spine length and brain stem length. The cervical spine length was varied from 95 mm to 125 mm and the brain stem length was varied from 46.4 mm to 52.6 mm. The analysis indicates that the coupling ratio would likely vary by ± 0.06 (2 standard deviations, range = 0.59 to 0.71) due to these geometric differences. This indicates that the uncertainty in the calculated strain is approximately 0.8% strain, meaning that the true average strain of injured players could lie within 9.7% and 11.3%, and the true average strain of the uninjured players could lie within the range of 4.6% to 6.2%. Regardless of the difference in coupling ratio, the same trend exists that the injured players had higher estimated strains and strain rates than the uninjured players.

The calculated strain presented in this dissertation represents a global strain along the axis of the cervical spinal cord and brain stem. This type of analysis does not incorporate local strains. These local strains may be higher due to the shear motion between the individual vertebral

bodies, the individual spinal segment ranges of motion, or the effects of the denticulate ligaments or spinal nerve roots tethering the cord to the spinal canal. On a microscopic level there may also be strain concentrations that occur along the axon or at the Nodes of Ranvier. This level of detail cannot be quantified based upon the approach taken in this dissertation and would require a very detailed central nervous system model.

A finite element model study was not conducted since a biofidelic and validated finite element model that incorporates the coupling of the spinal cord to the spinal canal could not be located. The development of such a model was beyond the scope of this dissertation. Future work could be conducted in this area by first assessing the coupling ratio in the human by way of cadaveric studies. This cadaveric data could then be used to validate a biofidelic finite element model of the spinal cord and brain stem. In addition to a validated human model, validated helmet finite element models must exist if a finite element modeling approach is conducted. This means that several other unknowns, such as coupling of the helmet to the head, the effects of helmet fit and chin strap forces, must be understood. Although several limitations exist in this study, the data support that tension in the upper spinal cord and brain stem is an important mechanism of concussion. The data supports that the upper neck forces as well as the strains in the cervical spinal cord and brain stem should be added to head kinematics for a more comprehensive evaluation of concussion.

CHAPTER 9 – CONCLUSIONS

The majority of recent biomechanical research has focused on head kinematics (velocities and accelerations) as a predictor of concussion. There is important direct evidence supporting that a mechanism of concussion is related to the tensile strain and strain rate in the upper cervical spinal cord and brain stem due to neck tension. Many of the signs and symptoms of concussion correlate to injury of the spinal cord, brain stem, and/or midbrain. There has been considerable new and older research in animals showing involvement of the brain stem and tissue degenerative changes in the cervical spinal cord and brain stem with concussive injury. Signs of concussion can occur as a result of pure tensile loading with no head impact.

The overall aim of this dissertation was to build upon this foundational research and to understand whether kinematics resulting in neck tension and the tensile strain and strain rate along the axis of the upper spinal cord and brain stem were biomechanical predictors of concussion. Two new laboratory impactors were designed and constructed to achieve these goals. The impactors were tested and found to be repeatable. The impactors were used to reconstruct twenty on-field collisions (n=18 helmet-to-helmet and n=2 helmet-to-chest (non-head impacts resulting in concussion)). The effects of helmet mass on ATD head and neck responses were also investigated during helmet-to-helmet and helmet-to-chest impacts (non-head impacts). These data were used to estimate the tensile strains and strain rates along the axis of the cervical spinal cord and brain stem. Based upon the results the following conclusions are drawn:

1. The new laboratory impactors were a repeatable method to recreate on-field collisions with one or two moving ATDs to represent the players. The impactors had a coefficient of variation of 0.02% relative to the target speed and the two impactors could be synchronized to within 1 millimeter or 1 millisecond of each other.

2. The laboratory methods in this dissertation were an improvement over previous methods. In this study, an instrumented ATD head, neck, and torso were used to represent each player, providing a more complete picture of head and torso kinematics and neck kinetics. The pre-impact momentum was more closely matched, and no constraining boundary conditions were imposed on the ATDs during the collisions.
3. In the laboratory reconstructions head ΔV relative to T1 was the single best predictor of injury (50% probability=5.35 m/s, $\chi^2=49.8$, 100% correct). It was followed by upper neck power (50% probability=3.24 kW, $\chi^2=36.7$, 94.4% correct) and neck tension (50% probability=894 N, $\chi^2=31.6$, 88.9% correct). Poorer predictors of injury were HIC₁₅ (50% probability=168, $\chi^2=17.5$, 80.6% correct), rotational velocity of the head relative to T1 (50% probability=30.2 rad/s, $\chi^2= 12.7$, 72.2% correct), and translational acceleration of the head (50% probability=70.2 g, $\chi^2=4.4$, 58.3% correct).
4. An impact to the chest can result in concussion. The two cases studied in this dissertation resulted in high neck tensile forces (Case A [LOC-out 3 weeks] = 2646 N, Case B [No LOC-out 1 week] = 1342 N) combined with forward flexion of the head relative to the torso. This is similar to the kinematics of a restrained occupant in a severe frontal automobile collision without an airbag.
5. The neck tension forces (+F_z) in the eighteen helmet-to-helmet laboratory reconstructions (1691±728 N) were higher than those previously reported in volunteer research but lower than cadaveric research resulting in ligamentous failure of the cervical spine. The high neck tension forces were combined with lateral (x-axis) and axial (z-axis) rotation of the head relative to T1 in the injured players.

6. A combination of neck tension force (distraction), lateral (x-axis) rotation, flexion, and axial (z-axis) rotation results in elongation of the cervical spine and the potential for tensile strains along the axis of the spinal cord and brain stem.
7. The time-varying product of tensile strain and strain rate along the axis of the cervical spinal cord and brain stem was the best tissue-level predictor of injury (50% probability=0.33 s⁻¹, $\chi^2=45.9$, 94.4% correct) when compared to strain and strain rate by themselves. This injury metric is consistent with previous research.
8. The magnitude of the tensile strains (6.8 % to 15.9 %) and strain rates (662 to 3112%/s) along the axis of the cervical spinal cord and brain stem in the injured players exceeded those in research which have resulted in concussion signs in in-vivo primate testing and transient axonal dysfunction in axonal tensile loading tests.
9. The combination of the research in this dissertation, the signs and symptoms of concussion, and the previous foundational research supports the theory that the tensile strains and strain rates along the axis of the cervical spinal cord and brain stem are an important mechanism of concussion.
10. The mass and inertia of the helmet increased the upper neck forces and moments in the Hybrid III 50th ATD in both helmet-to-helmet and helmet-to-chest (non-head impacts) collisions when compared to un-helmeted impacts.

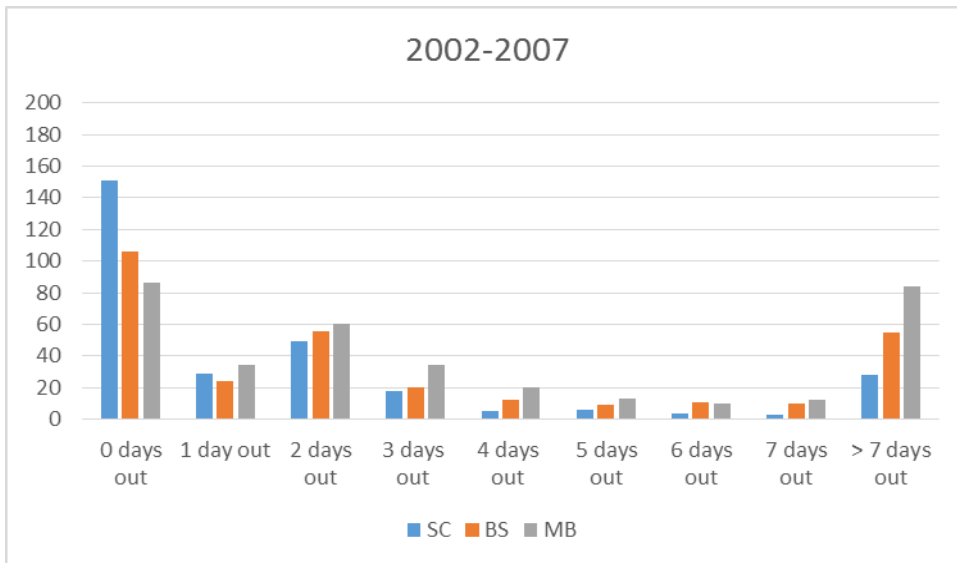
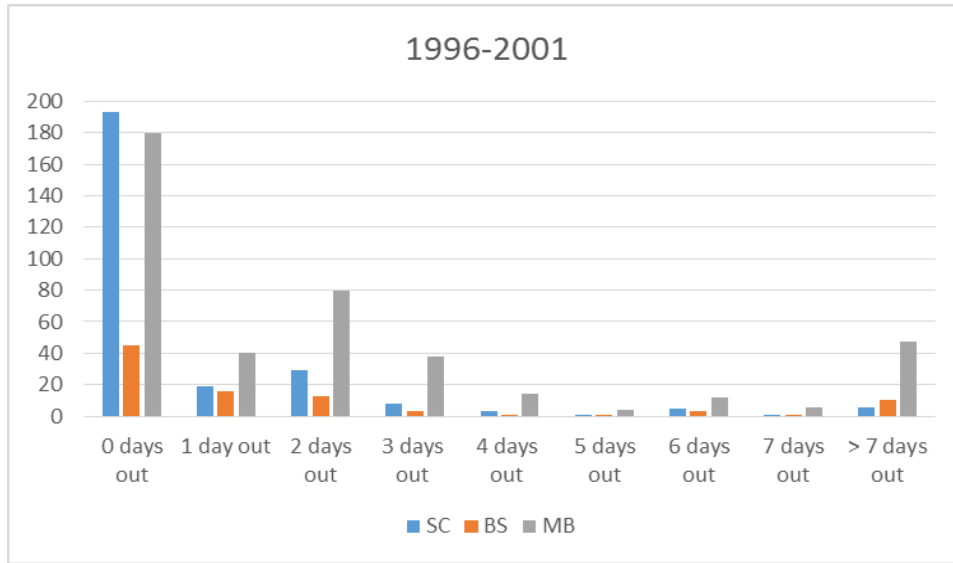
The research conducted in this dissertation supports earlier studies on the role of neck tension and strain in the upper cervical spine and brain stem as well as their rates of application as a cause for concussion. These biomechanical responses should be added to head kinematic responses for a more comprehensive evaluation of concussion.

APPENDIX A.1

Signs & Symptoms	Spinal Cord	Brainstem	Mid-Brain	Comments
1996-2001	78%	85%	92%	886 reported concussions
2002-2007	78%	86%	93%	854 reported concussions
General Symptoms				
Headaches	y	y	y	
Neck Pain	y	y	y	
Nausea	y	y	y	
Syncope		y	y	
Vomiting		y	y	
Back Pain	y			
Seizures				
Cranial Nerve Symptoms				
Dizziness	y	y	y	
Blurred Vision		y	y	
Vertigo	y	y	y	
Photophobia		y	y	
Tinnitus		y	y	
Diplopia		y	y	
Nystagamus	rarely	y	y	
Pupil Response		y	y	
Pupil Size		y	y	
Hearing Loss		y	y	
Memory Problems				
RGA Delayed			y	Possible thalamic dysfunction.
Info Processing Problems			y	Possible thalamic dysfunction.
Attention Problems			y	
AGA Delayed			y	
Cognition Problems				
Immediate Recall			y	Possible thalamic dysfunction.
Not Oriented to time			y	
Not Oriented to Place			y	
Not Oriented to Persons			y	
Somatic Complaints				
Fatigue	y	y	y	
Anxiety			y	
Personality Change			y	
Irritability		y	y	
Sleep Disturbance		y	y	
Loss of Appetite	y	y	y	
Depression		y	y	
Loss of Libido		y	y	
Loss of Consciousness				
		y	y	

Note: The remaining 8 percent of players had no reported symptoms in this data set.

Thank you to Dr. Ira Casson for his review of these symptoms and assessment of which could be related to signs and symptoms of spinal cord, brainstem or midbrain dysfunction.



1740 NFL players categorized by the potential source of the location of symptoms and the number of days out.

APPENDIX B.1 – Supplement for Chapter 4, Test Series 1

Impact Location	Helmet Condition	Impact Speed	Headform			Upper Neck Forces			Upper Neck Moments		
			Acceleration	ΔV	Lin. Momentum	Fx	Fy	Fz	Resultant	Resultant	
		(m/s)	(g)	(m/s)	(kgm/s)	(N)	(N)	(N)	(N)	(Nm)	
Location A	Un-helmeted	4.1	61.4	4.43	20.10	623	375	339	719	41.0	
			59.8	4.31	19.56	591	-374	314	690	37.8	
			62.3	4.49	20.40	641	-377	351	736	42.4	
		5.2	62.2	4.48	20.35	638	-374	354	732	42.7	
			99.9	6.30	28.62	882	460	670	975	59.2	
			99.1	6.14	27.87	872	-458	676	984	59.6	
		No facemask	4.1	96.1	6.46	29.33	886	-457	662	959	59.2
				104.5	6.31	28.66	889	-466	671	981	58.9
				-	-	-	-	-	-	-	-
			5.2	-	-	-	-	-	-	-	-
				-	-	-	-	-	-	-	-
				-	-	-	-	-	-	-	-
	Helmet	4.1	36.0	4.33	27.95	783	461	625	1023	59.5	
			35.7	4.31	27.82	817	-460	596	1027	61.2	
			36.1	4.34	28.03	792	-463	627	1023	59.7	
			36.1	4.34	28.01	740	-459	653	1019	57.5	
			53.6	6.01	38.82	987	632	1194	1569	77.7	
			54.1	5.85	37.78	989	-631	1215	1559	77.4	
		5.2	53.5	6.10	39.40	981	-642	1132	1509	74.4	
			53.2	6.08	39.26	992	-623	1236	1637	81.4	
			35.3	4.46	30.34	741	504	649	1050	62.1	
			36.4	4.44	30.27	733	-471	638	1038	61.1	
			36.6	4.52	30.79	739	-522	747	1118	61.0	
			32.7	4.40	29.97	750	-521	561	993	64.3	
	Helmet + 350 g	4.1	56.5	5.99	40.82	908	761	1294	1637	77.6	
			56.7	5.93	40.35	919	-764	1390	1656	78.3	
			57.1	5.98	40.71	915	-746	1263	1642	77.5	
			55.7	6.08	41.40	889	-774	1228	1614	76.8	
59.4			4.42	20.07	370	652	468	751	42.9		
58.8			4.40	19.99	373	-636	483	743	42.3		
5.2		62.5	4.54	20.59	378	-675	461	774	44.3		
		56.8	4.32	19.63	359	-646	461	737	42.2		
		82.5	5.96	27.07	472	853	895	1065	56.5		
		83.5	6.09	27.65	467	-855	893	1099	55.4		
		81.9	6.04	27.42	488	-856	930	1094	58.1		
		82.0	5.75	26.12	460	-847	862	1002	55.9		
No facemask	4.1	32.2	4.55	26.39	438	766	641	991	56.8		
		33.0	4.48	26.00	435	-770	644	980	55.9		
		32.6	4.53	26.25	452	-765	632	1000	58.3		
		31.1	4.64	26.91	428	-762	646	994	56.1		
		62.8	6.29	36.49	459	898	1122	1407	79.4		
		58.9	7.29	42.26	418	-829	1098	1373	75.5		
	5.2	70.3	4.40	25.53	519	-979	1151	1443	82.5		
		59.1	7.18	41.67	442	-888	1118	1403	80.3		
		31.9	4.31	27.86	354	959	664	1088	75.8		
		31.4	4.33	27.99	382	-954	638	1151	74.9		
		32.6	4.22	27.28	340	-960	707	1044	76.4		
		31.6	4.38	28.32	339	-962	648	1068	76.2		
Helmet	4.1	40.6	5.57	36.01	404	1118	1200	1491	88.6		
		45.3	5.97	38.60	437	-1170	1121	1504	92.6		
		45.0	5.82	37.57	385	-1120	1297	1498	84.0		
		31.5	4.93	31.87	389	-1065	1182	1471	89.3		
		29.4	4.29	29.19	342	1021	595	1127	84.0		
		28.2	4.21	28.66	363	-1024	641	1173	84.5		
	5.2	30.8	4.36	29.69	329	-1014	590	1103	82.7		
		29.2	4.29	29.22	334	-1025	554	1104	84.8		
		44.5	6.00	40.86	464	1331	1119	1598	109.8		
		46.8	6.04	41.14	490	-1347	1152	1621	111.3		
		43.9	6.02	41.01	455	-1321	1110	1605	108.6		
		42.9	5.93	40.41	448	-1325	1094	1568	109.4		
Location B	Un-helmeted	4.1	65.7	4.35	19.75	91	543	538	673	34.7	
			66.5	4.37	19.82	-94	-541	520	675	35.5	
			67.5	4.27	19.41	-82	-533	531	667	34.0	
		5.2	63.1	4.41	20.03	-97	-555	562	675	34.8	
			87.8	5.84	26.51	186	739	948	1083	44.5	
			88.9	5.89	26.72	-196	-753	957	1095	44.9	
		No facemask	4.1	87.9	5.85	26.55	-185	-735	953	1087	44.7
				86.7	5.78	26.25	-178	-729	933	1067	43.8
				39.5	4.35	25.21	99	583	733	912	35.5
			40.7	4.31	24.97	-100	-599	714	915	34.6	
			39.2	4.38	25.42	-102	-586	743	918	36.5	
			38.7	4.35	25.23	-95	-566	742	904	35.5	
	Helmet	4.1	55.9	5.83	33.80	169	791	1257	1416	51.0	
			57.6	5.85	33.94	-139	-812	1288	1407	50.4	
			53.7	5.77	33.48	-185	-773	1226	1406	51.9	
			56.3	5.86	33.99	-183	-788	1256	1435	50.8	
			37.5	4.35	28.09	177	608	809	1012	24.7	
			36.1	4.30	27.77	-180	-590	751	951	23.2	
		5.2	39.2	4.39	28.34	-163	-613	878	1072	22.9	
			37.4	4.36	28.17	-188	-622	797	1013	27.8	
			53.4	5.77	37.29	304	809	1420	1601	47.4	
			55.6	5.78	37.34	-293	-822	1365	1527	46.7	
			53.4	5.75	37.13	-329	-806	1450	1632	47.0	
			51.1	5.79	37.40	-289	-799	1446	1645	48.6	
	Helmet + 350 g	4.1	39.1	4.33	29.48	133	676	801	1019	33.7	
			40.8	4.40	29.94	-117	-666	700	925	28.6	
			38.8	4.28	29.12	-140	-683	873	1085	36.2	
			37.7	4.31	29.38	-143	-680	829	1048	36.4	
51.8			5.65	38.45	286	844	1518	1709	47.9		
52.1			5.66	38.54	-308	-862	1536	1723	54.1		
5.2		53.1	5.65	38.47	-267	-842	1554	1739	46.1		
		50.2	5.63	38.35	-282	-827	1465	1664	43.5		

Impact Location	Helmet Condition	Impact Speed	Headform			Upper Neck Forces			Upper Neck Moments	
			Acceleration	ΔV	Lin. Momentum	Fx	Fy	Fz	Resultant	Resultant
		(m/s)	(g)	(m/s)	(kgm/s)	(N)	(N)	(N)	(N)	(Nm)
Location D	Un-helmeted	4.1	61.7	4.49	20.40	690	396	501	880	55.8
			60.3	4.53	20.56	-685	-392	467	850	55.8
		62.7	4.42	20.08	-679	-387	507	887	55.2	
		62.1	4.53	20.56	-706	-410	527	904	56.5	
		5.2	84.7	6.03	27.38	1000	497	936	1413	75.4
			86.1	6.07	27.55	-1002	-503	927	1409	76.3
	No facemask	4.1	88.3	6.00	27.24	-975	-493	971	1416	74.4
			79.8	6.02	27.35	-1023	-495	911	1414	75.5
		5.2	41.8	4.14	24.04	696	435	733	1085	52.4
			44.1	4.16	24.13	-726	-430	753	1108	54.6
		5.2	41.7	4.17	24.19	-713	-434	730	1099	53.0
			39.5	4.10	23.79	-649	-442	718	1049	49.6
	Helmet	4.1	52.2	5.58	32.37	924	526	1079	1507	72.0
			52.1	5.55	32.17	-930	-529	1082	1514	72.4
		51.9	5.62	32.58	-913	-527	1089	1510	72.2	
		52.7	5.58	32.38	-930	-522	1067	1496	71.4	
		5.2	38.2	4.09	26.44	633	457	828	1129	46.1
			38.4	4.05	26.16	-623	-465	839	1131	46.2
	Helmet + 350 g	4.1	38.4	4.13	26.69	-631	-454	820	1121	46.3
			37.7	4.10	26.48	-645	-453	825	1135	46.0
		5.2	53.4	5.53	35.72	941	566	1364	1737	70.1
			54.6	5.50	35.52	-937	-566	1349	1730	70.3
		4.1	49.9	5.50	35.54	-910	-576	1361	1718	70.3
			55.8	5.59	36.10	-978	-556	1381	1765	69.8
	Helmet + 350 g	5.2	35.5	4.01	27.33	758	478	915	1263	50.9
			36.8	4.03	27.42	-758	-491	914	1249	51.6
		32.7	3.95	26.91	-728	-480	853	1212	51.8	
		37.1	4.06	27.65	-789	-464	976	1328	49.3	
		5.2	47.2	5.25	35.77	1055	539	1408	1832	74.5
			48.9	5.43	36.97	-1115	-579	1436	1890	76.0
46.5	5.07	34.55	-971	-525	1359	1745	73.1			
46.4	5.25	35.78	-1080	-513	1429	1861	74.5			

APPENDIX B.2 – Supplement for Chapter 4, Test Series 2, Impact Location C

Average of Location C, Impact speeds of 5.5, 7.4 m/s and 9.3 m/s																	
Helmet Mass	Total Mass		Acceleration		ΔV		Rot. Velocity		Trans. Momentum		Res. Upper Neck Force		Neck Tension		Res. Upper Neck Moment		
	(kg)	(kg)	(g)	(%)	(m/s)	(%)	(rad/s)	(%)	(kgm/s)	(%)	(N)	(%)	(N)	(%)	(Nm)	(%)	
Hybrid III - Head	0.00	4.54	0%	124.5	0%	7.14	0%	50.4	0%	32.4	0%	1759	0%	1338	0%	49.6	0%
Helmet A	1.50	6.04	33%	109.9	-12%	6.79	-5%	47.1	-7%	41.0	26%	2937	67%	2747	97%	70.3	42%
Helmet B	1.59	6.13	35%	98.6	-21%	6.94	-3%	48.8	-3%	42.5	31%	2971	69%	2761	98%	72.2	46%
Helmet C	1.84	6.38	41%	93.5	-25%	6.68	-7%	49.1	-2%	42.6	31%	2277	30%	2050	47%	72.7	47%
Helmet D	1.84	6.38	41%	101.4	-19%	6.78	-5%	49.7	-1%	43.3	33%	2340	33%	2076	49%	68.1	37%
Helmet E	1.85	6.39	41%	101.2	-19%	6.55	-8%	44.5	-12%	41.8	29%	2382	35%	2225	59%	74.6	51%
Helmet F	1.85	6.39	41%	106.1	-15%	6.74	-6%	47.6	-6%	43.1	33%	2273	29%	2207	58%	69.3	40%
Helmet G	1.91	6.45	42%	102.4	-18%	6.50	-9%	43.8	-13%	41.9	29%	2357	34%	2232	60%	70.7	45%
Helmet H	1.93	6.47	43%	86.4	-31%	6.40	-10%	42.3	-16%	41.4	28%	2397	36%	1988	42%	69.1	39%
Helmet I	1.98	6.52	44%	100.0	-20%	6.87	-4%	45.8	-9%	44.8	38%	2739	56%	2206	58%	77.4	56%
Helmet J	1.99	6.53	44%	85.8	-31%	6.25	-12%	39.6	-21%	40.8	26%	2361	34%	1821	35%	68.9	39%
Helmet K	2.00	6.54	44%	89.0	-29%	6.34	-11%	41.1	-18%	41.5	28%	2382	35%	1754	25%	70.6	42%
Helmet L	2.06	6.60	45%	86.5	-31%	6.55	-8%	47.0	-7%	43.2	33%	2123	21%	2176	56%	73.1	48%
Helmet M	2.08	6.62	46%	87.3	-30%	6.57	-8%	49.2	-2%	43.5	34%	2184	24%	2559	83%	83.9	69%
Helmet N	2.19	6.73	48%	87.8	-29%	6.35	-11%	45.0	-11%	42.7	32%	2030	15%	1696	21%	66.3	34%
Average			42%		-23%		-8%		-9%		31%		37%		56%		45%
Std Dev			4%		6%		3%		6%		3%		15%		22%		9%

Location C, Impact Speed = 5.5 m/s																	
Helmet Mass	Total Mass		Acceleration		ΔV		Rot. Velocity		Trans. Momentum		Res. Upper Neck Force		Neck Tension		Res. Upper Neck Moment		
	(kg)	(kg)	(g)	(%)	(m/s)	(%)	(rad/s)	(%)	(kgm/s)	(%)	(N)	(%)	(N)	(%)	(Nm)	(%)	
Hybrid III - Head	0.00	4.54	0%	89.0	0%	5.12	0%	37.5	0%	23.2	0%	834	0%	516	0%	22.2	0%
Helmet A	1.50	6.04	33%	79.7	-10%	4.95	-3%	33.9	-10%	29.9	29%	2177	161%	2030	293%	47.5	114%
Helmet B	1.59	6.13	35%	79.0	-11%	5.05	-1%	35.7	-9%	30.9	33%	2353	182%	2232	328%	47.6	114%
Helmet C	1.84	6.38	41%	68.2	-23%	4.89	-5%	34.2	-9%	31.2	34%	1600	92%	1476	186%	52.2	135%
Helmet D	1.84	6.38	41%	76.9	-14%	4.96	-3%	34.4	-8%	31.6	36%	1696	103%	1539	198%	45.5	105%
Helmet E	1.85	6.39	41%	71.7	-19%	4.92	-4%	33.0	-12%	31.4	35%	1462	75%	1592	208%	52.9	138%
Helmet F	1.85	6.39	41%	84.9	-5%	4.86	-5%	32.5	-13%	31.0	34%	1605	92%	1625	215%	48.8	120%
Helmet G	1.91	6.45	42%	76.1	-14%	4.66	-9%	33.6	-9%	30.1	29%	1705	104%	1715	232%	49.3	122%
Helmet H	1.93	6.47	43%	64.4	-28%	4.78	-7%	33.3	-11%	30.9	33%	1865	123%	1402	172%	45.0	102%
Helmet I	1.98	6.52	44%	76.2	-14%	4.99	-2%	32.4	-14%	32.5	40%	2046	145%	1336	159%	51.6	132%
Helmet J	1.99	6.53	44%	63.1	-29%	4.59	-10%	31.4	-16%	30.0	29%	1748	109%	1074	108%	47.4	113%
Helmet K	2.00	6.54	44%	65.7	-26%	4.73	-8%	32.6	-13%	30.9	33%	1752	110%	978	89%	44.8	102%
Helmet L	2.06	6.60	45%	67.3	-24%	4.78	-7%	34.1	-9%	31.5	36%	1283	54%	1570	204%	53.0	139%
Helmet M	2.08	6.62	46%	72.2	-19%	4.85	-5%	34.8	-7%	32.1	38%	1377	65%	1950	278%	60.5	172%
Helmet N	2.19	6.73	48%	62.0	-30%	4.62	-10%	31.7	-16%	31.1	34%	1332	60%	1040	101%	49.5	123%
Average			42%		-19%		-6%		-11%		34%		105%		198%		124%
Std Dev			4%		8%		3%		3%		3%		36%		68%		18%

Location C, Impact Speed = 7.4 m/s																	
Helmet Mass	Total Mass		Acceleration		ΔV		Rot. Velocity		Trans. Momentum		Res. Upper Neck Force		Neck Tension		Res. Upper Neck Moment		
	(kg)	(kg)	(g)	(%)	(m/s)	(%)	(rad/s)	(%)	(kgm/s)	(%)	(N)	(%)	(N)	(%)	(Nm)	(%)	
Hybrid III - Head	0.00	4.54	0%	117.1	0%	7.00	0%	49.8	0%	31.8	0%	1929	0%	1648	0%	55.1	0%
Helmet A	1.50	6.04	33%	106.6	-9%	6.64	-5%	46.6	-6%	40.1	26%	3369	75%	3216	95%	66.1	20%
Helmet B	1.59	6.13	35%	98.0	-16%	6.85	-2%	47.5	-5%	42.0	32%	3176	65%	2986	81%	69.0	25%
Helmet C	1.84	6.38	41%	91.4	-22%	6.62	-5%	49.2	-1%	42.2	33%	2309	20%	2218	35%	67.8	23%
Helmet D	1.84	6.38	41%	99.5	-15%	6.68	-5%	49.2	-1%	42.6	34%	2474	28%	2252	37%	61.7	12%
Helmet E	1.85	6.39	41%	99.9	-15%	6.46	-8%	43.9	-12%	41.3	30%	2658	38%	2529	54%	69.5	26%
Helmet F	1.85	6.39	41%	107.2	-8%	6.68	-5%	47.0	-5%	42.7	34%	2396	24%	2483	51%	66.3	20%
Helmet G	1.91	6.45	42%	95.7	-18%	6.42	-8%	42.7	-14%	41.4	30%	2274	18%	2506	52%	71.3	30%
Helmet H	1.93	6.47	43%	82.3	-30%	6.35	-9%	41.7	-16%	41.1	29%	2626	36%	2046	24%	66.0	20%
Helmet I	1.98	6.52	44%	92.0	-21%	6.85	-2%	45.8	-8%	44.6	40%	2921	51%	2521	53%	75.7	38%
Helmet J	1.99	6.53	44%	78.2	-33%	6.27	-10%	38.1	-23%	40.9	29%	2599	35%	1950	18%	67.2	22%
Helmet K	2.00	6.54	44%	85.2	-27%	6.28	-10%	39.7	-20%	41.0	29%	2645	37%	1678	2%	65.3	19%
Helmet L	2.06	6.60	45%	83.6	-29%	6.45	-8%	47.2	-5%	42.6	34%	2187	13%	2118	29%	69.1	26%
Helmet M	2.08	6.62	46%	87.1	-26%	6.44	-8%	50.3	1%	42.7	34%	2132	11%	2772	68%	84.5	54%
Helmet N	2.19	6.73	48%	82.5	-30%	6.25	-11%	44.2	-11%	42.1	32%	2088	8%	1787	8%	67.1	22%
Average			42%		-21%		-7%		-9%		32%		33%		43%		25%
Std Dev			4%		8%		3%		7%		3%		19%		26%		10%

Location C, Impact Speed = 9.3 m/s																	
Helmet Mass	Total Mass		Acceleration		ΔV		Rot. Velocity		Trans. Momentum		Res. Upper Neck Force		Neck Tension		Res. Upper Neck Moment		
	(kg)	(kg)	(g)	(%)	(m/s)	(%)	(rad/s)	(%)	(kgm/s)	(%)	(N)	(%)	(N)	(%)	(Nm)	(%)	
Hybrid III - Head	0.00	4.54	0%	167.5	0%	9.32	0%	63.8	0%	42.3	0%	2513	0%	2029	0%	71.4	0%
Helmet A	1.50	6.04	33%	143.3	-14%	8.78	-6%	60.8	-5%	53.0	25%	3264	30%	2995	48%	97.2	36%
Helmet B	1.59	6.13	35%	118.7	-29%	8.92	-4%	63.3	-1%	54.7	29%	3385	35%	3084	52%	100.0	40%
Helmet C	1.84	6.38	41%	120.9	-28%	8.52	-9%	64.0	0%	54.4	29%	2924	16%	2456	21%	98.0	37%
Helmet D	1.84	6.38	41%	127.7	-24%	8.70	-7%	65.6	3%	55.5	31%	2849	13%	2438	20%	97.2	36%
Helmet E	1.85	6.39	41%	132.0	-21%	8.26	-11%	56.6	-11%	52.8	25%	3026	20%	2554	26%	101.5	42%
Helmet F	1.85	6.39	41%	126.2	-25%	8.68	-7%	63.2	-1%	55.5	31%	2817	12%	2513	24%	92.7	30%
Helmet G	1.91	6.45	42%	135.2	-19%	8.43	-10%	55.0	-14%	54.4	29%	3092	23%	2474	22%	91.6	28%
Helmet H	1.93	6.47	43%	112.4	-33%	8.06	-13%	52.0	-19%	52.1	23%	2700	7%	2515	24%	96.2	35%
Helmet I	1.98	6.52	44%	131.9	-21%	8.78	-6%	59.3	-7%	57.2	35%	3248	29%	2759	36%	104.9	47%
Helmet J	1.99	6.53	44%	116.1	-31%	7.90	-15%	49.2	-23%	51.6	22%	2736	9%	2619	29%	92.2	29%
Helmet K	2.00	6.54	44%	116.1	-31%	8.02	-14%	51.0	-20%	52.5	24%	2750	9%	2605	28%	101.7	42%
Helmet L	2.06	6.60	45%	108.7	-35%	8.42	-10%	59.7	-7%	55.6	31%	2898	15%	2840	40%	97.2	36%
Helmet M	2.08	6.62	46%	102.5	-39%	8.42	-10%	62.4	-2%	55.8	32%	3043	21%	2954	46%	106.6	49%
Helmet N	2.19	6.73	48%	118.9	-29%	8.17	-12%	59.2	-7%	55.0	30%	2671	6%	2259	11%	82.1	15%
Average			42%		-27%		-9%		-8%		28%		18%		30%		36%
Std Dev			4%		6%		3%		8%		4%		9%		12%		8%

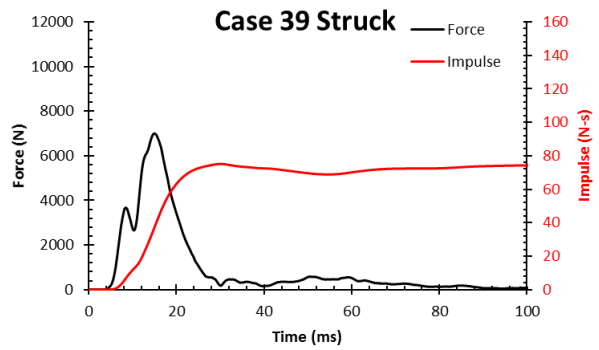
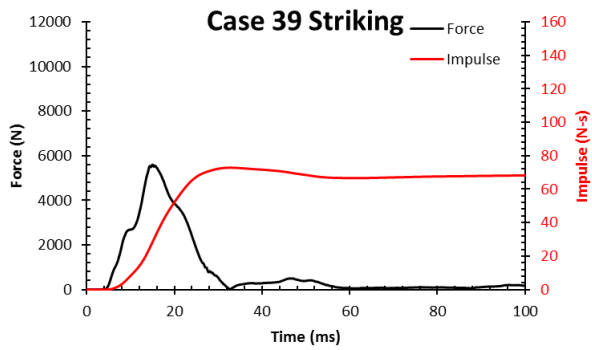
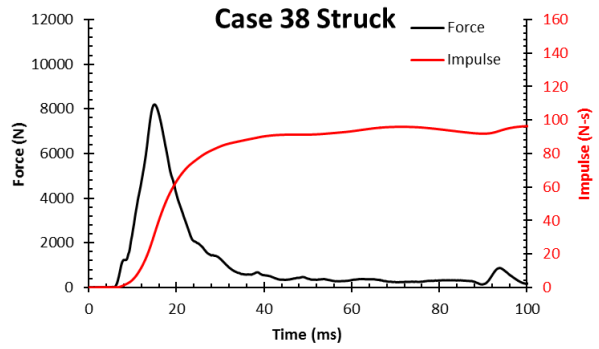
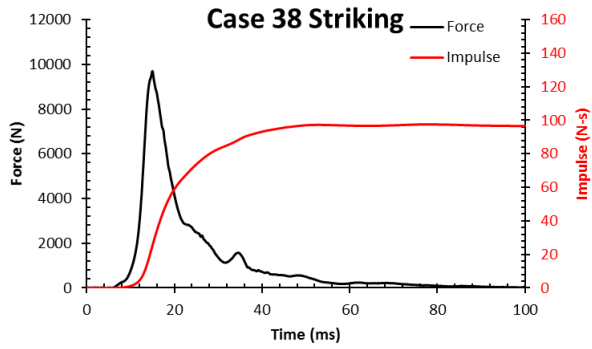
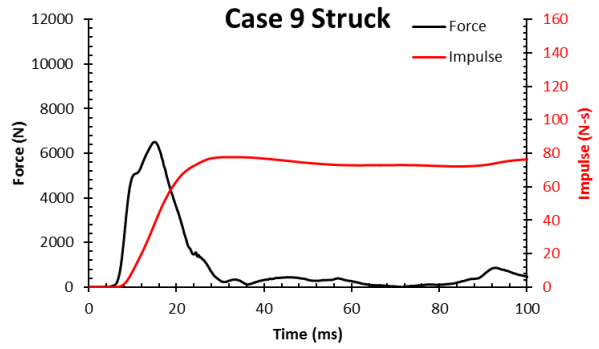
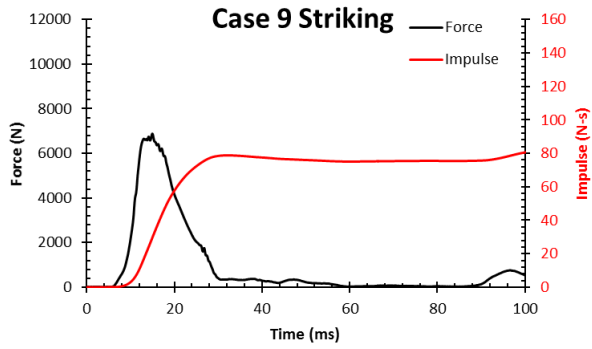
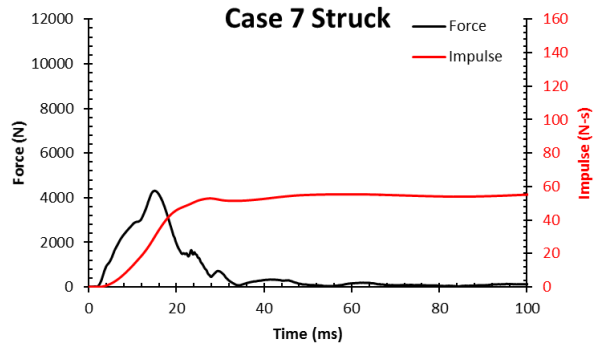
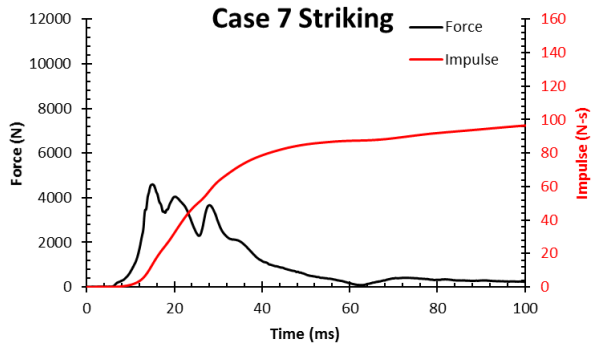
APPENDIX B.2 – Supplement for Chapter 4, Test Series 2, Impact Location D

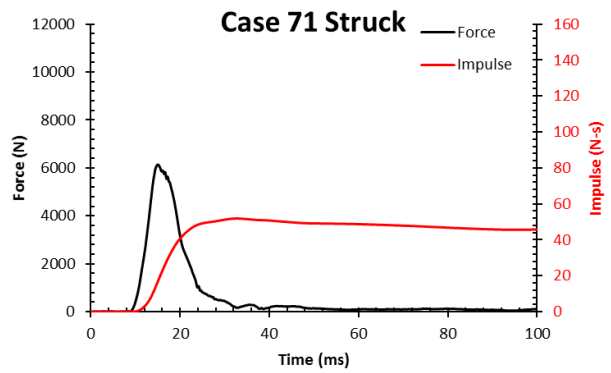
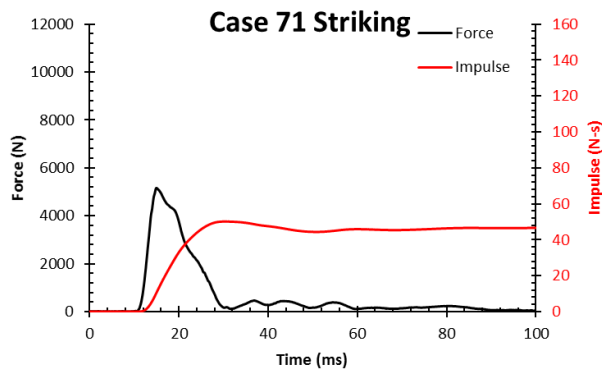
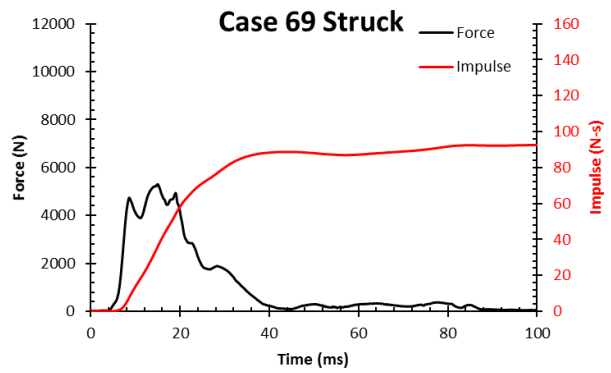
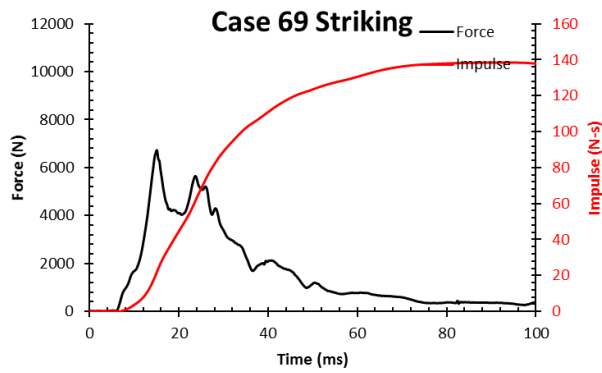
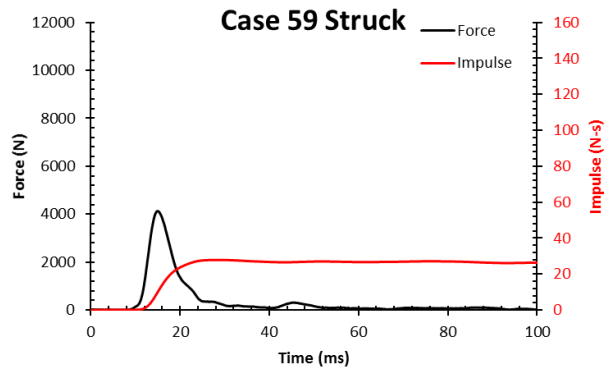
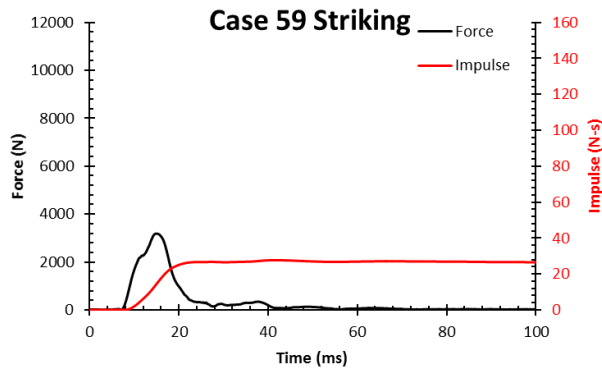
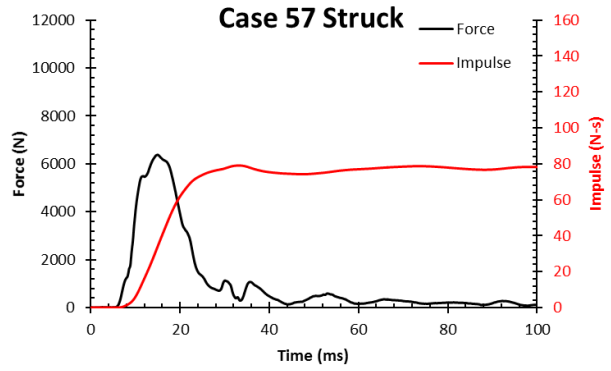
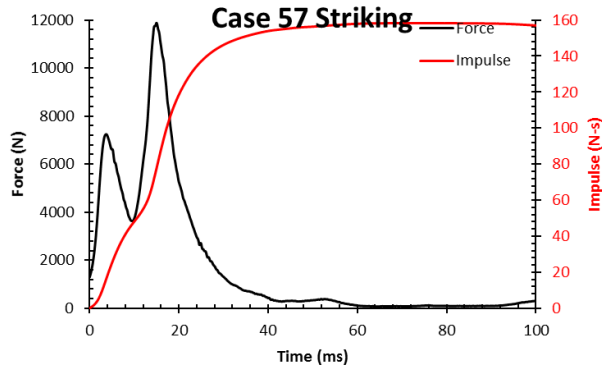
Average of Location D, Impact speeds of 7.4 m/s and 9.3 m/s																		
Helmet Mass	Total Mass		Acceleration		ΔV		Rot. Velocity		Lin. Momentum		Res. Upper Neck Force	Neck Tension	Res. Upper Neck Moment					
	(kg)	(kg)	(g)	(%)	(m/s)	(%)	(rad/s)	(%)	(kgm/s)	(%)	(N)	(N)	(Nm)	(%)				
Hybrid III - Head	0.00	4.54	0%	138.2	0%	8.56	0%	56.9	0%	38.9	0%	2251	0%	1820	0%	86.7	0%	
Helmet A	1.50	6.04	33%	112.4	-19%	7.37	-14%	60.8	7%	44.5	15%	2812	25%	2305	27%	97.4	12%	
Helmet B	1.59	6.13	35%	119.0	-14%	7.33	-14%	55.4	-3%	44.9	16%	2925	30%	2358	30%	101.6	17%	
Helmet C	1.84	6.38	41%	105.8	-23%	7.13	-17%	58.1	2%	45.5	17%	2882	28%	2419	33%	97.2	12%	
Helmet D	1.84	6.38	41%	121.0	-12%	6.99	-18%	57.8	2%	44.6	15%	2813	25%	2389	31%	91.0	5%	
Helmet E	1.85	6.39	41%	107.4	-22%	7.33	-14%	53.0	-7%	46.8	20%	2978	32%	2363	30%	111.6	29%	
Helmet F	1.85	6.39	41%	117.3	-15%	7.10	-17%	58.9	3%	45.3	17%	2836	26%	2603	43%	95.4	10%	
Helmet G	1.91	6.45	42%	122.8	-11%	7.09	-17%	51.7	-9%	45.8	18%	2738	22%	2504	38%	102.1	18%	
Helmet H	1.93	6.47	43%	96.7	-30%	6.71	-22%	49.1	-14%	43.4	12%	2899	29%	2442	34%	97.8	13%	
Helmet I	1.98	6.52	44%	109.4	-21%	6.74	-21%	52.9	-7%	43.9	13%	2833	26%	2479	36%	106.0	22%	
Helmet J	1.99	6.53	44%	106.6	-23%	6.46	-25%	52.0	-9%	42.2	8%	3003	33%	2448	34%	91.5	6%	
Helmet K	2.00	6.54	44%	92.2	-33%	6.54	-24%	51.5	-9%	42.8	10%	2795	24%	2397	32%	97.9	13%	
Helmet L	2.06	6.60	45%	107.5	-22%	7.40	-14%	53.9	-5%	48.8	26%	3028	35%	2393	31%	104.8	21%	
Helmet M	2.08	6.62	46%	107.9	-22%	7.33	-14%	59.8	5%	48.5	25%	2999	33%	2510	38%	102.5	18%	
Helmet N	2.19	6.73	48%	101.7	-26%	6.74	-21%	50.7	-11%	45.3	17%	2344	4%	2053	13%	78.2	-10%	
Average - % Change			42%		-21%				-18%		-4%		16%		27%		32%	15%
Std Dev			4%		6%			4%		6%		5%		7%		7%		9%

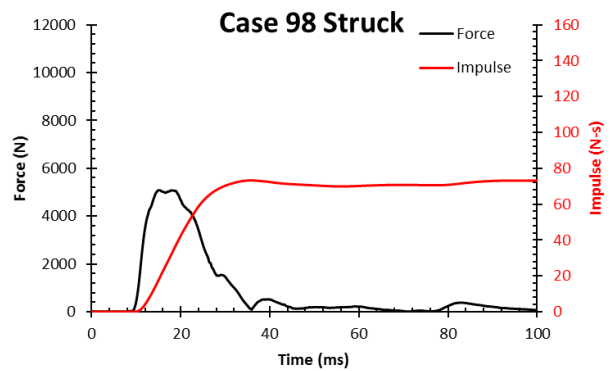
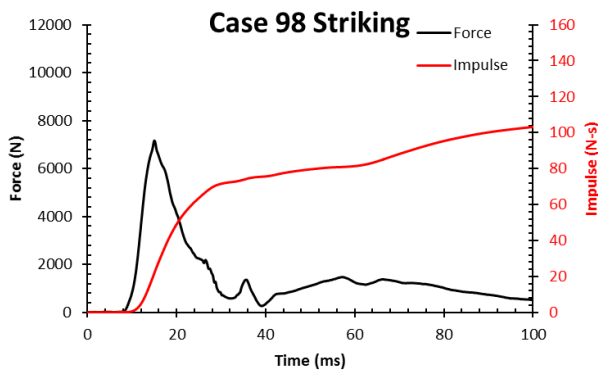
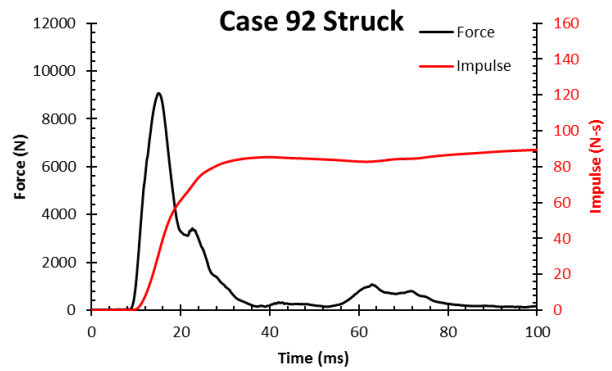
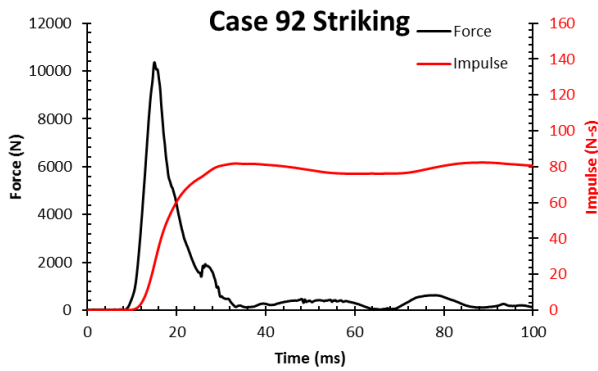
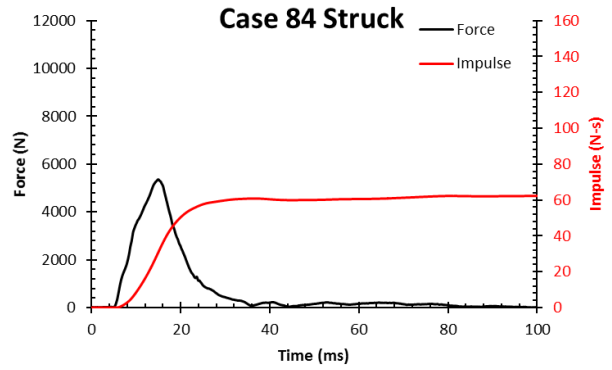
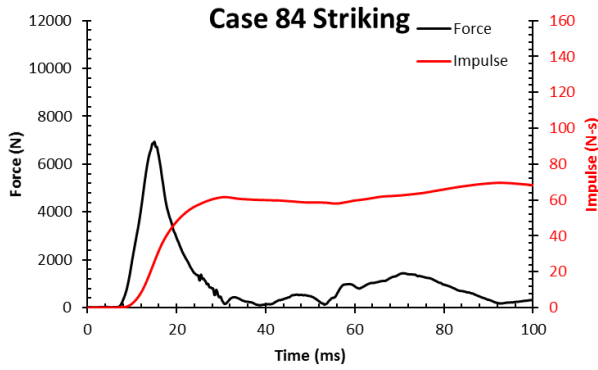
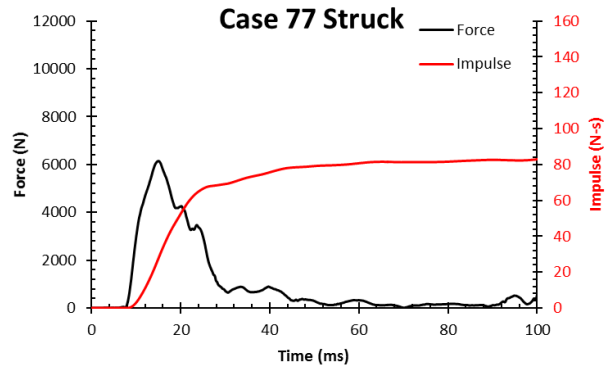
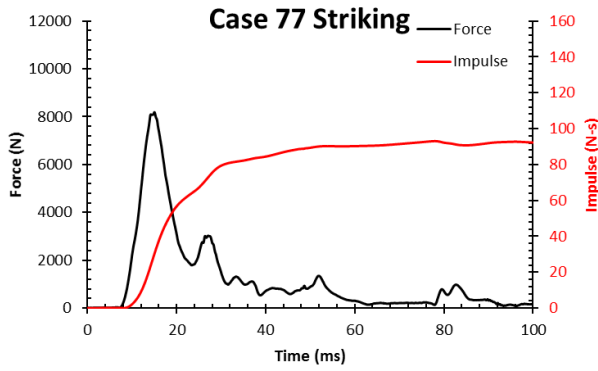
Location D, Impact Speed = 7.4 m/s																		
Helmet Mass	Total Mass		Acceleration		ΔV		Rot. Velocity		Lin. Momentum		Res. Upper Neck Force	Neck Tension	Res. Upper Neck Moment					
	(kg)	(kg)	(g)	(%)	(m/s)	(%)	(rad/s)	(%)	(kgm/s)	(%)	(N)	(N)	(Nm)	(%)				
Hybrid III - Head	0.00	4.54	0%	112.3	0%	6.62	0%	49.9	0%	30.0	0%	1821	0%	1416	0%	77.5	0%	
Helmet A	1.50	6.04	33%	94.4	-16%	6.49	-2%	51.8	4%	39.2	31%	2531	39%	2169	53%	78.5	1%	
Helmet B	1.59	6.13	35%	105.0	-6%	6.37	-4%	48.5	-3%	39.0	30%	2873	58%	2432	72%	84.1	9%	
Helmet C	1.84	6.38	41%	93.0	-17%	6.23	-6%	50.0	0%	39.7	32%	2621	44%	2144	51%	79.6	3%	
Helmet D	1.84	6.38	41%	105.7	-6%	6.13	-7%	49.8	0%	39.1	30%	2500	37%	2183	54%	76.5	-1%	
Helmet E	1.85	6.39	41%	93.1	-17%	6.48	-2%	46.4	-7%	41.4	38%	2887	59%	2312	63%	96.6	25%	
Helmet F	1.85	6.39	41%	102.1	-9%	6.16	-7%	50.0	0%	39.4	31%	2481	36%	2356	80%	72.4	-7%	
Helmet G	1.91	6.45	42%	102.7	-9%	6.30	-5%	45.6	-9%	40.6	35%	2189	20%	2552	80%	90.8	17%	
Helmet H	1.93	6.47	43%	79.3	-29%	5.98	-10%	43.4	-13%	38.7	29%	2848	56%	2283	61%	82.9	7%	
Helmet I	1.98	6.52	44%	89.3	-20%	5.98	-10%	45.8	-8%	39.0	30%	2562	41%	2513	77%	86.2	11%	
Helmet J	1.99	6.53	44%	94.5	-16%	5.74	-13%	42.7	-15%	37.5	25%	2947	62%	2454	73%	85.4	10%	
Helmet K	2.00	6.54	44%	77.8	-31%	5.82	-12%	44.9	-10%	38.1	27%	2626	44%	2172	53%	81.0	5%	
Helmet L	2.06	6.60	45%	100.1	-11%	6.53	-1%	45.5	-9%	43.1	44%	2929	61%	1826	29%	90.9	17%	
Helmet M	2.08	6.62	46%	97.8	-13%	6.49	-2%	48.8	-2%	43.0	43%	2652	46%	2288	62%	83.5	8%	
Helmet N	2.19	6.73	48%	83.6	-26%	5.87	-11%	42.0	-16%	39.5	31%	1906	5%	1656	17%	66.9	-14%	
Average			42%		-16%			-7%		-6%		33%		43%		59%		7%
Std Dev			4%		8%			4%		6%		5%		16%		18%		10%

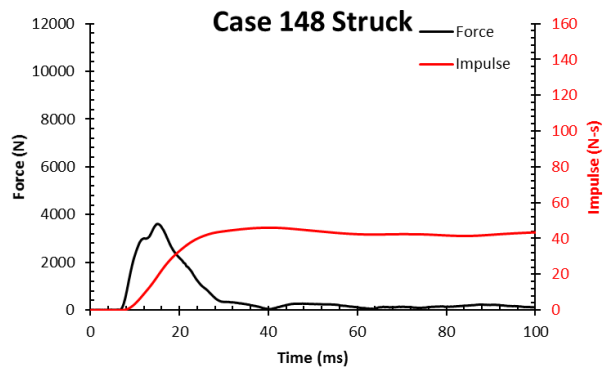
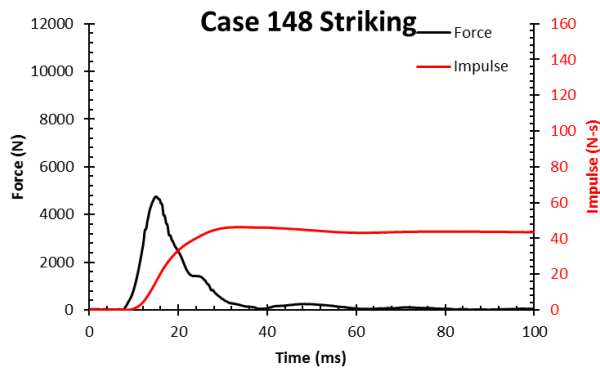
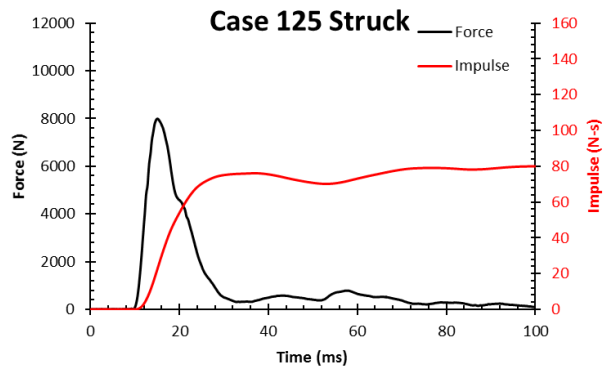
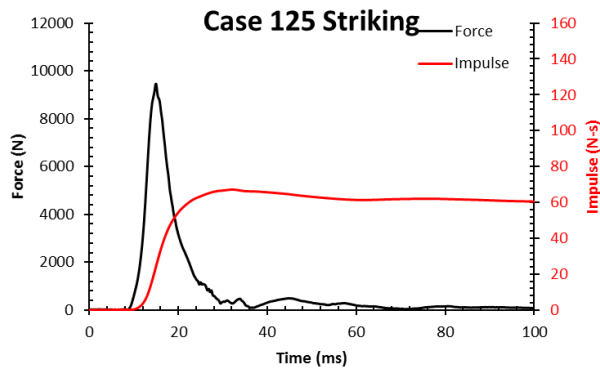
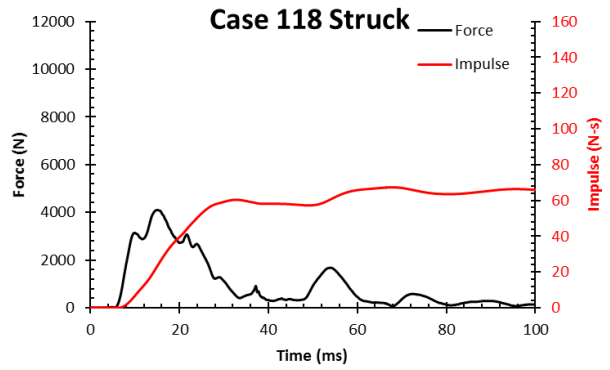
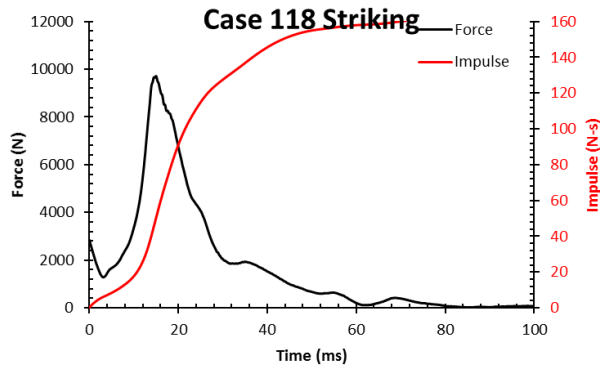
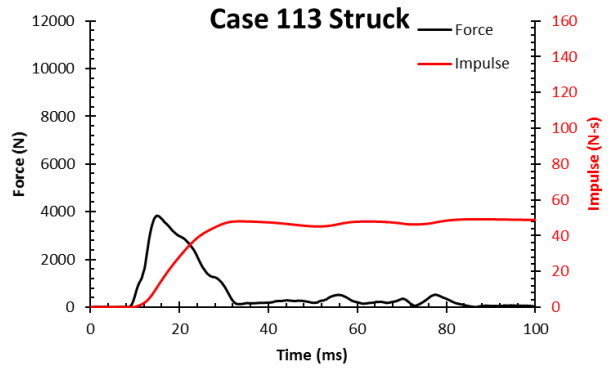
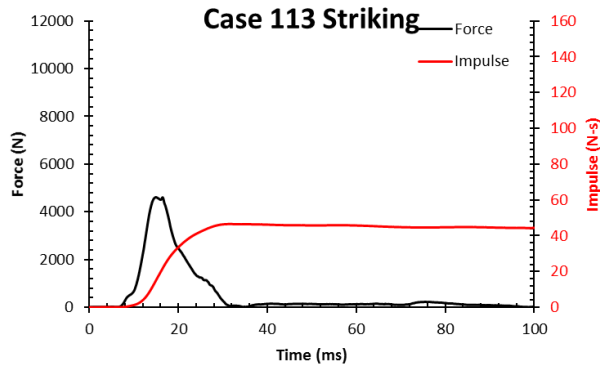
Location D, Impact Speed = 9.3 m/s																		
Helmet Mass	Total Mass		Acceleration		ΔV		Rot. Velocity		Lin. Momentum		Res. Upper Neck Force	Neck Tension	Res. Upper Neck Moment					
	(kg)	(kg)	(g)	(%)	(m/s)	(%)	(rad/s)	(%)	(kgm/s)	(%)	(N)	(N)	(Nm)	(%)				
Hybrid III - Head	0.00	4.54	0%	164.1	0%	10.50	0%	63.9	0%	47.7	0%	2680	0%	2225	0%	95.9	0%	
Helmet A	1.50	6.04	33%	130.5	-20%	8.25	-21%	69.8	9%	49.9	5%	3094	15%	2442	10%	116.3	21%	
Helmet B	1.59	6.13	35%	133.1	-19%	8.29	-21%	62.4	-2%	50.8	7%	2976	11%	2284	3%	119.1	24%	
Helmet C	1.84	6.38	41%	118.6	-28%	8.03	-24%	66.2	4%	51.2	7%	3142	17%	2694	21%	114.8	20%	
Helmet D	1.84	6.38	41%	136.4	-17%	7.85	-25%	65.8	3%	50.1	5%	3126	17%	2598	17%	105.6	10%	
Helmet E	1.85	6.39	41%	121.8	-26%	8.17	-22%	59.5	-7%	52.2	10%	3069	15%	2415	9%	126.5	32%	
Helmet F	1.85	6.39	41%	132.6	-19%	8.03	-24%	67.7	6%	51.3	8%	3191	19%	2651	19%	118.4	23%	
Helmet G	1.91	6.45	42%	142.9	-13%	7.89	-25%	57.7	-10%	50.9	7%	3287	23%	2456	10%	113.5	18%	
Helmet H	1.93	6.47	43%	114.0	-31%	7.44	-29%	54.8	-14%	48.1	1%	2950	10%	2601	17%	112.7	18%	
Helmet I	1.98	6.52	44%	129.5	-21%	7.49	-29%	60.0	-6%	48.9	2%	3103	16%	2445	10%	125.9	31%	
Helmet J	1.99	6.53	44%	118.7	-28%	7.17	-32%	61.4	-4%	46.8	-2%	3059	14%	2442	10%	97.6	2%	
Helmet K	2.00	6.54	44%	106.6	-35%	7.26	-31%	58.2	-9%	47.5	0%	2964	11%	2622	18%	114.8	20%	
Helmet L	2.06	6.60	45%	114.9	-30%	8.26	-21%	62.4	-2%	54.5	14%	3127	17%	2960	33%	118.6	24%	
Helmet M	2.08	6.62	46%	118.0	-28%	8.17	-22%	70.7	11%	54.1	13%	3345	25%	2732	23%	121.6	27%	
Helmet N	2.19	6.73	48%	119.9	-27%	7.61	-28%	59.5	-7%	51.2	7%	2782	4%	2450	10%	89.6	-7%	
Average			42%		-24%			-25%		-2%		15%		15%		15%		19%
Std Dev			4%		6%			4%		7%		5%		5%		7%		10%

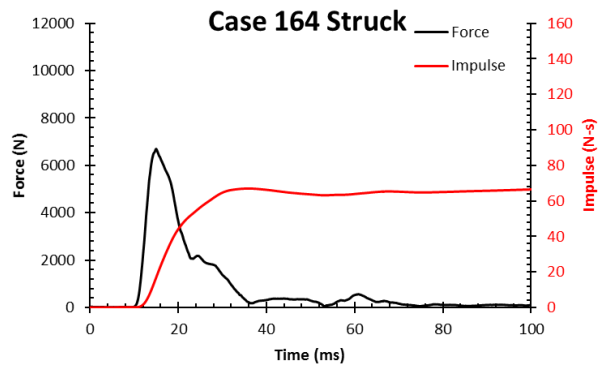
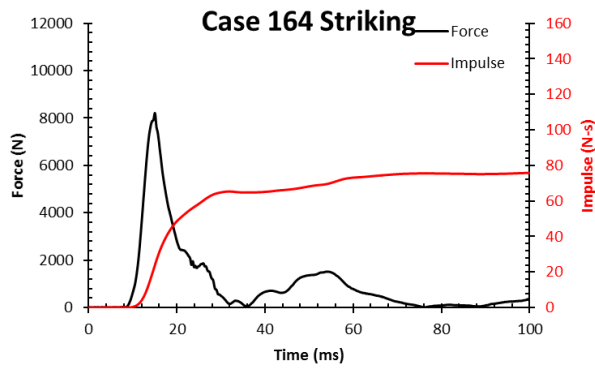
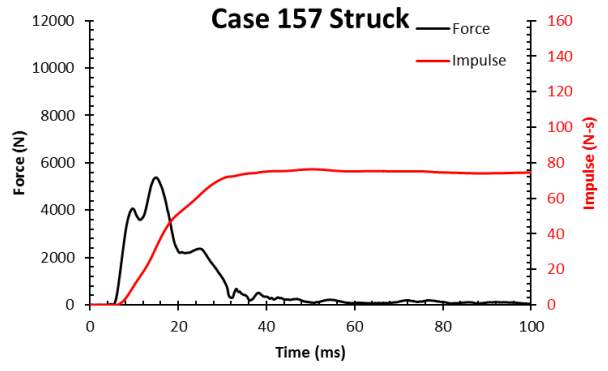
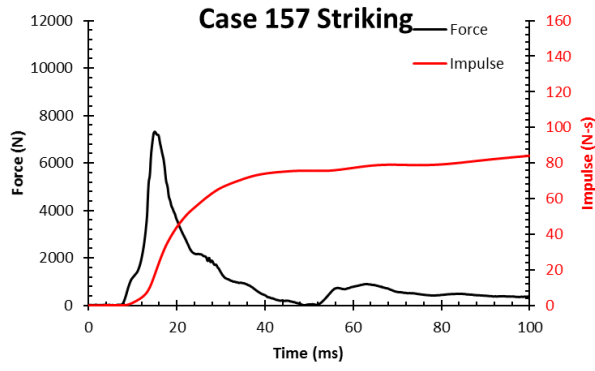
APPENDIX C.1 – IMPACT FORCE AND IMPULSE CURVES FOR EACH CASE





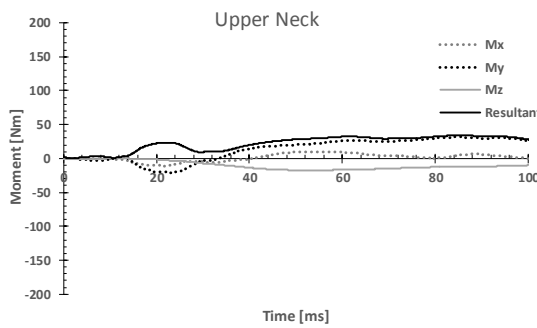
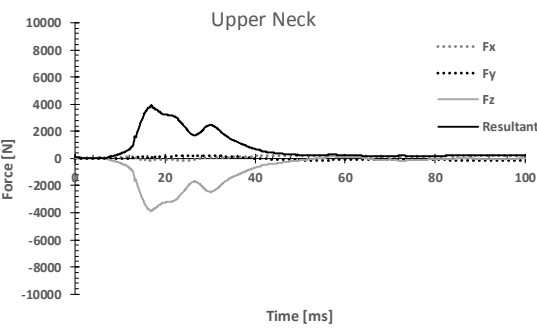
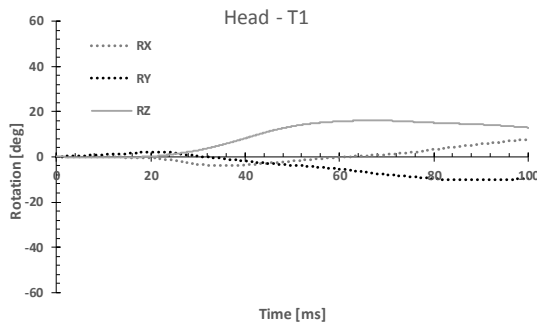
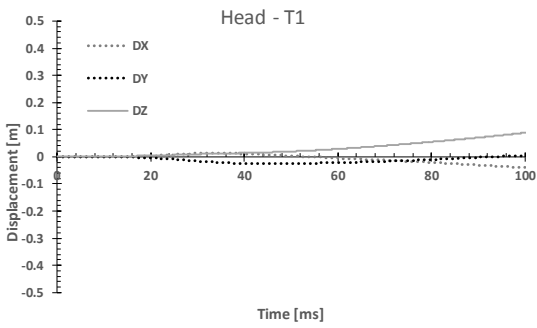
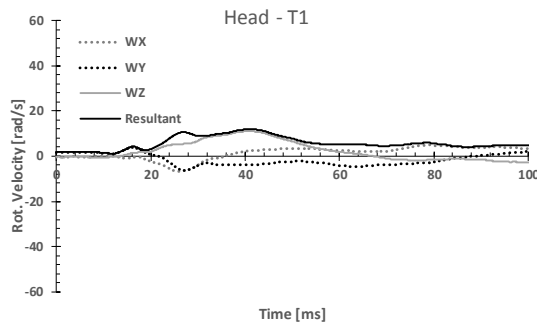
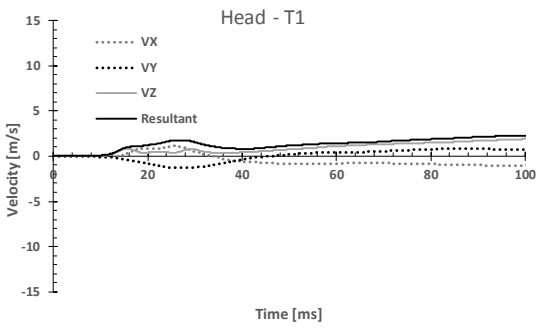
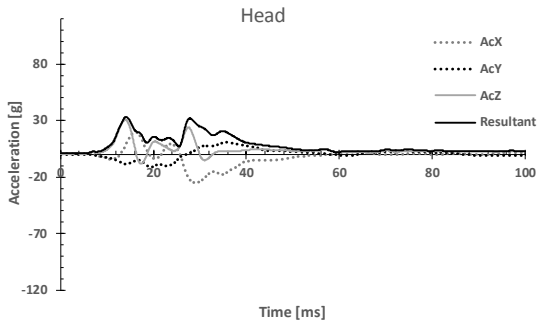




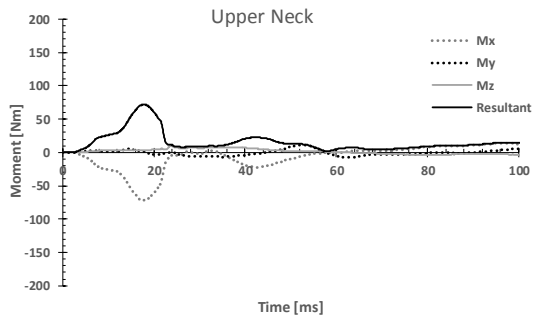
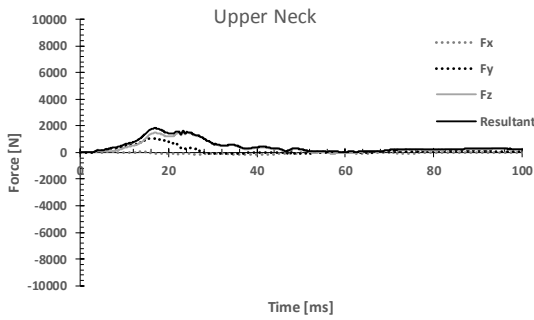
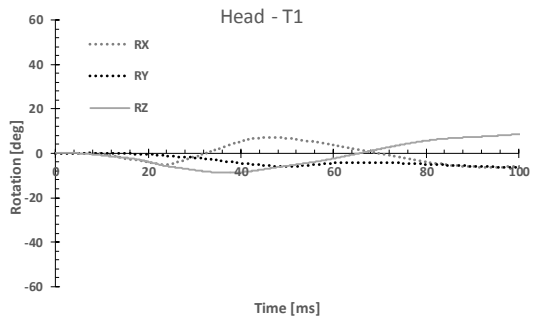
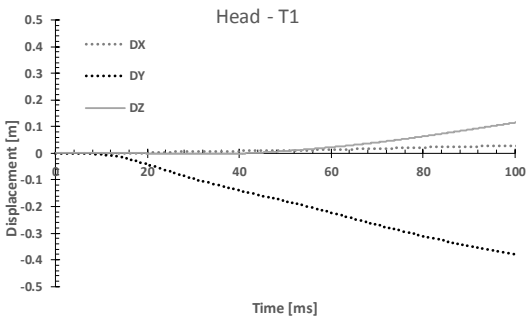
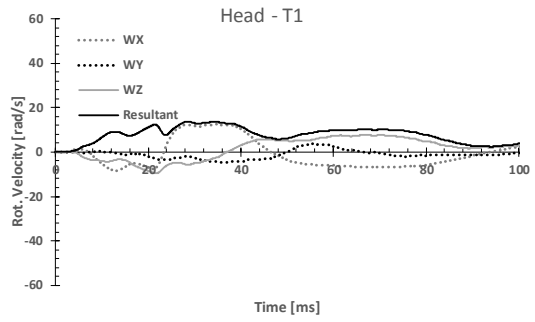
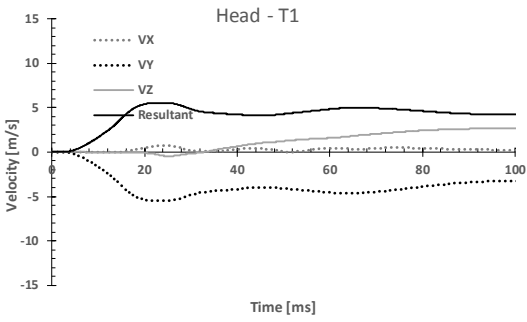
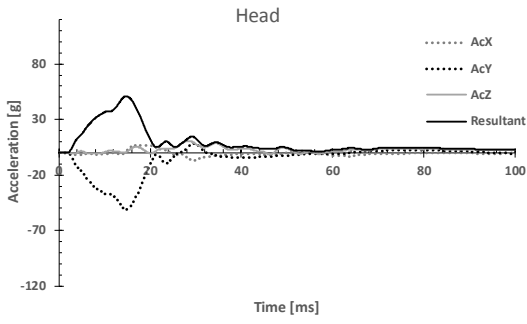


APPENDIX C.2 – ATD HEAD KINEMATICS AND NECK KINETICS FOR EACH CASE

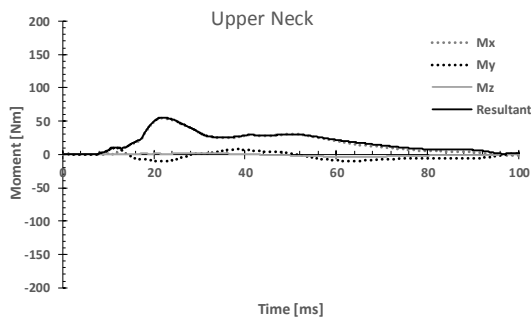
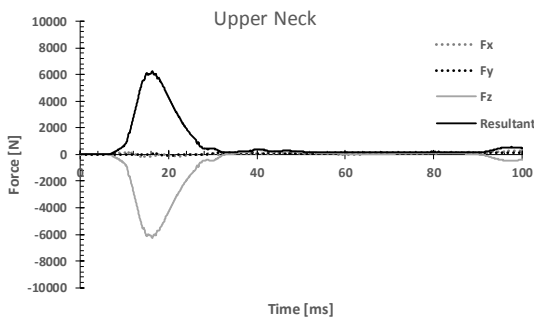
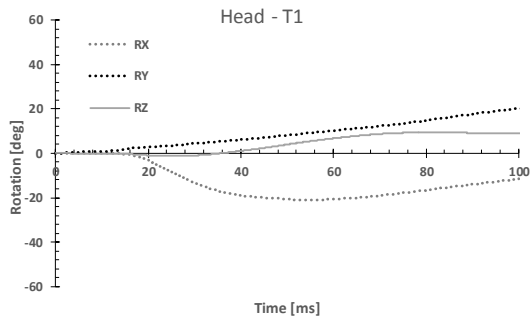
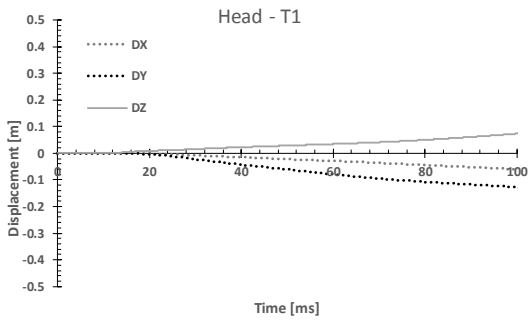
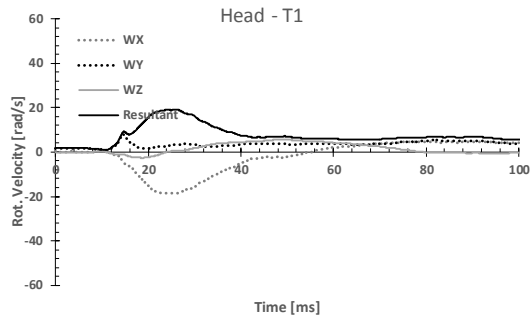
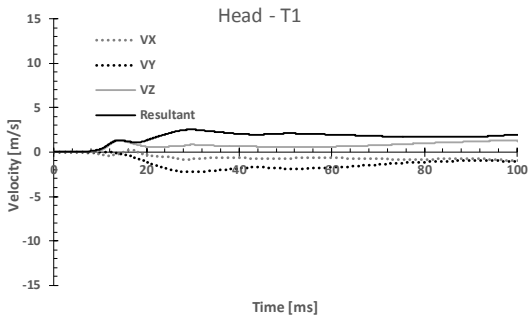
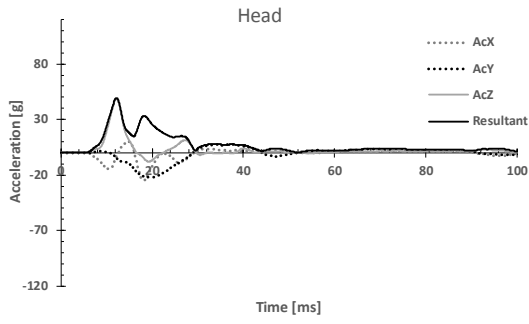
Case 7 Striking



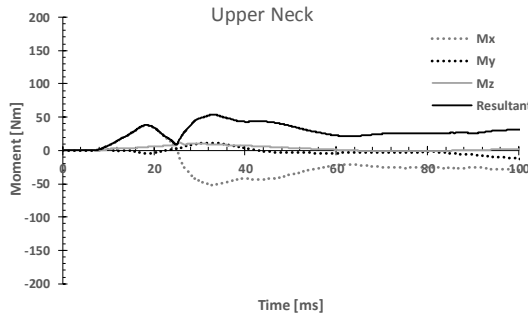
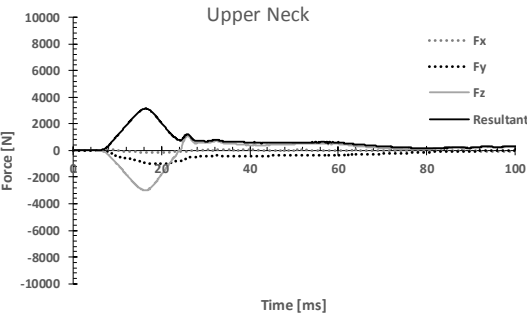
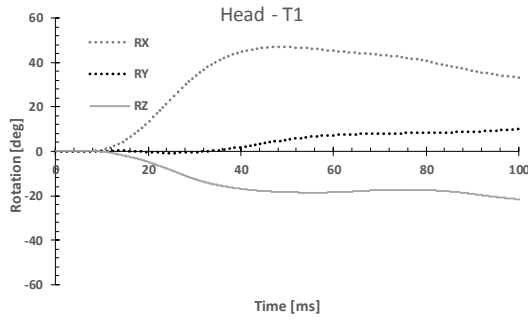
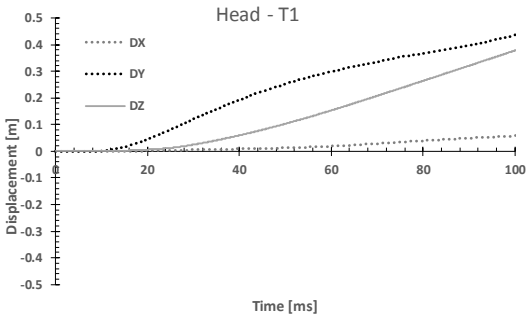
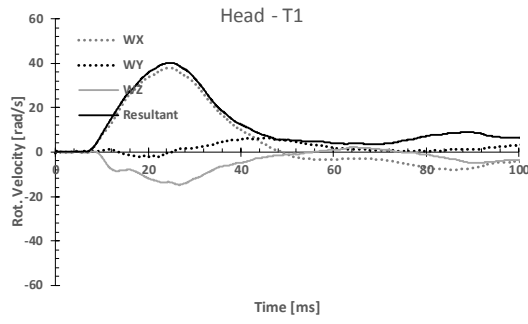
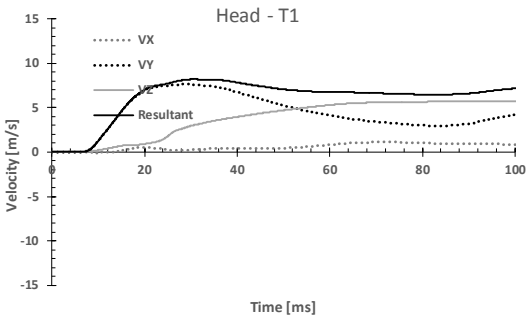
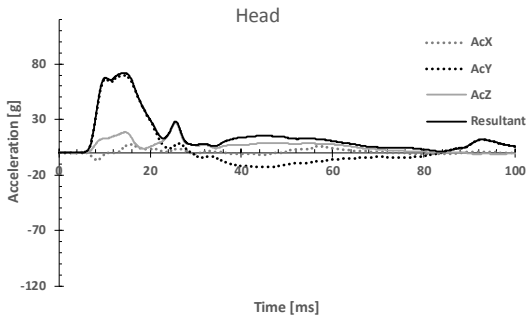
Case 7 Struck



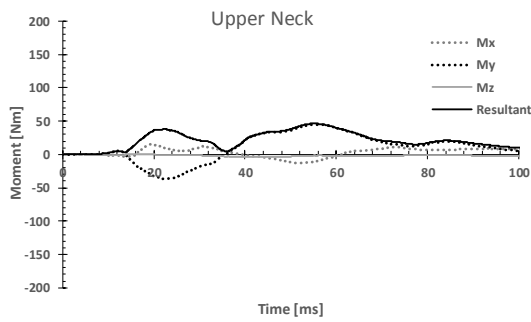
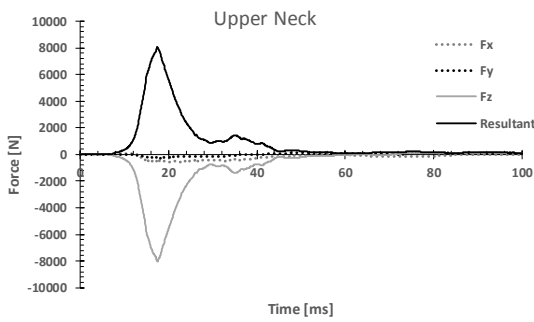
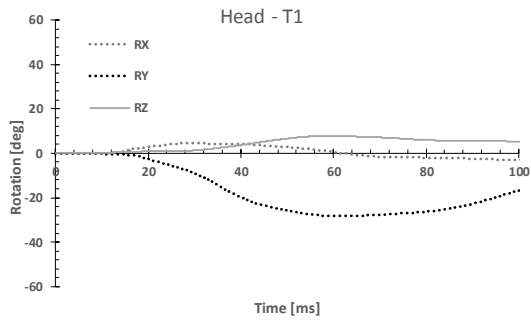
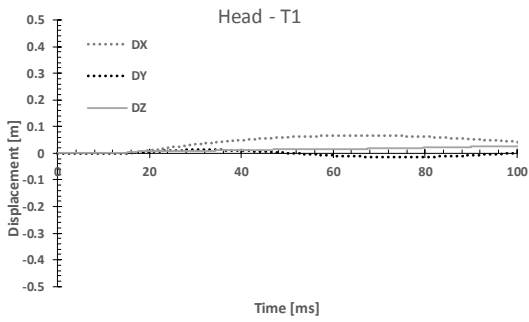
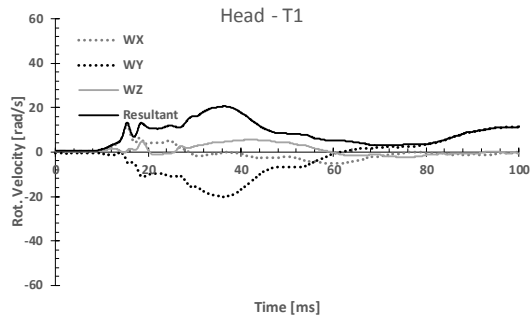
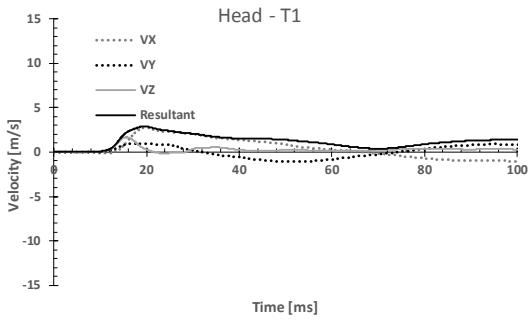
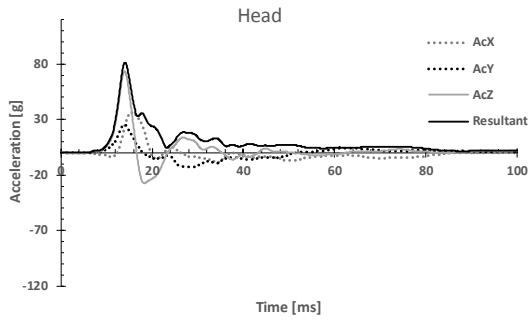
Case 9 Striking



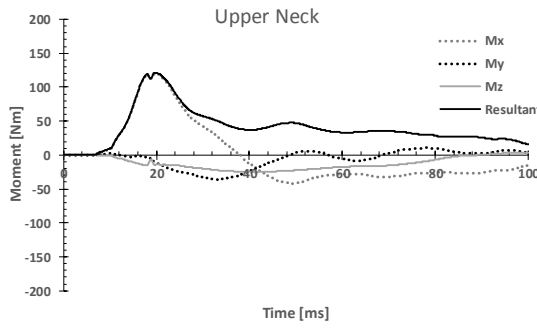
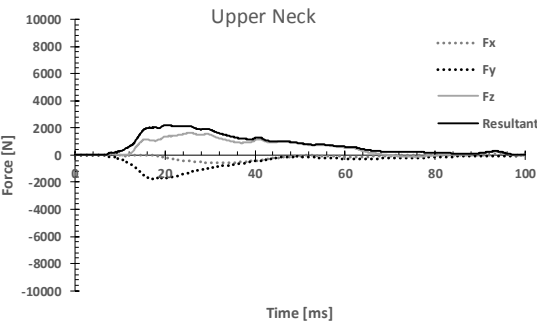
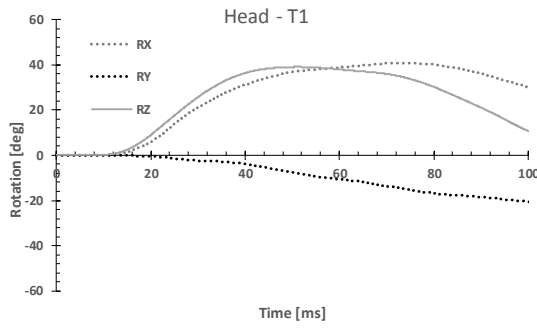
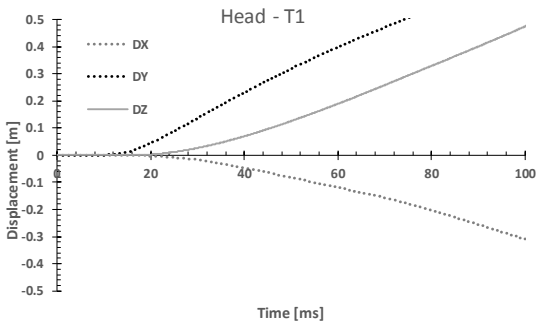
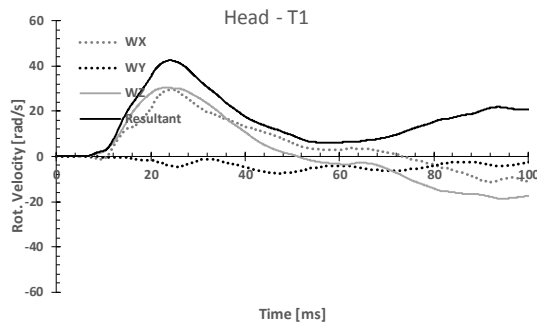
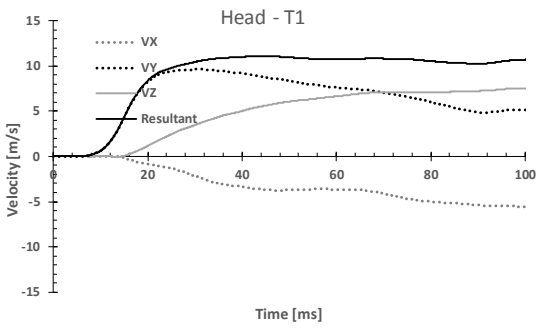
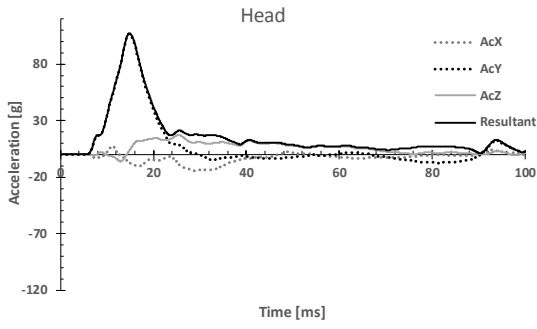
Case 9 Struck



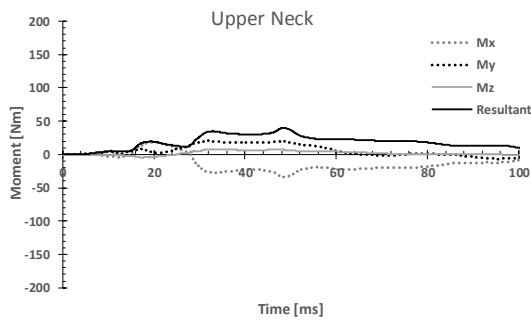
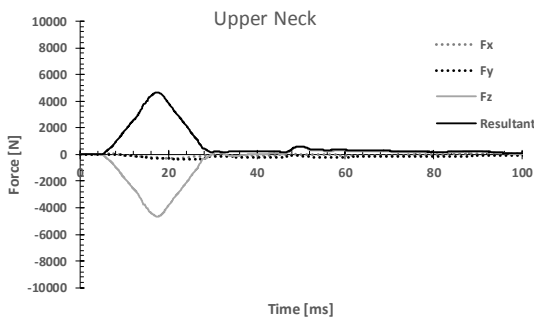
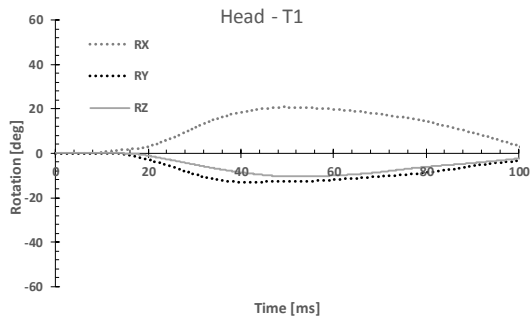
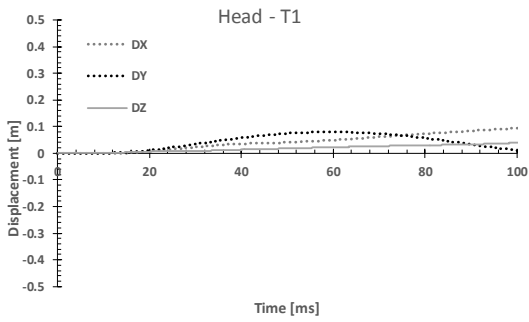
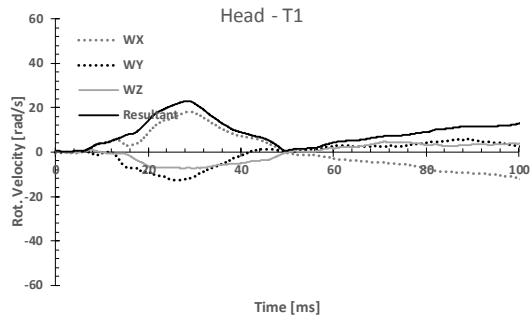
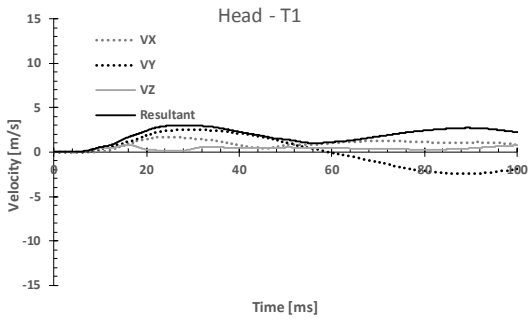
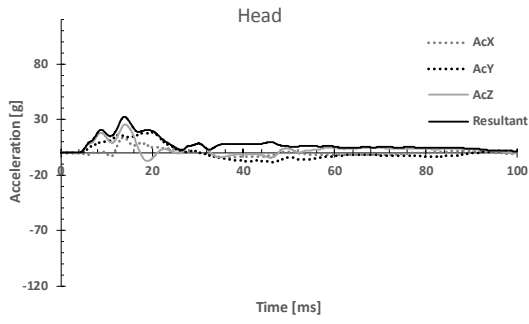
Case 38 Striking



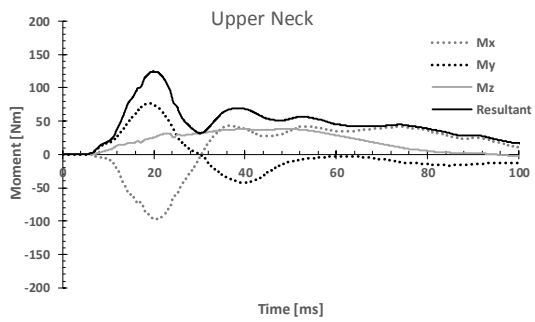
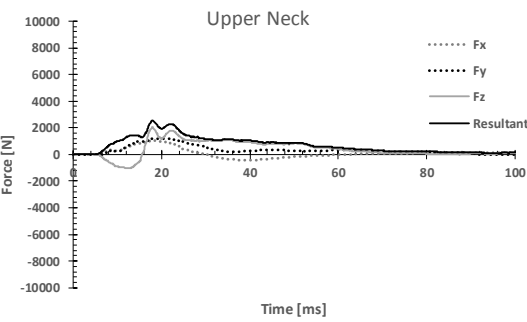
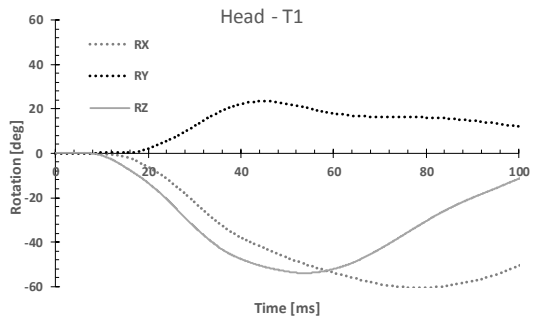
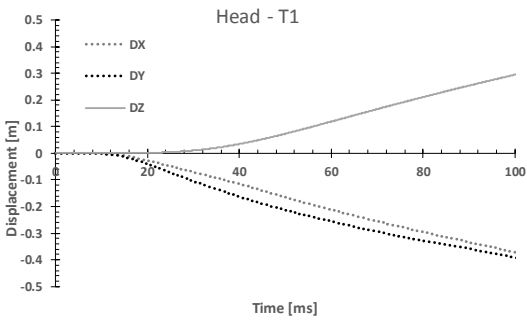
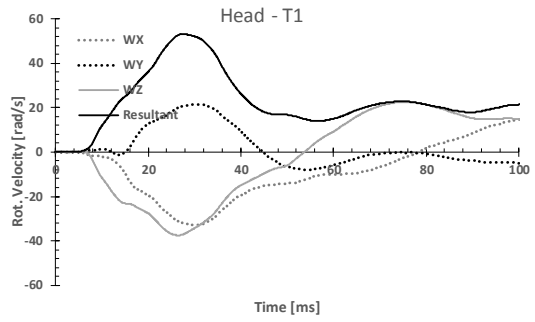
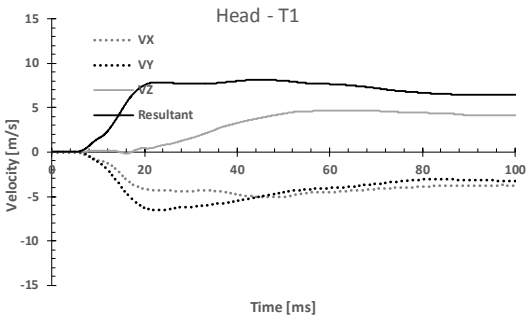
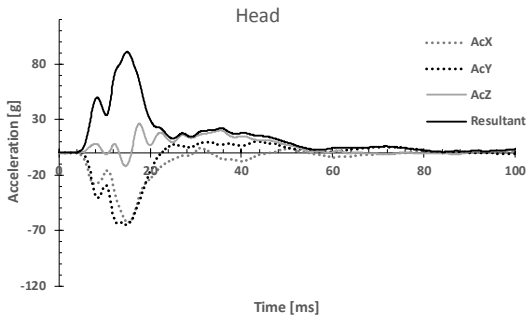
Case 38 Struck



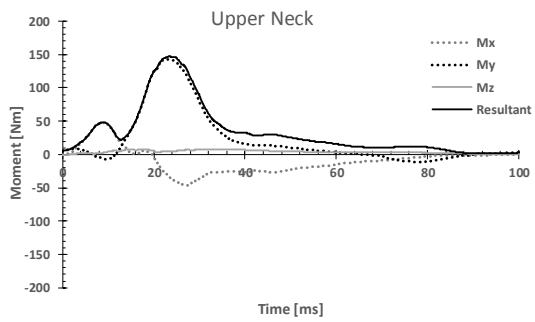
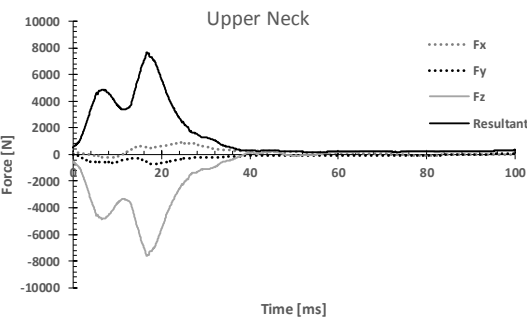
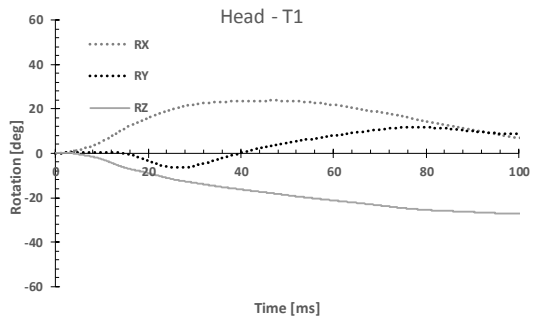
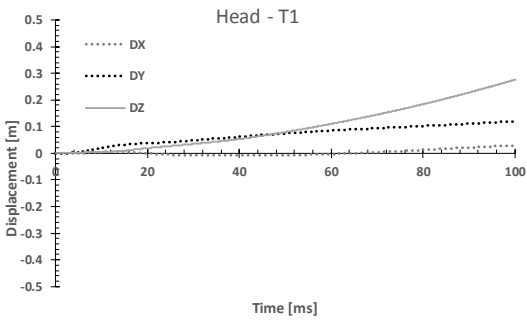
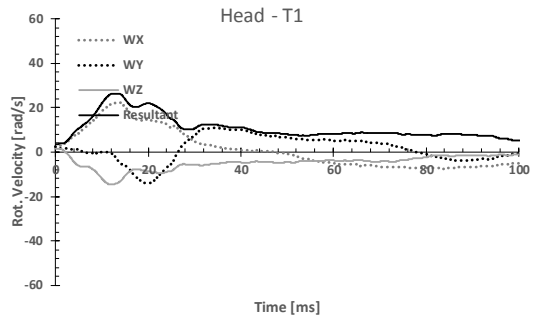
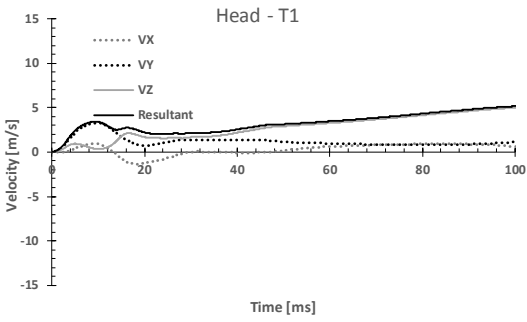
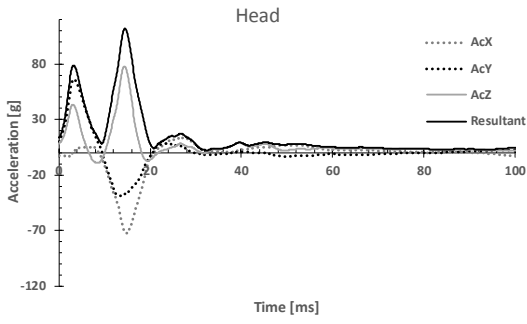
Case 39 Striking



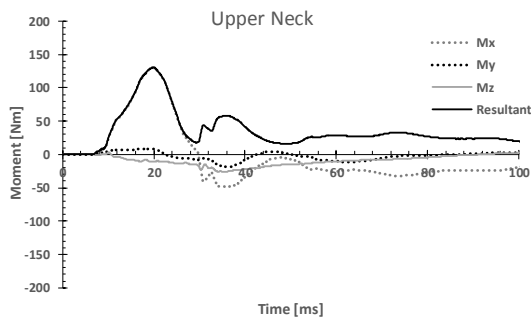
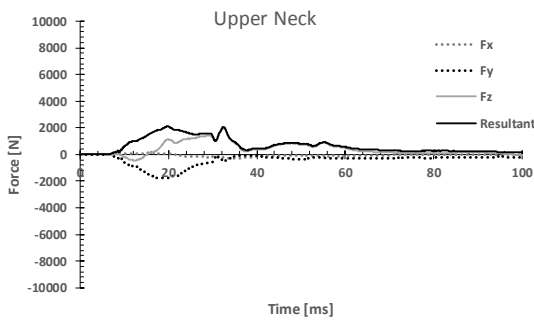
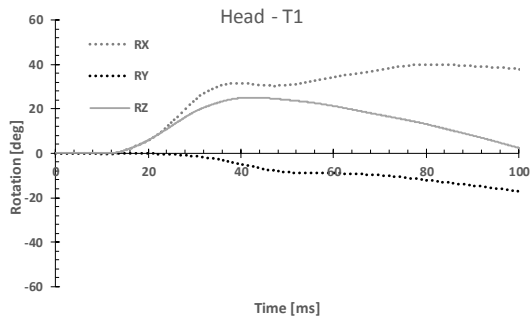
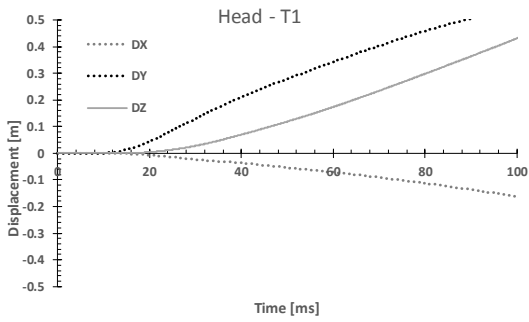
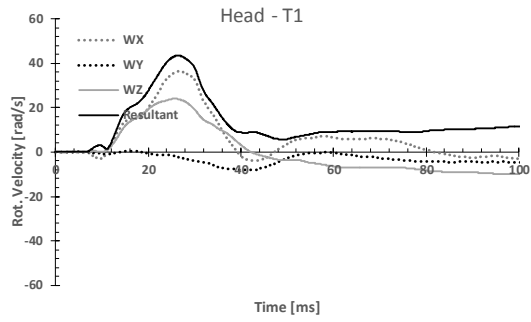
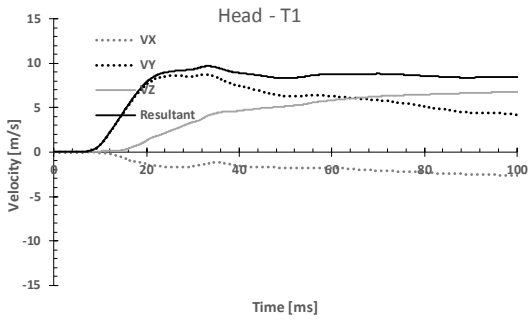
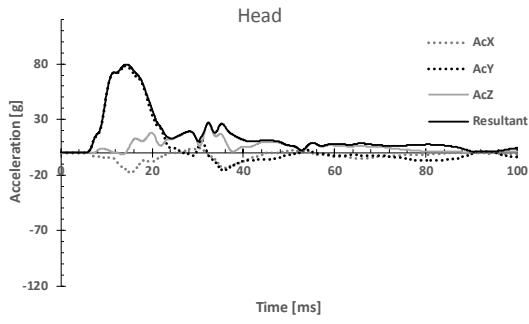
Case 39 Struck



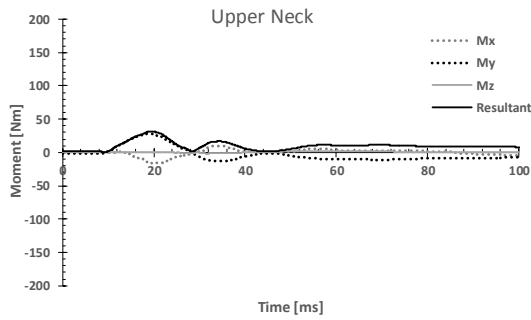
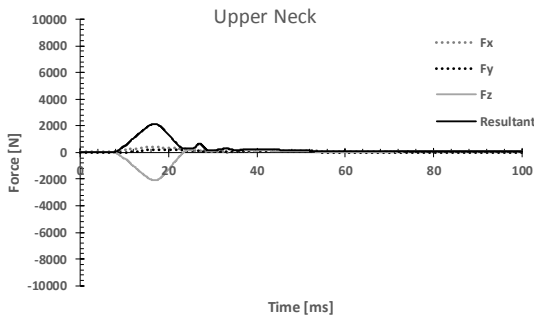
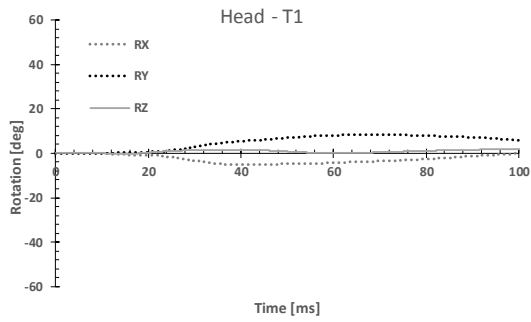
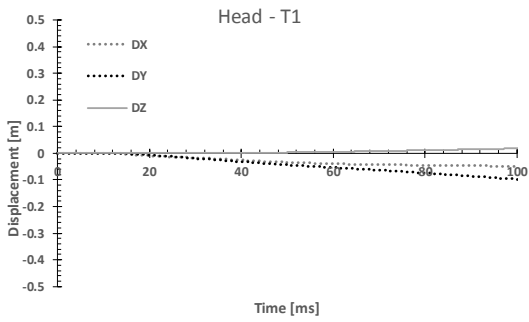
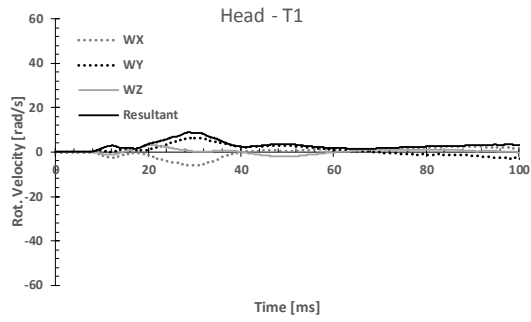
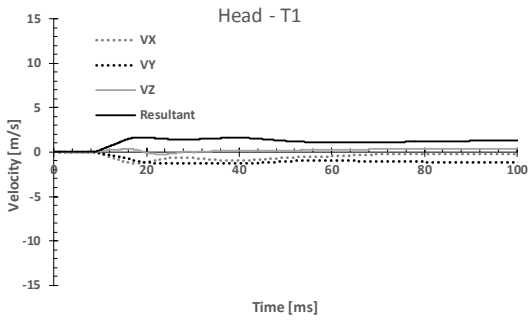
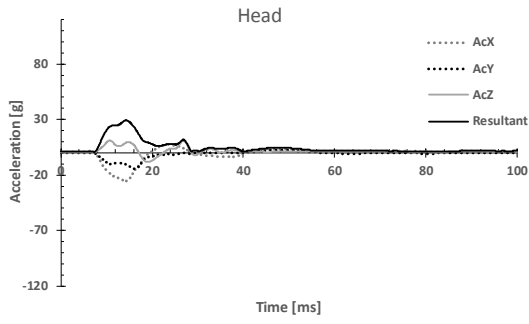
Case 57 Striking



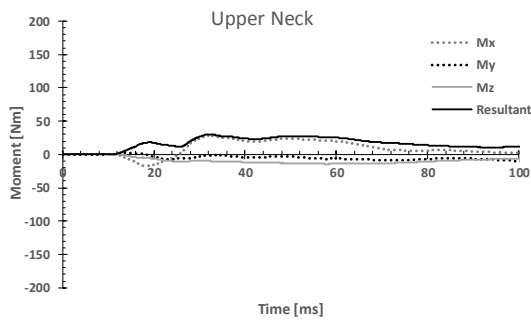
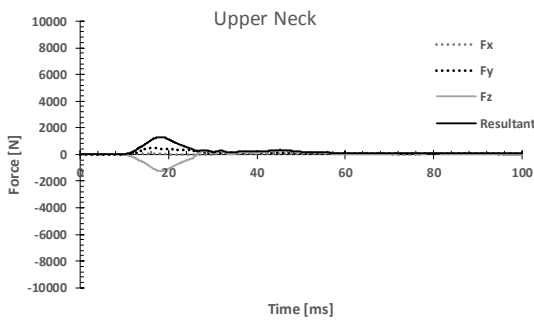
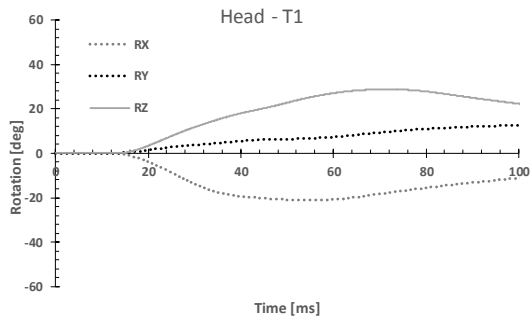
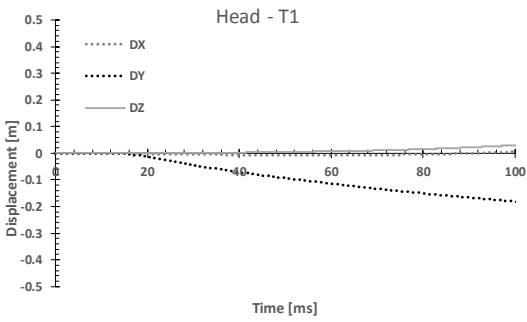
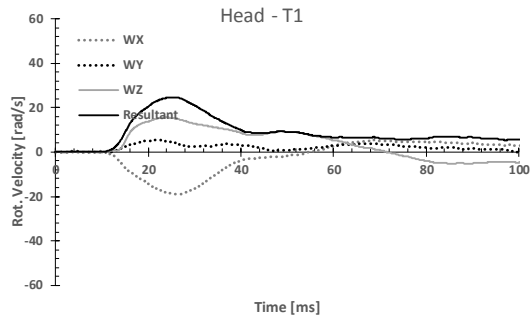
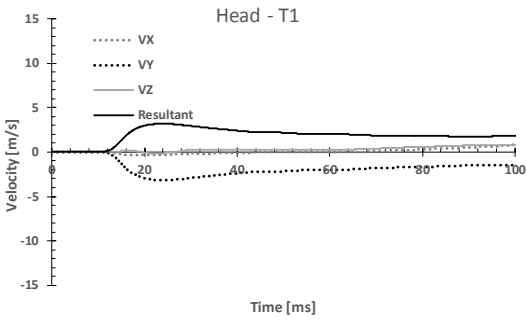
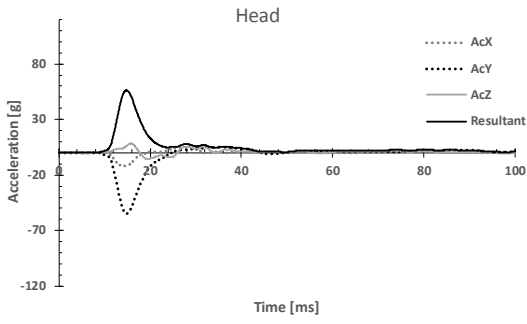
Case 57 Struck



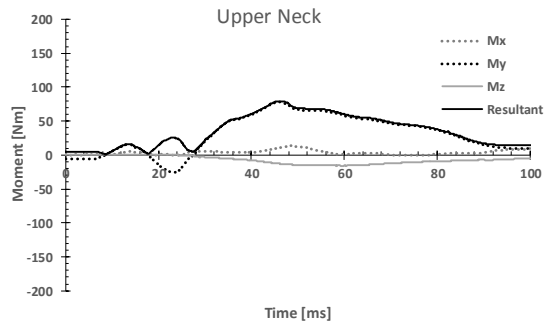
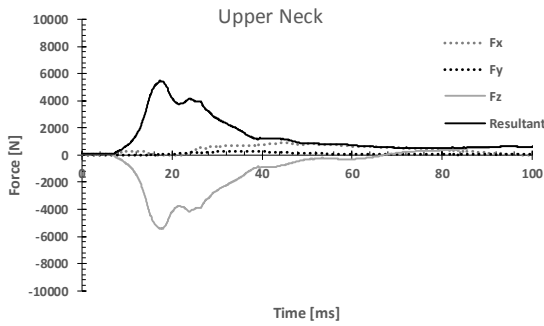
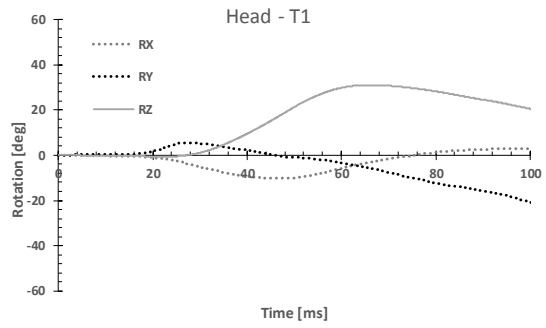
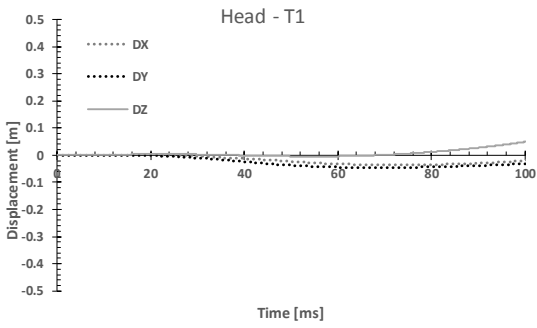
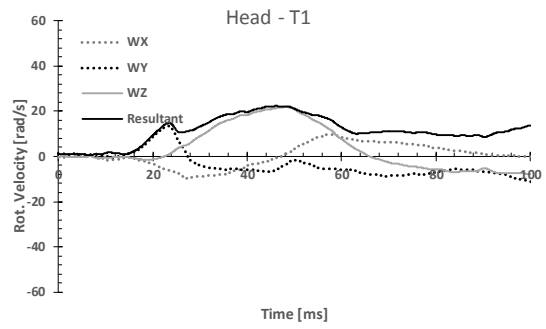
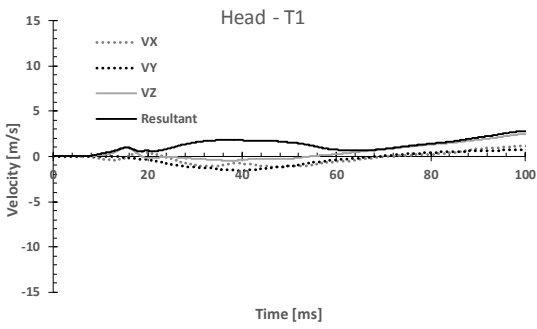
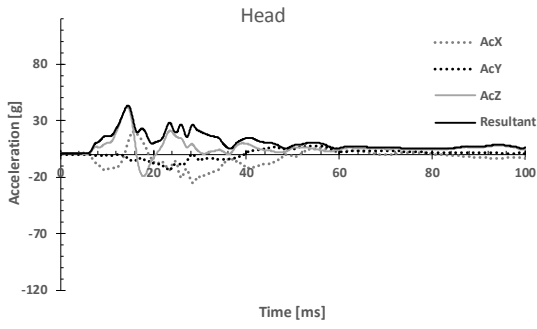
Case 59 Striking



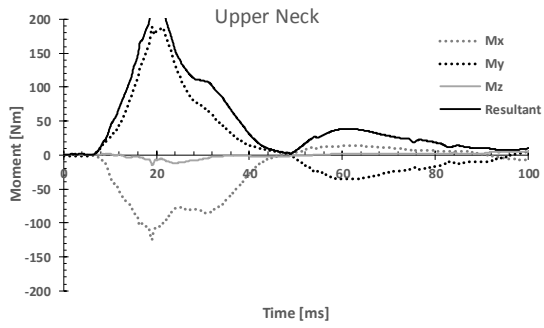
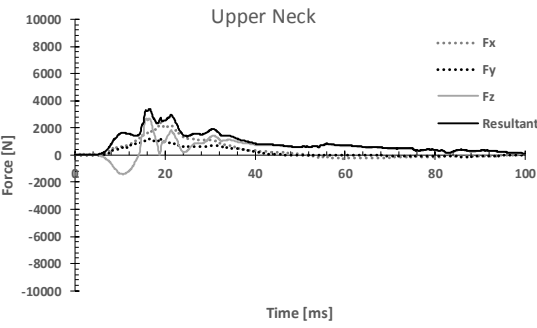
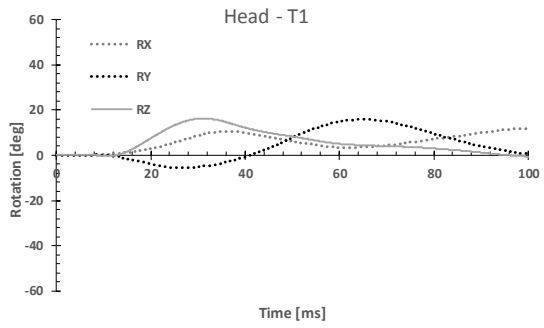
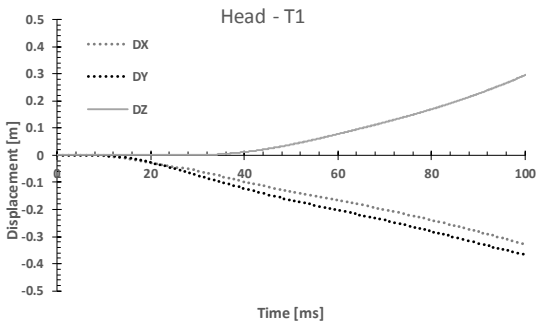
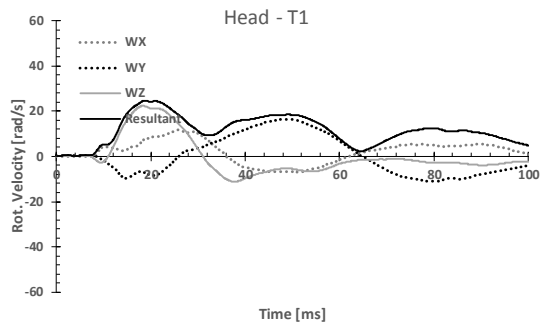
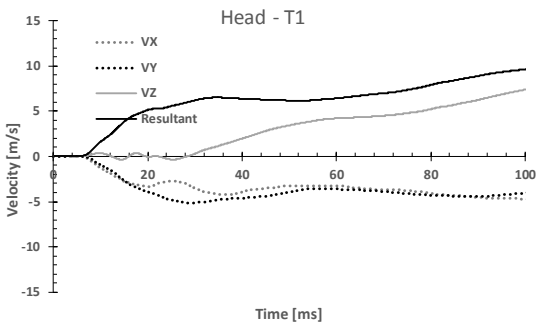
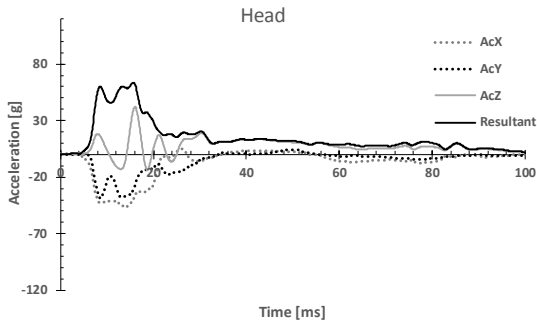
Case 59 Struck



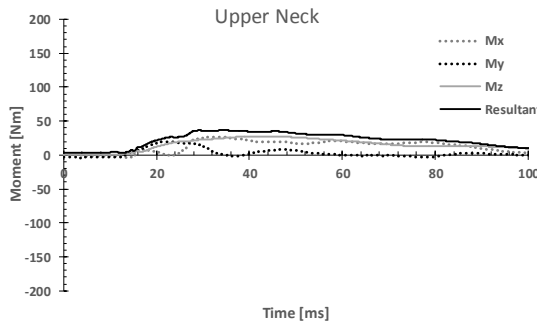
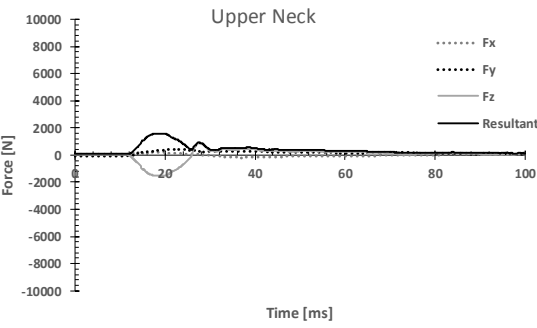
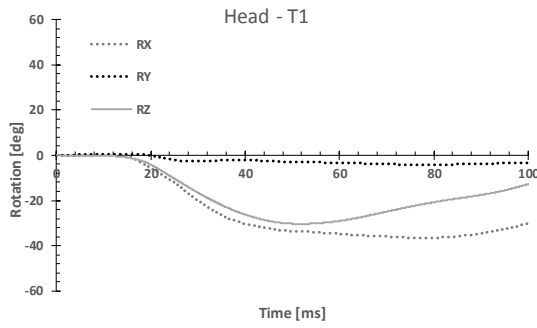
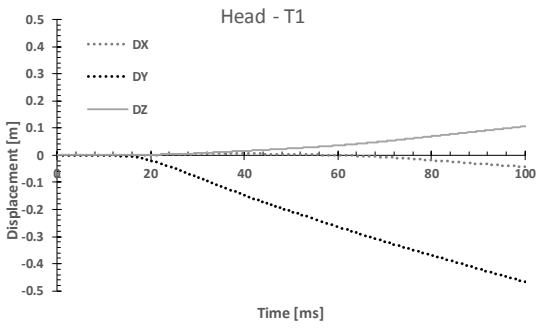
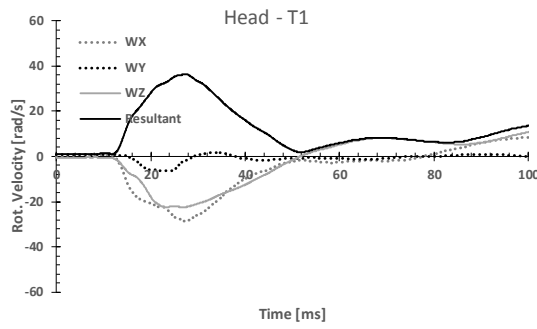
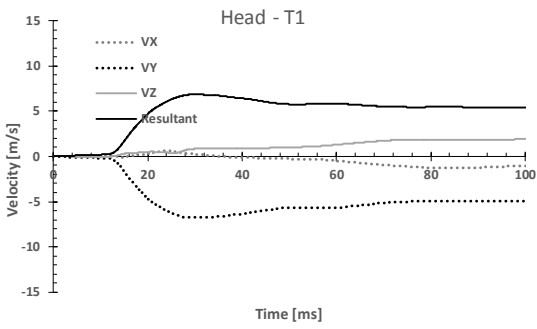
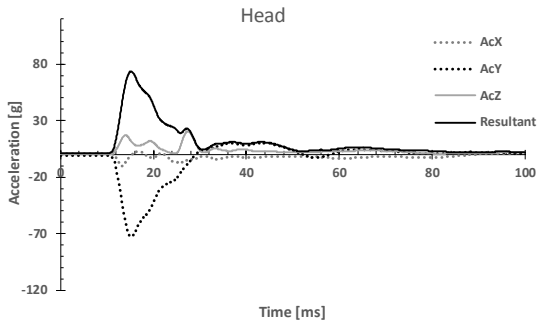
Case 69 Striking



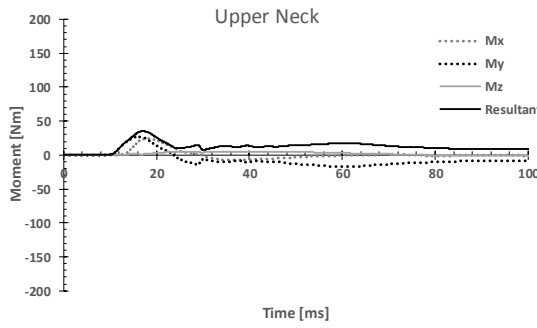
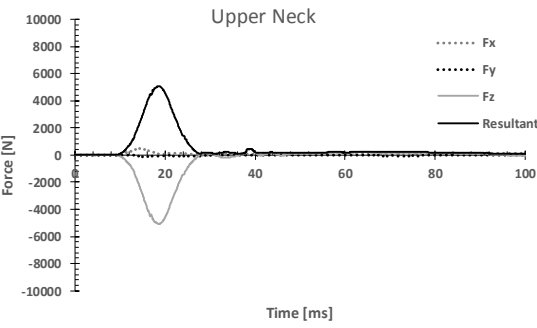
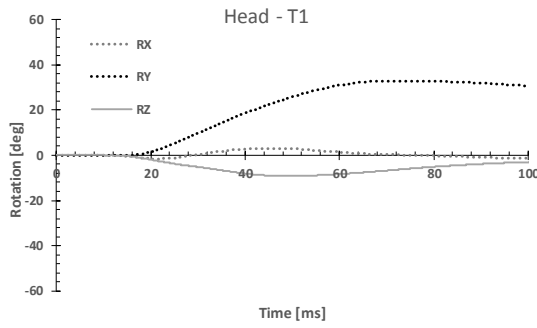
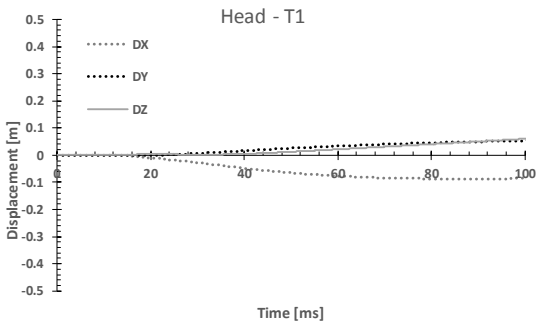
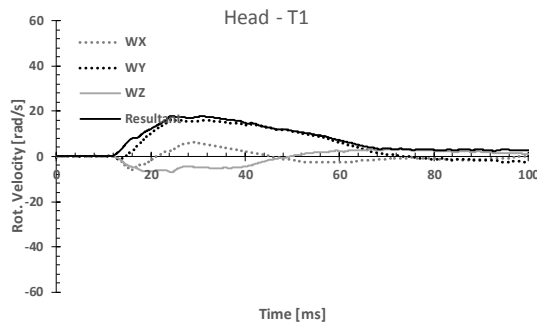
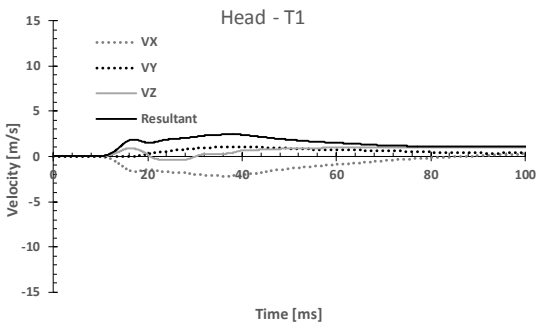
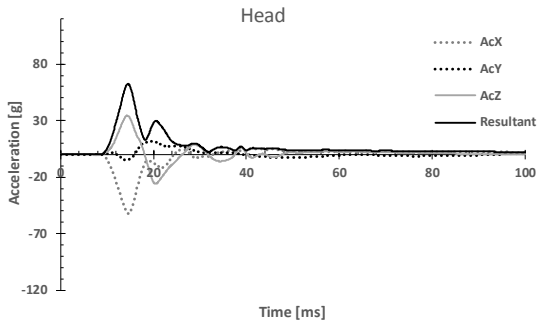
Case 69 Struck



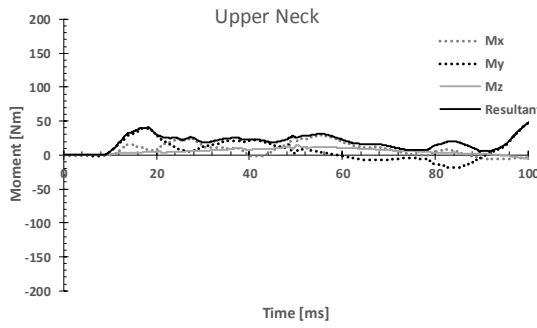
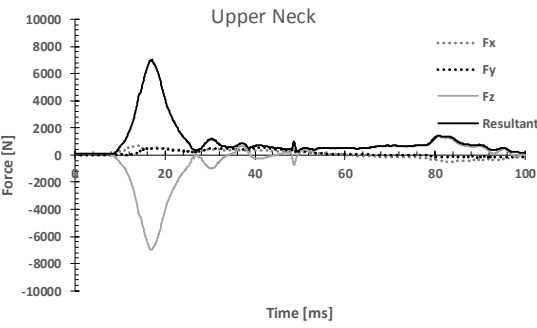
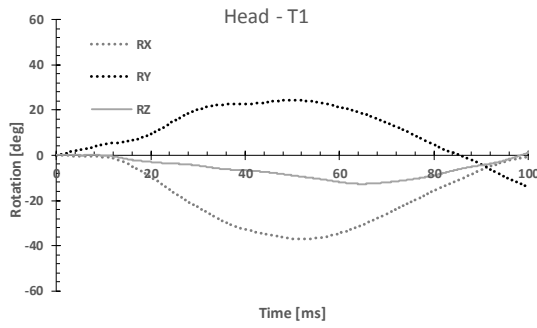
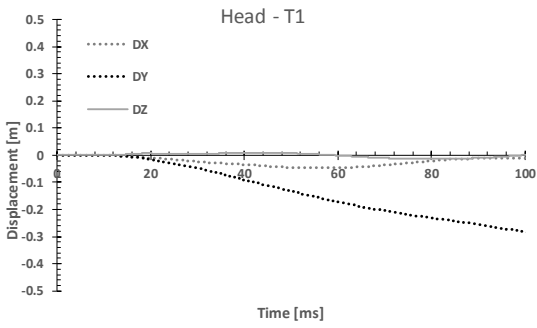
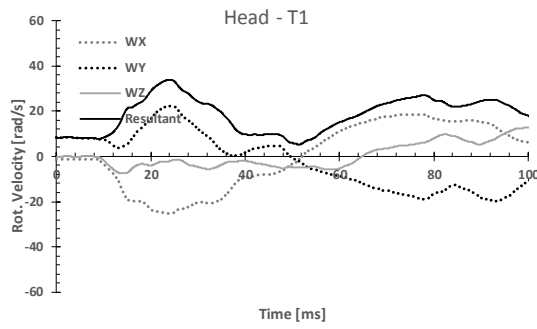
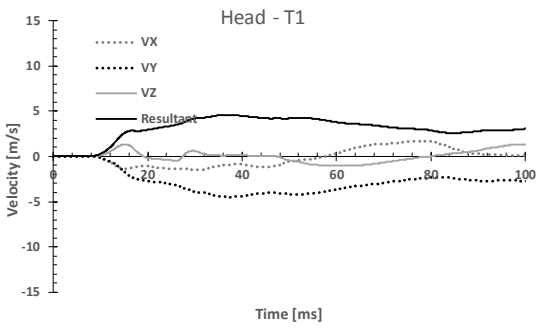
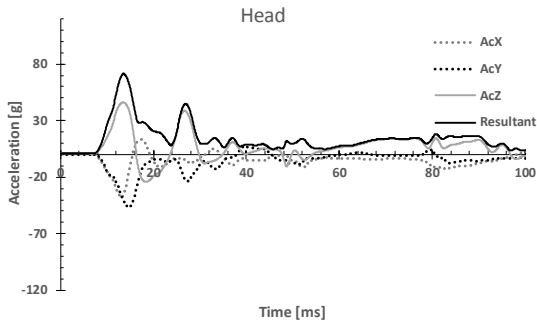
Case 71 Striking



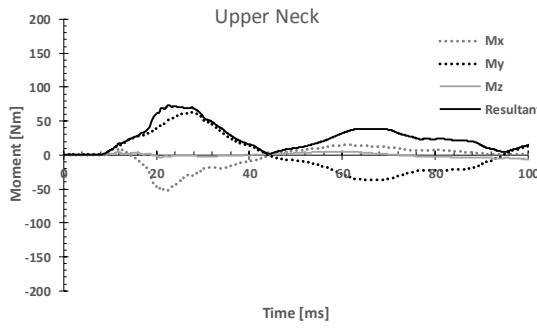
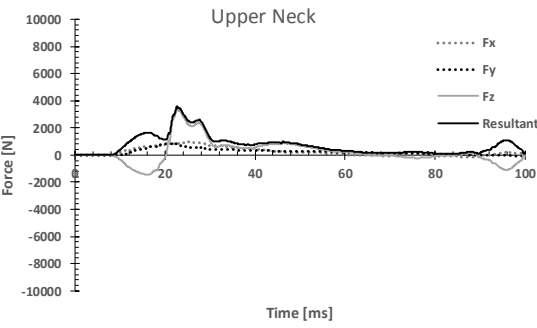
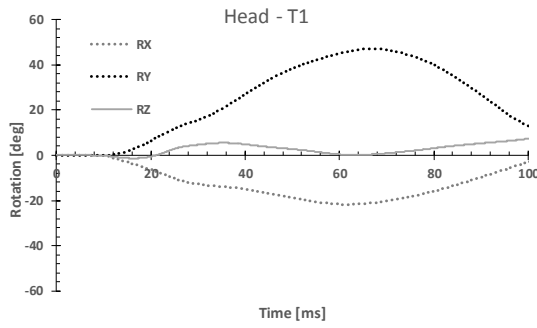
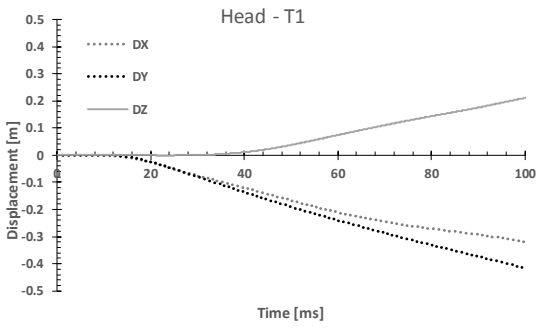
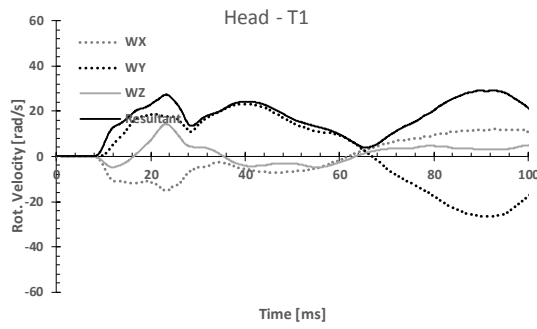
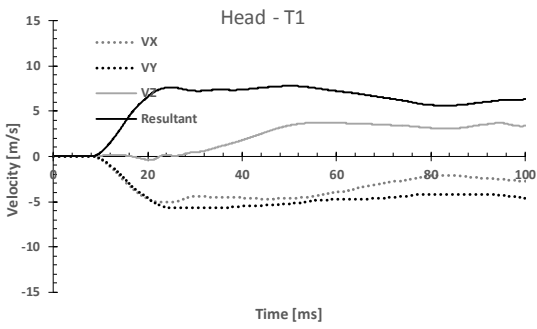
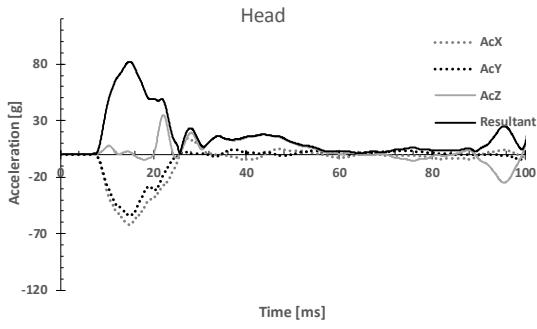
Case 71 Struck



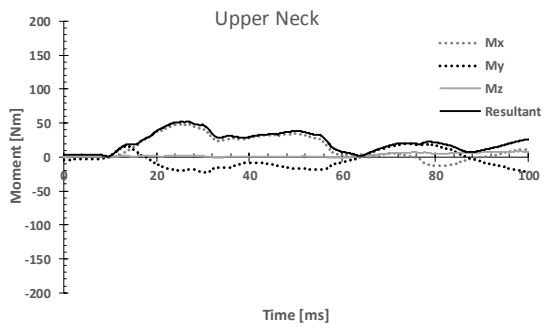
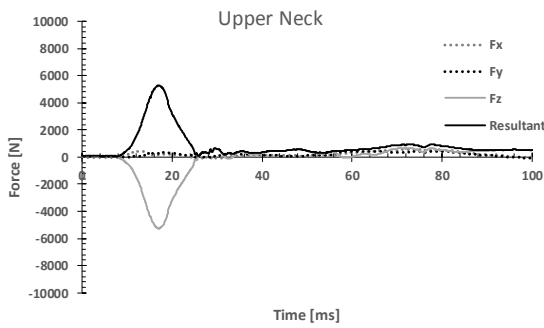
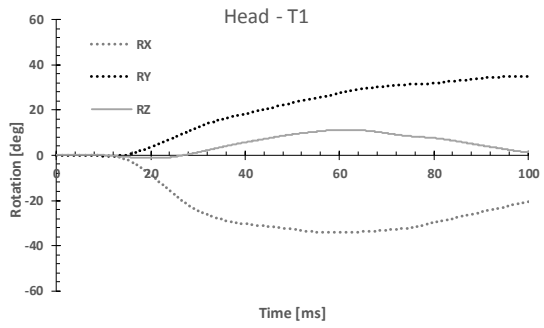
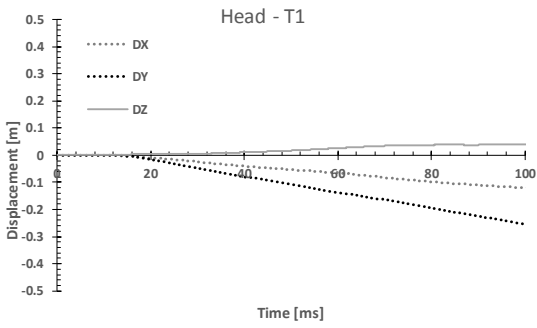
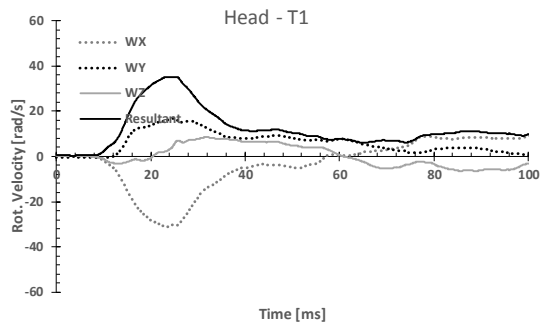
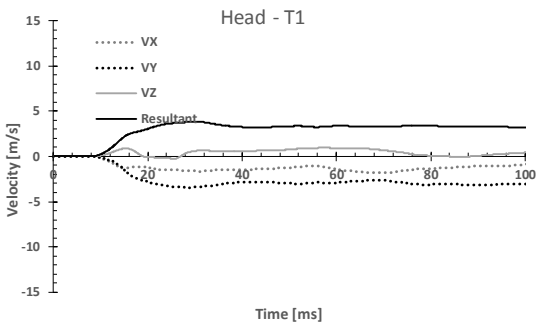
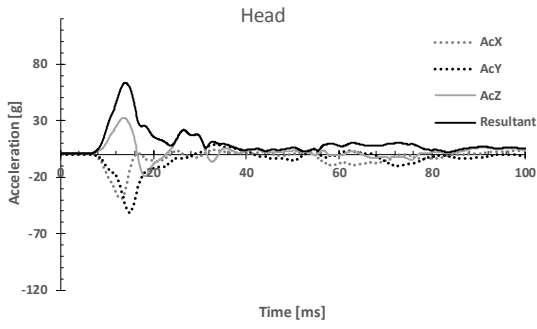
Case 77 Striking



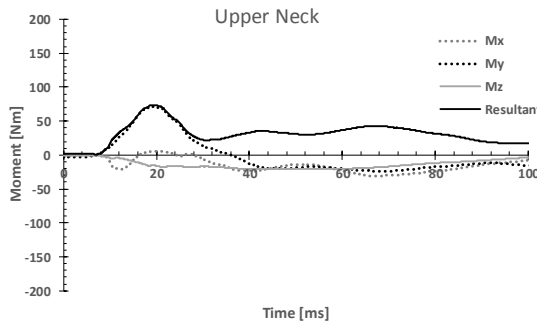
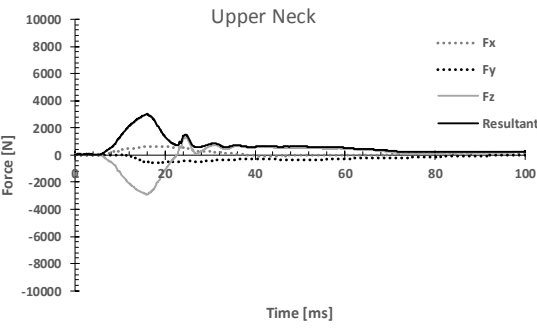
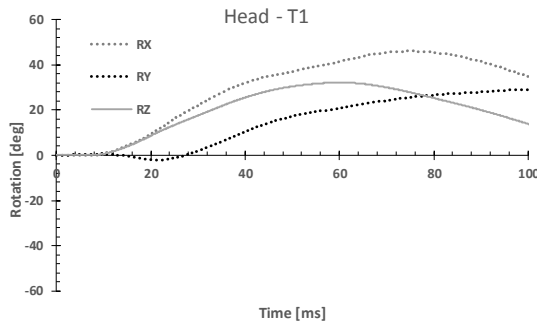
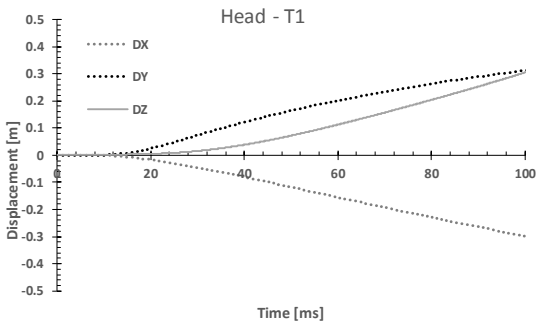
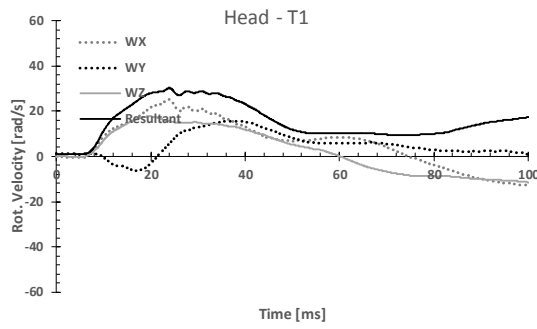
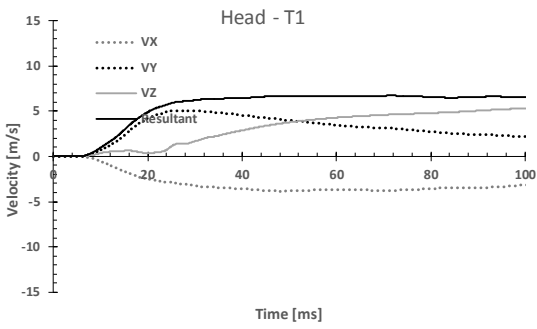
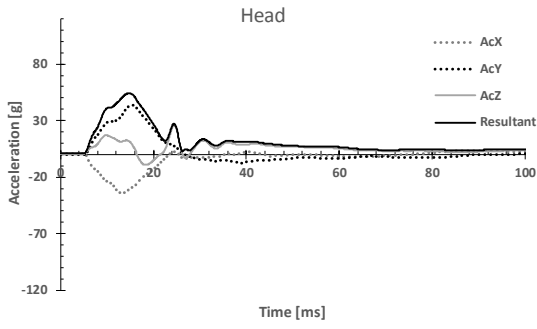
Case 77 Struck



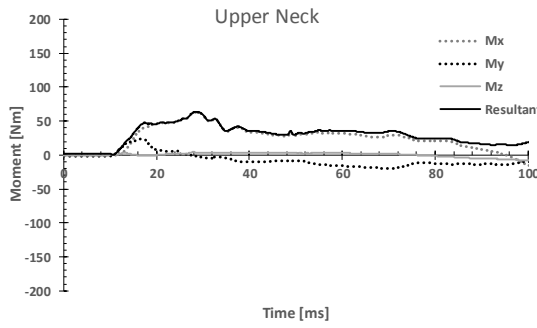
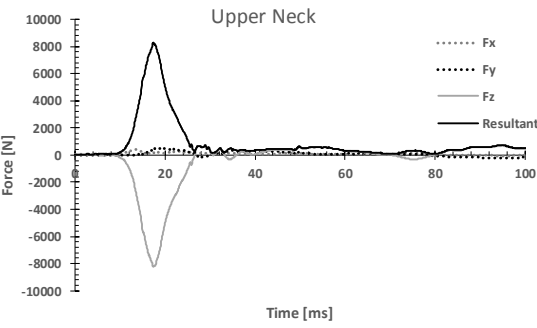
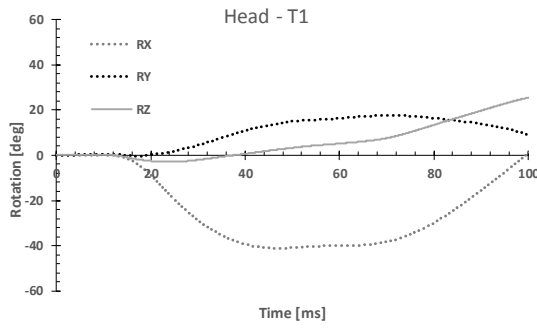
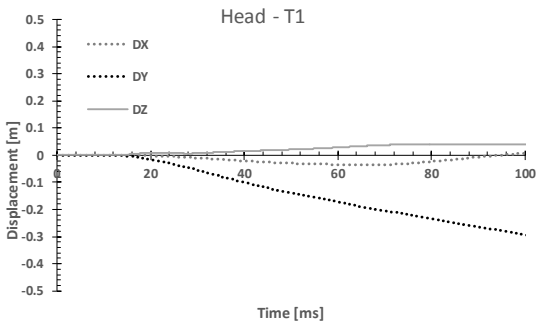
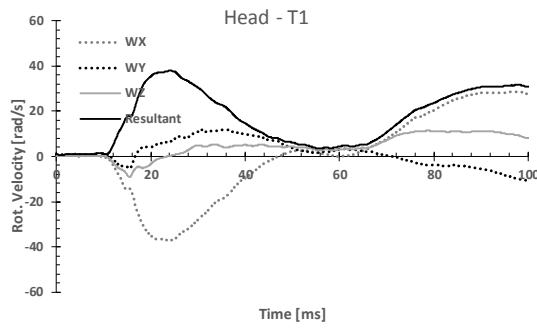
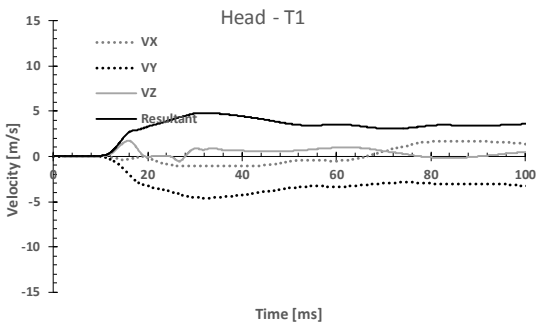
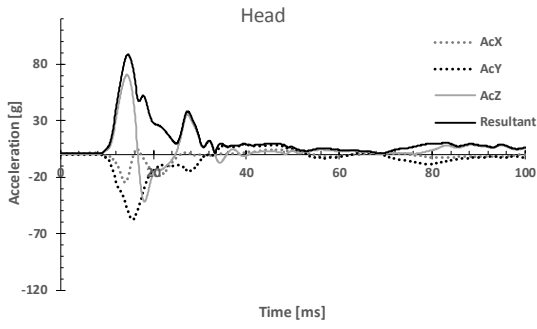
Case 84 Striking



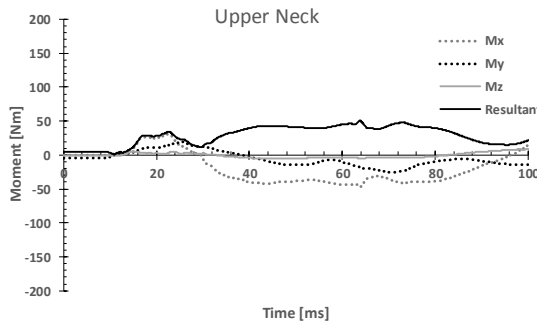
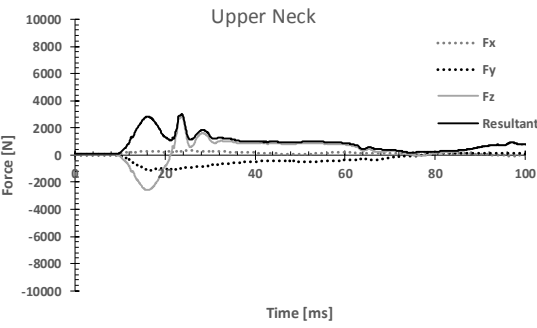
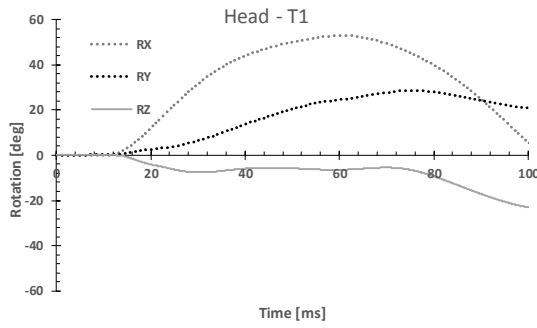
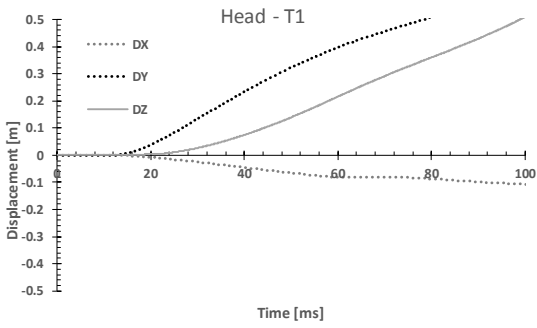
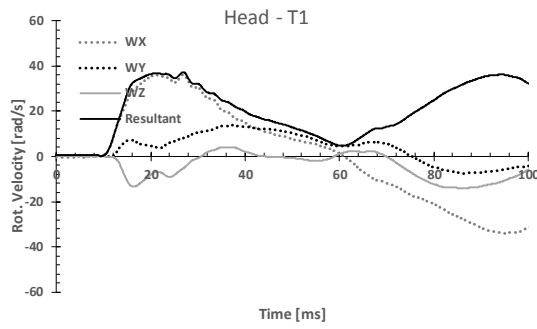
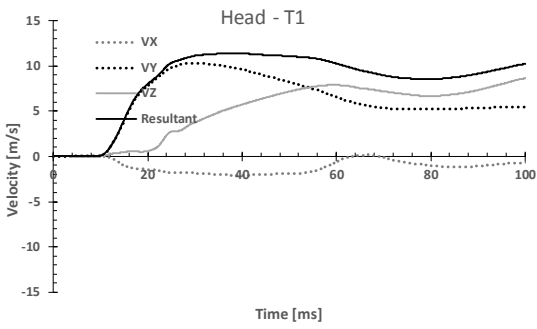
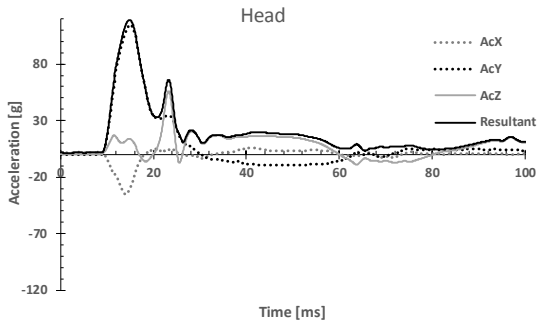
Case 84 Struck



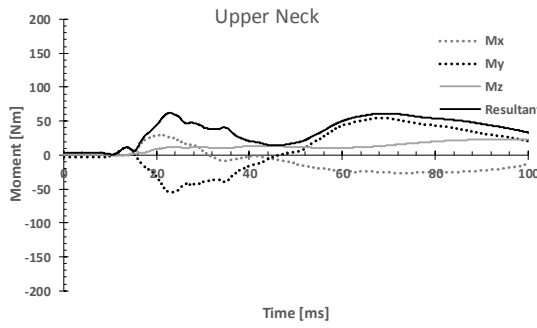
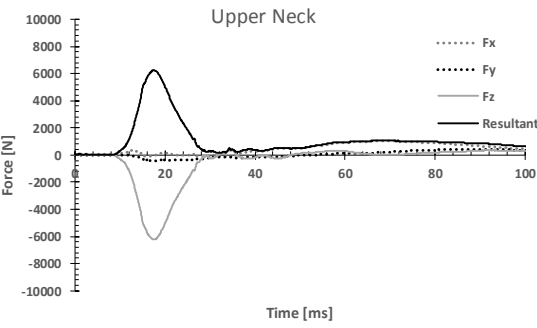
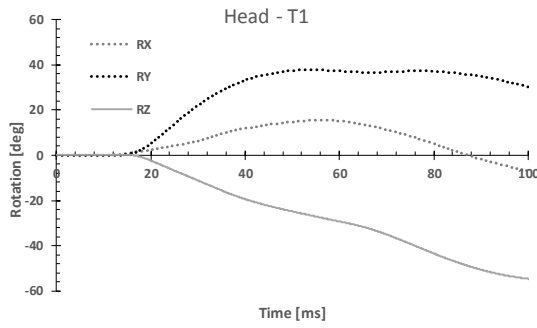
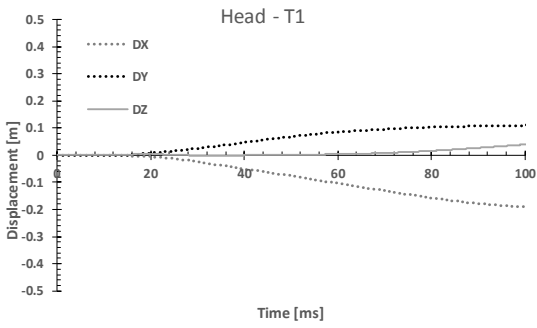
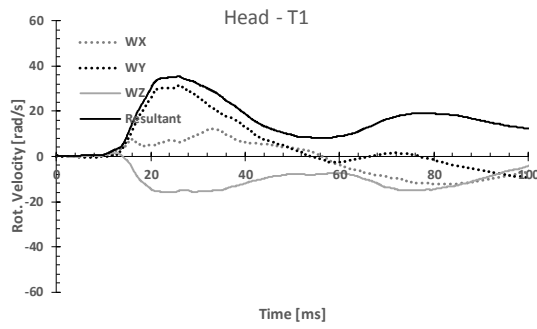
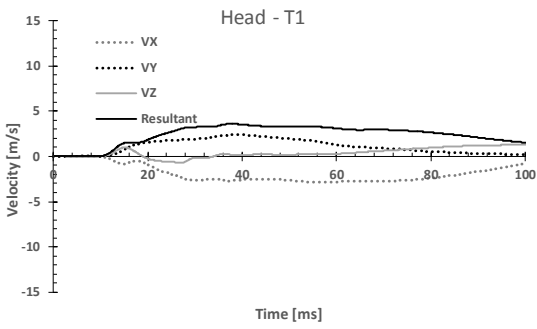
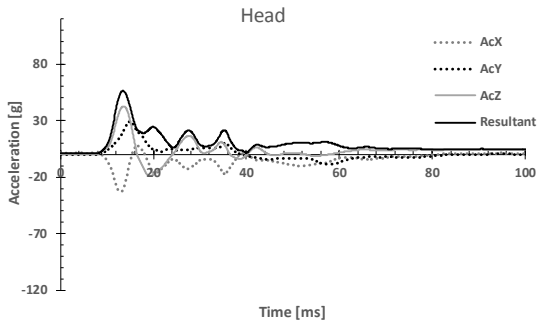
Case 92 Striking



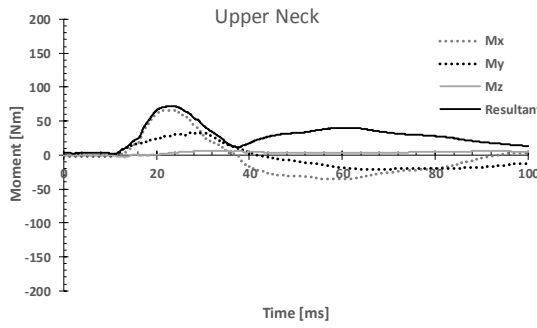
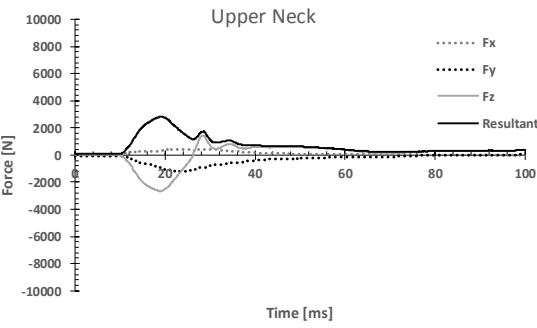
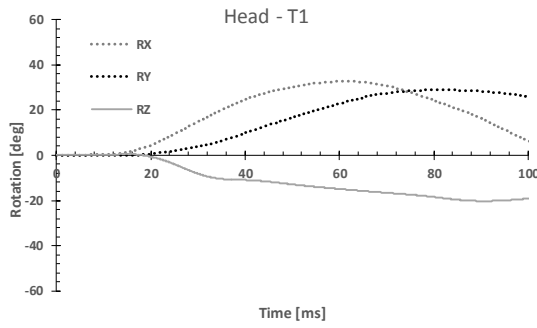
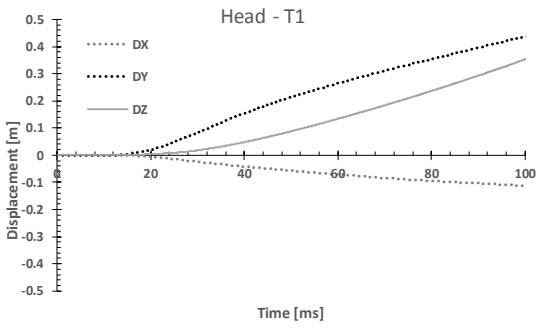
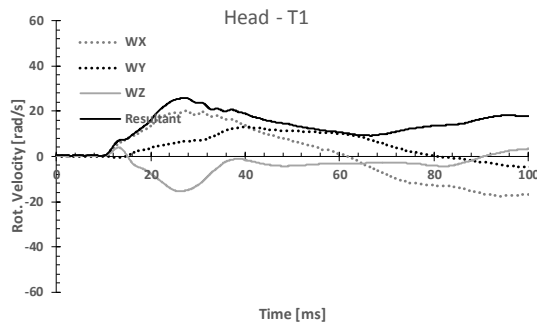
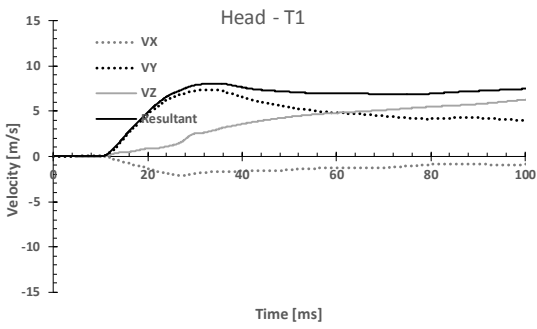
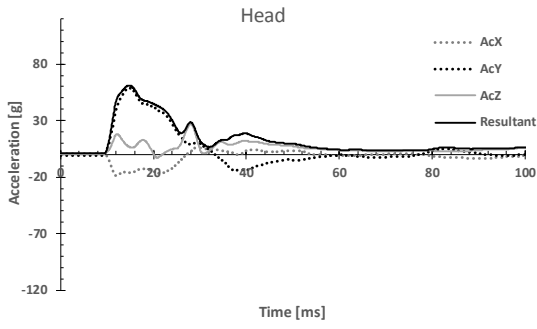
Case 92 Struck



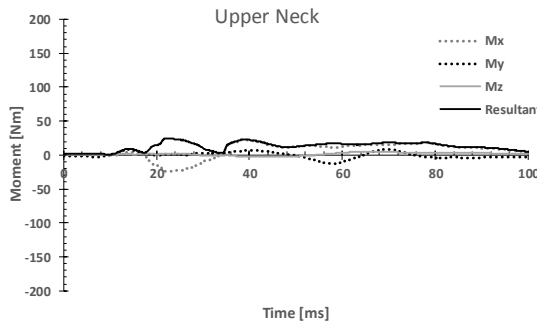
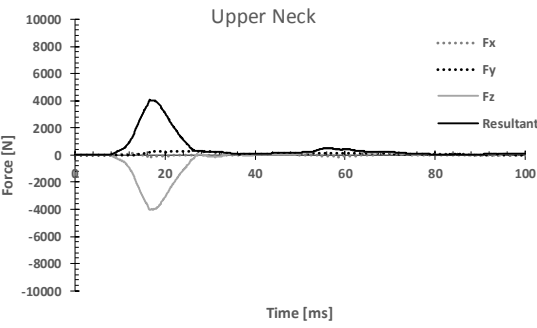
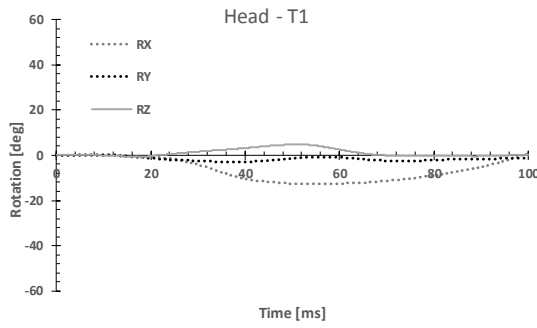
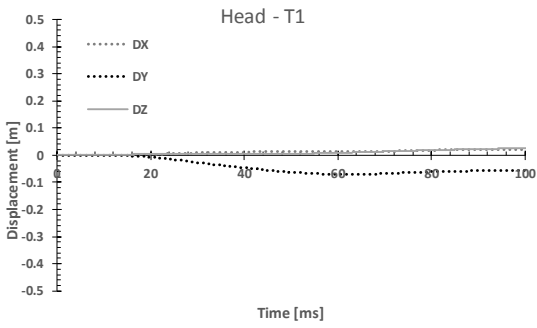
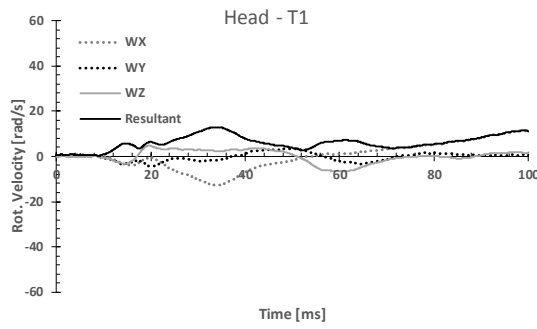
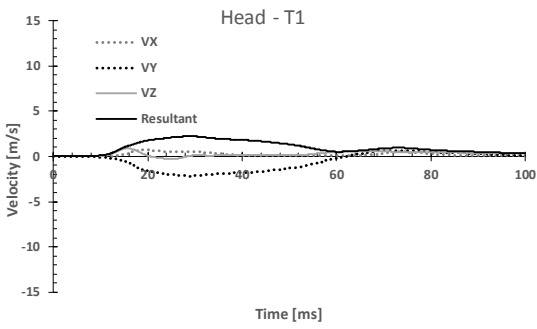
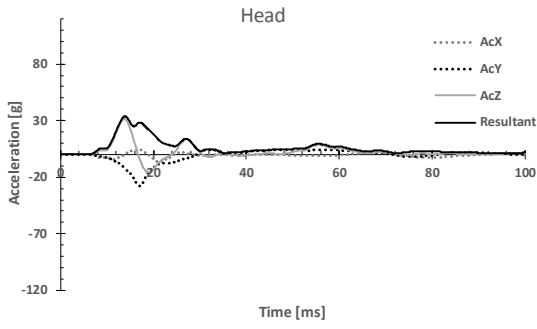
Case 98 Striking



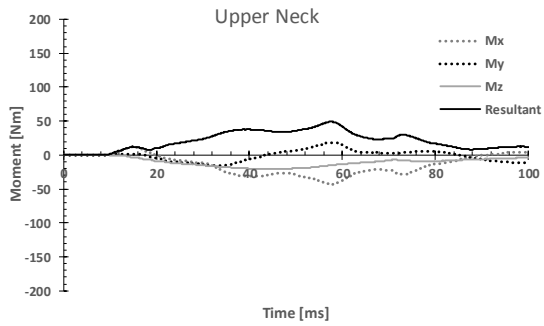
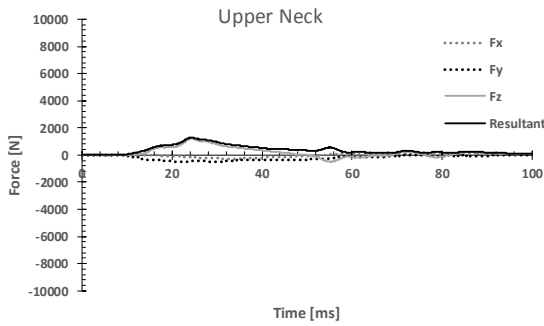
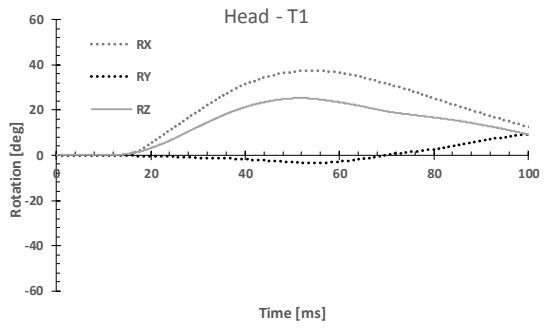
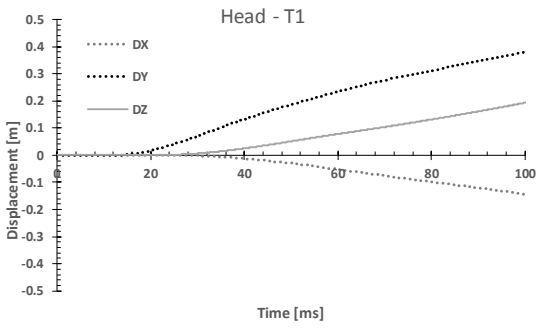
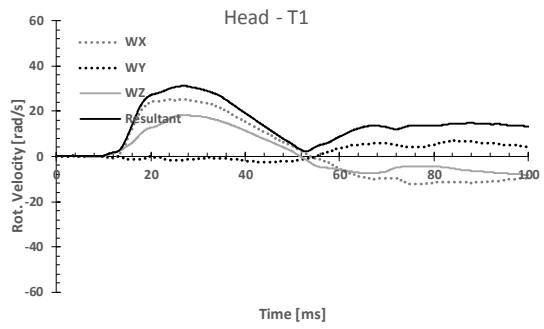
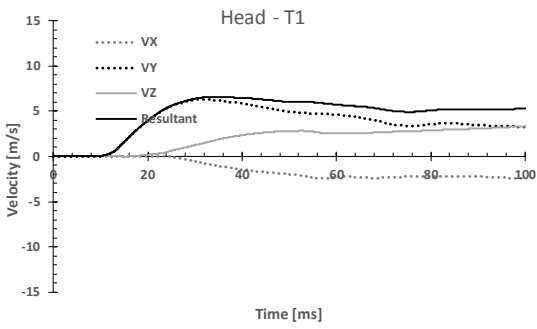
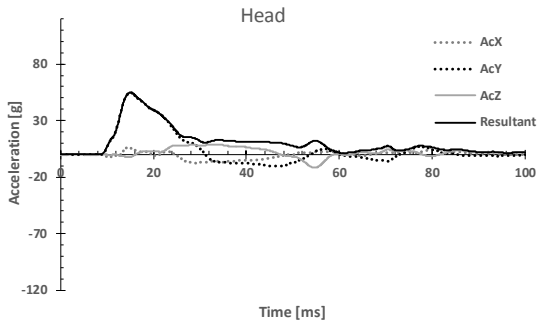
Case 98 Struck



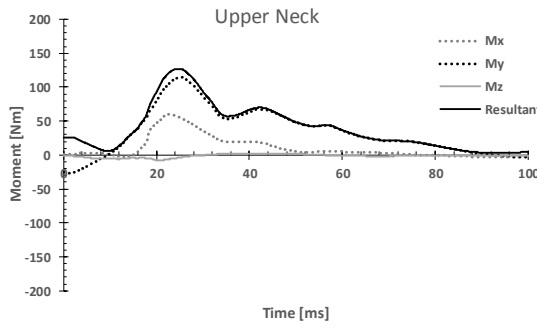
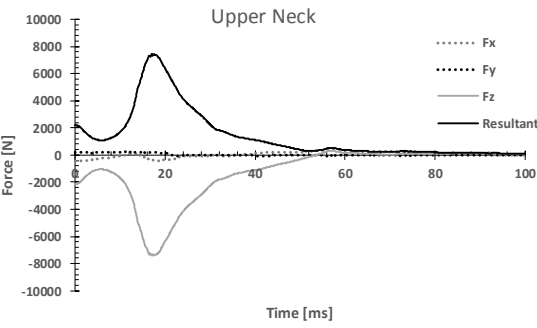
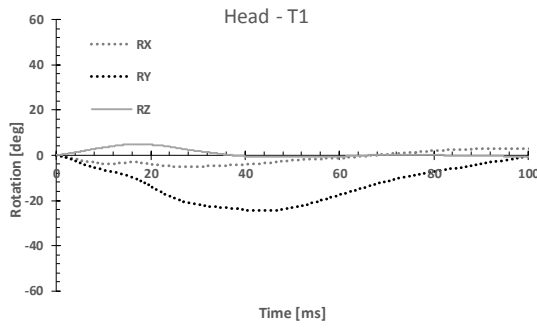
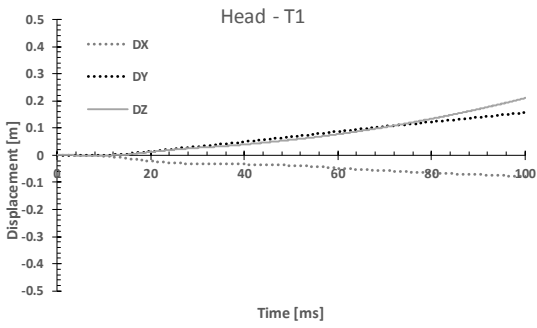
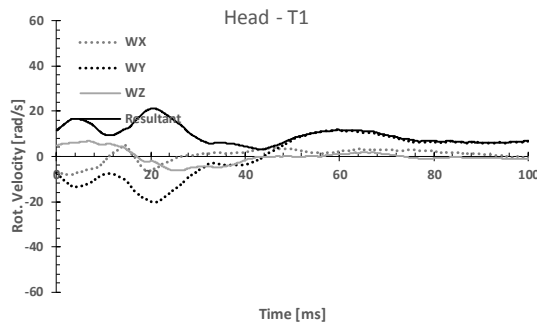
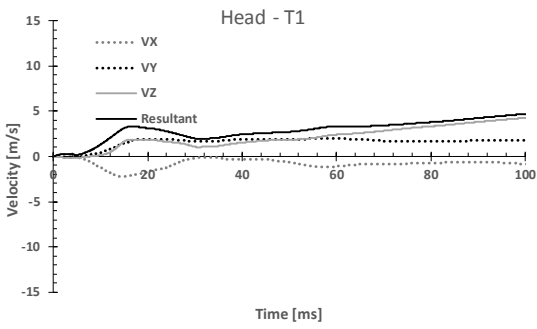
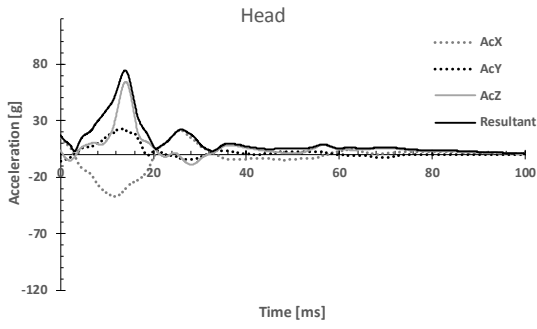
Case 113 Striking



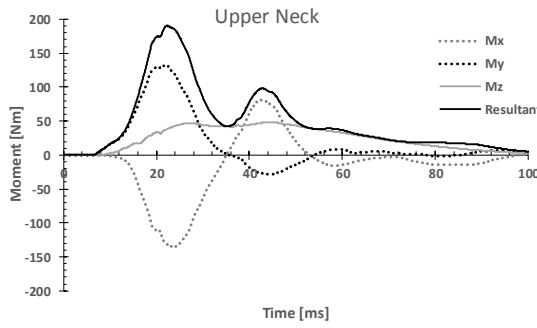
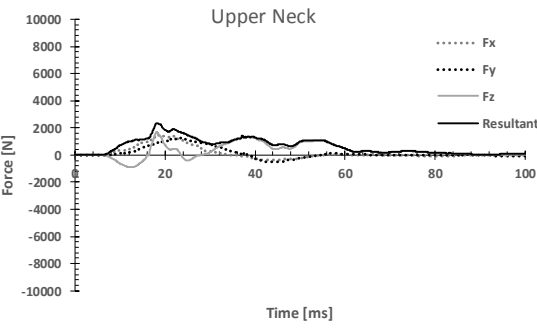
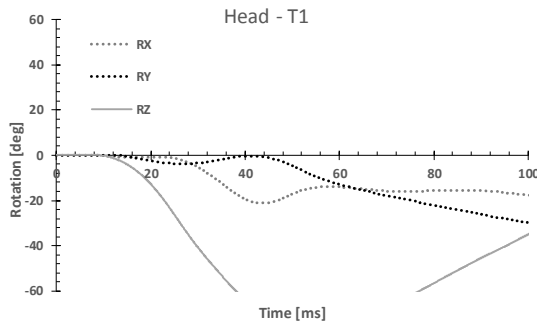
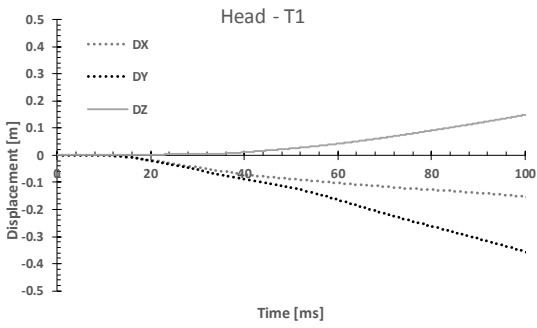
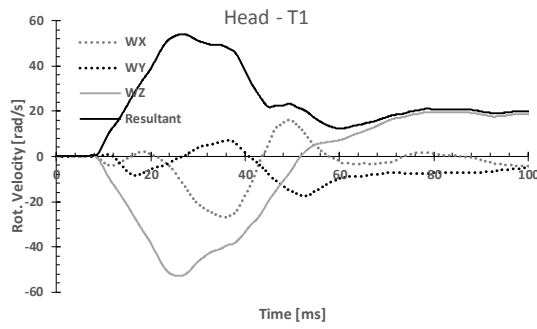
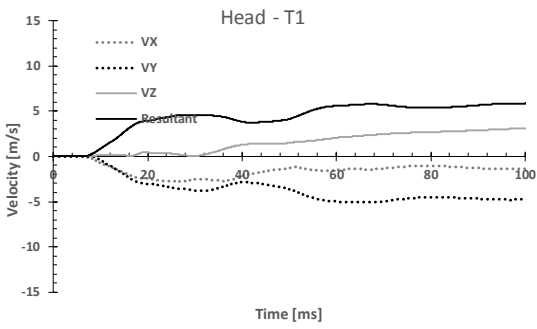
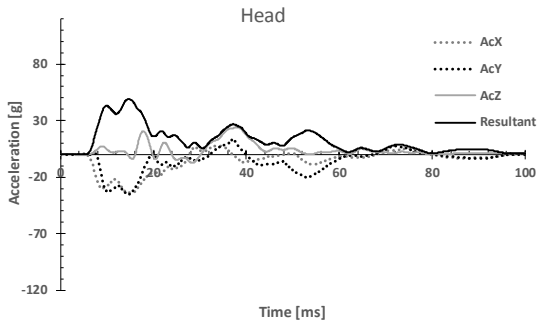
Case 113 Struck



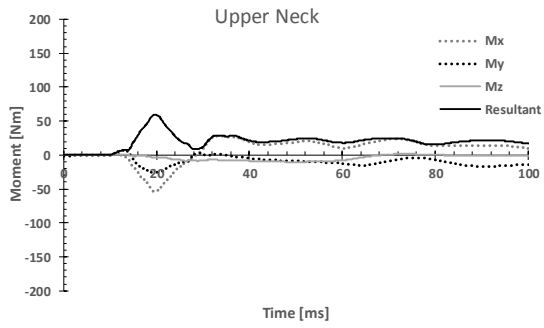
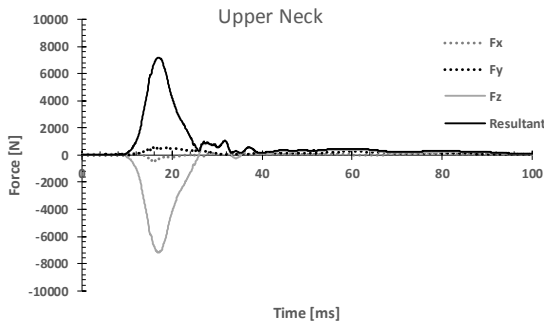
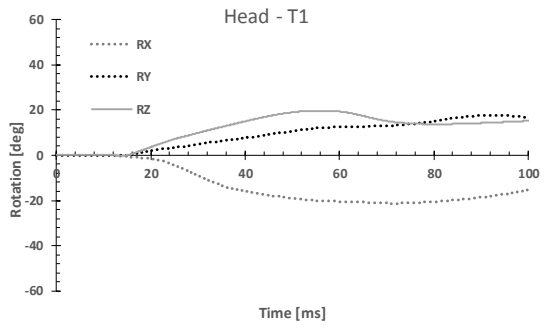
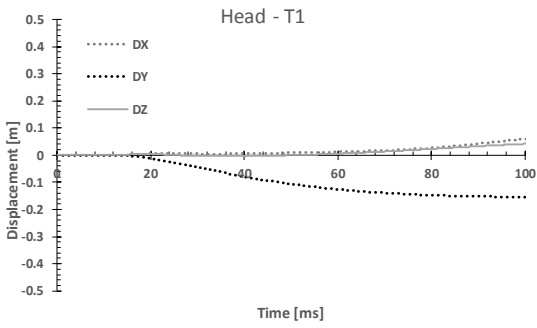
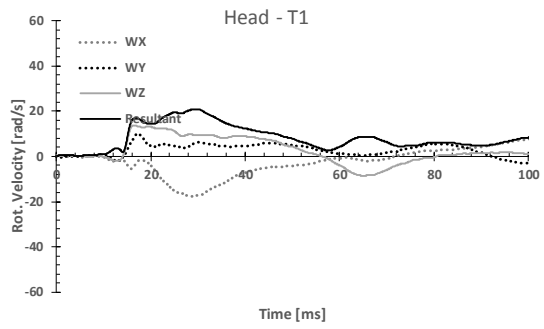
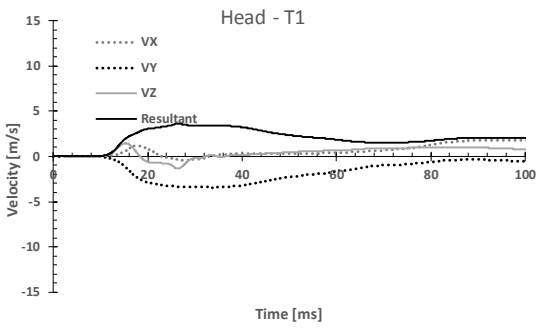
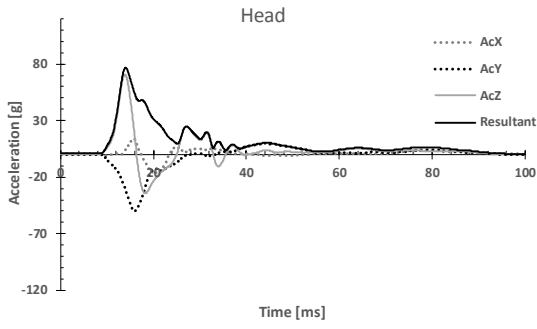
Case 118 Striking



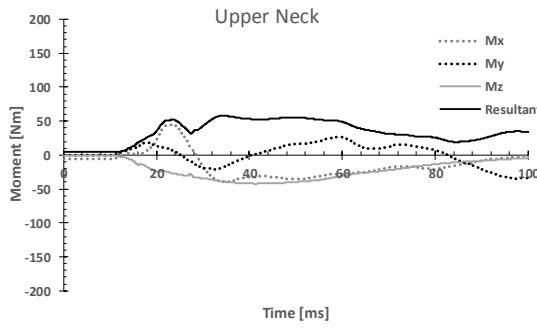
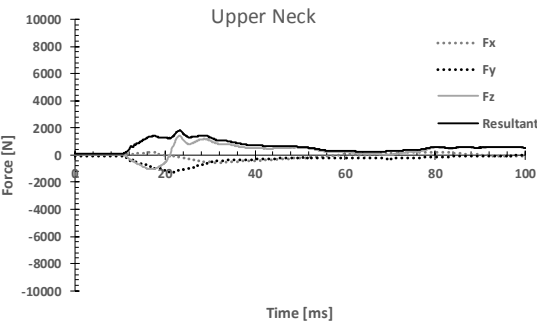
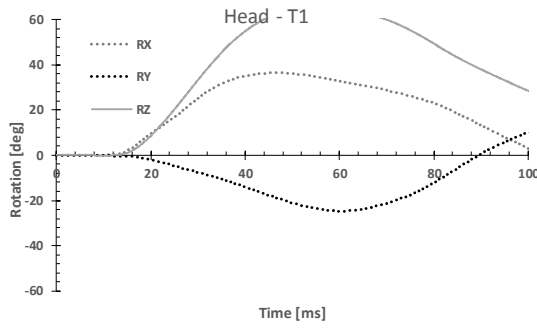
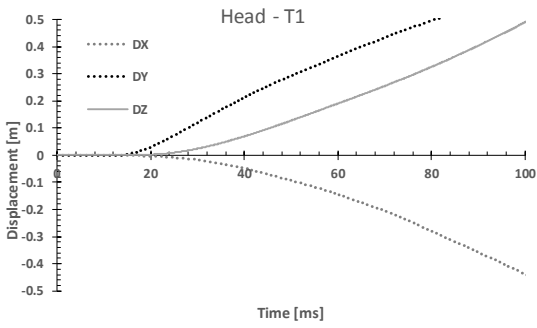
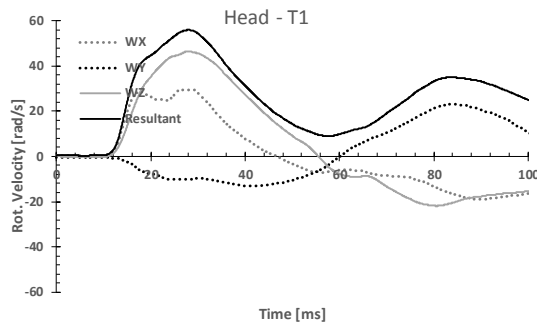
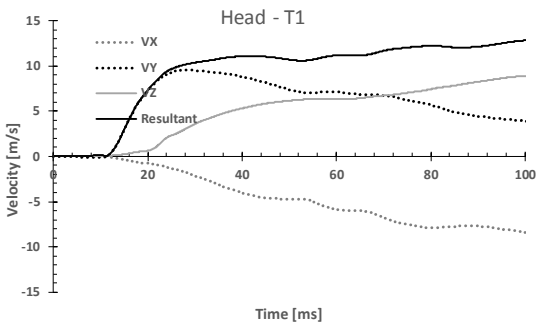
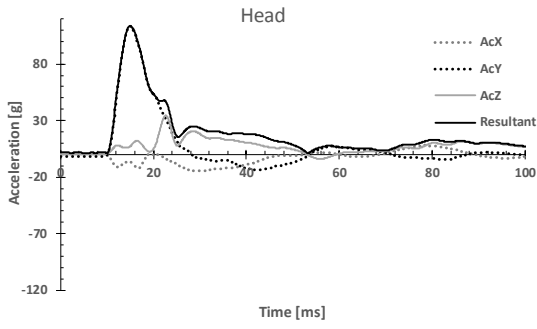
Case 118 Struck



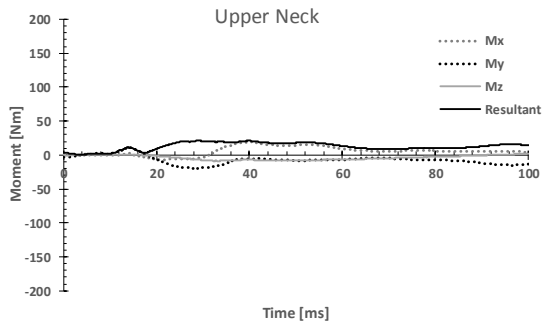
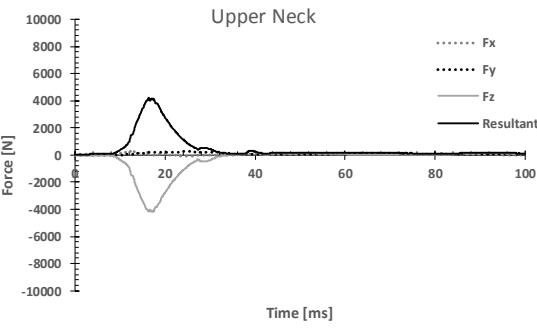
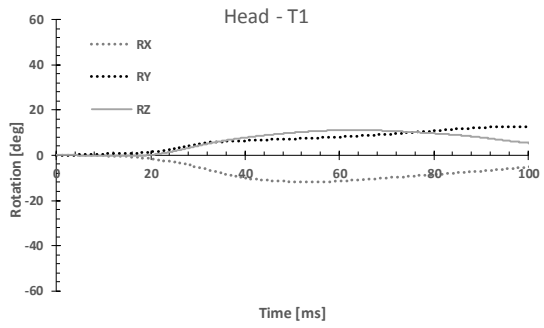
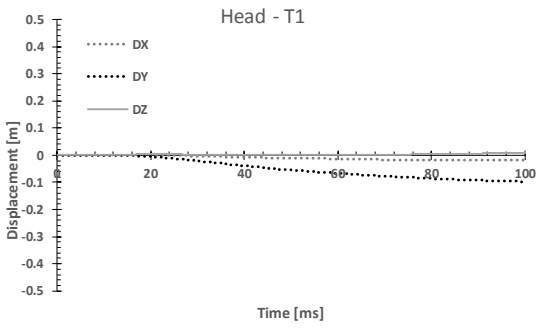
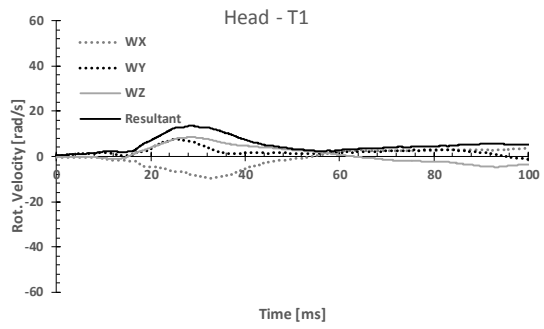
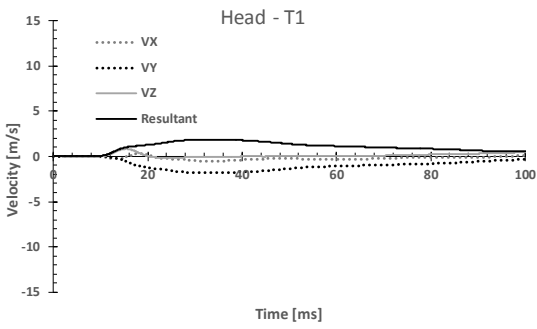
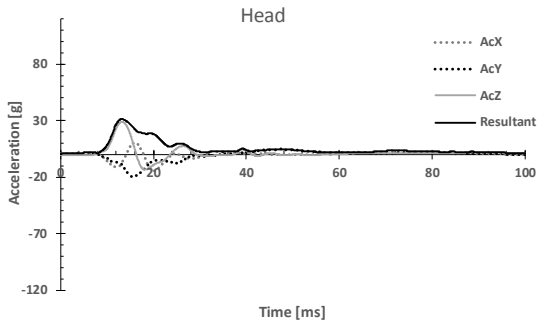
Case 125 Striking



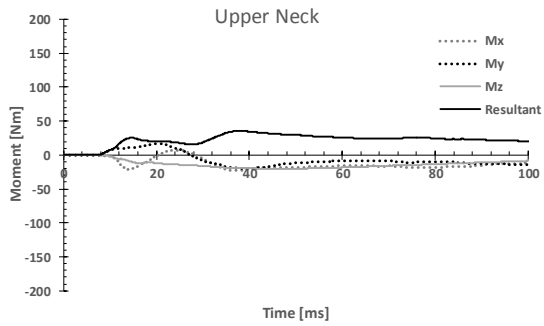
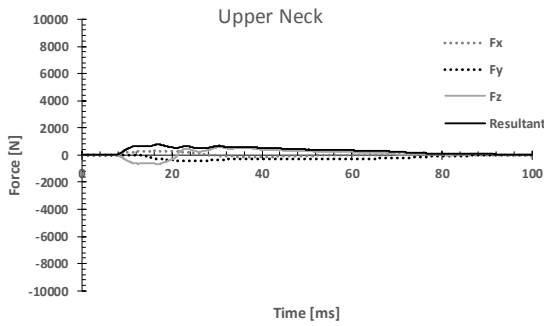
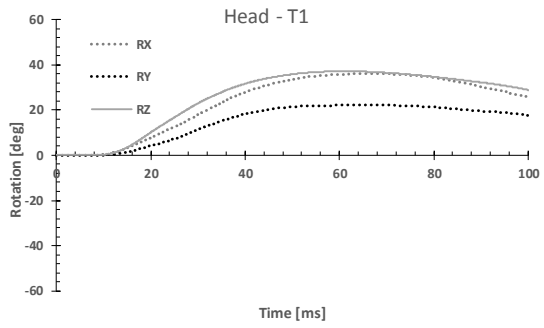
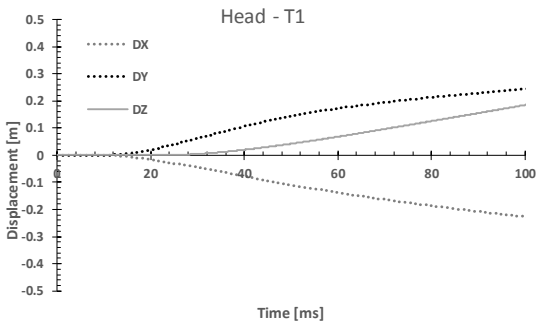
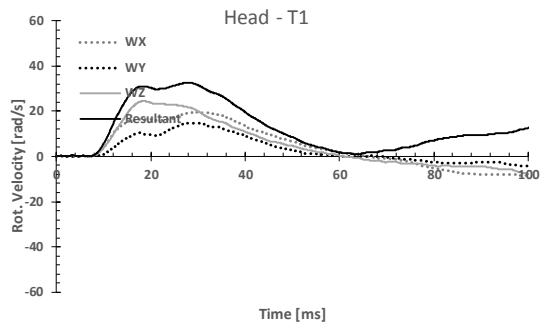
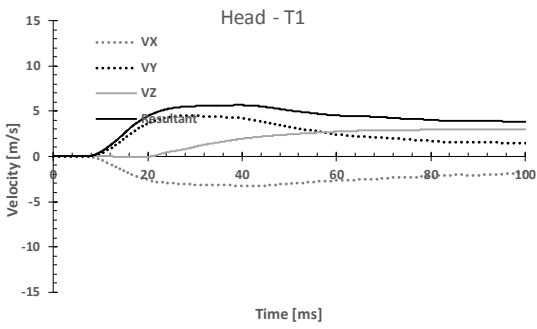
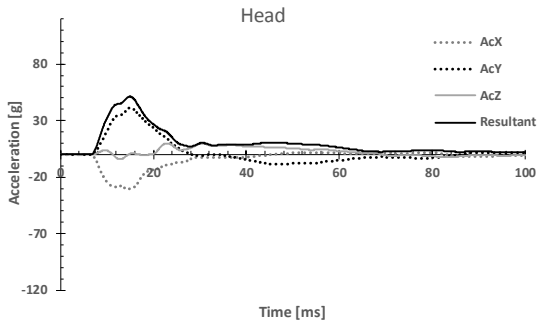
Case 125 Struck



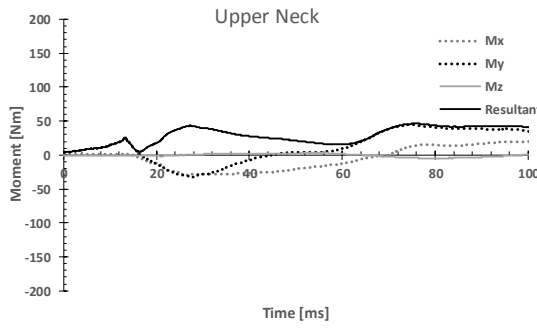
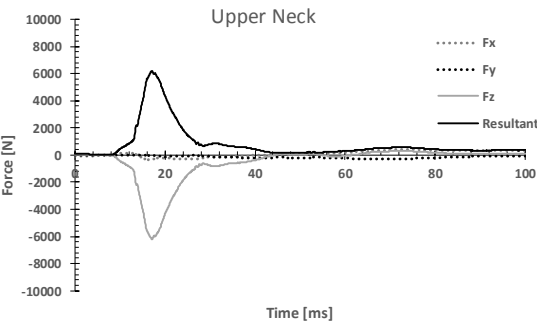
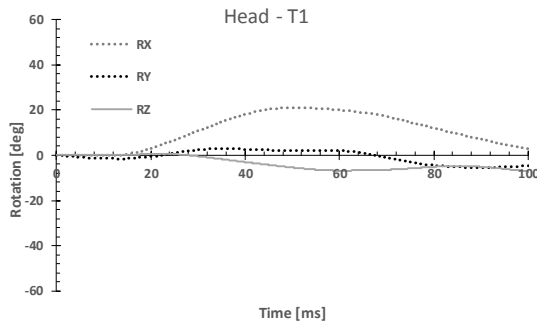
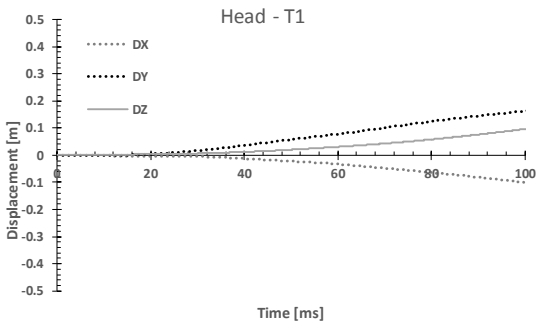
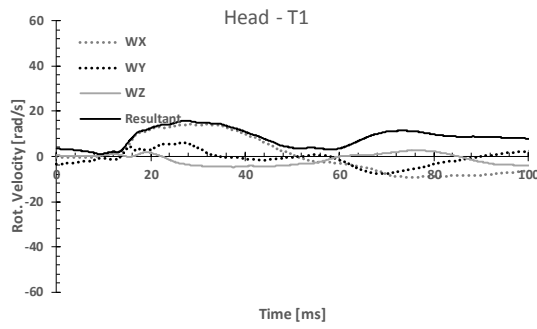
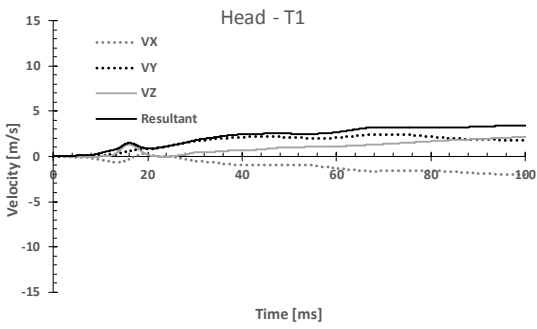
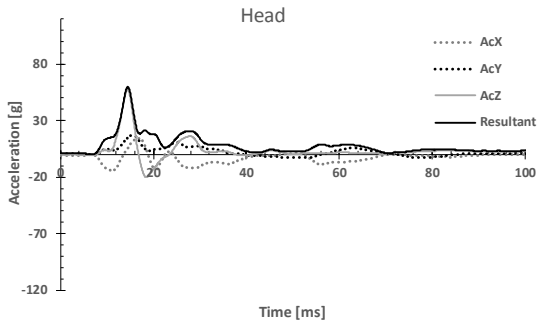
Case 148 Striking



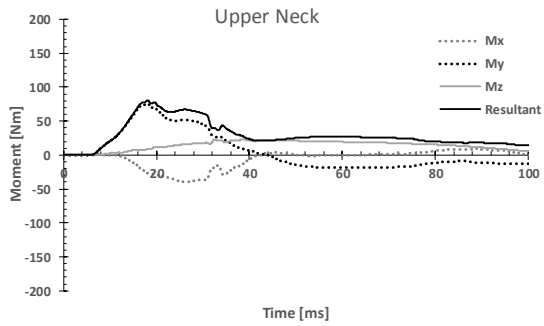
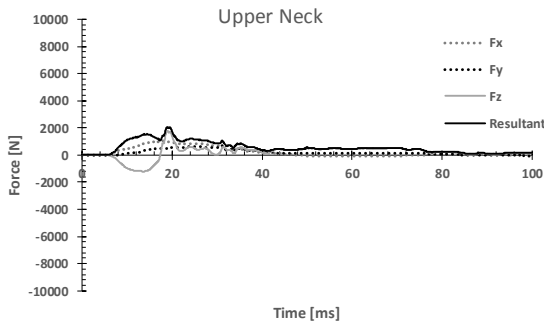
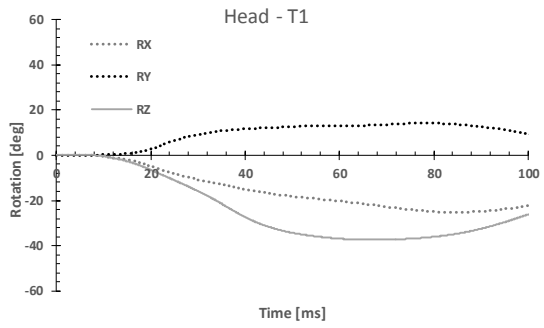
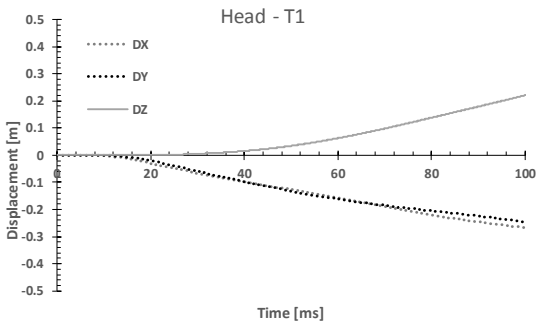
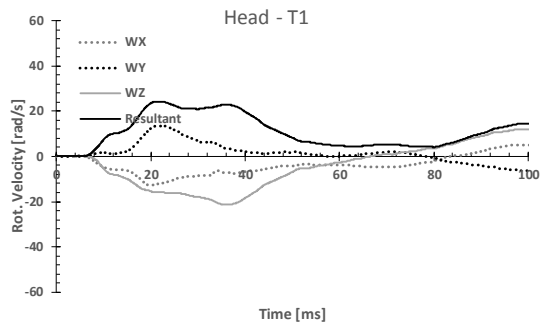
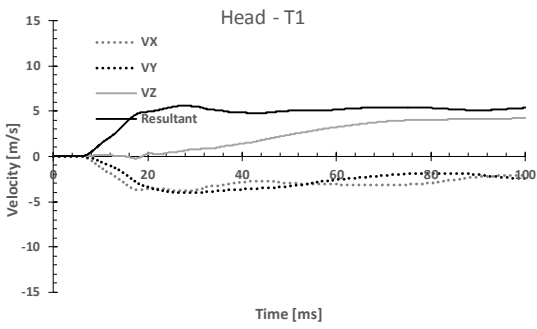
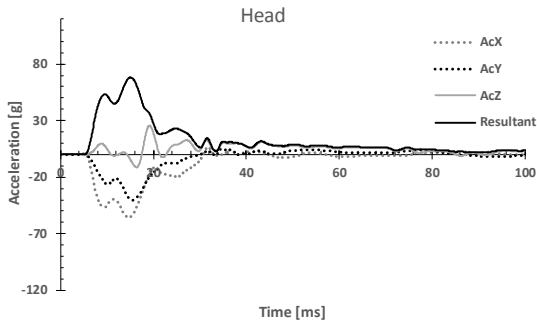
Case 148 Struck



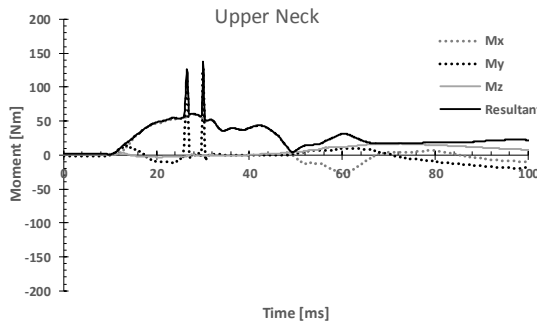
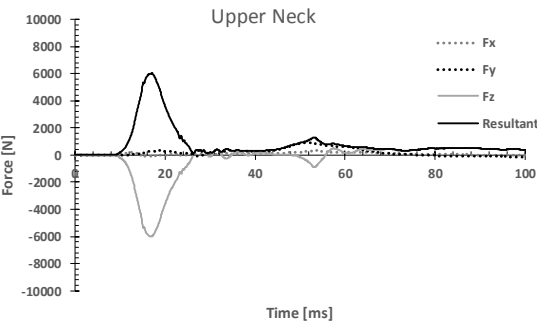
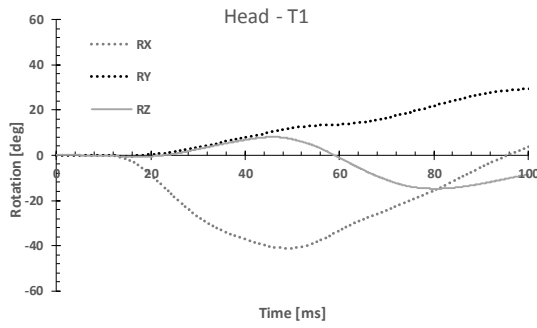
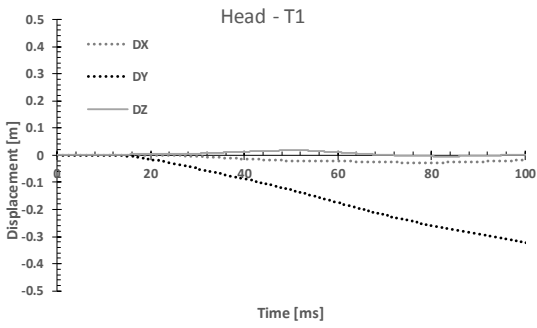
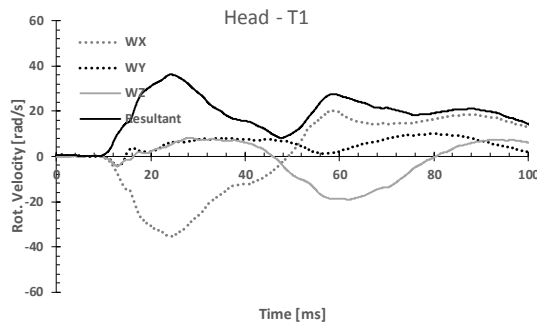
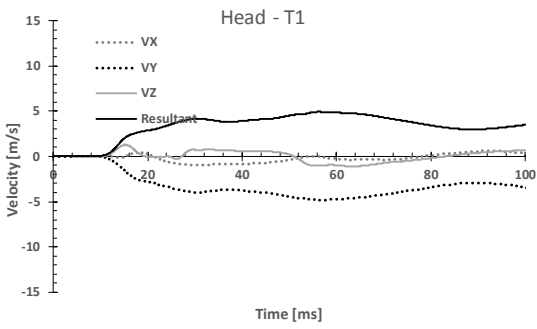
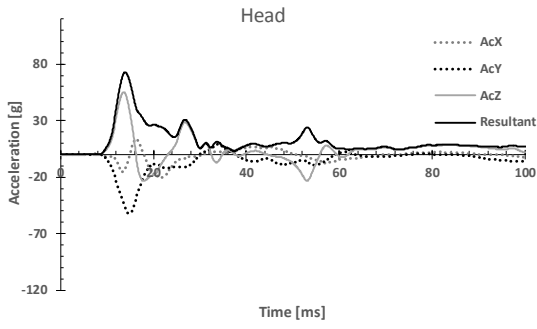
Case 157 Striking



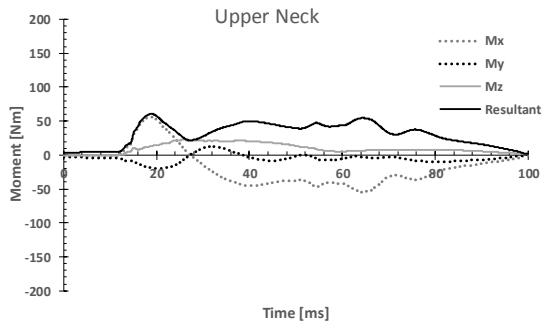
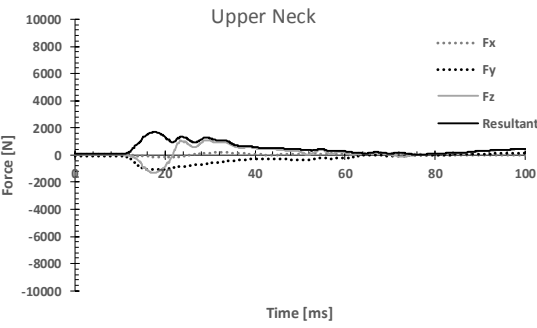
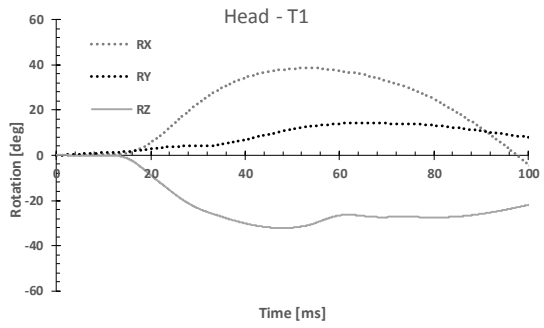
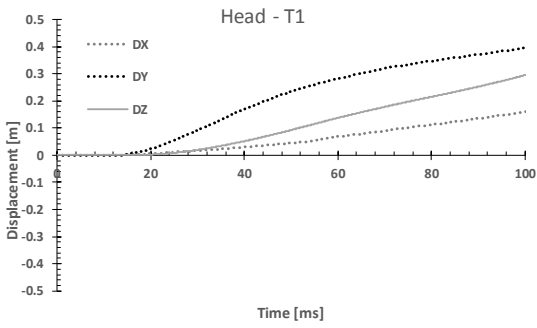
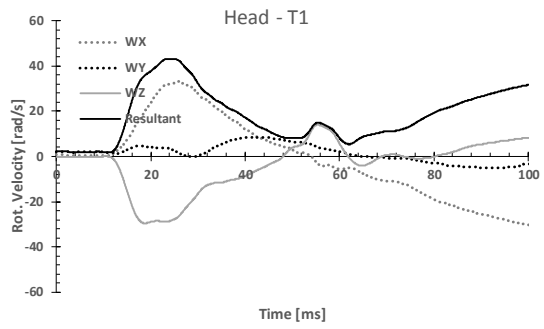
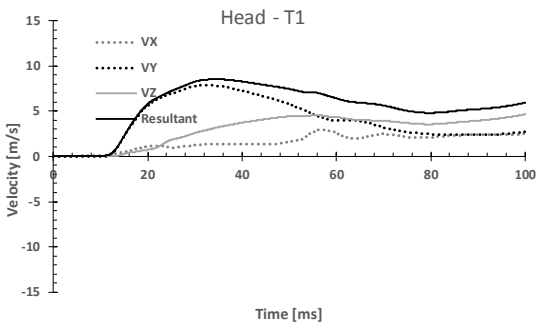
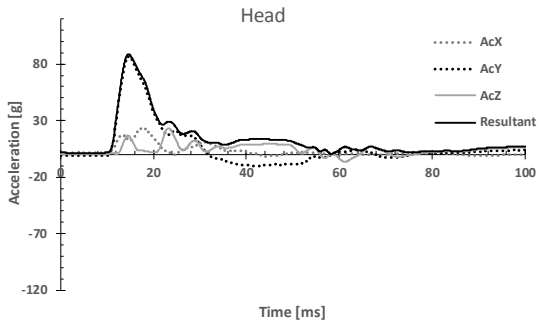
Case 157 Struck



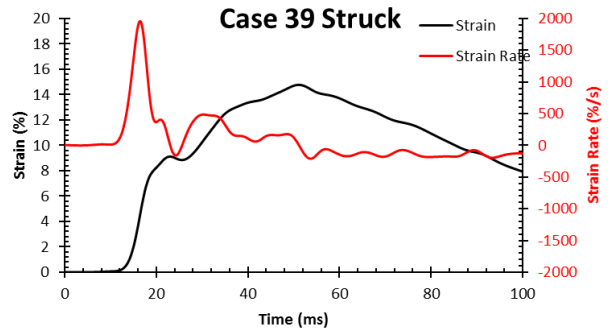
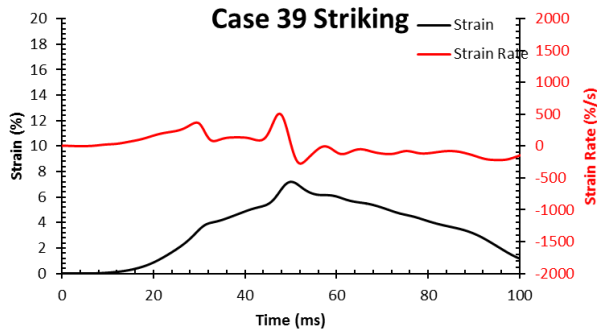
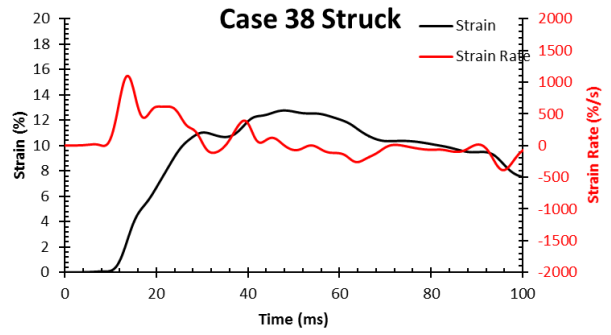
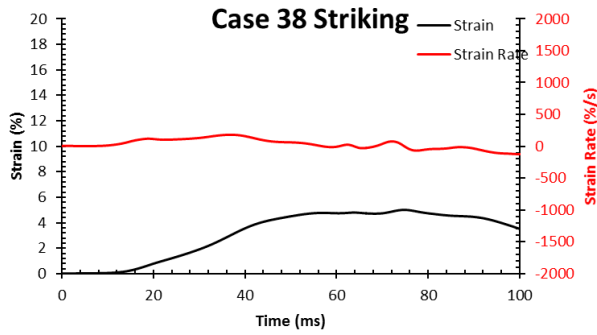
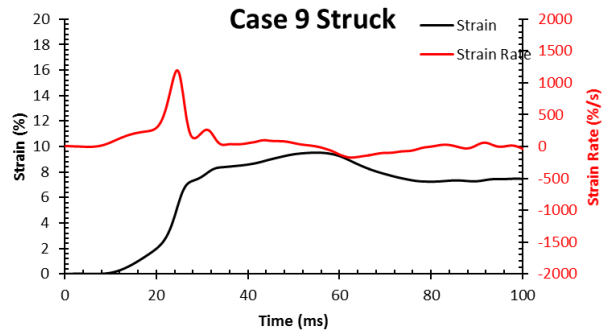
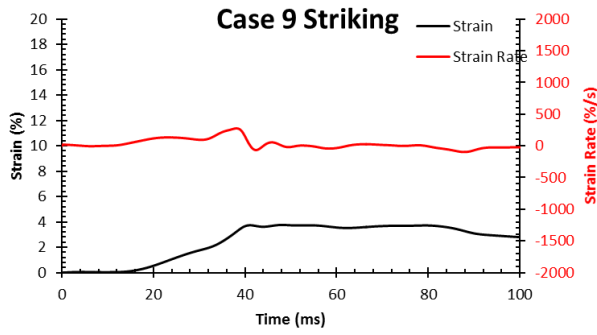
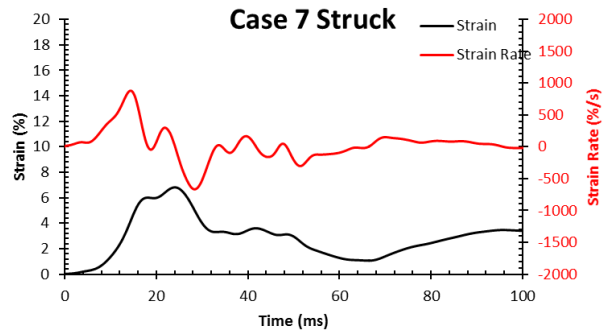
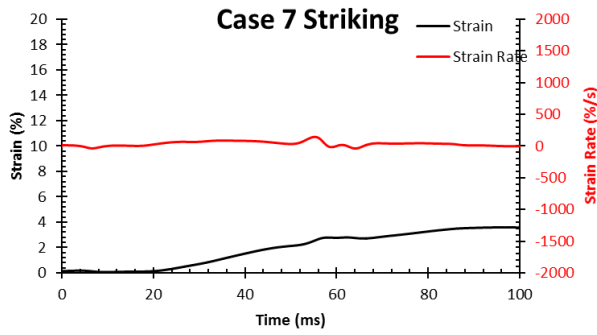
Case 164 Striking

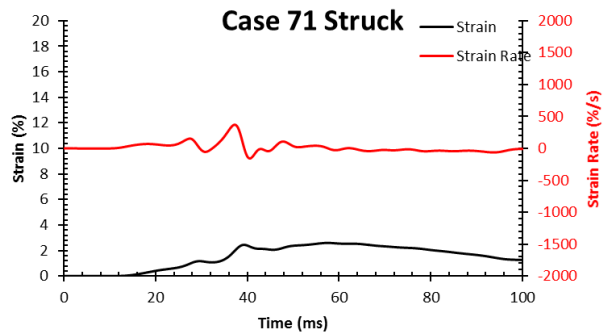
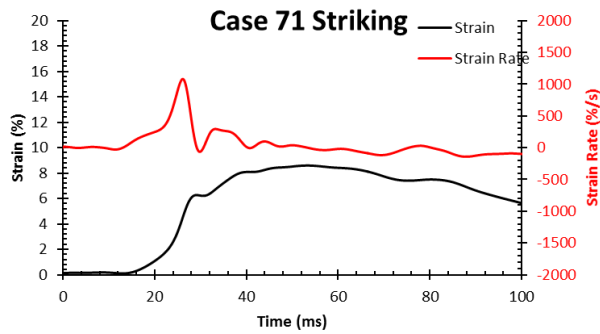
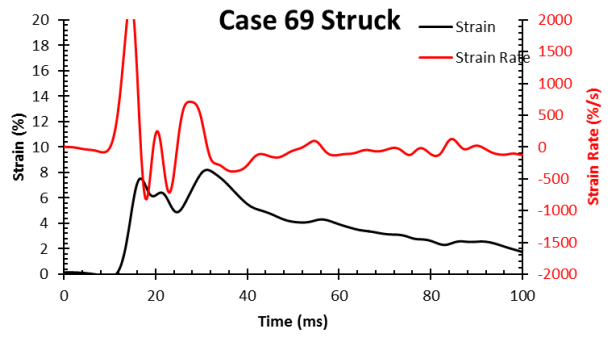
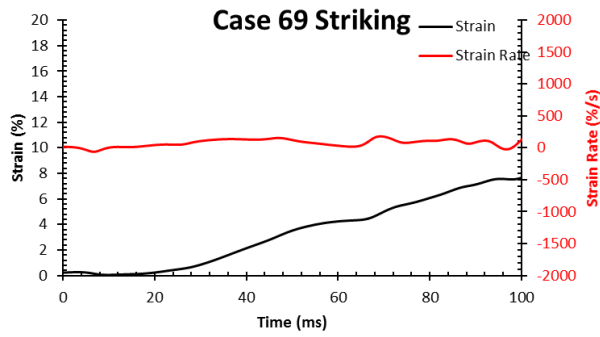
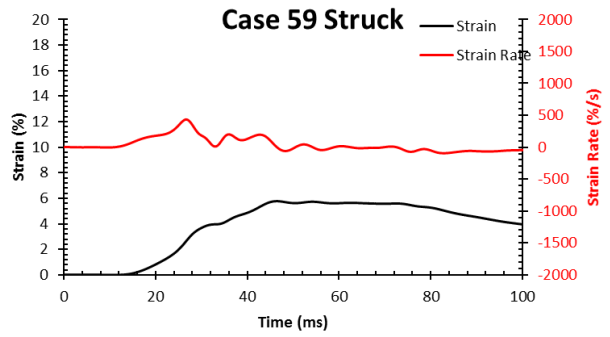
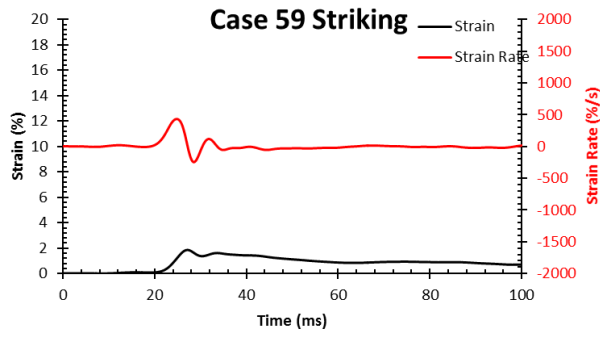
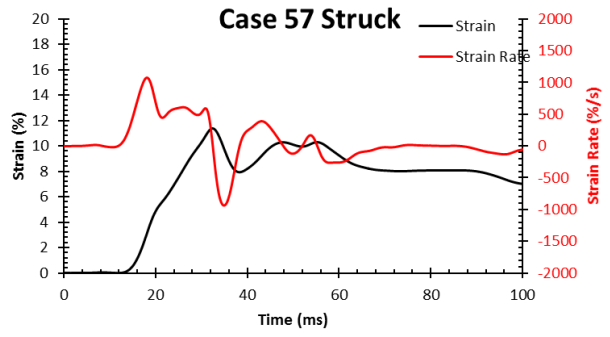
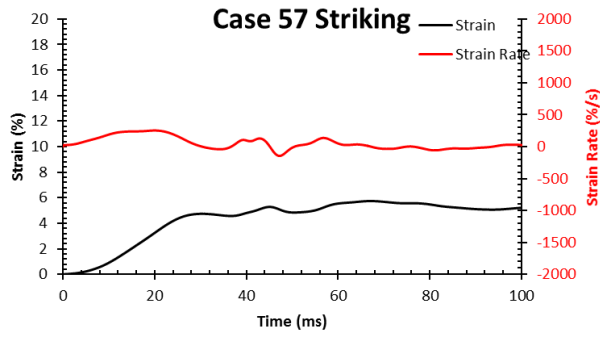


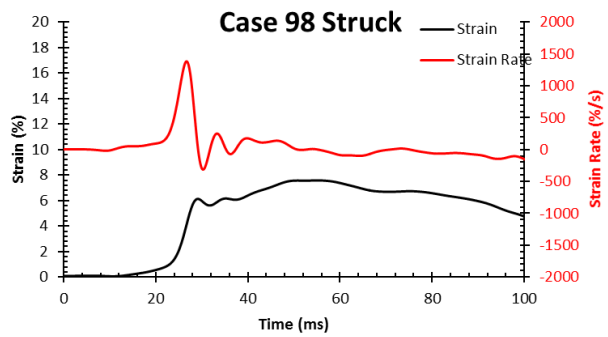
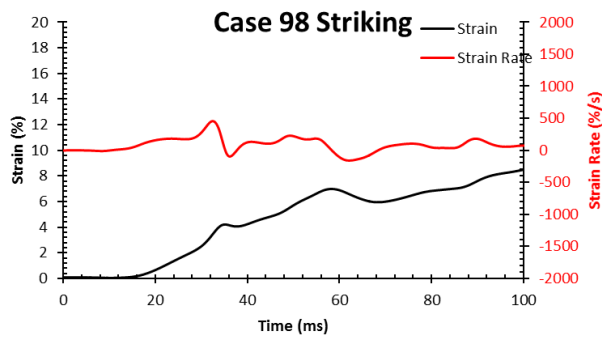
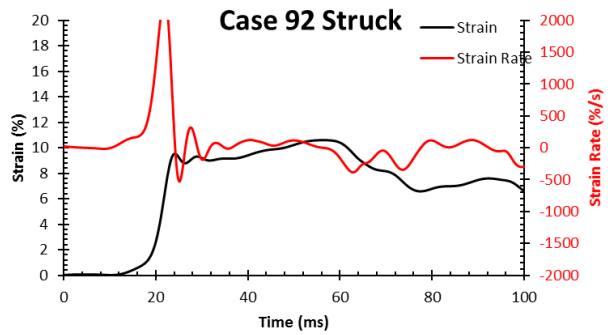
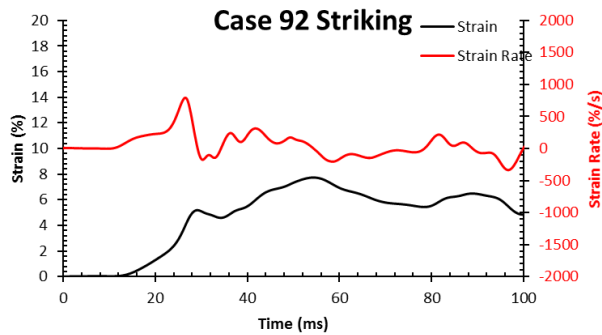
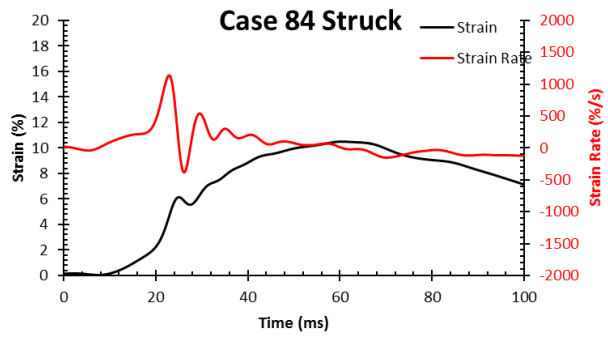
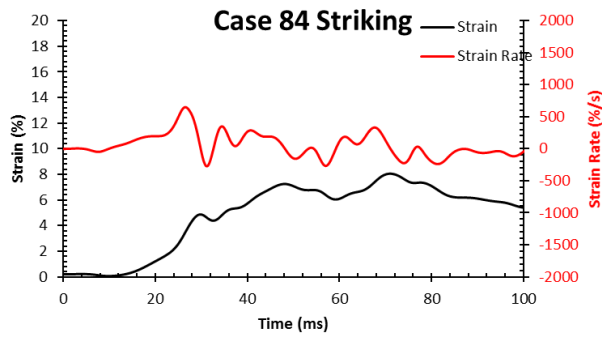
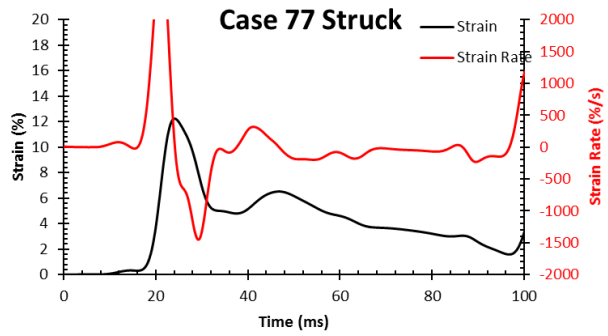
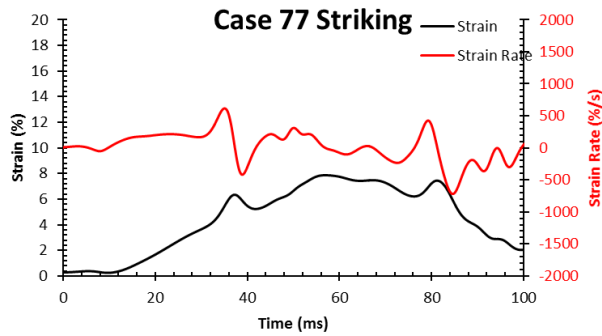
Case 164 Struck

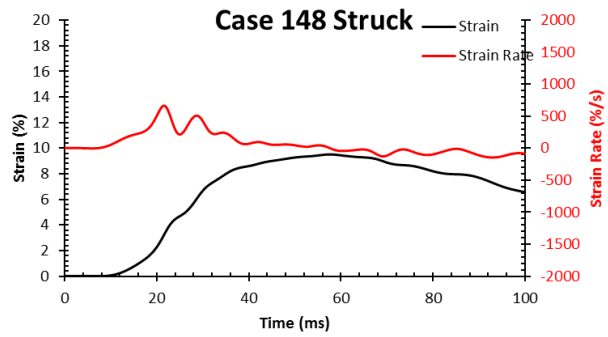
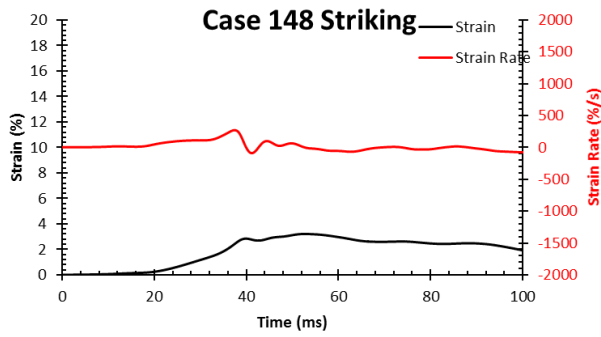
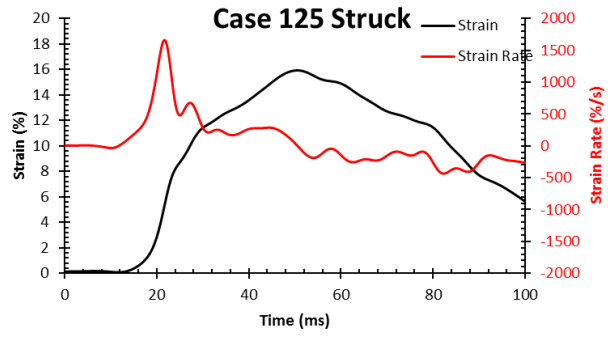
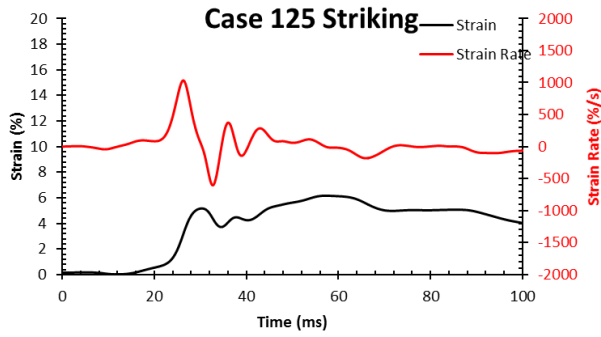
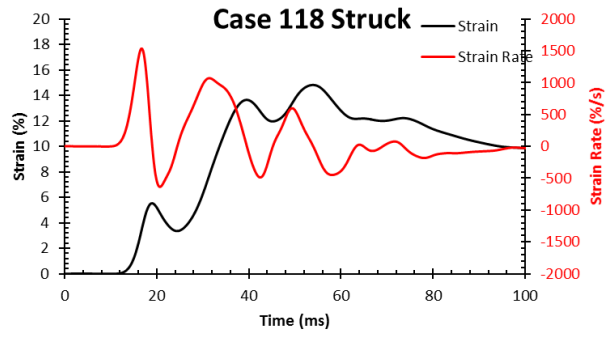
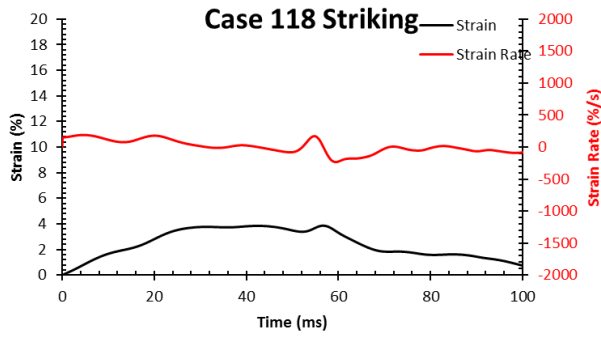
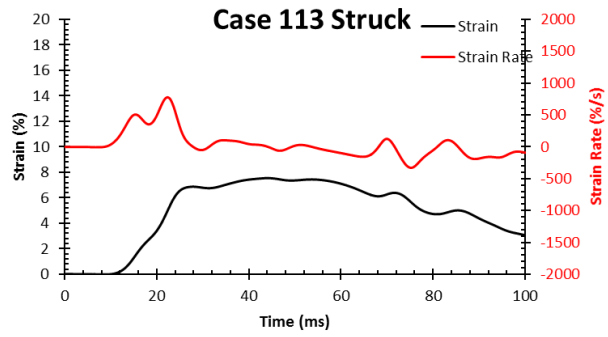
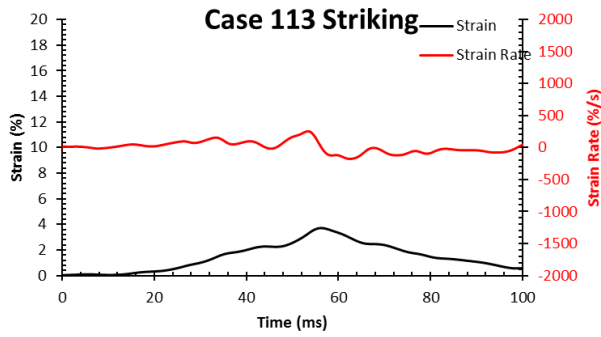


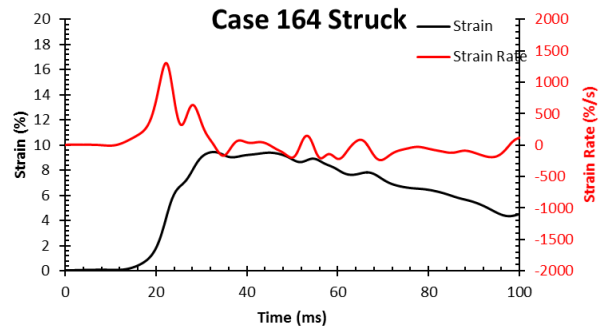
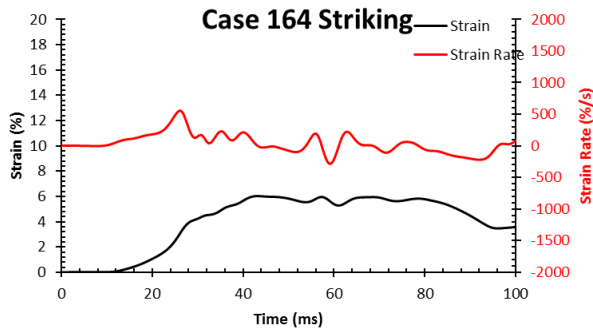
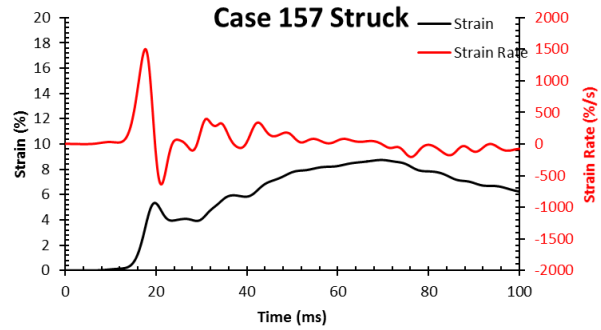
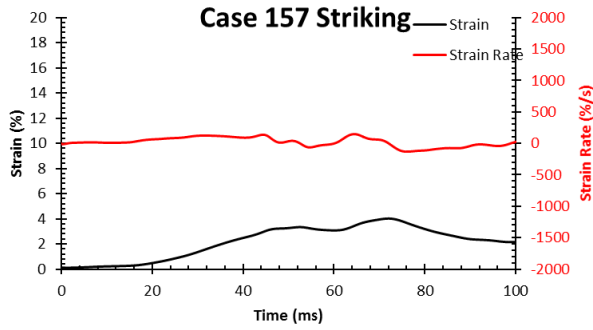
APPENDIX D.1 – ESTIMATED STRAIN AND STRAIN RATE IN THE SPINAL CORD AND BRAIN STEM FOR EACH CASE











REFERENCES

- [1] McCrory P, Meeuwse W H, Aubry M et al.: Consensus Statement on concussion in sport: the 4th International Conference on Concussion in Sport held in Zurich, November 2012. Br J Sports Med. 47. 250-258. 2013.
- [2] NFL Head, Neck and Spine Committee: NFL Head, Neck and Spine Committee's Protocols Regarding Diagnosis and Management of Concussion. 2015.
- [3] Casson I R, Viano D C, Powell J W, and Pellman E J: Twelve Years of National Football League Concussion Data. Sports Health. 2(6). 471-483. 2010.
- [4] Casson I R, Viano D C, Powell J W, and Pellman E J: Concussions Involving 7 or More Days Out in the National Football League. Sports Health. 3(2). 130-144. 2011.
- [5] Benson B W et al.: A prospective study of concussions among National Hockey League players during regular season games- the NHL-NHLPA Concussion Program. CMAJ. 183(8). 905-911. 2011.
- [6] McCrory P R and Berkovic S F. Video analysis of acute motor and convulsive manifestations in sport-related concussion. Neurology. 54(7). 1488-1491. 2000.
- [7] Tomlinson B E. Brain-stem lesions after head injury. Journal of clinical pathology supplement. 23(4). 154-165.
- [8] Oppenheimer D R. Microscopic lesions in the brain following head injury. J. Neurol. Neurosurg. Psychiat. 31. 299-306. 1968.
- [9] Hodgson VR, Thomas L M, and Khalil T: The Role of Impact Location in Reversible Cerebral Concussion. Society of Automotive Engineers. SAE831618. 1983.

- [10] Friede R: The pathology and mechanics of experimental cerebral concussion. Wadd Technical Report 61-256. Air Research and Development Command, United States Air Force, Wright-Patterson Air Force Base. 1961.
- [11] Friede R: Specific cord damage at the atlas level as a pathogenic mechanism in cerebral concussion. Journal of Neuropathology and experimental neurology. 19(2). 266-279. 1960.
- [12] Widmaier E P, Raff H, and Strang S T: Vander's Human Physiology: The Mechanisms of Body Function 10th Edition. McGraw-Hill. New York, New York. 2006.
- [13] Sances et al.: Experimental Studies of Brain and Neck Injury. Society of Automotive Engineers in Proceedings of 25th Stapp Car Crash Conference. SAE811032. 1981.
- [14] Lenox et al.: Development of neck injury tolerance criteria in human surrogates. I. Static tensile loading in the baboon neck: Preliminary observations. SAE Technical Sessions. 1982.
- [15] Pellman et al.: Concussion in Professional Football: Epidemiological Features of Game Injuries and Review of the Literature – Part 3. Neurosurgery. 54(1). 2004.
- [16] Viano D C, and Halstead D: Change in Size and Impact Performance of Football Helmets from the 1970s to 2010. Annals of Biomedical Engineering. 40:1:175-184. 2012a.
- [17] Viano D C, Whitnall C and Halstead D: Impact Performance of Modern Football Helmets. Annals of Biomedical Engineering 40:1: 160-174. 2012b.
- [18] Schwarz A, Bogdanich W and Williams J: N.F.L.'s Flawed Concussion Research and Ties to Tobacco Industry. The New York Times. March 24, 2016.
- [19] www.nfl.com. 30 Years of Health and Safety Rule Changes. Accessed April 2016.

- [20] Post A and Hoshizaki T B: Rotational Acceleration, Brain Tissue Strain, and the Relationship to Concussion. Journal of Biomechanical Engineering. Vol. 137. 2015.
- [21] Hodgson V R and Thomas L M: Acceleration Induced Shear Strains in a Monkey Brain Hemisection. Society of Automotive Engineers. SAE791023. 1979.
- [22] Gurdjian E S, Webster J E, Lissner H R: Observations on the Mechanism of the Brain Concussion, Contusion, and Laceration. Surg., Gynec., & Obstet. Vol. 101, pp. 680-690, 1955.
- [23] Gurdjian E S, Lissner H R, Patrick L M: Concussion – Mechanism and Pathology. 7th Stapp Car Crash Conference. 1965.
- [24] Hodgson V R, Gurdjian E S, Thomas L M: Experimental Skull Deformation and Brain Displacement Demonstrated by Flash X-Ray Technique. Journal of Neurosurgery. Vol. 15 (5), pp. 549-552, 1966.
- [25] Hodgson V R, Thomas L M, Gurdjian E S, Fernando O U, Greenberg S W, and Chason J: Advances in Understanding of Experimental Concussion Mechanisms. Society of Automotive Engineers. SAE 690796, 1969.
- [26] Gurdjian E S, Hodgson V R, Thomas L M, and Patrick L M: High Speed Techniques in Head Injury Research. Med. Sci. Vol. 18 (11), pp. 45-56, 1967.
- [27] Gurdjian E S, Thomas L M, and Hodgson V R: Comparison of Species Response to Concussion. 9th Stapp Car Crash Conference. 1966.
- [28] Breig A. 1960. Biomechanics of the Central Nervous System. Almqvist and Wiskell. Stockholm, Sweden.

- [29] Ommaya A K, Hirsch AE, Martinez J L: The Role of Whiplash in Cerebral Concussion. Stapp Car Crash Conference. SAE 660804, 1966.
- [30] Hollister N R, Jolley W P, Horne R G. Biophysics of concussion – Part I. Wright Air Development Center Technical Report 58-193. 1958.
- [31] Denny-Brown D, and Russell W R: Experimental Cerebral Concussion. Brain. 64:2 and 3. 1941.
- [32] Smith et al.: Immediate coma following inertial brain injury dependent on axonal damage in the brain stem. Journal of Neurosurgery. Vol. 93. P 315-322. 2000.
- [33] Hansson et al.: Neck Flexion Induces Larger Deformation of the Brain Than Extension at a Rotational Acceleration, Closed Head Trauma. Advances in Neuroscience. Volume 2014. Article ID 945869. 2014.
- [34] Endo E, Suzuki H, et al.: Kinematic Analysis of the Cervical Cord and Cervical Canal by Dynamic Neck Motion. Asian Spine Journal. 8(6). 747-752. 2014.
- [35] Yuan Q, Dougherty L, Margulies S: In Vivo Human Cervical Spinal Cord Deformation and Displacement in Flexion. Spine. 23:15: 1677-1683, 1998.
- [36] Smith CG: Changes in length and position of the segments of the spinal cord with changes in posture of the monkey. Radiology. 66(2). 259-266. 1956.
- [37] Ishii T et al.: Kinematics of the Upper Cervical Spine in Rotation – In Vivo Three-Dimensional Analysis. Spine. 29(7). E139-E144. 2004a.
- [38] Ishii T et al.: Kinematics of the Subaxial Cervical Spine in Rotation – In Vivo Three-Dimensional Analysis. Spine. 29(24). 2826-2831. 2004b.

- [39] Ishii T et al.: Kinematics of the Cervical Spine in Lateral Bending – In Vivo Three-Dimensional Analysis. Spine. 31(2). 155-160. 2006.
- [40] White A A and Panjabi M M: Clinical Biomechanics of the Spine, 2nd Edition. JB Lippincott Company. 1990.
- [41] Kroeker S G and Ching R P: Coupling between the spinal cord and cervical vertebral column under tensile loading. Journal of Biomechanics. 46: 773-779. 2013.
- [42] Dibb A T et al.: Tension and Combined Tension-Extension Structural Response and Tolerance Properties of the Human Male Ligamentous Cervical Spine. Journal of Biomechanical Engineering. 131. August 2009.
- [43] Pellman E J et al.: Concussion in Professional Football: Reconstruction of Game Impacts and Injuries. Neurosurgery 53: 799 – 812, 2003.
- [44] Viano D C, Casson I R, and Pellman E J: Concussion in Professional Football: Biomechanics of the Struck Player – Part 14. Neurosurgery 61(2). 313-327. 2007.
- [45] Collins C L et al.: Neck Strength: A Protective Factor Reducing Risk for Concussion in High School Sports. J Primary Prevent 35: 309-319. 2014.
- [46] Giordano C and Kleiven S: Evaluation of Axonal Strain as a Predictor for Mild Traumatic Brain Injuries Using Finite Element Modeling. 58th Stapp Car Crash Journal. 2014.
- [47] Antona-Makoshi J, Davidsson J, Ejma S, and Ono K: Reanalysis of monkey head concussion experiment data using a novel monkey finite element model to develop brain tissue injury reference values. IRCOBI Conference. pp 441-454. IRC-12-54. 2012.

- [48] Ono K, Kikuchi A, Nakamura M, Kobayashi H, Nakamura N: Human Head Tolerance to Sagittal Impact Reliable Estimation Deduced from Experimental Head Injury Using Subhuman Primates and Human Cadaver Skulls. Society of Automotive Engineers in Proceedings of the 24th Stapp Car Crash Conference. SAE 801303, 1980.
- [49] Zhang L, Yang K H, King A: A Proposed Injury Threshold for Mild Traumatic Brain Injury. Journal of Biomechanical Engineering 126: 226-236, 2004.
- [50] Viano D C, Casson I R, Pellman E J, Zhang L, King A I, Yang K H: Concussion in Professional Football: Brain Responses by Finite Element Analysis – Part 9. Neurosurgery 57: 5: 891-915, 2005.
- [51] Takhouas E G et al.: Development of Brain Injury Criterion (BrIC). Stapp Car Crash Journal. 57. P 243-266. 2013.
- [52] Naidich T P et al.: Duvernoy's Atlas of the Human Brain Stem and Cerebellum. Springer-Verlag/Wien. New York. 2009.
- [53] Chancey V C et al.: A kinematic and anthropometric study of the upper cervical spine and the occipital condyles. Journal of Biomechanics. Vol. 40. P. 1953-1959. 2007.
- [54] Anderst W J et al.: Continuous cervical spine kinematics during in vivo dynamic flexion-extension. The Spine Journal. 14. 1221-1227. 2014.
- [55] Ceylan D et al.: The denticulate ligament: anatomical properties, functional and clinical significance. Acta Neurochir. 154. P 1229-1234. 2012.
- [56] Mucha A et al.: A Brief Vestibular/Ocular Motor Screening (VOMS) Assessment to Evaluate Concussions. The American Journal of Sports Medicine. 42(10). 2479-2486. 2014.

- [57] Bogduk N: The anatomical basis for cervicogenic headache. J Manipulative Physiol Ther. 15(1). 67-70. 1992.
- [58] Bogduk N: Anatomy and physiology of headache. Biomed Pharmacother. 49(10). 435-445. 1995.
- [59] www.nocsae.org. Standard Performance Specification for Newly Manufactured Football Helmets. May 2012. Accessed December 2014.
- [60] Pellman E J, Viano D C, Tucker A M and Casson I R: Concussion in Professional Football: Location and Direction of Helmet Impacts – Part 2. Neurosurgery 53:6. 2003b.
- [61] Viano, D.C., 2012c. Biomechanics of Brain Injury. In: Zasler, Nathan D., Katz, Douglas I., Zafonte, Ross D. (Eds.), Brain Injury Medicine, 2nd ed. Demos Medical, New York, NY. (Chapter 10).
- [62] Jadischke R, Viano D C, Dau N, King A I and McCarthy J: On the accuracy of the Head Impact Telemetry (HIT) System used in football helmets. Journal of Biomechanics 46: 2310-2315. 2013.
- [63] Viano D C, Pellman E J, Withnall C and Shewchenko, N.: Concussion in Professional Football: Performance of Newer Helmets in Reconstructed Game Impacts – Part 13. Neurosurgery 59: 3. 2006.
- [64] Pellman E J, Viano D C, Withnall C, Shewchenko N, Bir C A and Halstead P D: Concussion in Professional Football: Helmet Testing to Assess Impact Performance – Part 11. Neurosurgery 58:1. 2006.

- [65] Padgaonkar A J, Krieger K W, King A I: Measurement of angular acceleration of a rigid body using linear accelerometers. *Journal of Applied Mechanics* 42. 552-556, 1975.
- [66] Mertz H J, Irwin A L, Prasad P. Biomechanical and scaling bases for frontal and side impact injury assessment reference values, SAE 2003-22-0009, *Stapp Car Crash Journal*, 47:155-188, 2003.
- [67] Hardy W N, Mason M J, Foster C D, Shah C S, Kopacz J M, Yang K H, King A I, Bishop J B, Bey M, Anderst W and Tashman S: A Study of the Response of the Human Cadaver Head to Impact. 51st Stapp Car Crash Conference. SAE2007-22-0002, 2007.
- [68] Hardy W N, Foster C D, Mason M J, Yang K H, King A I and Tashman S: Investigation of Head Injury Mechanisms Using Neutral Density Technology and High Speed Biplanar X-Ray. 45th Stapp Car Crash Conference. SAE2001-22-0016.
- [69] Piziali R, Hopper R, Girvan D, and Merala R: Injury Causation in Rollover Accidents and the Biofidelity of Hybrid III Data in Rollover Tests. SAE Technical Paper 980362. 1998.
- [70] McIntosh A S and Patton D A: Boxing headgear performance in punch machine tests. *British Journal of Sports Medicine*. 49(17): 1108 – 1112. 2015.
- [71] Bartsch A, Benzel E, Miele V and Prakash V: Impact test comparisons of 20th and 21st century American football helmets. *Journal of Neurosurgery*. November. 2011.
- [72] Newman J A, Beusenbergh M C, Shewchenko N, Withnall C and Fournier E: Verification of biomechanical methods employed in a comprehensive study of mild traumatic brain injury and the effectiveness of American football helmets. *Journal of Biomechanics* 38: 1469-1481, 2005.

[73] www.nocsae.org. Standard Performance Specification for Newly Manufactured Ice Hockey Helmets. March 2016. Accessed February 2017.

[74] <http://www.nfl.com/combine/tracker>. The National Football League. Accessed April 2015.

[75] Mertz H J, Irwin A L, Melvin J W, Stalnaker R L and Beebe M S: Size, weight and biomechanical impact response requirements for adult size small female and large male dummies. Society of Automotive Engineers. SAE890756. 1989.

[76] Mertz H J, Jarrett K, Moss S, Salloum M and Zhao Y: The Hybrid III 10-Year-Old Dummy. In *Stapp Car Crash Journal*. 45: 2001-22-0014. 2001.

[77] Backaitis S H and Mertz H J. Hybrid III: The First Human-Like Crash Test Dummy. Society of Automotive Engineers. SAE PT-44.

[78] Instrumentation for Impact Test – Part 1 – Electronic Instrumentation. Society of Automotive Engineers. March 1995. SAE J211-1.

[79] Jadischke R A. Football helmet fitment and its effects on helmet performance. MS Thesis, Wayne State University, Detroit, MI. 2012.

[80] Ishii M, Ono K and Kubota M. Factors influencing the repeatability and reproducibility of the dummies used for rear-end impact evaluation. IRCOBI Conference. Madrid, Spain. 2006.

[81] Shaw J, Probst E and Donnelly B. Evaluation of the 95th percentile HIII large male dummy. Enhanced Safety of Vehicles Conference. Paper number 07-0228. 2007.

[82] Hodgson V R. Tolerance of the head and neck to –Gx inertial loading of the head. Technical Report No. 11. Wright Patterson Air Force Base. 1981.

- [83] Stapp J P. Human Tolerance to Severe, Abrupt Acceleration. Gravitational stress in aerospace medicine. P.165-188. 1951.
- [84] Hutchinson M G. Concussions in the National Hockey League (NHL): The Video Analysis Project. PhD Dissertation. University of Toronto. 2011.
- [85] Elkin B S, Elliott J M, Siegmund G P. Whiplash injury or concussion? A possible biomechanical explanation for concussion symptoms in some individuals following a rear-end collision. J Orthop Sports Phys Ther 46(10):874-885, 2016.
- [86] Jadischke R, Viano D C, McCarthy J, King A I. The effects of helmet weight on Hybrid III head and neck responses by comparing unhelmeted and helmeted impacts. Biomech Eng 1;138(10), 2016.
- [87] Ommaya A K. Trauma to the nervous system. Hunterian Lecture delivered at the Royal College of Surgeons England. P. 317-347. 1965.
- [88] King A I, Nakhla S S, Mital N K. Simulation of head and neck response to $-G_x$ and $+G_z$ impacts, in AGARD Conference No, 253, Models and Analogues for the Evaluation of Human Biodynamic Response, Performance and Protection. Paper 7A, AGARD-NATO, 1979.
- [89] Mao H, Zhang L, Jiang B, Genthikatti V V, et al.: Development of a Finite Element Human Head Model Partially Validated With Thirty Five Experimental Cases. Journal of Biomechanical Engineering. 135. 2013.
- [90] Fice J B: Numerical Modeling of Whiplash Injury. Master's Thesis. University of Waterloo. 2010.

- [91] Dvorak J, Panjabi M M, Novotny J E and Antinnes J A. In vivo flexion/extension of the normal cervical spine. *Journal of Orthopaedic Research* Vol. 9, P. 828-834, 1991.
- [92] Yliniemi E M, Pelletiere J A, Doczy E J, et al. Dynamic tensile failure mechanics of the musculoskeletal neck using a cadaver model. *Journal of Biomechanical Engineering* 131, May 2009.
- [93] Yliniemi E M. Dynamic tensile neck injury: A post mortem human study. University of Washington. 2005.
- [94] McIntosh A S, Patton D A, Frechede B, et al. The biomechanics of concussion in unhelmeted football players in Australia: a case-control study. *BMJ Open* 2014; 4:e005078.doi:10.1136/bmjopen-2014-005078
- [95] Funk J R, Duma S M, Manoogian S J and Rowson S. Biomechanical risk estimates for mild traumatic brain injury. *Ann Proc Assoc Adv Automot Med* 51:343-361, 2007.
- [96] Rowson S and Duma S M. Development of the STAR evaluation system for football helmets: integrating player head impact exposure and risk of concussion. *Ann Biomed Eng* 39(8): 2130-2140, 2011.
- [97] Mertz H J and Patrick L M. Investigation of the kinematics and kinetics of whiplash. Society of Automotive Engineers. SAE670919, 1967.
- [98] Mertz H J and Patrick L M. Strength and response of the human neck. Society of Automotive Engineers. SAE 710855, 1971.

- [99] Thunnissen J, Wismans J, Ewing C L and Thomas D J. Human volunteer head-neck response in frontal flexion: a new analysis. Society of Automotive Engineers. SAE 952721, 1995.
- [100] Van Ee C A, Nightingale R W, Camacho D L A, et al. Tensile properties of the human muscular and ligamentous cervical spine. In: *Proceedings of 44th Stapp Car Crash Conference*, Paper No. SC2000-01-SC07, 2000.
- [101] Maiman D J, Coates J, Myklebust J B. Cord/spine motion in experimental spinal cord injury. *Journal of Spinal Disorders* 2(1) 14-19, 1989.
- [102] Singh A, Kallakuri S, Chaoyang C and Cavanaugh J M. Structural and functional changes in nerve roots due to tension at various strains and strain rates: an in-vivo study. *Journal of Neurotrauma*, 26(4), April 2009.
- [103] Margulies S S, Meaney D F, Bilston L B, et al. In vivo motion of the human cervical spinal cord in extension and flexion. 1992 International IRCOBI Conference on the Biomechanics of Impacts, P. 213-224, September 1992.
- [104] Kuwazawa Y, Pope M, Bashir W, et al. The length of the cervical cord: effects of postural changes in healthy volunteers using positional magnetic resonance imaging. *Spine*, Vol. 31 Number 17, P. E579-E583, 2006.
- [105] Yoganandan N, Pintar F A, Maiman D J, et al. Human head-neck biomechanics under axial tension. *Med. Eng. Phys.* 18(4), 289-294, 1996.
- [106] Chancey V C, Nightingale R W, Van Ee C A, et al. Improved estimation of human neck tensile tolerance: reducing the range of reported tolerance using anthropometrically correct

muscles and optimized physiologic initial conditions. In: *Stapp Car Crash Journal Volume 47*. Paper No. 2003-22-0008, 2003.

[107] Harrison D E, Caillet R, Harrison D D, Troyanovich S J, and Harrison S O. Reviews of the literature. A review of biomechanics of the central nervous system – part II: spinal cord strains from postural loads. *Journal of Manipulative & Physiological Therapeutics*. 22(5). 322-332. 1999.

[108] Newman J, Beusenbert M, Fournier E, Shewchenko N, et al.: A new biomechanical assessment of mild traumatic brain injury: Part 1 – Methodology. IRCOBI Conference. Spain. 1999.

[109] Prasad P and Mertz H J: The Position of the United States Delegation to the ISO Working Group 6 on the use of HIC in the Automotive Environment. Society of Automotive Engineers SAE851246, 1985.

[110] Viano D C et al.: Measurement of Head Dynamics and Facial Contact Forces in the Hybrid III Dummy. Society of Automotive Engineers. SAE861891. 1986.

[111] Viano D C et al.: Concussion in Professional Football: Comparison with Boxing Head Impacts – Part 10. *Neurosurgery*. 57:6:1154-1171. 2005.

[112] Viano D C and Parenteau C S: Analysis of Head Impacts Causing Neck Compression Injury. *Traffic Injury Prevention*. 9(2):144–152, 2008.

[113] Lau I V and Viano D C: The Viscous Criterion: Bases and Applications of an Injury Severity Index for Soft Tissues. *Society of Automotive Engineers*. SAE861882. 1986.

- [114] Viano D C and Lau I V: A Viscous Tolerance Criterion for Soft Tissue Injury Assessment. Journal of Biomechanics. 21(5). 387-399. 1988.
- [115] DiLorenzo F A: Power and Bodily Injury. Society of Automotive Engineers. 760014. 1976.
- [116] Newman J A et al.: A Proposed New Biomechanical Head Injury Assessment Function – The Maximum Power Index. Society of Automotive Engineers. SAE2000-01-SC16. 2000.
- [117] King A I, Yang K H, Zhang L, Hardy W and Viano D C: Is Head Injury Caused by Linear or Angular Acceleration? IRCOBI Conference. Lisbon, Portugal. September 2003.
- [118] Ji et al.: In Vivo Measurements of Human Brain Displacement. Stapp Car Crash Journal. 2004-22-0010. 2004.
- [119] Ji and Margulies: In Vivo pons motion within the skull. Journal of Biomechanics. Vol. 40. P. 92-99. 2007.
- [120] Salem et al.: In vivo three-dimensional kinematics of the cervical spine during maximal axial rotation. Manual Therapy. Vol. 18. P. 339-344. 2013.
- [121] Antona-Makoshi J.: Reanalysis of primate head impact experiments to clarify mild traumatic brain injury kinematics and thresholds. Thesis. Chalmers University of Technology. Gothenburg, Sweden. 2013.
- [122] Myers B S, McElhaney J H and Nightingale R: Cervical Spine Injury Mechanisms. 107-155. *In* Levine R S. Head and Neck Injury. Society of Automotive Engineers. P-276. 1994.
- [123] <http://www.ghbmc.com/>. Global Human Body Models Consortium. Accessed January 2017.

- [124] Galbraith J A, Thibault L E, and Matteson D R: Mechanical and Electrical Responses of the Squid Giant Axon to Simple Elongation. Journal of Biomechanical Engineering. 115(1). 13-22. 1993.
- [125] Viano D C and Lovsund P: Biomechanics of Brain and Spinal-Cord Injury: Analysis of Neuropathologic and Neurophysiologic Experiments. Journal of Crash Prevention and Injury Control. 1(1). 35-43. 1999.
- [126] Li Y, Zhang L, Kallakuri, Zhou R and Cavanaugh J M: Injury Predictors for Traumatic Axonal Injury in a Rodent Head Impact Acceleration Model. Stapp Car Crash Journal. 55. 25-47. 2011.
- [127] Reid J D. Effects of flexion-extension movements of the head and spine upon the spinal cord and nerve roots. J. Neurol. Neurosurg. Psychiat. 23. 214-221. 1960.
- [128] Maiman D J, Myklebust J B, Ho K C, and Coats J: Experimental Spinal Cord Injury Produced by Axial Tension. Journal of Spinal Disorders. 2:1:6-13. 1989.
- [129] Kallakuri S, Li Y, Zhou R et al.: Impaired axoplasmic transport is the dominant injury induced by an impact acceleration injury device: An analysis of traumatic axonal injury in pyramidal tract and corpus callosum of rats. Brain Research. 1452. 29-38. 2012.
- [130] Viano D C, Hamberger A, Bolouri H and Saljo A: Evaluation of Three Animal Models for Concussion and Serious Brain Injury. Annals of Biomedical Engineering. 40:1: 213-226. 2012.
- [131] Thibault L A and Gennarelli T A: Biomechanics of Diffuse Brain Injuries. Society of Automotive Engineers. SAE856022. 1985.

- [132] Cusick J F et al.: Effects of vertebral column distraction in the monkey. *Journal of Neursurgery*. 57: 651-659. 1982.
- [133] Ewing C L and Thomas D J: *Human Head and Neck Response to Impact Acceleration*. Naval Aerospace Medical Research Laboratory (NAMRL). Monograph 21. 1972.
- [134] National Highway Transportation Administration. United States Department of Transportation. <https://www.nhtsa.gov/research-data>. Washington, DC, USA. Accessed January 2016.
- [135] *The Abbreviated Injury Scale 1980 Revision*. American Association for Automotive Medicine. Morton Grove, IL. 1980.

ABSTRACT**BIOMECHANICS OF CONCUSSION:
THE IMPORTANCE OF NECK TENSION**

by

RONALD JADISCHKE**August 2017****Advisors:** Dr. Albert King and Dr. David Viano**Major:** Biomedical Engineering**Degree:** Doctor of Philosophy

Linear and angular velocity and acceleration of the head are typically correlated to concussion. Despite improvements in helmet performance to reduce accelerations, a corresponding reduction in the incidence of concussion has not occurred (National Football League [NFL] 1996 – present).

There is compelling research that forces on and deformation to the brain stem are related to concussion. The brain stem is the center of control for respiration, blood pressure and heart rate and is the root of most cranial nerves. Injury to the brain stem is consistent with most symptoms of concussion reported in the National Football League and the National Hockey League, such as headaches, neck pain, dizziness, and blurred vision. In the Hybrid III anthropomorphic test device (ATD), the upper neck load cell is in close proximity to the human brain stem.

This study found that the additional mass of a football helmet onto the Hybrid III headform increases the upper neck forces and moments in response to helmet-to-helmet impact and helmet-to-chest impacts. A new laboratory impactor device was constructed to simulate collisions using two moving Hybrid III ATDs. The impactor was used to recreate on-field

collisions (n=20) in American football while measuring head, neck and upper torso kinematics. A strong correlation between upper neck forces, upper neck power and the estimated strains and strain rates along the axis of the upper cervical spinal cord and brain stem and concussion was found. These biomechanical responses should be added to head kinematic responses for a more comprehensive evaluation of concussion.

AUTOBIOGRAPHICAL STATEMENT

EDUCATION

B.A.Sc. Mechanical Engineering (Honors-Automotive Option), University of Windsor, 2002.
M.S. Biomedical Engineering (Impact Biomechanics), Wayne State University, Detroit, MI. 2012.
PhD Biomedical Engineering (Impact Biomechanics), Wayne State University, Detroit, MI. 2017.

EXPERIENCE

Mr. Jadischke has always been involved in athletics, including a variety of contact and non-contact sports. His interest in concussion research has grown due to his involvement in contact sport and his exposure to concussions. His current research interest is focused on the biomechanics of concussion in pursuit of understanding a potential mechanism and threshold of concussion.

Since 2005 Mr. Jadischke has been employed with McCarthy Engineering Inc. in Windsor, Ontario. He has developed an impact testing facility and is currently involved in helmet testing and the laboratory reconstruction of concussion-causing hits as a part of various ongoing research projects. In other motor vehicle collision reconstruction work at McCarthy Engineering, he specializes in motor vehicle collision reconstruction, vehicle fitness inspections, seat belt investigations and impact biomechanics. He is also a partner at Vehiclemetrics Inc. wherein they have developed a method to acquire vehicle systems parameters for use in automobile collision simulations and acquire geometric data for occupant modeling.

Prior to joining McCarthy Engineering Inc., Mr. Jadischke was the design team leader responsible for vehicle heating and air conditioning components and their integration into the heating and air conditioning systems. He has also obtained a variety of automotive related research and development, design and manufacturing experience while enrolled in the University of Windsor's Co-operative Engineering Program.